PHYSICS-BASED DYNAMIC MODEL FOR REVERSIBLE LIQUID-TO-LIQUID HEAT PUMP SYSTEMS

Development, validation and simulation with different systems, time-scales, operation conditions and working mode switch.

Universidad del País Vasco
Euskal Herriko Unibertsitatea

Erik Salazar Herrán

Thesis for the degree of Doctor of Philosophy in
Energy Efficiency and Sustainability in Engineering and Architecture

Supervisors: Ph.D. Koldobika Martin Escudero
Ph.D. Luis Alfonso del Portillo Valdes

Thermal Engineering Department
University of the Basque Country (UPV/EHU)
October, 2019

Abstract

The energetic problem is an issue that concerns the entire world. For instance, heating and cooling in buildings accounts for around the 80% of total final energy use in buildings, of which the 75% is still generated from fossil fuels and only 19% from renewable energy. In this context, Heat Pump systems (HP) are one of the most promising technologies to reduce fossil energy consumption for heating and cooling in buildings. Additionally, newer and more efficient heat pump technology would improve the energy sustainability of the building in which it is used.

In order to develop new HPs, there are two important aspects. The improvement of the components and the improvement of the joint system. The components would improve by optimizing geometrical parameters and materials, among others. Regarding the joint system, the main goal is to improve the control loop of the system. Nowadays, the best way to address these aspects is by the dynamic modeling of the components and systems that could simulate accurately their behavior. During this thesis a model for reversible liquid-to-liquid HP has been developed.

Firstly, a review is presented on the state-of-the-art of residential HPs and the advances on their modeling. A general energy background is presented. In it, the main global energy problems, heating and cooling handicaps in buildings and the latest energy policies are presented. Then, a brief description of HP operation principles, types of HPs and their role in the energy transition is depicted. Additionally, different tests with HPs conducted by the community are described. Finally, the advances in mathematical modeling of vapor compression cycles are reviewed explaining the different approaches to model them, the advantages and disadvantages of those approaches and the already existing models.

Then, the physics-based dynamic model to simulate the behavior of reversible liquid-to-liquid HPs is presented. The model of each component of the HP is developed separately and then they are joined together. The model is implemented in Matlab/Simulink environment.

A refrigerant-to-liquid plate heat exchanger (PHEX) model was developed using the Finite Control Volume method. The behavior of PHEXs either if they are working as condensers or as evaporators can be simulated. Moreover, they allow the user to choose the configuration of the PHEX between parallel-flow and counter-flow. The equations

and their implementation have been presented.

After that, the model is validated in micro-scale situations, understanding that the micro-scale is the time scale at which fast transient-states are produced. Examples include operation condition changes, working mode switches or system start-ups.

Different tests under different transient situations were developed. Measurements have been used to validate the model under heating, cooling and start-up situations. Simulation results present good agreement with test data.

Once the model was validated under different micro-scale transient situations, working mode switch was simulated. The reversible behavior of the system was simulated by starting in cooling mode, switching to heating mode and going back to cooling mode. Since experimental data of working mode switches was not available, it was not possible to compare the simulation results with test data. However, the obtained results could have a good alignment to the actual behavior of the system during a working mode switch.

Finally, the model was used to simulate the behavior of other HP under macro-scale situations, understanding that the macro-scale is the time scale at which the dynamics of the system are studied during long time periods. With it, the utility of the model to obtain the performance of the system is studied. With respect to micro-scale simulations, the discretization of the model into finite volumes was reduced to the half.

The HP used (different from that used in micro-scale tests), test rig and tests procedure is explained. Then, the model is validated under the cooling working mode. A good agreement is observed between test data and simulation results in water temperatures but the compressor power consumption is underestimated. After that, a system energy performance study was conducted in order to clarify the divergences between test data and simulation results. It was concluded that by improving the compressor model more accurate results could be obtained.

To summarize, the validity of the model can be asserted to simulate liquid-to-liquid HPs with accurate results. It can be used to carry out micro- and macro-scales simulations under different working modes and configurations of PHEXs. Additionally, working mode switch simulations can be carried out.

Acknowledgments

I want to express my gratitude to all the people, who directly or indirectly, have contributed to the elaboration of this thesis. It would never have been possible without their support.

Firstly, to my supervisors. To Koldo, for his close and pleasant manners and for guiding me during my first steps in the research field. For his help, advice, dedication and availability. To Luis, for encouraging me to take this challenge, for the trust placed in me from the first moment and the experience provided.

To the people of the department and ENEDI members for creating a friendly and close work environment. Also for the willingness to help when I have needed. A special mention to Irati and Ana, for all the joint support we have given during these years and for all the good times.

To Nagore, Fernando and Pedro for their availability and help during my first steps with Simulink.

To Professor Alleyne for allowing me to spend some of the most special months of my life in Illinois. For sharing his wisdom, advice and experience. To all the Alleyne Research Group, especially to Herschel and Chris for their advice and help whenever I had needed it.

To the members of the applied thermodynamics section of the ETSI of the UPM, to Ignacio, for their kindness, generosity and help during my stays in Madrid.

To Emilio Navarro for his altruistic collaboration and Saunier Duval Vitoria for the data and help received.

Finally, to my parents, Sheila, Maria, family and friends for always being there.

Many thanks to all of you.

Nomenclature

Symbols

A	area $[m^2]$
Bo	Boiling number $[-]$
c	specific heat $[kJ\ kg^{-1}\ K^{-1}]$
C_v	valve coefficient $[m^2]$
D_h	hydraulic diameter $[m]$
G	mass flux $[kg\ m^{-2}\ K]$
h	enthalpy $[kJ\ kg^{-1}]$
$\dot{h}$	enthalpy time derivative $[kJ\ kg^{-1}\ s^{-1}]$
L	plates width $[m]$
m	mass $[kg]$
$\dot{m}$	mass flow rate $[kg\ s^{-1}]$
N	number of finite volumes
Nu	Nusselt number
p_{co}	corrugation pitch $[m]$
P	pressure $[kPa]$
$\dot{P}$	pressure time derivative $[kPa\ s^{-1}]$
Pr	Prandtl number
$\dot{q}$	heat transfer rate $[kW\ s^{-1}]$
Re	Reynolds number
t	time $[s]$
T	temperature $[K]$
V	volume $[m^3]$
x	plates length in the flow direction $[m]$

Greek letters

α	convection heat transfer coefficient $[kW\ m^{-2}\ K^{-1}]$

β	chevron angle [rad]
Δ	difference/increase
η	efficiency
∂	partial derivative
ρ	density [$kg\,m^{-3}$]
$\dot{\rho}$	density time derivative [$kg\,m^{-3}\,s^{-1}$]

Subscripts

ave	average property
c	cross-sectional area
comp	compressor
cv	control volume
Eq	equivalent
h	at constant enthalpy
i	control volume index
in	inlet
isen	isentropic
n	last finite volume
out	outlet
p	at constant pressure
r	pressures ratio
R	refrigerant
s	heat transfer area
S	secondary fluid
c	cross-sectional area
valve	valve
W	wall/plate

Acronyms

ASHP Air Source Heat Pump

ASHPWH Air Source Heat Pump Water Heater

COP Coefficient of Performance

DHW Domestic Hot Water

EER Energy Efficiency Ratio

EEV Electronic Expansion Valve

EU European Union

FCV Finite Control Volume

GSHP Ground Source Heat Pump

HEX Heat Exchanger

HVAC Heating Ventilation and Air Conditioning

HP Heat Pump system

HTC Heat Transfer Coefficient

MB Moving Boundary

MFR Mass Flow Rate

NE Normalized Error

PHEX Plate Heat Exchanger

RTF Real Time Factor

SAHP Solar Assisted Heat Pump

SPF Seasonal Performance Factor

TXV Thermostatic Expansion Valve

UNFCCC United Nations Framework Convention on Climate Change

USA United States of America

VCC Vapor Compression Cycle

4WV Four Way Valve

Contents

Chapter 1

INTRODUCTION

During this first chapter an overview of the state of the art will be presented. It will firstly involve the current global energy framework and a revision of global and European agreements and policies regarding the main objectives of energy consumption and emissions reduction. Then, a brief introduction to heat pump systems and its role in the energy transition will be given. It will be followed by a review of the experimental tests with heat pump systems that have been carried out over the world during the last years. Finally, the advances that have taken place in vapor compression cycles modeling for different approaches and components will be revised, with a greater emphasis in physics-based models.

1.1 Energy Background

1.1.1 Energy global framework

Energy plays a very important role in the development of the society and countries. Energy consumption is needed to develop any kind of economic activity. Therefore, global primary energy consumption grows annually. In the last 25 years, primary energy consumption has increased almost a 60% (Figure 1.1). This growth is more evident in areas under development as shown in Figure 1.2. Moreover, it is estimated to continue growing in the next 20 years between 18 and 38% under recent energy policies and barely decrease under ambitious energy policies (Figure 1.1).

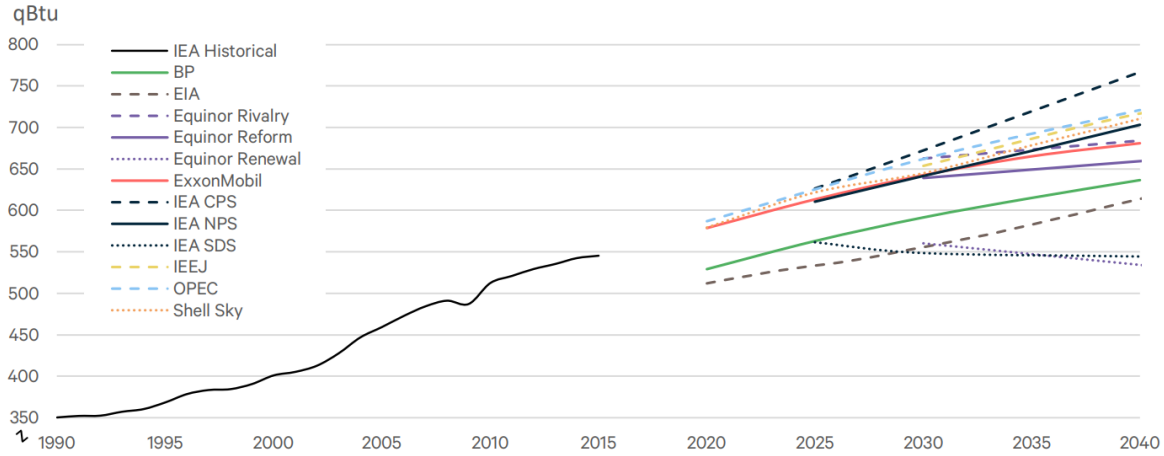

Figure 1.1: Historic global primary energy consumption and future estimations under different scenarios [1].

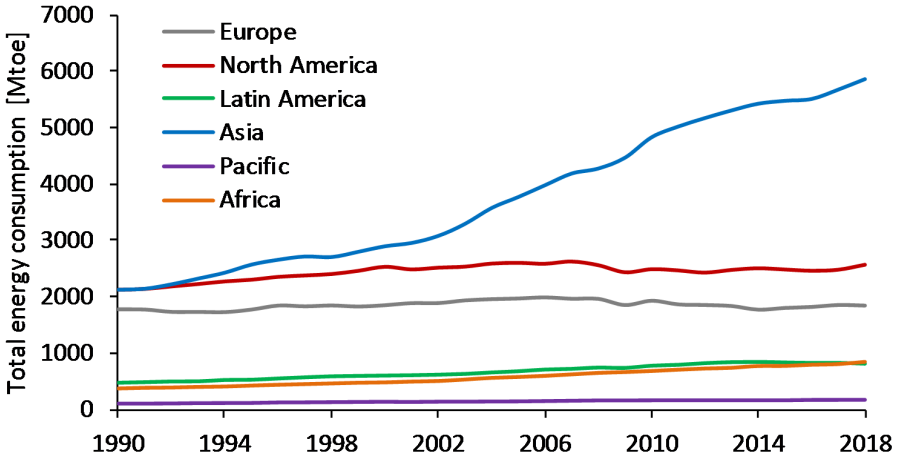

Figure 1.2: Total energy consumption by regions [2].

The main energy consumption is given in industrial, transport and residential sectors, which in 2017 monopolize the 79% of the total world final energy consumption (Figure 1.3). Nowadays, that energy is mainly produced from non-renewable sources as can be seen in Figure 1.4.

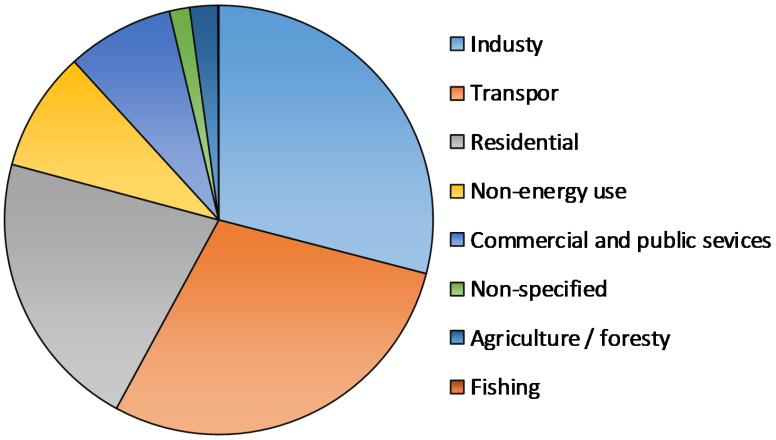

Figure 1.3: Global total final energy consumption by sector [3].

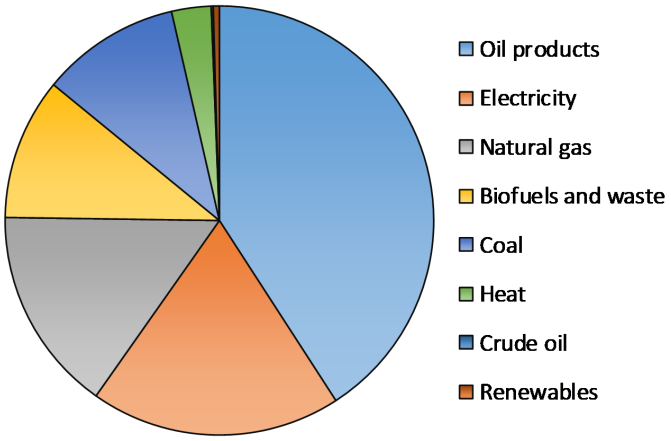

Figure 1.4: Global total final energy consumption by source [3].

In this context, the exponential growth of energy consumption from non-renewable sources has led to different serious problems:

- ***Environmental problems***

The environmental problems such as climatic change are caused primarily by the overwhelming progress of the human species and its growth of greenhouse gas emissions.

Two main environmental problems are produced by the increase of gas emissions to the atmosphere.

On the one hand, the greenhouse effect caused by an unnatural concentration of greenhouse gases in the Earth's atmosphere is powering the global warming. The major gases that contribute to the greenhouse effect are the water vapor and the carbon dioxide, which are mainly produced by fossil fuels burning activities.

On the other hand, the ozone layer depletion. The ozone concentration prevents the most harmful UVB wavelengths from passing through the atmosphere. Nevertheless, ozone-depleting substances such as halocarbon refrigerants, CFCs, HCFCs and solvents, are causing a decrease in the ozone atmospheric concentration.

- ***Fossil fuels scarcity***

Fossil fuels are the most consumed primary energy nowadays. Moreover, the increase of energy demand worldwide [4] have increased fossil fuels consumption, even with the increase of renewable energy sources [5]. For instance, in Figure 1.5 can be seen the global primary energy demand growth by fuel in each leading world regions from 2017 to 2018.

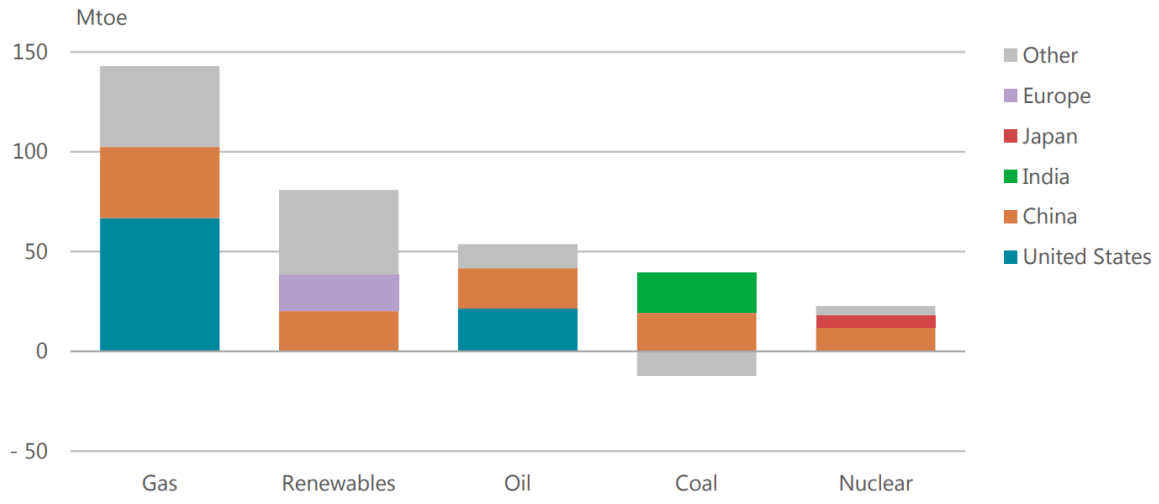

Figure 1.5: Global primary energy demand growth by fuel and leading world regions from 2017 to 2018 [5].

Nevertheless, the reservoirs of fossil fuels are not inexhaustible. It is calculated that the depletion time for oil, coal and gas is of approximately 35, 107 and 37 years respectively from 2006 [6].

Moreover, production countries are different from consumption countries, generating

geopolitical tensions between nations. In Figures 1.6 and 1.7 can be seen the difference between oil production and consumption countries, respectively.

Figure 1.6: Oil production areas [7].

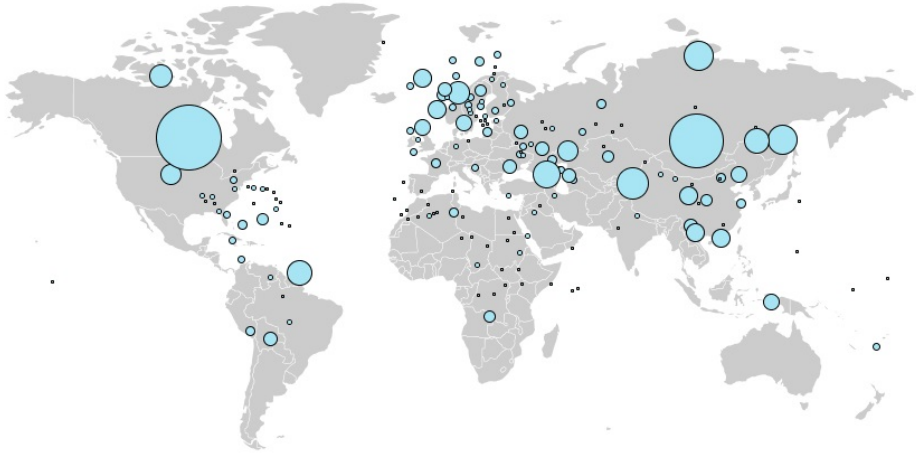

Figure 1.7: Oil consumption areas [7].

- ***Enhancement of the social inequality between countries***

There is a proved relationship between the energy consumption of a society and its economic growth [8–10]. For instance, in Figure 1.8 can be seen how the most developed countries have much more energy consumption. Therefore, an energy unequal consumption between countries leads in an unequal economic growth.

The reduction of this problems goes through an energetic transition towards a less energy consumption and a higher use of renewable energy sources.

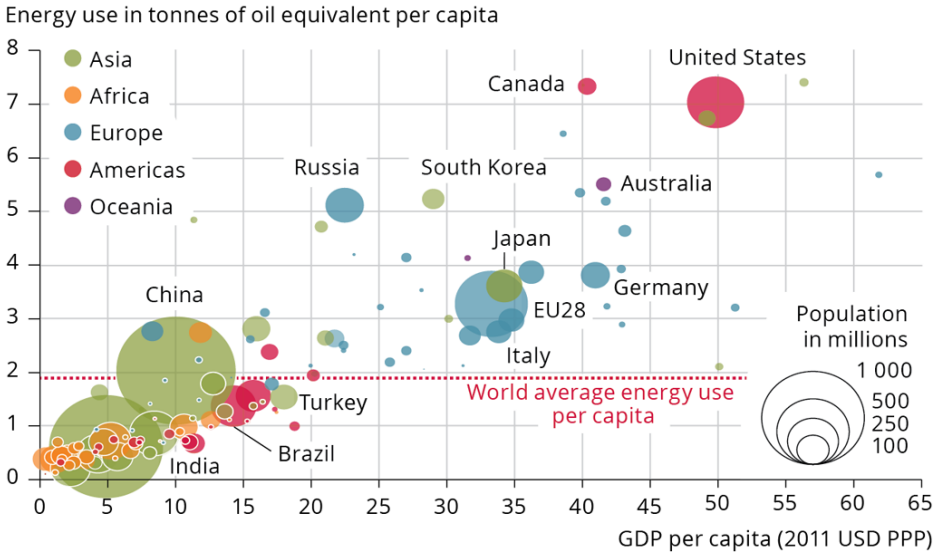

Figure 1.8: Energy consumption VS Gross Domestic Product for different countries [11].

1.1.2 Heating and cooling in buildings

As seen in Figure 1.3, residential sector accounts more than 20% of the total global energy consumption. In Europe, that percentage increase up to 27% [12].

The sources of residential energy consumption varies for different locations. For instance, in Figure 1.9 is shown the comparison of energy sources in residential sector in 2017 between United States of America (USA) and European Union (EU). However, it can be asserted that the use of non-renewable sources is predominant.

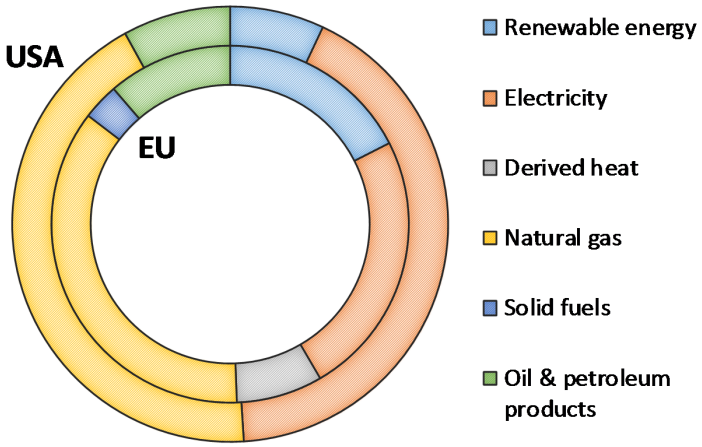

Figure 1.9: Comparison of energy sources in residential sector in 2017 between USA and EU [12, 13] .

The final energy consumption by end-use in the residential sector is divided as shown in Figure 1.10. Space heating accounts for around 50 - 65% of the dwellings energy

consumption. Taking into account all the heating and cooling systems it grows up to 70 - 79%. Cooling currently accounts for around 5% of energy consumption but it is growing rapidly due to, among others, the increase in the global temperature [14].

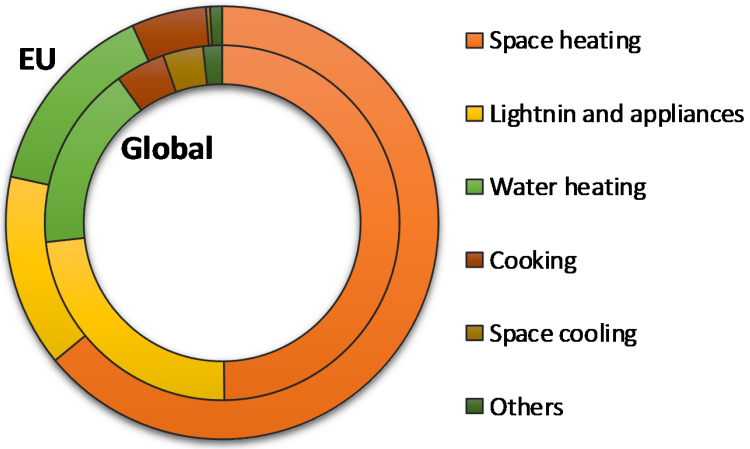

Figure 1.10: Final energy consumption by end-use in the residential sector [15].

Moreover, for the case of EU, Figure 1.11 shows the main energy sources for each type of end-use. In EU, for space heating and Domestic Hot Water (DHW) production, around 23% and 10% respectively is produced from renewable energy sources [12]. Globally, space heating production from renewable sources decreases to around 10% [16]. It entails a considerable environmental impact due to the related CO2, NOx and CFCs emissions [17].

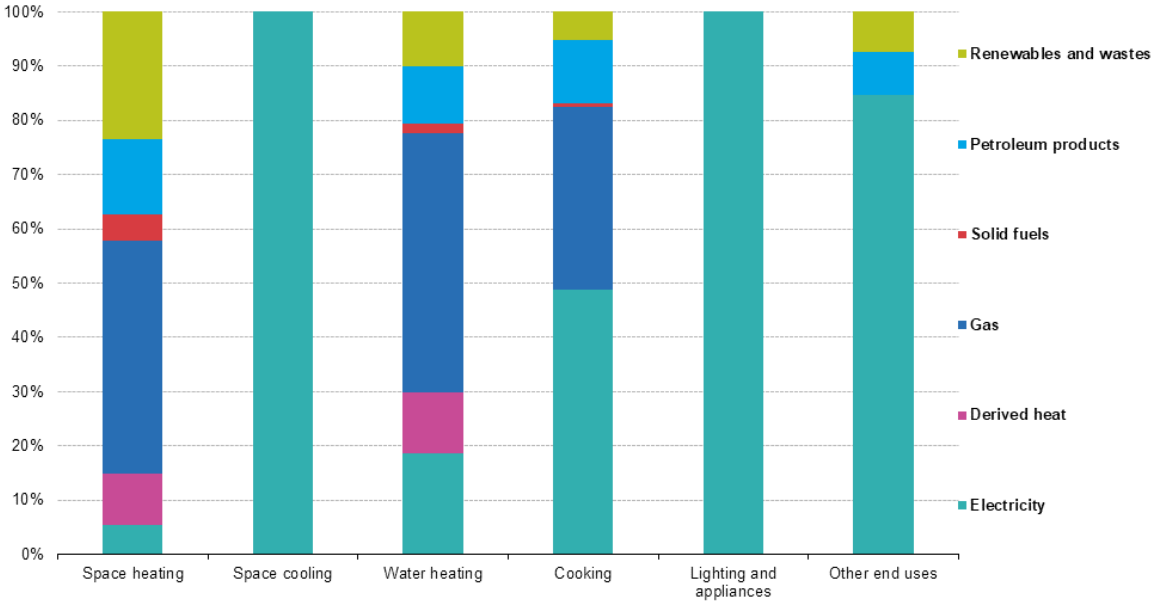

Figure 1.11: Main energy sources for each type of end-use in the residential sector [12].

Almost half of the EU's buildings have individual boilers installed before 1992, with efficiency of 60% or less [18]. Decisions on replacing old appliances are typically made under pressure, when the heating system breaks down. Moreover, desirable information is not easily available for most consumers. This leads them to continue using older, conventional and less efficient technologies [19].

For the specific case of Spain, half of dwellings have conventional individual boiler for space and hot water production and hardly 23% are equipped with clean technologies, such as heat pumps systems (Figure 1.12a). Regarding cooling systems, the use of electric technologies increases up to 78%. However, the implementation rate of cooling systems in Spain is around 49% [20]. They are mainly used in hot and Mediterranean climatic zones (Figure 1.12b).

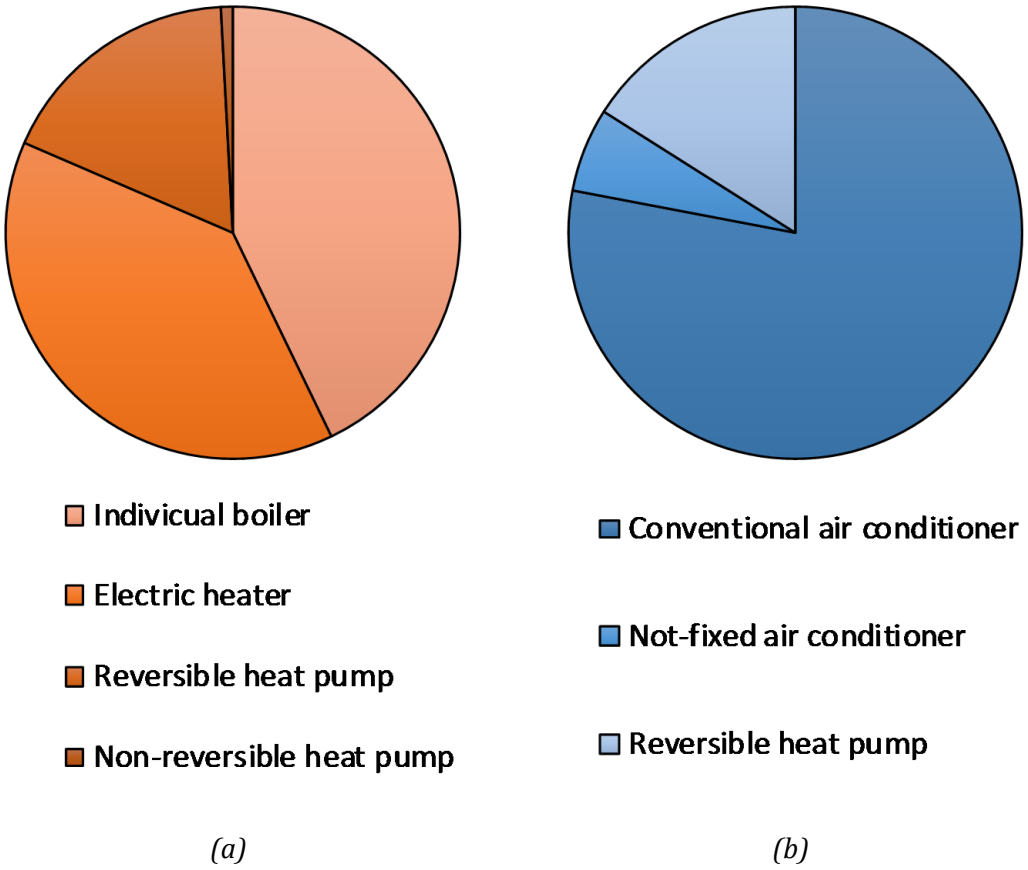

Figure 1.12: Heating (a) and cooling (b) systems used in residential bilding in Spain [20]

Bearing all this in mind, cooling and heating present a great opportunities to reduce greenhouse gas emissions from the residential sector and move towards a more sustainable future. Clean heating and cooling means providing heat and cool without emitting CO2, noxious gases or particulates. It can be provided by different clean systems

from which one of the most promising technology are the heat pumps [21].

1.1.3 Global and European energy policies

With the objective of reducing the global emissions some policies and agreements have been signed during last years. Some are agreements that have been reached between different countries around the world while others are policies implemented in specific regions.

Since it is not possible to enumerate and describe all of them, the most representative global agreements and European Directives that were signed during the last years will be presented chronologically.

Montreal Protocol on Substances that Deplete the Ozone Layer

This is the first international treaty signed to battle the environmental issues and the first universally ratified treaty in United Nations history. It was signed in 1987 as a result of the Vienna Convention for the Protection of the Ozone Layer by 197 parties (196 states and the European Union). It is focused in the reduction of halogenated hydrocarbons that deplete stratospheric ozone [22].

United Nations Framework Convention on Climate Change (UNFCCC)

It was signed in Rio de Janeiro in 1992 by 43 countries, which were considered as the developed countries and the economies in transition. Its main goal was to stabilize greenhouse gases concentrations in the atmosphere at a level that would prevent dangerous anthropogenic interference with the climate system [23].

European Directive 93/76/CEE

This is the first European Directive regarding the energy efficiency in buildings. The purpose of this Directive was to limit the carbon dioxide emissions by improving energy efficiency implementing programmes in the following fields [24]:

- Energy certification of buildings.

- The billing of heating, air-conditioning and hot water costs on the basis of actual consumption.
- Third-party financing for energy efficiency investments in the public sector.
- Thermal insulation of new buildings.
- Regular inspection of boilers.
- Energy audits of undertakings with high energy consumption.

This Directive encouraged EU members to work on the improvement of the energy efficiency in buildings but did not impose any obligation to any of them.

In 2006 this Directive was replaced by the Directive 2006/32/EC.

Kyoto Protocol

The Kyoto Protocol was adopted in Japan in 1997 to extends the UNFCCC treaty of 1992 [25]. It entered into force in 2005 and its first commitment period started in 2008 and ended in 2012. The objective of this protocol was to reduce the emissions of the six main greenhouse gases.

European Directive 2002/91/CE

The objective of this Directive was to promote the improvement of the energy performance of buildings, taking into account outdoor climatic and local conditions, as well as indoor climate requirements and cost-effectiveness [26].

This directive introduce the energy certification of buildings, the application of minimum requirements on the energy performance of new and major renovation buildings, a general methodology for the calculation of the buildings energy performance and a regular inspection of boilers and air-conditioning systems.

This directive also introduced for the first time the definition of a “heat pump” as a device or installation that extracts heat at low temperature from air, water or earth and supplies it to the building.

In 2010 this Directive was replaced by the Directive 2010/31/UE.

European Directive 2006/32/CE

This directive on energy end-use efficiency and energy services replaced the Directive 93/76/CEE. It main purpose was to enhance the cost-effective improvement of energy end-use efficiency by providing the necessary tools to remove existing barriers that impede the efficiency and by creating the conditions for the development and promotion of a market for energy services. It also imposed to State members the submission of Energy Efficiency Action Plans [27].

In 2012 this Directive was replaced by the Directive 2012/27/UE.

European Directive 2009/28/EC

This Directive on the promotion of the use of energy from renewable sources was signed on 23 April 2009 and established a common framework for the promotion of energy from renewable sources [28]. It set mandatory national overall targets and measures for the use of energy from renewable sources.

On this purpose, it was set that aerothermal, geothermal and hydrothermal heat energy captured by heat pumps shall be taken into account for the calculation of the sum of gross final consumption of energy from renewable sources for heating and cooling if the final energy output significantly exceeds the primary energy input required to drive the heat pumps.

The amount of energy captured by heat pumps to be considered energy from renewable sources for the purposes of this Directive E_{res} shall be calculated in accordance with the following formula:

$$E_{res} = Q_{usable}(1 - 1/SPF) \tag{1.1}$$

where Q_{usable} is the estimated total usable heat delivered by heat pumps and Seasonal Performance Factor (SPF) is the estimated average seasonal performance factor of the heat pumps. Only heat pumps with a minimum SPF can be considered as renewable energy systems.

SPF is the term that determine the performance of a real installation, contrary to the Coefficient of Performance (COP) that evaluates the performance under controlled labor-

atory environment [29].

European Directive 2010/31/UE

With the aim of reduce the energy consumption of the EU by 20%, reduce the greenhouse gas emissions by 20% and implements the measures established in the Commission Communication entitled "Action plan for energy efficiency: realizing the potential" [30], in 2010 was signed the Directive 2010/31/UE on the energy performance of buildings. This directive ratified the requirements established in the Directive 2002/91/CE and introduce the concept of nearly zero-energy buildings and the independent control systems for energy performance certificates [31].

This directive redefined the heat pump definition given in the Directive 2002/91/CE and introduced the concept of reversible heat pumps.

European Directive 2012/27/UE

The Directive 2012/27/EU on energy efficiency established a common framework of measures for the promotion of energy efficiency within the Union in order to ensure the achievement of the Union's 2020 20% headline target on energy efficiency and to pave the way for further energy efficiency improvements beyond that date [32].

Paris agreement

The Paris Agreement is the latest agreement signed by the UNFCCC. It was signed in 2015 and for the first time brings all nations into a common cause to undertake ambitious efforts to combat climate change and adapt to its effects, with enhanced support to assist developing countries to do so [33].

The Paris Agreement central aim was to strengthen the global response to the threat of climate change by keeping a global temperature rise below 2 degrees Celsius with respect to pre-industrial (1990) levels. Additionally, the agreement aims to strengthen the ability of countries to deal with the impacts of climate change.

The Paris Agreement entered into force on 4 November 2016.

1.2 Heat pump systems

Heat Pump system (HP) are mechanical systems driven by electric energy with the objective of transfer heat from a heat source to a heat sink. The great majority of HPs work on the principle of the Vapor Compression Cycle (VCC) (Figure 1.13), consisting of an outdoor Heat Exchanger (HEX) (as evaporator), a compressor, an indoor HEX (as condenser) and an expansion valve. A volatile liquid, known as the refrigerant fluid, is used to transport the heat in the closed HP cycle [34].

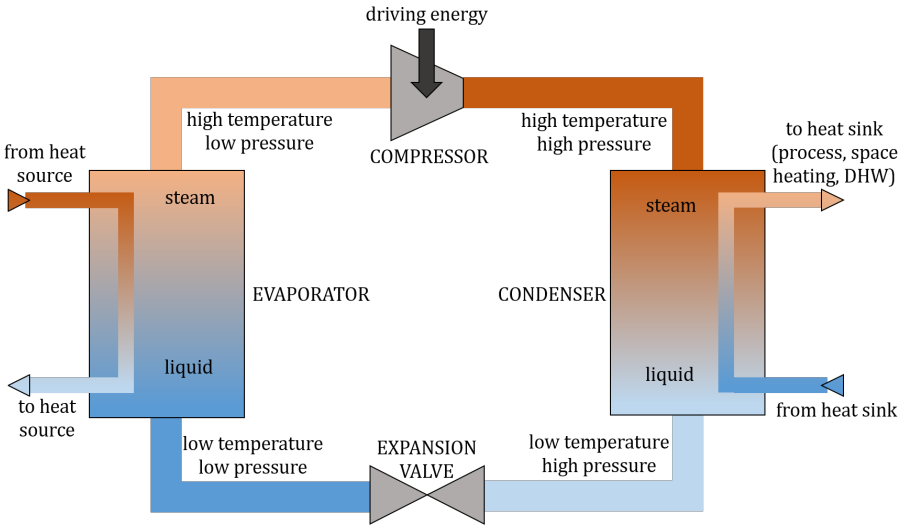

Figure 1.13: Vapor compression cycle scheme.

In the condenser and evaporator HEXs, heat is transferred between the refrigerant fluid and other fluid used in the heat source and sink, known as secondary fluid. Depending on the HP, the sink can be water or air. Similarly, the heat sources depend on the HP, being the most common ones the ambient air, the subsoil, groundwater reservoirs or surface water reservoirs. The combination of these heat sinks and sources defines the HP classification.

1.2.1 Heat pumps classification

Depending on the heat source and sink combinations, HPs can be classified as air-to-air HP, air-to-water HP, water-to-water HP and water-to-air HP. This classification defines the HEX utilized for the heat transfer between the secondary fluid and the refrigerant fluid.

- **Air-to-air HP:** Uses outdoor air as the heat source and indoor air as the heat sink.
- **Air-to-water HP:** Uses outdoor air as the heat source and transfers heat to indoor water.
- **Water-to-water HP:** Also known as liquid-to-liquid HP, takes heat from outdoor water and transfers heat to indoor water.
- **Water-to-air HP:** Also known as liquid-to-air HP, takes heat from outdoor water and transfers heat to indoor air.

On the other hand, depending on the heat source, they can be differentiated between Air Source Heat Pump (ASHP) and Ground Source Heat Pump (GSHP).

- **Air Source Heat Pump:** It takes heat from outdoor air and transfer it to the refrigerant fluid. The most common ASHP are air-to-air HP, so then, the refrigerant transfer the heat to indoor air. Nevertheless, it also can be transferred to water (i.e. to radiators water).
- **Ground Source Heat Pump:** Subsoil or outdoor water reservoirs are used as the heat source. When heat is taken form the subsoil it is usually utilized a ground-coupled HEX in order to exchange heat between the subsoil and the used secondary fluid, which then will transfer to the refrigerant fluid. In these cases, in cold climates, the secondary fluid is usually a water mixture with glycol to avoid the freezing of the water. In case of using water reservoirs, it can be a closed loop, which uses a coupled HEX, or an open loop, where the water of the reservoir exchange directly the heat with the refrigerant fluid in the outdoor HEX.

Additionally, nowadays, an important number of HPs are designed with the capability of reverse the working cycle of the system and use them to cool down the indoor air or water instead of heating it. These systems are commonly known as reversible HPs and are achieved by placing a Four Way Valve (4WV) between the HEXs and the compressor.

The operation cycle of a reversible HP depends on the working mode of the system: heating or cooling modes. During the heating mode, the system absorbs heat from the heat source, transfers it to the refrigerant fluid of the system's closed circuit and, later, this heat is transferred to the indoor air or water. Therefore, the indoor HEX works as the condenser and the outdoor HEX as the evaporator. On the contrary, in the cooling mode, the system cools the indoor air or water by extracting heat from it by means of

the refrigerant and transferring it outside. In this case, the condenser is the outdoor HEX and the evaporator the indoor HEX.

There are two main situations in which reversible HPs are used. Firstly, when the HP is wanted to supply both heating and cooling demands. For instance, during the summer time, when the HP is working on cooling mode in order to cover the refrigeration demand and a punctual heating demand is given such as a DHW demand. At that moment, the working mode is switched and the system goes from the cooling mode to the heating mode.

Secondly, in ASHP, in cold climates it is common that the ambient air moisture freezes around the refrigerant tubes of the outdoor HEX forming an ice layer. It drastically reduces the heat transmission between the air and refrigerant decreasing the performance of the system [35, 36]. In this cases, the cycle is reversed in order to increase the temperature of the refrigerant fluid that goes through the outdoor unit during a given time and melt the ice. Then, the cycle is reversed again to continue supplying space heating or DHW to the building. This cycles are commonly known as defrosting cycles.

Apart from the presented HPs types, there exist other minority used types of HPs. Some of them are variations of the previously described ones, other are hybrid systems and others are systems that use a different working cycle instead of VCC.

- **Air Source Heat Pump Water Heater (ASHPWH):** These systems are similar to an ASHP,but the condenser instead of being a HEX, is a coil immersed in a water tank with the objective of heat the water of the tank. ASHPWH are utilized mainly for DHW production [37, 38].
- **Solar Assisted Heat Pump (SAHP):** These systems use the sun radiation as the heat source to evaporate the refrigerant fluid before sending it to the compressor. There are different types of SAHP such as direct-expansion SAHP [39], air-source SAHP [40] or photovoltaic/thermal-solar SAHP [41].
- **Absorption HP:** Instead of using a VCC driven by electric/mechanical energy, these systems use the absorption cooling cycles using an absorber and a generator [42, 43]. They are very useful when both heating and cooling are required simultaneously. Although there exist residential absorption HPs [44], they are more usual in the industry.
- **Air-ground dual source HP:** These systems can use either air or ground as heat

sources. The control of the system chose which source use at each time depending on the operation and ambient conditions [45, 46]. This technology is under development and it is not very used yet.

On the other hand, there are many refrigerant fluids that can be utilized in the closed loop of a HP. The ideal refrigerant would be natural, with low global warming potential, low ozone depletion potential, good thermochemical properties and safe. Nowadays, the objective is to remove from the market the most environmentally harmful refrigerants and improve the technology to use safely natural hydrocarbons such as propane [47].

1.2.2 Heat Pump role in the energy transition

Energy transition is 'a pathway toward transformation of the global energy sector from fossil-based to zero-carbon by the second half of this century' [48]. It involves the decarbonisation of electric energy production, industrial processes, transport and Heating Ventilation and Air Conditioning (HVAC) sector, among others.

Regarding residential sector, district heating and demand electrification are two of the most promising solutions for the reduction of energy consumption and emissions from heating and cooling [19]. However, electricity must come from renewable sources in order to get clean heating and cooling.

Nevertheless, energy efficiency progress is overshadowed by continued investments in carbon-intensive and less-efficient heating technologies. Fossil fuels still supply most space and water heating needs in buildings. Therefore, direct emissions from heating remains at 80% of the total direct emissions from buildings [49]. Clean systems such as HP technologies propose notable potential to decrease emissions from residential sector.

Energy performance of HPs have been proved to be better than conventional systems for space heating, cooling and DHW production [50, 51]. Having the GSHP systems a better performance than the ASHP systems due to two main reasons. The higher temperature of the ground against the ambient air and the no need of carrying out defrosting cycles that decrease system performance [52, 53]. Additionally, as presented previously, it has been boosted the use of HPs recognizing them as part of renewable energy technologies (European Directive 2009/28/EC [28]). However, the drawback

is that HPs are more expensive than boilers [54].

In this context, Asaee et al. [55] developed a techno-economic research to study the feasibility of converting Canadian building stock into almost zero consumption buildings. The study was developed using a validated energy model to simulate the energy demands of buildings in Canada. With the model 17,000 different houses were recreated in which conventional heating and cooling systems were replaced by an air-to-water HP, an auxiliary boiler and a thermal storage tank.

The results showed that the changes mentioned in the thermal facilities could be made in 6.3 million Canadian homes, which would lead to a 36% of reduction in Canada's final energy consumption from buildings. On the other hand, it was ensured the reduction of primary energy consumption in those provinces where renewable energies have a significant weight in the generation of electric energy. Consequently, the consumption of fossil fuels as well as greenhouse gases emissions would be significantly reduced. However, the authors noted the impossibility of carrying out the improvement of thermal installations without governmental economic aid or incentive programs.

1.2.3 Manufacturers as a key factor

The reduction of investment costs, enhancement of systems energy performance, use of more environmentally friendly refrigerant fluids and reduction of the payback time would make the HP technologies even more competitive in the residential heating and cooling market. In this context, HPs manufacturers plays an important role. They have the opportunity to develop new more efficient systems to achieve the energetic sustainability.

According to various studies, HP sales in 2018 increased with respect to 2017 in different European countries such as Finland [56], Ireland [57] and Germany [58]. Moreover, annual HP sales in the world have been more than doubled, from 1.8 million units in 2012 to over 4 million in 2017, with year-on-year growth of 30% [16]. This demonstrates the progress of HP technologies, which are increasingly competitive, commanded by manufacturers. Nevertheless, the sales of HPs should increase significantly [49].

1.3 Experimental tests with Heat Pumps

Experimental tests can be carried out both under laboratory conditions and under real conditions. The usefulness of them depends on the purpose of the test. When tests are developed in a laboratory, the operation conditions of the system are controlled and the measurements are usually more accurate. Therefore, the performance of the system can be better calculated and the elements of the system more accurately characterized. Tests under real conditions are developed by monitoring a whole system in a real building with real usage along days, weeks, months or even years. This tests are usually utilized to analyze the seasonal performance and characterize the behavior of the whole system.

On the other hand, while tests under real conditions are always dynamic tests that depends on the indoor and outdoor conditions, laboratory tests can be developed both under steady or dynamic conditions. Tests under steady conditions are achieved by fixing the operation conditions of the system and waiting until the steady-state for those conditions are given. If the goal of the tests is to characterize the performance of the system for a given conditions or validate a static model, steady tests are suitable.

Nevertheless, when a dynamic model wanted to be validated or the performance of the system for variable conditions wanted to be studied, dynamic tests are needed. They can be carried out by varying the operation conditions of the system during its operation or testing it under the ambient variable conditions.

1.3.1 Tests under laboratory conditions

Byrne et al. [59, 60] conducted experimental tests under laboratory conditions for simultaneous heating and cooling with an ASHP. Firstly, they characterized for different operation conditions the ASHP under steady laboratory tests and then they analyzed the dynamic behavior of the defrosting cycle.

Thermal dynamic analysis of a multi-functional ASHP system for heating, cooling and DHW production was made in comparison with a conventional ASHP system (only heating and cooling) by Sun et al. [61] Energy and exergy efficiencies were calculated. It was concluded that for both heating and cooling mode, the multi-functional ASHP system had better energy and exergy performance. Defrosting cycles of ASHP were

also experimentally analyzed with laboratory tests [62, 63].

Zheng et al. [53] developed a performance and exergetic experimental study comparing a GSHP and an ASHP. The test was carried out in North China under steady conditions, using seawater as the energy source for the GSHP. Due to the decrease of the heat transfer performance caused by the frost formation, the results showed a better performance of the GSHP.

Cakir et al. [64] developed a laboratory steady experimental test in which a multifunctional HP was tested. It was able to run in four modes, namely air-to-air, air-to-water, water-to-water and water-to-air. Water tanks were used to simulate water sources. Results showed that the HP unit which has the maximum COP was the water to air system followed by the water to water system (Figure 1.14).

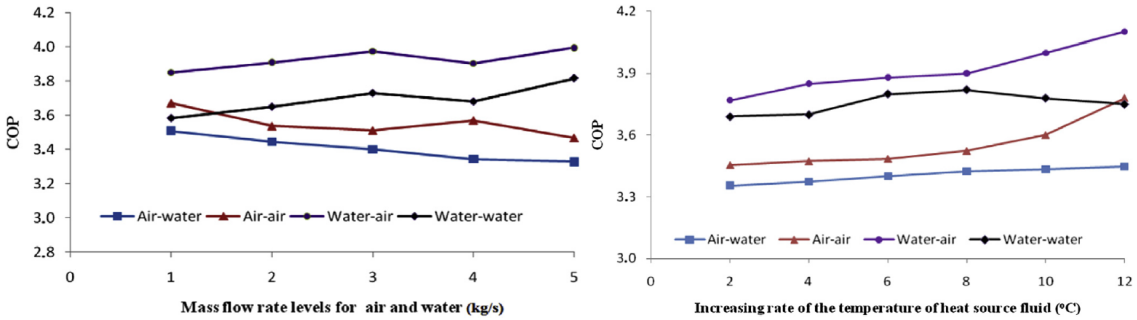

(a) *(b)*

Figure 1.14: COP change for different HP functions versus increasing of the evaporator fluid mass flow rate (a) and temperature (b) [64].

Sebarchievici et al. [65] tested a reversible GSHP and compared different working modes (space heating and space cooling, both with and without DHW production). This test was developed under laboratory dynamic conditions during one month. They concluded that the COP for space heating and cooling is similar and that the DHW production decreases the performance of the system (Figure 1.15).

Pitarch et al. [66] tested in the laboratory a GSHP under different fixed conditions in which a separated subcooler was added after the condenser for DHW production. In this case, propane (R290) was used as refrigerant fluid. Obtained results showed a high degree of performance improvement by adding the subcooler.

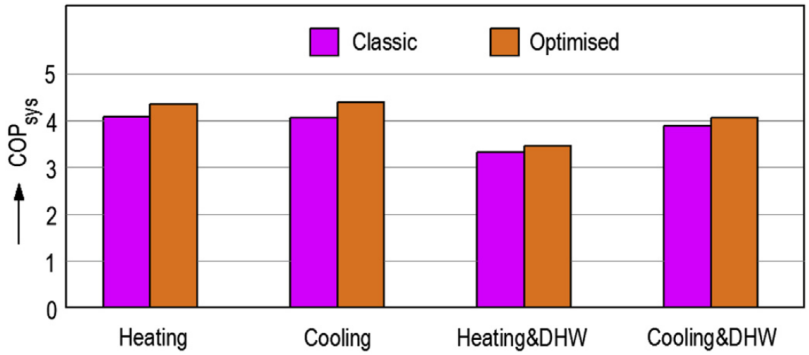

Figure 1.15: Variation of COP in different operation modes of GSHP [65].

1.3.2 Tests under real conditions

Regarding tests under real conditions, Luo et al. [67] continuously monitored a GSHP in south Germany during four years to analyze heating and cooling performance. In northwest China, a GSHP system of a residential district was compared with a traditional air conditioner proving the greater efficiency of the HP [68]. Also in China, in Shanghai, a water heat exchanger was coupled to a domestic ASHP in order to produce DHW. This system was compared with conventional DHW systems and the reduction of energy consumption was demonstrated [69].

Sivasakthivel et al. [70] tested a GSHP for cooling and heating in an Himalayan city. The results showed a better COP in the heating mode than in the cooling mode (Figure 1.16). On the other hand, in order to predict the long-term performance of a GSHP system, it was monitored during two years in East China by Yan et al. [71].

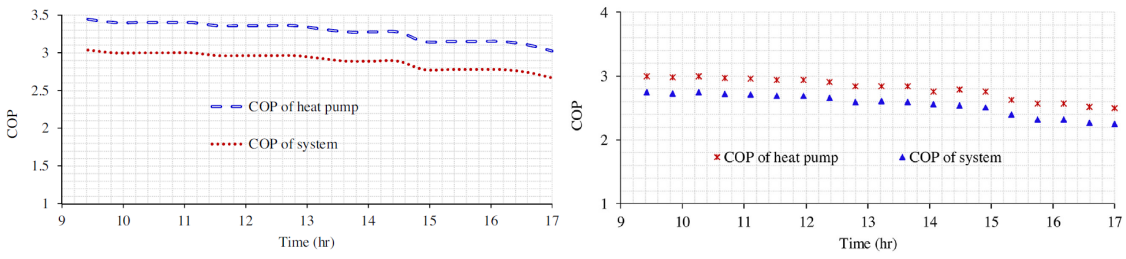

Figure 1.16: COP of the HP and the whole system under heating (a) and cooling (b) modes [70].

Some authors have developed experimental tests in which different energy sources have been compared under real conditions. Urchueguía et al. [72] carried out an experiment in European Mediterranean coast were a GSHP and a ASHP were compared

in heating and cooling modes. For a whole climatic season, the results showed that the GSHP system consume less primary energy (Figure 1.17).

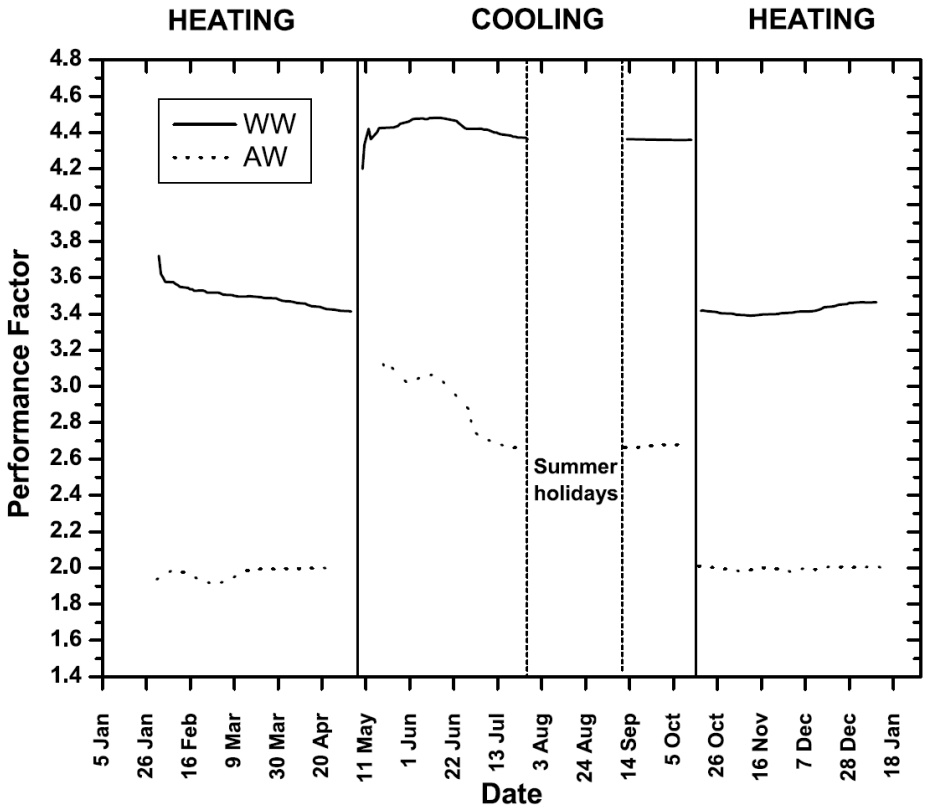

Figure 1.17: System performance evolution for both HP systems and both working modes during one year [72].

Romani et al. [73, 74] compared in a test cubicle the performance of radiant wall coupled to a GSHP with a conventional ASHP. The comparison was carried out both for the heating and for the cooling modes. In both of them was demonstrated the energy saving potential of the radiant wall coupled to a GSHP.

Another comparison was carried out by Schibuola et al. [52] in Venice. Using the lagoon water a heat source, a GSHP system was compared with an ASHP, a condensing boiler and an air-cooled chiller in both the cooling and the heating modes. It was proved the major efficiency of the GSHP.

Dikic et al. [75] carried out a comparison between SAHP, GSHP and ASHP for space heating. Additionally, they studied also different combined systems, such as ground source SAHP, air source SAHP and air-ground dual source HP. All tests were carried out in a test room under dynamic conditions in the east region of Turkey. The COP of the SAHP was the highest for single source systems whereas the ground source SAHP

system was the highest for double source systems. COP values for multiple source systems were higher than for the single source systems. Exergetic analysis was also carried out favoring in this case single source systems, especially GSHP system.

Dai et al. [76] study experimentally the heating performance of a ground source SAHP during the coldest month in China. On the other hand, Verma et al. [77] carried out the study of a ground source SAHP from December to January in India. Both studies concluded that the performance of a GSHP system increased when it is assisted with solar energy, especially when DHW is demanded during the night due to the storage capacity of the tanks.

1.4 Vapor compression cycles modeling

Systems modeling is the representation of a real behavior by means of applying physical laws, empirical regressions and/or correlations. Now, it will be firstly introduced to the different approaches that can be followed for modeling VCC. Secondly, VCC physics-based dynamic models that can be found along the literature will be presented. Finally, models of VCC components will be revised.

1.4.1 Different approaches for VCC modeling

Steady VS dynamic models

Steady models have been widely used in the industry, becoming a commonly required practice for VCC design [78]. Nevertheless, steady models assumes as constants the variables that interact in the model without taking into account the variability of them over time. Dynamic models take into account those variations representing and predicting the behavior of the system over the time. In Figure 1.18 can be seen the graphic definition of both approaches.

It is accepted by the modeling community that dynamic system operation can be approximated by series of quasi steady-state operation conditions taking a reduced time-step in comparison with the simulation time [79]. However, this assumption cannot be accepted for any situation. For instance, if the aim of the model is to simulate the

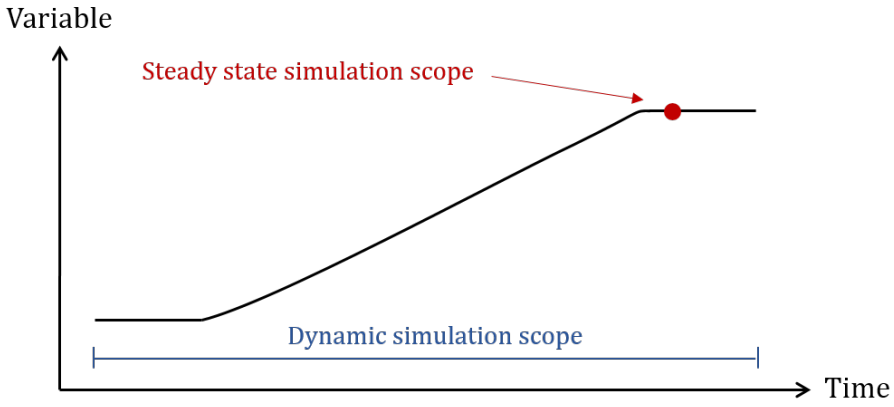

Figure 1.18: Graphic definition of steady and dynamic state.

dynamic control of a system, it cannot be done by approximation due to the suddenness and high speed of the transient-state. For those situations, dynamic simulations must be performed.

Regarding HVAC models, many authors have developed steady models. Most of them with the objective of calculate the energy performance of a system for a given operation conditions. For instance, Underwood et al. [80] developed a parametric steady model for an ASHP that can be parameterized and fitted either from field, laboratory or manufacturers data. Tran et al. [81] used regressions from tests data to predict the COP of an ASHPWH. Kinab et al. [82] developed a model to calculate the performance of a reversible HP by modeling and simulating separately the components of the system using physic equations and approaches.

In fact, there exist different widely used software developed to simulate the behavior of HVAC systems under steady-state conditions, such as DOE/ORNL [83] developed by Oak Ridge National Laboratory (ORNL), CYCLE_D-HX [84] developed by the National Institute of Standards and Technology (NIST), IMST-ART [85] by the IMST research group from the Technical University of Valencia and VapCyc [86] by Center of Environmental Energy Engineering from University of Maryland.

However, steady models are not able to predict transient-states. This limit its utility in fields like control systems, fails prediction or systems design. For that purposes, dynamic models are needed.

On the other hand, SPF is a term needed to calculate the amount of captured energy to be considered as renewable energy. It is commonly calculated by long-term real field measurements [29], which requires an important monetary investment. Never-

theless, it can be calculated by data obtained with a validated dynamic model without the necessity of develop long-term tests.

Tests-based VS physics-based models

In tests-based models, also known as data-based, black box or lumped parameters models, the unknown variables at each step-time are calculated by means of empirical correlations and regressions fitted to experimental data using maths and statistics. Those equations had been previously created using data obtained from laboratory or field tests. This kind of models are used to predict with high accuracy the behavior of a given system under given steady conditions [87, 88]. Additionally, they can be utilized also to predict dynamic behavior [89]. Nevertheless, this kind of models only can be used to predict the behavior of the system that have been previously tested. If any component of the system is altered, the model would no longer be valid. Therefore, the versatility of tests-based models is low.

On the other hand, physics-based models use physical laws to simulate the behavior of the system, providing great accuracy and the opportunity to simulate different components and configurations. Underwood [90] reviewed GSHP simulations, comparing models based on transfer functions and physics-based models, emphasizing the accuracy of the latter. Similarly, Rasmussen [91] compared physics-based and data-based models, highlighting the versatility of the former.

However, the complexity of developing and implementing physics-based models is greater than test-based models. Therefore, test-based models could be more appropriate for some fields, such as performance studies of a given system in different locations. Additionally, the computational load of a physics-based model is also greater than a test-based one.

Micro-scale VS macro-scale models

Depending on the purpose of the model, it can be approached from two different points of views: macro-scale and micro-scale. On the one hand, the purpose of simulations carried out by macro-scale models is to get a general view of the system behavior, over hours, days or months, in order to predict the seasonal performance of a given system.

The performance during transient-states, such as start-up, shut-down and working

mode switches are not taken into account in macro-scale models. It would increase the model complexity and computational time while the results would hardly vary due to the negligible time of those transient-states in comparison with the total simulation time.

On the other hand, micro-scale models focus on the behavior of the system during short time periods in which aggressive transient-states are given. Seconds-based time scales are usually used in order to understand the physical behavior of systems under fast transitory states.

1.4.2 VCC systems physics-based dynamic models

Micro-scale models

Regarding physics-based micro-scale dynamic models to simulate VCC systems, one of the most known tool is the commercial software Thermosys [92], which is able to carry out dynamic simulations of different vapor compression systems [93][79]. This software works in Matlab/Simulink environment [94] and was developed by the Alleyne Research Group of the University of Illinois at Urbana-Champaign. Different components can be used to simulate different VCCs. For instance, non-reversible air source refrigeration systems can be simulated with this software [95]. Additionally, Li et al [96], based on Thermosys software, developed a dynamic model of a cooling vapor compression cycle with which the shut-down and start-up operations were analyzed.

In Modelica environment [97] different component libraries have been developed to simulate the dynamic behavior of VCC systems. TIL Suite [98] and ThermoCycle [99] are the most known ones. For instance, a transient modeling of a flash tank vapor injection HP was developed by Qiao et al. [100, 101] using Modelica environment to capture the transient heat transfer and flow phenomena. Similarly, Qiao et al. [102] presented a dynamic heat exchanger and frost growth model to account for the non-uniform frost formation during winter operation of a vapor injection HP.

Koury et al. [103] also presented a physics-based dynamic model of a low cost ASHP for residential water heating and validated it experimentally. As said before, one of the most usefulness of micro-scale models are the capability of simulate and predict fast transient-states of systems. Regarding HPs, the most common fast transient-states are

the produced by the start-ups and shut-downs of the systems and by the working mode switching.

For instance, start-ups and shut-downs cycles of a VCC were simulated and analyzed by Li et al. [96], Lee et al. [104], Hermes et al. [105], Andrade et al. [106] and Jeong et al. [107].

Working mode switching are very common in HPs due to its capability to reverse the cycle thanks to the 4WV. As explained before, it can be given for two main reasons: supply punctual heating or cooling demand and to carry out defrosting cycles.

Concerning reverse-cycle dynamic modeling, Qiao et al. [108] presented a model in Modelica of an ASHP system to analyze its transient characteristics during the defrosting cycle. A physics-based model of the frost formation and melting is detailed and developed. The models used to simulate the behavior of the HP components were validated in [100, 102]. Both frost formation and melting models, as well as the simulation during the defrosting cycle, were not compared with experimental tests.

Macro-scale models

Dynamic macro-scale models of different HVAC systems have been studied over the last few years. However, there are not many studies carried out with physics-based models. Calise et al. [109] developed a dynamic model of three different layouts of solar heating and cooling systems and analyzed the daily transient energy performance. Specifically, dynamic macro-models of HPs can be found in the recent bibliography. Buonomano et al. [110] analyzed the system's power consumption, operation costs and environmental impact of a water loop HP in hourly, daily and seasonal scales. The performance factor of a dual-source HP was seasonally and annually analyzed by Grossi et al. [111]. Furthermore, the HP included in a polygeneration system was dynamically simulated by Calise et al. [112]. The electric, thermal and economic analysis was presented on a daily, weekly and yearly basis.

1.4.3 VCC components dynamic physics-based models

When modeling dynamic systems such as VCC systems, it must bear in mind that not all the components of the system have equal dynamics. In fact, when modeling a dy-

namic system, usually the dynamics of the model are governed by the components with slowest dynamics.

For instance, in the case of HPs, the heat exchangers have slower dynamics than the components that regulate the Mass Flow Rate (MFR), such as compressors or valves [113, 114]. This causes that the challenge when modeling HPs relies in modeling slow dynamic components such as heat exchangers.

Heat exchangers modeling

For HEX physics-based models, different modeling and resolution methods can be found. Among others, two of the most commonly used methods are the Moving Boundary (MB) [115] and Finite Control Volume (FCV) [116]. While FCV divides the total length of the HEX into a finite number of volumes of equal size, the MB method divides it into a reduced number of unequal finite volumes of variable size. The sizes of those finite volumes varies along the simulation and depends on a chosen property, such as mean void fraction [117]. Garcia et al. [118] summarized the references in which transient models of heat exchangers for refrigeration systems appeared.

Regarding modeling methods, some comparisons between both methods have been presented over the last few years. Bendapudi et al. [119] compared them in a shell-and-tube heat exchanger of a centrifugal chiller system. The results were compared with experimental data and it was concluded that, during steady-states, MB was faster reaching equal accuracy. Nevertheless, during transient-states, the FCV formulation was found to be more robust. Pangborn et al. [120] made a comparison between modeling an air-to-liquid HEX with both FCV and MB methods, concluding that the computational time of MB was lower than that of FCV, maintaining a good order of accuracy in both cases. Desideri et al. [121] compared MB and FCV methods in a Plate Heat Exchanger (PHEX) concluding the similar good grade of accuracy of both methods and highlighting the lower computational time of the MB approach. Similar conclusions were were reached by Bonilla et al. [122] simulating an evaporator of a direct solar steam facility.

On the other hand, Rodriguez et al. [123] compared four different dynamic modeling paradigms for an air-to-refrigerant evaporator. It was compared FCV method with three MB methods: enthalpy, void fraction and density based MB. They highlighted the advantages of the FCV method due to the no need of switching triggers, thresholds

or tolerances to reach accurate results. However the asserted that it is done at the expenses of a higher computational time.

The MB methods has been widely used in air-to-liquid HEX dynamic modeling, as described in [91, 124, 125]. For instance, Ibrahim et al. [51] used it to predict the energy performance of an ASHPWH and Bonilla et al. [122] used for the simulations of condensers and evaporators of a solar-thermal power plant. McKinley et al. [126] developed a nonlinear switched MB model to simulate air-to-liquid HEXs.

Regarding refrigerant-to-liquid HEX, Sangi et al. [127] used a combined MB and discretized methods to carry out simulations of GSHPs in Modelica and Li et al. [128] to model the condensers and evaporators of an underwater system. The use of MB method makes it difficult to develop a liquid-to-refrigerant HEX with counter-flow configuration. For instance, Bell et al. [129] developed an MB model for counter-flow HEX, but was only able to predict stationary states. Chu et al. [130] were able to model a counter-flow PHEX but they had to use a MB-FCV coupling algorithm.

In FCV models, Ozana et al. [131] implemented a dynamic model of a steam superheater HEX of an industrial boiler using the FCV method. It was validated for both parallel and counter-flow connections. Nevertheless, it was not necessary to model the phase change of the fluids. Bendapudi et al. [132] developed a centrifugal chiller system model using the FCV method for the shell-and-tube heat exchanger, focusing on aspects like mesh dependence, integrator order and step-size. It was concluded that an increase in the number of finite control volumes increases the simulation accuracy up to a limit. Srihari et al. [133] analyzed the effect of the maldistribution of the flow into the PHEX channels for single-phase fluids using a FCV model. Moreover, the transient performance of the air side of an air-to-water HP under frosting conditions was analyzed using a dynamic FCV model by Gao et al. [134].

Compressors modeling

The most widely used compressors in VCC systems are the scroll and reciprocating compressors. Along years, many numerical studies have been carried out regarding the modeling of both scroll and reciprocating compressors. The complexity of those models depends, among others, in their purpose. Complex models are usually used to compressors design issues. For instance, Link et al. [135] developed a model to predict the start-ups and shut-downs transients of reciprocating compressors. A literature

review about the recent publications of refrigerant scroll compressors modeling was written by Byrne et al. [47]. In there, many geometrical, empirical and semi-empirical models can be found.

Nevertheless, when the compressor is modeled inside a more complex system such as a VCC, rarely complex geometrical models are utilized to describe the behavior of the compressor. It would lead in a more complex model that would hardly improve the model accuracy due to the uncertainties and assumptions that are involved in the system. In this cases, simple models are utilized to describe compressors behavior [51, 95, 118].

Moreover, it must be take into account that, as said before, the dynamics of the compressor are much faster than the HEX ones. Therefore, compressor can be simulate as and static component inside a dynamic model if the HEXs are modeled dynamically [51, 124, 136]. Nevertheless, some authors have applied time variables to the static modeling approach transforming the static compressor model into a quasi-static model [95, 137].

Expansion devices modeling

Inside VCC systems, different expansion devices can be found, such as Thermostatic Expansion Valve (TXV), Electronic Expansion Valve (EEV) and capillary tubes [138]. Nowadays, the main expansion device of the refrigerant cycle usually is an EEV due to its fast regulation capacity and precise control [139, 140].

Regarding valves modeling, in the literature can be found high accuracy models of expansion valves. For example, Cao et al. [141] develop a neural network model to model the refrigerant flow thorough an electronic expansion valve and Ndiaye et al. [142] modeled the bleed port of a thermostatic expansion valve.

However, similarly to compressor models, in systems like VCC the dynamics and inertial effects of the valves are usually neglected and they are statically modeled [95, 114, 136].

Chapter 2

MOTIVATION & GOALS

During this chapter, firstly the project motivation will be described. Then, the main goals of the thesis and the contributions to both scientific community and HVAC industry will be presented. Finally, the structure of the thesis document will be explained.

2.1 Project motivation

The energetic problem is an issue that concerns all entire world. Heating and cooling in buildings accounts for around the 80% of total final energy use, of which the 75% is still generated from fossil fuels and only 19% from renewable energy [18]. In this context, Heat Pump systems are one of the most promising technologies to reduce fossil energy consumption for heating and cooling in buildings [143]. Additionally, newer and more efficient heat pump technology would improve the energy sustainability of the building in which it is used.

In order to develop new HPs, there are two important aspects. The improvement of the components and the improvement of the joint system. The components would improve by optimizing geometrical parameters and materials, between others. In the joint system, the main goal is to improve the control loop of the system. Nowadays, the best way to address these aspects is by the dynamic modeling of the components and systems that could simulate accurately their behavior.

These dynamic models should fulfill the following requirements:

- Full dynamic model.
- Capability to carry out heating, cooling and DHW production modes simulations.
- Capability to simulate micro-scale transient simulations. Understanding as micro-scale the time scale at which fast transient-states are produced. For instance, operation conditions changes, working mode switches or system start-ups.
- Capability to simulate macro-scale dynamic simulations. Understanding as macro-scale the time scale at which the dynamic of the system is studied during long time periods. With it, the performance of the system is obtained, such as COP, Energy Efficiency Ratio (EER) or SPF.
- Possibility to use different components to create a system.
- Possibility to change physical specifications of the components and the working fluids.

In this thesis, it will be described the development and validation of a reversible liquid-to-liquid HP model capable to carry out micro- and macro-scale simulations.

There exist different modeling environments in which systems dynamic models can be developed and simulated, such as AMESim [144], Modelica [97] or Matlab/Simulink [94]. For this thesis it was chosen to use Matlab/Simulink environment for the following reasons:

- Many HVAC systems manufacturers develop and test their control loops with Simulink.
- It is one of the most used programming and modeling environment in the HVAC engineering. Therefore, is common to find Matlab/Simulink software already installed in engineering companies.
- The high optimized capability of interaction between the drag and drop modeling Simulink environment and the numerical computing Matlab environment.

However, there are also some drawbacks when using Matlab/Simulink environment to model physic facilities. For instance, the signals in Simulink are unidirectional and the direction is set before the simulations.

Regarding the different modeling approaches described in Section 1.4.1, the model will be developed as a physics-based dynamic model that will be able to simulate both micro- and macro-scales simulations. It would give the possibilities of predict both fast transient situations, such as working mode switches, and long time situations, such as monthly system performance.

Additionally, PHEX model will be developed using FCV method. The main reason of chosen this method is the versatility that offers it to simulate different HEXs configurations and types. For instance, by using FCV method, during this thesis it will be presented a model that simulates the dynamic behavior of a refrigerant-to-liquid PHEX that can work indistinctly in counter- or parallel-flow and both as a condenser and as an evaporator.

Now, goals, contributions and structure of the thesis will be described.

2.2 Goals

The main goals of this thesis are the followings:

1. **To develop a physics-based dynamic model to simulate reversible liquid-to-liquid HPs.** The model must be able to simulate the dynamic behavior of a reversible liquid-to-liquid heHP under different situations and configurations.

2. **To validate the developed model under fast transient situations.** One of the requirements of the model is to simulate the behavior of the system during transient simulations in a micro-scale of time such as drastic change in operation conditions, start-up situations or working mode switches. Therefore, the model must be validated under micro-scale situations.

3. **To carry out dynamic simulations during a working mode switch.** In order to prove the validity of the model to simulate reversible HPs, working mode switches from the heating mode to the cooling mode and vice-versa must be achieved.

4. **To validate the model under large time scale situations.** The last requirement of the model it to carry out simulations under macro-scale situations. Therefore, simulation results must be validated against large time scale experimental tests.

5. **Flexible model.** The developed model must be flexible to simulate HPs of different sizes and configurations, allowing the user to change the specifications fo the used components.

Additionally, to reach those main goals, some specific objectives must be achieved.

- To elaborate a comprehensive analysis of the state of the art in the field where the study is focused: reversible HPs operation, experimental test with HPs, mathematical dynamic models of HPs and dynamic characterization of HPs.
- To develop the mathematical model of each component of the system separately.
- To look for the appropriate simulation environment and become familiar with the implementation of the dynamic models in it.
- To joint the different components together.
- To design a test methodology to validate the model under different dynamic situations.
- To carry out the data reduction, synchronization and treatment of experimental test measurements.

2.3 Contributions

The contributions of this thesis can be separated into two groups. The first one is the contributions to the scientific community. The other one includes HVAC industry and more specifically HPs manufacturers. Some contributions are horizontal to both groups.

Contributions to scientific community

- A detailed overview about residential HPs is presented. It is reviewed the European legislation and global agreements regarding HPs, which supports a greater use of HPs for production of DHW, space heating and space cooling. The basic principles of operation and the different types of residential HPs that can be found in the market are explained. Additionally, the different field and laboratory experimental tests that have been carried out within last years are presented.
- Different approaches to carry out VCC mathematical models are presented. A review of the scientific community advances in VCC physics-based models are presented, focusing in the PHEXs mathematical dynamic modeling.
- A model that can predict the dynamic behavior of a HP during both fast transient-states and slow dynamic situations is developed.
- A dynamic HP model to simulate working mode switches is developed.
- A model that can simulate the behavior of a PHEX working both as a condenser or as an evaporator is developed. Moreover, the same model can work under different configurations of the PHEX, such as counter-flow and parallel-flow connections.
- An uncommon thermal facilities test methodology is presented.

Contribution to HVAC industry

- The developed model is able to simulate accurately HP systems varying the specifications of the used components such as geometrical characteristics, configurations and working fluids. It is useful to simulate the behavior of new systems

or components during the design stages.

- Validated components or systems can be saved and libraries can be created. Thus, new systems configurations or different operation conditions can be simulated.
- As the model is implemented in Matlab/Simulink, the developed control loops of the manufacturers can be implemented in the model.
- With the same model, both micro-scale and macro-scale simulations can be carried out. It allows the user to predict the behavior of the system both for fast transient situations, such as start-ups, and for long time operations to study the system performance.

2.4 Document structure

The thesis is divided in six independent chapters. However, in many cases along the document are found references to other chapters or sections of the document.

Chapter 1 includes the introduction to the thesis presenting an exhaustive state of the art about residential HPs and the advances on its modeling. Firstly, a general energy background is presented. In it, the main global energy problems, heating and cooling handicaps in buildings and the latest energy policies are presented. Then, a brief description of HPs operation principles, types of HPs and their role in the energy transition is depicted. Additionally, different tests with HPs conducted by the community are described. Finally, the advances in mathematical modeling of VCC and its components are reviewed. In **Chapter 2**, the objectives of this thesis and the contributions to both scientific community and HVAC industry are presented.

In **Chapter 3**, the model development is presented. Equations to characterize each of the system component are presented and transformed in order to implement them in Matlab/Simulink. The model block of each component is presented, explaining them individually and collectively. Finally, apart from the implemented equations, the complementary information that is needed to carry out simulations are defined and explained.

The model is used for micro-scale validations and simulations in **Chapter 4**. Firstly, the used test facility and followed methodology to carry out tests for micro-scale validation

are presented. Different transient situations are tested by varying the operation conditions and the working mode of the system. Then, the validation during the heating mode, the cooling mode and the system start-up is showed. Finally, a switching mode simulation is presented, explaining the considerations for carrying out the simulation and discussing the obtained results.

Chapter 5 presents the utilization of the model for macro-scale simulations. Firstly, the test rig and the carried out tests are explained. in this case, the difference between tests is the demanded cooling load and therefore, the ON/OFF time ratio. With those tests, the validation of the model in macro-scale situations is given. Then, it is compared the system performance during tests and simulations.

Finally, in **Chapter 6**, the scientific works that have been produced during the development of this thesis, the conclusions that can be drawn from this research and the proposed working lines that can be followed are presented.

Apart from the main chapters, the document includes some annexes where additional information is given. In **Annex I**, some images about the interior of the component model subsystems are shown. Then, in **Annex II**, the code written in the "S-funtions" is given. In it, the FCV equations to simulate the dynamic behavior of PHEXs are implemented. As said before, in Chapter 4 the validation in micro-scale is presented. However, in it, only some representative comparisons between test data and simulation results are presented. Thus, **Annex III** collects the remaining carried out comparisons. Similarly, in **Annex IV** are collected the comparisons in macro-scale that are not shown in Chapter 5.

Chapter 3

HEAT PUMP SYSTEM MODEL

During this chapter, the model to simulate the behavior of liquid-to-liquid heat pump systems will be presented. It is firstly presented the governing equations that simulates the dynamic behavior of the system and the modifications of the equations that are needed to implement them in the simulation environment. The implementation in matrix mode of the PHEX equations is also explained. Then, the interface of the model with a specific explanation of each component in given. Finally, in addition to the equations, the complementary information and data that is needed to carry out the simulations is presented and explained.

3.1 Introduction

As said during the introductory chapter, the model is able to simulate liquid-to-liquid HP systems under different circumstances such as water cooling, water heating, working mode switches, start-ups and shut-downs situations.

The model is entirely developed in Matlab/Simulink environment implementing physic equations and using the FCV method. Differently from the models that are usually found in bibliography for HPs simulations, this model does not use any experimental correlations nor regressions to carry out the simulations with the exceptions of the empirical correlations that will be later presented to calculate the Heat Transfer Coefficient (HTC) of the fluids inside the PHEXs. The model is developed with physic equations and components data provided by manufacturers.

Additionally, the PHEXs model simulates the behavior of a PHEXs indistinctly if it is working as a condenser or as an evaporator. Moreover, it simulates both counter-flow and parallel-flow connections.

There exist two kind of components in VCC systems. Some of them are responsible of regulating the MFR, such as compressors and valves, while others regulate the high and low working pressures, such as HEXs. The dynamics of the PHEXs are much slower than the dynamics of the compressor and the valve. Thus, the dynamics of the system is assumed to be dominated by the dynamics of the heat exchangers. Therefore, ir order to simplify the model, the compressor and the valve are modeled as static components.

For models of those components that regulate refrigerant MFR, inlet and outlet refrigerant pressures must be known. Otherwise, for components that regulate the refrigerant pressure, the inlet and outlet refrigerant MFRs must be known.

During this chapter, the implemented governing equations to simulate the behavior of the different components of the HP such as the compressor, the EEV, and PHEXs will be firtly presented and transformed until reach the equations that can be implemented in the chosen modeling environment.

Once the equations have been obtained, it will be explained the methodology to implement the dynamic equations of the PHEXs using the FCV method for a N number of FCV. Then, an example of a three finite volumes PHEX will be presented both for counter-flow and parallel-flow connections.

3.2 Governing equations

Now, the equations that model the behavior of the different components of a basic liquid-to-liquid HP will be presented.

It is assumed that each component of the system is thermally insulated from the surroundings, taken them as adiabatic systems. Therefore, there will not be heat losses or gains to/from the ambient air.

On the other hand, pressure losses between components (inside pipes) are negligible. Consequently, it will be assumed two pressure levels: high-pressure and low-pressure.

Moreover, regarding pipes, since pressure losses are negligible and heat transfer to/-from surroundings is null, the refrigerant energy at the outlet of one component will be equal to the refrigerant energy at the inlet of the next component. Therefore, pipes will not be modeled. Outlet properties will be directly sent to the inlet port of the corresponding component.

Neglecting pipes modeling is widely used in HVAC systems modeling [51, 90, 145]. Similarly, taken assumptions can be easily find along the literature [100, 114, 146]

3.2.1 Compressor

As said before, compressor is statically modeled. Both refrigerant MFR and outlet enthalpy are calculated by means of algebraic equations. Equation (3.1) and (3.2) are used to calculate the refrigerant MFR and the outlet enthalpy respectively.

$$\dot{m}_{comp} = \rho_{in} \cdot V_{comp} \cdot \eta_{vol} \tag{3.1}$$

$$h_{out,comp} = h_{in} + \frac{1}{\eta_{isen}}(h_{out,isen} - h_{in}) \tag{3.2}$$

The compressor power is calculated with an energy balance assuming an adiabatic compression.

$$W_{comp} = \dot{m}_{comp} \cdot (h_{out} - h_{in}) \tag{3.3}$$

While the irreversibilities inside the compressor are measured with the isentropic efficiency, the friction and mechanical losses are given by the volumetric efficiency.

3.2.2 Electronic expansion valve

The EEV model calculates the refrigerant mass flow as a consequence of the current valve position and cycle pressures. The EEV is modeled statically and it is assumed to have an isenthalpic thermodynamic behavior. The mass flow regulation is described by the relationship presented in Equation (3.4).

$$\dot{m}_{valve} = C_v \cdot \sqrt{\Delta P \cdot \rho_{in}} \tag{3.4}$$

The valve coefficient (C_v) depends on the EEV type and can be determined experimentally.

3.2.3 Four ways valve

The 4WV is the component that allows the reversibility of the system. By switching the inlet and outlet ports of the valve, the system can switch from the cooling working mode to the heating working mode and vice versa. Nevertheless, the reversibility is internally given by switching the inlet signals to the components. It will be detailed explained in Section 4.7.

On the other hand, it is known that losses are given inside 4WVs, such as pressure drops, heat losses and fluid leakages from high-pressure to low-pressure side [147]. However, through experimental tests it was observed that this losses are chaotic, random and hard to predict.

Therefore, taking into account the randomness of these phenomenon and that in the model it is not needed such valve to allow the system reversibility, the 4WV model is not modeled.

3.2.4 Plate heat exchanger

Unlike the compressor and EEV, PHEX are modeled dynamically, using partial differential equations to model the behavior of the refrigerant fluid, secondary fluids and intermediate plates. At the time of modeling the behavior of the PHEX, some assump-

tions have been taken into account. This assumptions are widely used for HVAC systems dynamic modeling [113, 114, 120, 121, 136].

- Pressure drops through the PHEX will be neglected. Although there exist pressure drops, they can be neglected since are usually lower than $20kPa$ [148, 149]. Moreover, at the time of validate the model, those values can be lower than the inherit error of the used measurement device. Taken them into account would lead in a more complex model and the accuracy ot results would not improve.
- The maldistribution of the refrigerant mass flow is neglected, so it is supposed that it is uniformly distributed in the different channels of the PHEX.
- Axial thermal energy conduction is negligible.
- It is supposed that the heat exchangers are totally insulated from the surroundings.
- Fluid flow through PHEX is modeled as one-dimensional.
- For the calculation of the heat transfer rate, the PHEX are reduced to two channels and one plate heat exchanger. Nevertheless, once the heat transfer rate is calculated, it is multiplied by two to take into account the fact that each channel is confined between two plates.
- The FCV method is adopted to carry out the calculations.
- It is supposed that the density and velocity of the secondary fluid remain constant along all the PHEX.

Refrigerant equations

The refrigerant fluid is the fluid that undergoes a phase change when it circulates through the PHEX. It can be condensed going from superheated gas to subcooled liquid or evaporated going from two-phase fluid to superheated gas. Additionally, it can go out from the PHEX as a two-phase fluid if the transferred heat between fluids is insufficient to conclude the condensation or evaporation processes.

During transient-states, properties of the refrigerant fluid change with time and along PHEX, with the exception of pressure, which do not change along PHEX. In order to model the changes of the fluid properties, energy and mass conservation equations

are applied to the refrigerant fluid. Momentum conservation equation is not applied due to, as said before, the pressure drop through the PHEX is negligible.

Refrigerant mass: Equation 3.5 presents the mass conservation equation for the refrigerant fluid. Nevertheless, this equation is not suitable for being implemented in a simulation code, so it must be transformed. Equations transformation is similar to the followed by Rasmussen [114] for a single-phase heat exchanger. Firstly, each term is integrated along the length of the heat exchanger. Then, each term of Equation 3.6 is transformed separately.

$$\frac{\partial(\rho_{_R} A_c)}{\partial t} + \frac{\partial(\dot{m}_{_R})}{\partial x} = 0 \tag{3.5}$$

$$\int_0^x \frac{\partial(\rho_{_R} A_c)}{\partial t} dx + \int_0^x \frac{\partial(\dot{m}_{_R})}{\partial x} dx = 0 \tag{3.6}$$

Regarding the first term of the equation, extracting the cross-sectional area from the integrator and applying the Leibniz integral rule [150], Equation 3.7 is obtained.

$$\int_0^x \frac{\partial(\rho_{_R} A_c)}{\partial t} dx = A_c \left[\frac{d}{dt} \int_0^x \rho_{_R} dx \right] \tag{3.7}$$

Then, the integral equation is solved (Equation 3.8).

$$A_c \left[\frac{d}{dt} \int_0^x \rho_{_R} dx \right] = V \dot{\rho}_{_R} \tag{3.8}$$

Finally, enthalpy and pressure are taken as independent variables for calculating the density time derivative, reaching Equation 3.9.

$$V \dot{\rho}_{_R} = V \left[\left(\left| \frac{\partial \rho}{\partial P} \right|_h \dot{P}_R \right) + \left(\left| \frac{\partial \rho}{\partial h} \right|_P \dot{h}_R \right) \right] \tag{3.9}$$

The second term is transformed by solving the integral and Equation 3.10 is gotten.

$$\int_0^x \frac{\partial(\dot{m}_{_R})}{\partial x} dx = \dot{m}_{_{R,\,out}} - \dot{m}_{_{R,\,in}} \tag{3.10}$$

Substituting the terms of the Equation (3.6) and reordering them, Equation (3.11) is obtained.

$$V\left[\left(\left|\frac{\partial\rho}{\partial P}\right|_h \dot{P}_R\right) + \left(\left|\frac{\partial\rho}{\partial h}\right|_P \dot{h}_R\right)\right] + \dot{m}_{R,\,out} - m\dot{m}_{R,\,in} = 0 \tag{3.11}$$

where $\left|\frac{\partial\rho}{\partial P}\right|_h$ represents the refrigerant density variation with respect to the pressure variation at constant enthalpy and $\left|\frac{\partial\rho}{\partial h}\right|_P$ represents the refrigerant density variation with respect to the enthalpy variation at constant pressure [151].

The mass conservation equation applied to the refrigerant fluid is now in function of the pressure and enthalpy time derivatives.

Refrigerant energy: Equation 3.12 presents the energy conservation equation applied to the refrigerant fluid. It must be transformed following similar steps than for the refrigerant mass. Firstly, $cT = h$ equality is applied, getting Equation 3.13. This is because during the refrigerant phase changes, pressure and temperature are dependent properties. Therefore, the calculations are simplified if the independent variables to calculate the rest of the properties of the refrigerant fluid are the enthalpy (h) and the pressure (P).

$$\frac{\partial(\rho_R A_c c_R T_R)}{\partial t} - \frac{\partial(A_c P_R)}{\partial t} + \frac{\partial(m_R c_R T_R)}{\partial x} = \alpha_R L(T_R - T_W) \tag{3.12}$$

$$\frac{\partial(\rho_R A_c h_R)}{\partial t} - \frac{\partial(A_c P_R)}{\partial t} + \frac{\partial(m_R h_R)}{\partial x} = \alpha_R L(T_R - T_W) \tag{3.13}$$

Then, each term of Equation 3.13 is integrated along the length of the heat exchanger resulting in Equation 3.14 Now, spatial dependency can be removed.

$$\int_0^x \frac{\partial(\rho_R A_c h_R)}{\partial t}dx - \int_0^x \frac{\partial(A_c P_R)}{\partial t}dx + \int_0^x \frac{\partial(m_R h_R)}{\partial x}dx = \int_0^x \alpha_R L(T_R - T_W)dx \tag{3.14}$$

Regarding the first term of the equation, extracting the cross-sectional area from the integrator and applying the Leibniz integral rule, Equation 3.15 is obtained.

$$\int_0^x \frac{\partial(\rho_R A_c h_R)}{\partial t}dx = A_c\left[\frac{d}{dt}\int_0^x (\rho_R h_R)dx\right] \tag{3.15}$$

Then, solving and assuming average properties inside the PHEX, Equation 3.16 is obtained.

$$A_c\left[\frac{d}{dt}\int_0^x(\rho_R h_R)dx\right] = V(\dot{\rho}_R h_{R,ave} + \dot{h}_R \rho_{R,ave}) \tag{3.16}$$

Enthalpy and pressure are taken as independent variables for calculating the density time derivative. Assuming that, Equation 3.17 is reached.

$$V(\dot{\rho}_R h_{R,ave} + \dot{h}_R \rho_{R,ave}) = V\left[\left[\left(\left|\frac{\partial\rho}{\partial P}\right|_h \dot{P}_R\right) + \left(\left|\frac{\partial\rho}{\partial h}\right|_P \dot{h}_R\right)\right] h_{R,ave} + \dot{h}_R \rho_{R,ave}\right] \tag{3.17}$$

Second term is transformed by extracting the cross-sectional area from the integral and integrating the time derivative of the pressure, which results in Equation 3.18.

$$\int_0^x \frac{\partial(A_c P_R)}{\partial t}dx = V\dot{P}_R \tag{3.18}$$

Integrating the third term, Equation 3.19 is obtained.

$$\int_0^x \frac{\partial(\dot{m}_R h_R)}{\partial x}dx = \dot{m}_{R,out} h_{R,out} - \dot{m}_{R,in} h_{R,in} \tag{3.19}$$

Integrating the right side of the Equation 3.14, Equation 3.20 is reached.

$$\int_0^x \alpha_R L(T_R - T_W)dx = \alpha_R A_s(T_R - T_W) \tag{3.20}$$

Finally, joining all the transformed terms together (Equation 3.17 - 3.20) and reordering them, Equation 3.21 is obtained.

$$\begin{aligned}\left(\left|\frac{\partial\rho}{\partial P}\right|_h h_{R,ave} - 1\right)V\dot{P}_R + \left(\left|\frac{\partial\rho}{\partial h}\right|_P h_{R,ave} + \rho_{R,ave}\right)V\dot{h}_R + \\ \dot{m}_{R,out} h_{R,out} - \dot{m}_{R,in} h_{R,in} = \alpha_R A_s(T_R - T_W)\end{aligned} \tag{3.21}$$

Now, the energy conservation equation applied to the refrigerant fluid has been modified in order to be implemented in a simulation code. It is in function of the pressure and enthalpy time derivatives so the phase change of the fluid can be taken into account and simulated.

Secondary fluids equations

The velocity and the density of the secondary fluid, generally water or a mixture of water and Ethylene-Glycol, is assumed to be constant along all the heat exchanger. This leads to not needing to apply the equation of the mass conservation for the secondary fluid.

Equation 3.22 presents the energy conservation equation for secondary fluid. Differently from refrigerant fluid, the secondary fluid will remain in liquid-phase along all the PHEX. Therefore, it can be directly calculated the temperature variation instead of enthalpy variation.

Since the secondary fluid is assumed as incompressible fluid, the variation of the pressure is neglected. Therefore, the partial derivative of the pressure with respect of time does not appear in Equation 3.22.

$$\frac{\partial(\rho_S A_c c_S T_S)}{\partial t} + \frac{\partial(m_S c_S T_S)}{\partial x} = \alpha_S L(T_W - T_S) \tag{3.22}$$

The following steps carried out to transform the equation in order to be suitable for being implemented in a simulation code are similar to the previously followed for the refrigerant energy conservation equation.

Each term of Equation 3.22 is integrated along the length of the heat exchanger.

$$\int_0^x \frac{\partial(\rho_S A_c c_S T_S)}{\partial t} dx - \int_0^x \frac{\partial(m_S c_S T_S)}{\partial x} dx = \int_0^x \alpha_S L(T_W - T_S) dx \tag{3.23}$$

Transforming the first term of Equation 3.23 and assuming average properties, Equation 3.24 is obtained. Note that the density of the secondary fluid remains constant.

$$\int_0^x \frac{\partial(\rho_S A_c c_S T_S)}{\partial t} dx = V \rho_{S,\,ave} c_{S,\,ave} \dot{T}_S \tag{3.24}$$

Transforming second and the right terms of Equation 3.23, Equations 3.25 and 3.26 respectively are gotten.

$$\int_0^x \frac{\partial(\dot{m}_S c_S T_S)}{\partial x} dx = \dot{m}_S c_{S,\,ave}(T_{S,\,out} - T_{S,\,in}) \tag{3.25}$$

$$\int_0^x \alpha_S L(T_W - T_S) dx = \alpha_S A_{Ss}(T_W - T_S) \tag{3.26}$$

Finally, joining Equations 3.24 - 3.26, Equation 3.27 is obtained.

$$V\rho_{S,ave}c_{S,ave}\dot{T}_S + \dot{m}_S c_{S,ave}(T_{S,out} - T_{S,in}) = \alpha_S A_s(T_W - T_S) \tag{3.27}$$

By implementing the Equation 3.27 in a simulation code, the secondary fluid temperature variation with respect to time in a PHEX can be calculated.

Plates equations

The temperature variation of the intermediate plate is described by applying the energy conservation equation. It is presented in Equation 3.28 and no transformations are needed.

$$m_W c_W \dot{T}_W = \alpha_R A_s(T_R - T_W) - \alpha_S A_s(T_S - T_W) \tag{3.28}$$

The temperature of the plate depends on the mass and the thermal properties of the plate material and the heat transferred to or from both refrigerant and secondary fluids.

3.3 Heat exchanger model implementation

Once the equations have been transformed into temporal derivative equations, they are discretized into different FCVs. For an N number finite control volumes, 3.11, 3.21, 3.27 and 3.28 are transformed into Equations 3.29 - 3.32.

$$V_{cv}\left(\left|\frac{\partial\rho}{\partial P}\right|_h\right)_i \dot{P}_R + V_{cv}\left(\left|\frac{\partial\rho}{\partial h}\right|_P\right)_i \dot{h}_R + \dot{m}_{R,out,i} - \dot{m}_{R,in,i} = 0 \tag{3.29}$$

$$\begin{aligned} V_{cv}\left[\left(\left|\frac{\partial\rho}{\partial P}\right|_h\right)_i h_{R,i} - 1\right]\dot{P}_R + V_{cv}\left[\left(\left|\frac{\partial\rho}{\partial h}\right|_P\right)_i h_{R,i} + \rho_{R,i}\right]\dot{h}_{R,i} + \\ \dot{m}_{R,out,i}h_{R,out,i} - \dot{m}_{R,in,i}h_{R,in,i} = \alpha_{R,i}A_{s,cv}(T_{R,i} - T_{W,i}) \end{aligned} \tag{3.30}$$

$$V_{cv}\rho_{S,i}c_{S,i}\dot{T}_{S,i} + \dot{m}_S c_{S,i}(T_{S,out,i} - T_{S,in,i}) = \alpha_{S,i}A_{s,i}(T_{W,i} - T_{S,i}) \tag{3.31}$$

$$m_{W,cv}c_W\dot{T}_{W,i} = \alpha_{R,i}A_{s,cv}(T_{R,i} - T_{W,i}) - \alpha_{S,i}A_{s,cv}(T_{S,i} - T_{W,i}) \tag{3.32}$$

Heat transfer rates between fluids and plates ($\dot{q}_i$) are defined in Equations 3.30, 3.31

and 3.32 as $\alpha_i A_{s,cv} \Delta T_i$.

This equations are now implemented in the chosen simulation environment, Matlab/Simulink [94]. Specifically, the model has been constructed in Simulink. This simulation tool of Matlab environment allows the user to build and design simulation blocks models by a drag and drop system. Additionally, Simulink is integrated in Matlab and data can be easily transferred from one to the other. Because of that, although the model has been built in Simulink, the governing equations of the PHEXs have been implemented in a Matlab code by means of a the Simulink block "S-function". This block allows to implement algorithms in Matlab code and then call to it from Simulink during the simulation of the model. Then, in order to implement the presented equations in a S-function, they are reorganized into a matrix equation.

$$\begin{bmatrix} V_{cv}\left[\left(\left|\frac{\partial\rho}{\partial P}\right|_h\right)_i h_{R,i} - 1\right] & V_{cv}\left[\left(\left|\frac{\partial\rho}{\partial h}\right|_P\right)_i h_{R,i} + \rho_{R,i}\right] & 0 & 0 \\ V_{cv}\left(\left|\frac{\partial\rho}{\partial P}\right|_h\right)_i & V_{cv}\left(\left|\frac{\partial\rho}{\partial h}\right|_P\right)_i & 0 & 0 \\ 0 & 0 & V_{cv}\rho_{S,i}c_{S,i} & 0 \\ 0 & 0 & 0 & m_{W,cv}c_W \end{bmatrix} \times \begin{bmatrix} \dot{P}_R \\ \dot{h}_{R,i} \\ \dot{T}_{S,i} \\ \dot{T}_{W,i} \end{bmatrix} = \begin{bmatrix} \dot{m}_{R,in,i}h_{R,in,i} - \dot{m}_{R,out,i}h_{R,out,i} + 2\dot{q}_{R,i} \\ \dot{m}_{R,in,i} - \dot{m}_{R,out,i} \\ -\dot{m}_S c_{S,i}(T_{S,out,i} - T_{S,in,i}) + 2\dot{q}_{S,i} \\ \dot{q}_{R,i} + \dot{q}_{S,i} \end{bmatrix} \tag{3.33}$$

Both heat transfer rates ($\dot{q}_R$ and $\dot{q}_S$) are multiplied by two because every refrigerant or secondary fluid are in contact with two intermediate plates, except for the boundary secondary fluid channels.

In order to solve Equation 3.33, the inlet and outlet MFRs of the refrigerant fluid must be known. When a steady-state is calculated, both are equal. Nevertheless, during a transient-state, expansion and compression devices regulate the refrigerant MFR and can be different. On the other hand, the inlet enthalpy of the refrigerant fluid and the inlet temperature and MFR of the secondary fluid must also be known.

As will be shown later, when Equation 3.33 is extended to an arbitrary number of control volumes and the refrigerant inlet and outlet MFRs are known, the intermediate

MFRs must be calculated at each time step. These intermediate refrigerant MFRs will be moved to the second term of the matrix equation, forming another state vector.

In the aggregate, for each time step, $4N$ derivative states and integrations must be solved, of which, the first corresponds to the pressure, from the second to N+1 to the refrigerant enthalpies, from N+2 to $2N$+1 to the secondary fluid temperatures, from $2N$+2 to $3N$+1 to the intermediate wall temperatures and from $3N$+2 to $4N$ to the refrigerant intermediate MFRs. Nevertheless, only the refrigerant energy and mass equations have to be solved together. The energy equation of plates and secondary fluid can be removed from the matrix and solved separately, thus the computational time is reduced.

On the other hand, at the time of applying the presented formulation to a fixed number of FCVs, counter-flow and parallel-flow connections must be differentiated. Figure 3.1 and Figure 3.2 show a graph description of a PHEX discretized in N number of FCVs for counter-flow and parallel-flow connections, respectively.

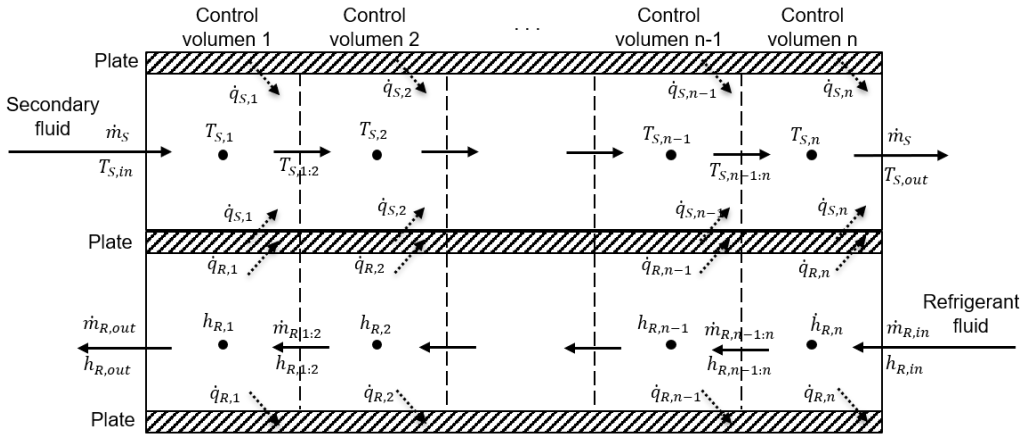

Figure 3.1: Finite control volume counter-flow PHEX model.

As can be seen, the outlets and inlets of the refrigerant fluid are inverted when the connection of the PHEX is in counter-flow or parallel-flow. The inversion of the refrigerant fluid allows the model to be used in reversible HPs which can heat and cool-down water, depending on the user demands.

3.3.1 Arbitrary number of FCVs case

Equation 3.33 will now be extended to N control volumes formulation for both a counter-flow and a parallel-flow connection.

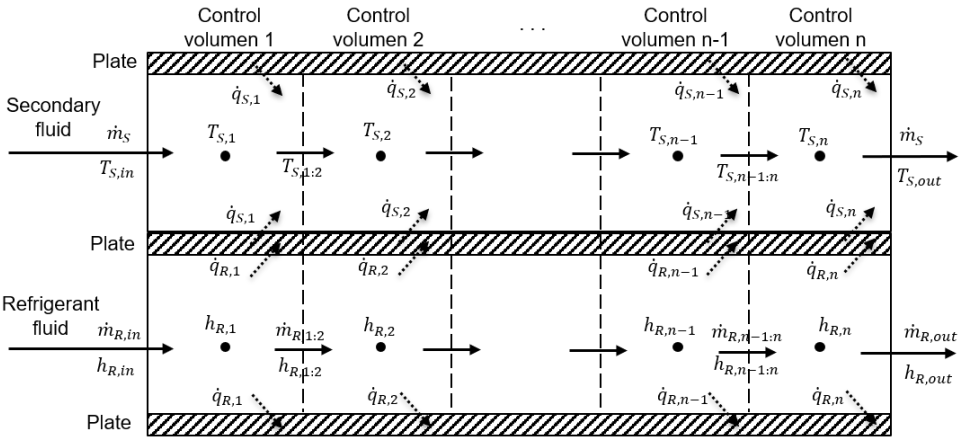

Figure 3.2: Finite control volume parallel-flow PHEX model.

Equation 3.34 and Equation 3.35 show the matrix equations that solve the refrigerant energy and mass equations for counter-flow and parallel-flow PHEX, respectively.

As the secondary fluid and plates energy equation can be solved separately, they have been removed from the refrigerant matrix. Equation 3.36 shows the secondary fluid energy matrix equation and Equation 3.41 shows the intermediate plate energy matrix equation. They are equal regardless of the connection of the PHEX.

$$\begin{bmatrix} Z_1 & Z_3 & Z_5 \\ Z_2 & Z_4 & Z_6 \end{bmatrix} \times \begin{bmatrix} \dot{P}_R \\ \dot{h}_{R,1} \\ \cdots \\ \dot{h}_{R,n} \\ \dot{m}_{R,1:2} \\ \cdots \\ \dot{m}_{R,n-1:n} \end{bmatrix} = \begin{bmatrix} -\dot{m}_{R,out} h_{R,out} + 2\dot{q}_{R,1} \\ 2\dot{q}_{R,2} \\ \cdots \\ 2\dot{q}_{R,n-1} \\ \dot{m}_{R,in} h_{R,in} + 2\dot{q}_{R,n} \\ -\dot{m}_{R,out} \\ 0 \\ \cdots \\ 0 \\ \dot{m}_{R,in} \end{bmatrix} \tag{3.34}$$

$$\begin{bmatrix} Z_1 & Z_3 & Z_7 \\ Z_2 & Z_4 & Z_8 \end{bmatrix} \times \begin{bmatrix} \dot{P}_R \\ \dot{h}_{R,1} \\ \dots \\ \dot{h}_{R,n} \\ \dot{m}_{R,1:2} \\ \dots \\ \dot{m}_{R,n-1:n} \end{bmatrix} = \begin{bmatrix} -\dot{m}_{R,in} h_{R,in} + 2\dot{q}_{R,1} \\ 2\dot{q}_{R,2} \\ \dots \\ 2\dot{q}_{R,n-1} \\ \dot{m}_{R,out} h_{R,out} + 2\dot{q}_{R,n} \\ -\dot{m}_{R,in} \\ 0 \\ \dots \\ 0 \\ \dot{m}_{R,out} \end{bmatrix} \tag{3.35}$$

$$[Z_9] \times \begin{bmatrix} \dot{T}_{S,1} \\ \dots \\ \dot{T}_{S,n} \end{bmatrix} = \begin{bmatrix} \dot{m}_S c_{S,1} (T_{S,in} - T_{S,1:2}) + 2\dot{q}_{S,1} \\ \dots \\ \dot{m}_S c_{S,n} (T_{S,n-1:n} - T_{S,out}) + 2\dot{q}_{S,n} \end{bmatrix} \tag{3.36}$$

$$\begin{bmatrix} m_{W,cv} c_W \end{bmatrix} \times \begin{bmatrix} \dot{T}_{W,1} \\ \dots \\ \dot{T}_{W,n} \end{bmatrix} = \begin{bmatrix} \dot{q}_{R,1} - \dot{q}_{S,1} \\ \dots \\ \dot{q}_{R,n} - \dot{q}_{S,n} \end{bmatrix} \tag{3.37}$$

Sub-matrices of Equations 3.34 - 3.36 are presented below.

$$[Z_1] = \begin{bmatrix} V_{cv} \left[\left(\left| \frac{\partial \rho}{\partial P} \right|_h \right)_1 h_{R,1} - 1 \right] \\ V_{cv} \left[\left(\left| \frac{\partial \rho}{\partial P} \right|_h \right)_2 h_{R,2} - 1 \right] \\ \dots \\ V_{cv} \left[\left(\left| \frac{\partial \rho}{\partial P} \right|_h \right)_{n-1} h_{R,n-1} - 1 \right] \\ V_{cv} \left[\left(\left| \frac{\partial \rho}{\partial P} \right|_h \right)_n h_{R,n} - 1 \right] \end{bmatrix}$$

$$[Z_2] = \begin{bmatrix} V_{cv}\left(\left|\frac{\partial \rho}{\partial P}\right|_h\right)_1 \\ V_{cv}\left(\left|\frac{\partial \rho}{\partial P}\right|_h\right)_2 \\ \dots \\ V_{cv}\left(\left|\frac{\partial \rho}{\partial P}\right|_h\right)_{n-1} \\ V_{cv}\left(\left|\frac{\partial \rho}{\partial P}\right|_h\right)_n \end{bmatrix}$$

$$[Z_3] = \begin{bmatrix} V_{cv}\left[\left(\left|\frac{\partial \rho}{\partial h}\right|_P\right)_1 h_{R,1} + \rho_{R,1}\right] & 0 & .. & 0 & 0 \\ 0 & V_{cv}\left[\left(\left|\frac{\partial \rho}{\partial h}\right|_P\right)_2 h_{R,2} + \rho_{R,2}\right] & .. & 0 & 0 \\ \dots & \dots & \dots & \dots & \dots \\ 0 & 0 & \dots & V_{cv}\left[\left(\left|\frac{\partial \rho}{\partial h}\right|_P\right)_{n-1} h_{R,n-1} + \rho_{R,n-1}\right] & 0 \\ 0 & 0 & \dots & 0 & V_{cv}\left[\left(\left|\frac{\partial \rho}{\partial h}\right|_P\right)_n h_{R,n} + \rho_{R,n}\right] \end{bmatrix}$$

$$[Z_4] = \begin{bmatrix} V_{cv}\left(\left|\frac{\partial \rho}{\partial h}\right|_P\right)_1 & 0 & \dots & 0 & 0 \\ 0 & V_{cv}\left(\left|\frac{\partial \rho}{\partial h}\right|_P\right)_2 & \dots & 0 & 0 \\ \dots & \dots & \dots & \dots & \dots \\ 0 & 0 & \dots & V_{cv}\left(\left|\frac{\partial \rho}{\partial h}\right|_P\right)_{n-1} & 0 \\ 0 & 0 & \dots & 0 & V_{cv}\left(\left|\frac{\partial \rho}{\partial h}\right|_P\right)_n \end{bmatrix}$$

$$[Z_5] = \begin{bmatrix} -h_{1:2} & 0 & 0 & ... & 0 & 0 & 0 \\ h_{1:2} & -h_{2:3} & 0 & ... & 0 & 0 & 0 \\ 0 & h_{2:3} & -h_{3:4} & ... & 0 & 0 & 0 \\ ... & ... & ... & ... & ... & ... & ... \\ 0 & 0 & 0 & ... & h_{\text{n-3:n-2}} & -h_{\text{n-2:n-1}} & 0 \\ 0 & 0 & 0 & ... & 0 & h_{\text{n-2:n-1}} & -h_{\text{n-1:n}} \\ 0 & 0 & 0 & ... & 0 & 0 & h_{\text{n-1:n}} \end{bmatrix}$$

$$[Z_6] = \begin{bmatrix} -1 & 0 & 0 & ... & 0 & 0 & 0 \\ 1 & -1 & 0 & ... & 0 & 0 & 0 \\ 0 & 1 & -1 & ... & 0 & 0 & 0 \\ ... & ... & ... & ... & ... & ... & ... \\ 0 & 0 & 0 & ... & 1 & -1 & 0 \\ 0 & 0 & 0 & ... & 0 & 1 & -1 \\ 0 & 0 & 0 & ... & 0 & 0 & 1 \end{bmatrix}$$

$$[Z_7] = \begin{bmatrix} h_{1:2} & 0 & 0 & ... & 0 & 0 & 0 \\ -h_{1:2} & h_{2:3} & 0 & ... & 0 & 0 & 0 \\ 0 & -h_{2:3} & h_{3:4} & ... & 0 & 0 & 0 \\ ... & ... & ... & ... & ... & ... & ... \\ 0 & 0 & 0 & ... & -h_{\text{n-3:n-2}} & h_{\text{n-2:n-1}} & 0 \\ 0 & 0 & 0 & ... & 0 & -h_{\text{n-2:n-1}} & h_{\text{n-1:n}} \\ 0 & 0 & 0 & ... & 0 & 0 & -h_{\text{n-1:n}} \end{bmatrix}$$

$$[Z_8] = \begin{bmatrix} 1 & 0 & 0 & ... & 0 & 0 & 0 \\ -1 & 1 & 0 & ... & 0 & 0 & 0 \\ 0 & -1 & 1 & ... & 0 & 0 & 0 \\ ... & ... & ... & ... & ... & ... & ... \\ 0 & 0 & 0 & ... & -1 & 1 & 0 \\ 0 & 0 & 0 & ... & 0 & -1 & 1 \\ 0 & 0 & 0 & ... & 0 & 0 & -1 \end{bmatrix}$$

$$[Z_9] = \begin{bmatrix} V_{cv}\rho_{S,1}c_{S,1} & 0 & ... & 0 & 0 \\ 0 & V_{cv}\rho_{S,2}c_{S,2} & ... & 0 & 0 \\ ... & ... & ... & ... & ... \\ 0 & 0 & ... & V_{cv}\rho_{S,n-1}c_{S,n-1} & 0 \\ 0 & 0 & ... & 0 & V_{cv}\rho_{S,n}c_{S,n} \end{bmatrix}$$

Equations 3.34 - 3.37 present the equations for a N FCVs model. Now, an example for the case in which three FCVs are taken will be presented.

3.3.2 Three FCVs example case

Equation 3.33 will now be extended to a three control volumes formulation for both counter-flow and parallel-flow connections.

Figure 3.3 and Figure 3.4 show schematically the three control volume counter-flow and parallel-flow PHEX, respectively. Equation 3.38 and Equation 3.39 show the refrigerant matrix equations for counter-flow and parallel-flow PHEX, respectively. Equations 3.40 and 3.41 shows the secondary fluid and intermediate plates energy matrix equation.

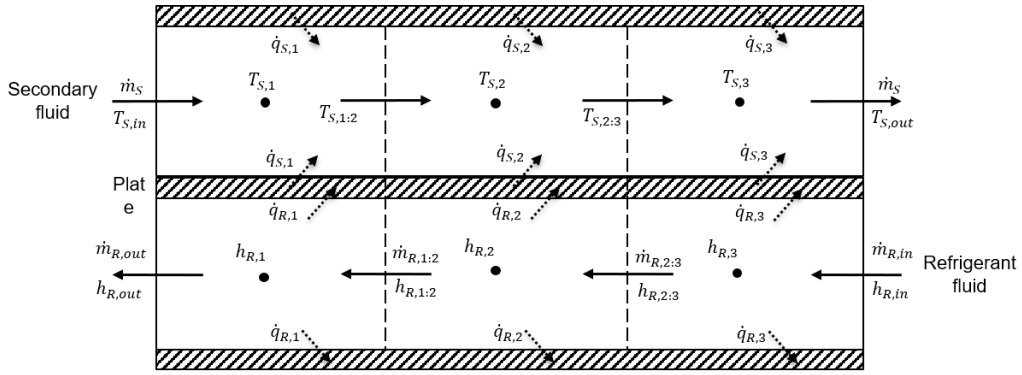

Figure 3.3: Three FCV counter-flow PHEX model.

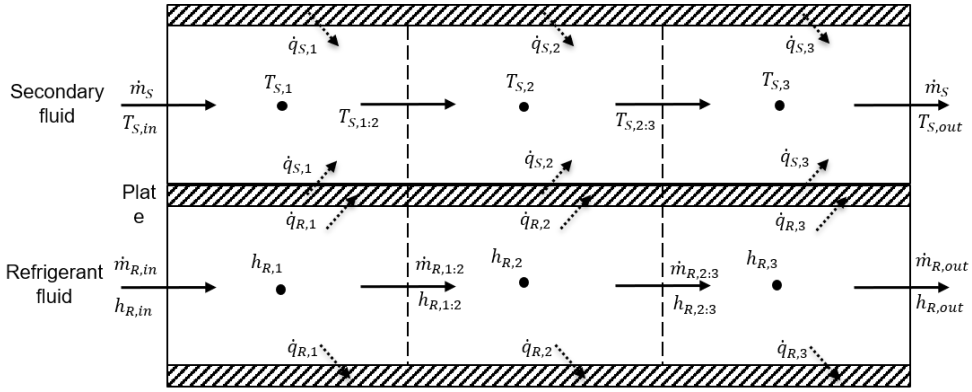

Figure 3.4: Three FCVs parallel-flow PHEX model.

$$\begin{bmatrix} Z_1 & Z_3 & Z_5 \\ Z_2 & Z_4 & Z_6 \end{bmatrix} \times \begin{bmatrix} \dot{P}_R \\ \dot{h}_{R,1} \\ \dot{h}_{R,2} \\ \dot{h}_{R,3} \\ \dot{m}_{R,1:2} \\ \dot{m}_{R,2:3} \end{bmatrix} = \begin{bmatrix} -\dot{m}_{R,out} h_{R,out} + 2\dot{q}_{R,1} \\ 2\dot{q}_{R,2} \\ \dot{m}_{R,in} h_{R,in} + 2\dot{q}_{R,3} \\ -\dot{m}_{R,out} \\ 0 \\ \dot{m}_{R,in} \end{bmatrix} \tag{3.38}$$

$$\begin{bmatrix} Z_1 & Z_3 & Z_7 \\ Z_2 & Z_4 & Z_8 \end{bmatrix} \times \begin{bmatrix} \dot{P}_R \\ \dot{h}_{R,1} \\ \dot{h}_{R,2} \\ \dot{h}_{R,3} \\ \dot{m}_{R,1:2} \\ \dot{m}_{R,2:3} \end{bmatrix} = \begin{bmatrix} \dot{m}_{R,in} h_{R,in} + 2\dot{q}_{R,1} \\ 2\dot{q}_{R,2} \\ -\dot{m}_{R,out} h_{R,out} + 2\dot{q}_{R,3} \\ \dot{m}_{R,in} \\ 0 \\ -\dot{m}_{R,out} \end{bmatrix} \tag{3.39}$$

$$[Z_9] \times \begin{bmatrix} \dot{T}_{S,1} \\ \dot{T}_{S,2} \\ \dot{T}_{S,3} \end{bmatrix} = \begin{bmatrix} \dot{m}_S c_{S,1}(T_{S,in} - T_{S,1:2}) + 2\dot{q}_{S,1} \\ \dot{m}_S c_{S,2}(T_{S,1:2} - T_{S,2:3}) + 2\dot{q}_{S,2} \\ \dot{m}_S c_{S,3}(T_{S,2:3} - T_{S,out}) + 2\dot{q}_{S,3} \end{bmatrix} \tag{3.40}$$

$$\left[m_{W,cv} c_W\right] \times \begin{bmatrix} \dot{T}_{W,1} \\ \dot{T}_{W,2} \\ \dot{T}_{W,3} \end{bmatrix} = \begin{bmatrix} \dot{q}_{R,1} - \dot{q}_{S,1} \\ \dot{q}_{R,2} - \dot{q}_{S,2} \\ \dot{q}_{R,3} - \dot{q}_{S,3} \end{bmatrix} \tag{3.41}$$

Sub-matrices of Equations 3.38 - 3.40 are presented in Table 3.1.

Equations 3.38 - 3.41 present the equations for a three FCVs model, but they can easily extended to an arbitrary number of control volumes to achieve better accuracy in the results.

Table 3.1: Sub-matrices of Equations 3.38 - 3.40.

Z_1	$\begin{bmatrix} V_{cv}\left[\left(\left\|\frac{\partial\rho}{\partial P}\right\|_h\right)_1 h_{R,1} - 1\right] \\ V_{cv}\left[\left(\left\|\frac{\partial\rho}{\partial P}\right\|_h\right)_2 h_{R,2} - 1\right] \\ V_{cv}\left[\left(\left\|\frac{\partial\rho}{\partial P}\right\|_h\right)_3 h_{R,3} - 1\right] \end{bmatrix}$
Z_2	$\begin{bmatrix} V_{cv}\left(\left\|\frac{\partial\rho}{\partial P}\right\|_h\right)_1 \\ V_{cv}\left(\left\|\frac{\partial\rho}{\partial P}\right\|_h\right)_2 \\ V_{cv}\left(\left\|\frac{\partial\rho}{\partial P}\right\|_h\right)_3 \end{bmatrix}$
Z_3	$\begin{bmatrix} V_{cv}\left[\left(\left\|\frac{\partial\rho}{\partial h}\right\|_P\right)_1 h_{R,1} + \rho_{R,1}\right] & 0 & 0 \\ 0 & V_{cv}\left[\left(\left\|\frac{\partial\rho}{\partial h}\right\|_P\right)_2 h_{R,2} + \rho_{R,2}\right] & 0 \\ 0 & 0 & V_{cv}\left[\left(\left\|\frac{\partial\rho}{\partial h}\right\|_P\right)_3 h_{R,3} + \rho_{R,3}\right] \end{bmatrix}$
Z_4	$\begin{bmatrix} V_{cv}\left(\left\|\frac{\partial\rho}{\partial h}\right\|_P\right)_1 & 0 & 0 \\ 0 & V_{cv}\left(\left\|\frac{\partial\rho}{\partial h}\right\|_P\right)_2 & 0 \\ 0 & 0 & V_{cv}\left(\left\|\frac{\partial\rho}{\partial h}\right\|_P\right)_3 \end{bmatrix}$
Z_5	$\begin{bmatrix} -h_{1:2} & 0 \\ h_{1:2} & -h_{2:3} \\ 0 & h_{2:3} \end{bmatrix}$
Z_6	$\begin{bmatrix} -1 & 0 \\ 1 & -1 \\ 0 & 1 \end{bmatrix}$
Z_7	$\begin{bmatrix} h_{1:2} & 0 \\ -h_{1:2} & h_{2:3} \\ 0 & -h_{2:3} \end{bmatrix}$
Z_8	$\begin{bmatrix} 1 & 0 \\ -1 & 1 \\ 0 & -1 \end{bmatrix}$
Z_9	$\begin{bmatrix} V_{cv}\rho_{S,1}c_{S,1} & 0 & 0 \\ 0 & V_{cv}\rho_{S,2}c_{S,2} & 0 \\ 0 & 0 & V_{cv}\rho_{S,3}c_{S,3} \end{bmatrix}$

3.4 Model interface

During this section, the model final interface will be presented and some explanations about it will be given. Each component will be presented separately and then, the

whole model together. For each components, inlets and outlets will be explained. In Annex I, the model subsystems of each component are presented. Similarly, in Annex II, programmed S-functions for the implementation of PHEXs equations is written down.

First of all, the explanation given in Section 3.3 about the needed inputs to solve the the equations of each component must be extended. As said in Section 3.1, there are two kind of components: those which regulate the refrigerant MFR and those which regulate the refrigerant working pressures. These different blocks must be interspersed. For instance, having a HEX, which is a block that regulates the pressure, the anterior and posterior blocks must be those which regulate the MFR, such as valves or compressors.

It is because in order to solve the equations of blocks that regulate the refrigerant MFRs, it must be known the inlet and outlet refrigerant pressures. Similarly, to solve the equations of blocks that regulate the refrigerant pressure, it must be known the inlet and outlet MFRs. This will be clearly seen in the figures of the present section.

3.4.1 Compressor

In Figure 3.5 the block that simulates the behavior of a compressor can be seen. It can be used either for a scroll compressor or a reciprocating compressor since the equations presented in Section 3.2.1 generally calculates the outlet refrigerant MFR, enthalpy and consumed power in function of the inlet properties, cycle pressures.

Block inputs

- **Flow in:** This input is a three variables vector. The first of them represents the inlet pressure in [kPa], the second one is the inlet temperature in [°C] and the last one represents the inlet enthalpy in [kJ/kg]. This input port must be connected to 'Flow out' outlet port of the evaporator.
- **Up-stream pressure:** This input port is a single variable that represents the outlet pressure in [kPa]. In a simple HP, it will be the condensation pressure calculated in the condenser.

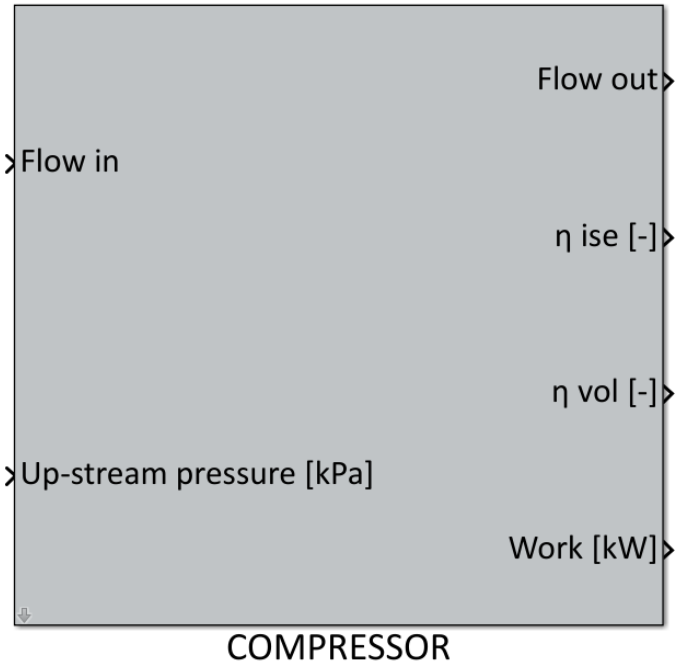

Figure 3.5: Compressor model block.

Block outputs

- **Flow out:** This output is a three variables vector. The first of them represents the refrigerant outlet MFR in [kg/s], the second one is the outlet temperature in [°C] and the last one represents the outlet enthalpy in [kJ/kg].
- η_{ise}**:** It shows the calculated isentropic efficiency of the compressor at each step time.
- η_{vol}**:** It shows the calculated volumetric efficiency of the compressor at each step time.
- **Work:** It represents the power consumption of the compressor in order to compress the refrigerant fluid in [kW].

3.4.2 Electronic Expansion Valve

The block to simulate the EEV is presented in Figure 3.6. It can be used for any kind of EEV if the valve coefficient in function of the opening degree is known.

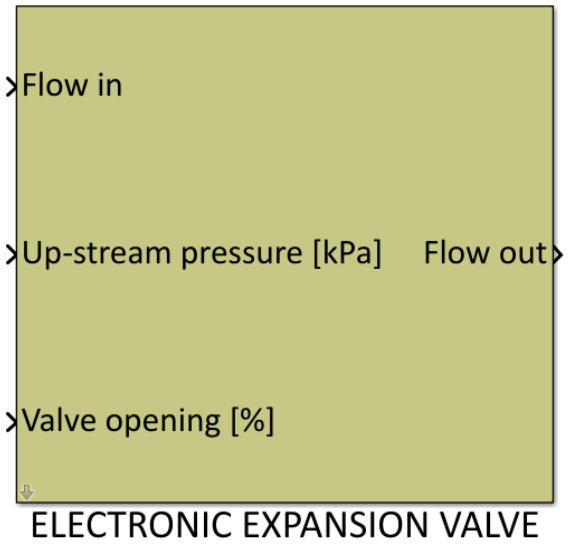

Figure 3.6: Compressor model block.

Block inputs

- **Flow in:** This input is a vector with the same three variables presented in the compressor block. This input port must be connected to 'Flow out' outlet port of the condenser.
- **Up-stream pressure:** This input port is a single variable that represents the outlet pressure in [kPa]. In a simple HP, it will be the evaporation pressure calculated in the evaporator.
- **Valve opening:** It is a single variable that represents the opening degree of the EEV at each time step. It is a percentage between 0 and 100%.

Block outputs

- **Flow out:** This output is a vector with the same three variables presented in the compressor block.

3.4.3 Indoor Unit PHEX

In Figure 3.7 can be seen the block used to simulate the indoor unit PHEX. As explained before, it can work indistinctly as a condenser and as an evaporator. When the system

is working in heating mode, this blocks works as a condenser and as an evaporator during the cooling mode.

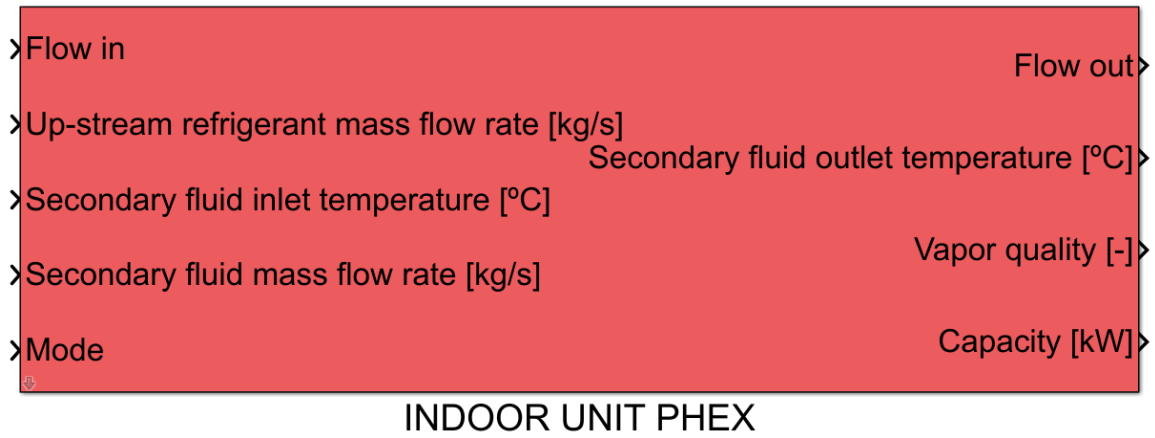

Figure 3.7: Indoor Unit PHEX model block.

Block inputs

- **Flow in:** This input is a three variables vector. The first of them represents the inlet refrigerant MFR in [kg/s], the second one is the inlet temperature in [°C] and the last one represents the inlet enthalpy in [kJ/kg]. This input port must be connected to 'Flow out' outlet port of the compressor when working in heating mode and to 'Flow out' of the EEV when working in cooling mode.
- **Up-stream refrigerant mass flow rate:** This input port is a single variable that represents the outlet refrigerant MFR in [kg/s].
- **Secondary fluid inlet temperature:** It is the inlet temperature of the secondary fluid in [°C].
- **Secondary fluid mass flow rate:** It is the MFR of the secondary fluid in [kg/s].
- **Mode:** It is a single variable port that defines the working mode that will be simulated. The value must be 1 for heating mode or 0 for cooling mode. With this information, the PHEX block can know if it is working as a condenser or as an evaporator.

Block outputs

- **Flow out:** This output is a three variables vector. The first of them represents the refrigerant outlet pressure in [kPa], the second one is the outlet temperature in [°C] and the last one represents the outlet enthalpy in [kJ/kg].
- **Secondary fluid outlet temperature:** It is the outlet temperature of the secondary fluid in [°C].
- **Vapor quality:** It is a N variables vector that represents the vapor quality of the refrigerant at each FCV of the PHEX.
- **Capacity:** It is the heat transfer given between fluids at each time step expressed in [kW].

3.4.4 Outdoor Unit PHEX

In Figure 3.8 can be seen the block used to simulate the outdoor unit PHEX. Similarly to the indoor unit, it can work indistinctly as a condenser and as an evaporator but in the opposite situations.

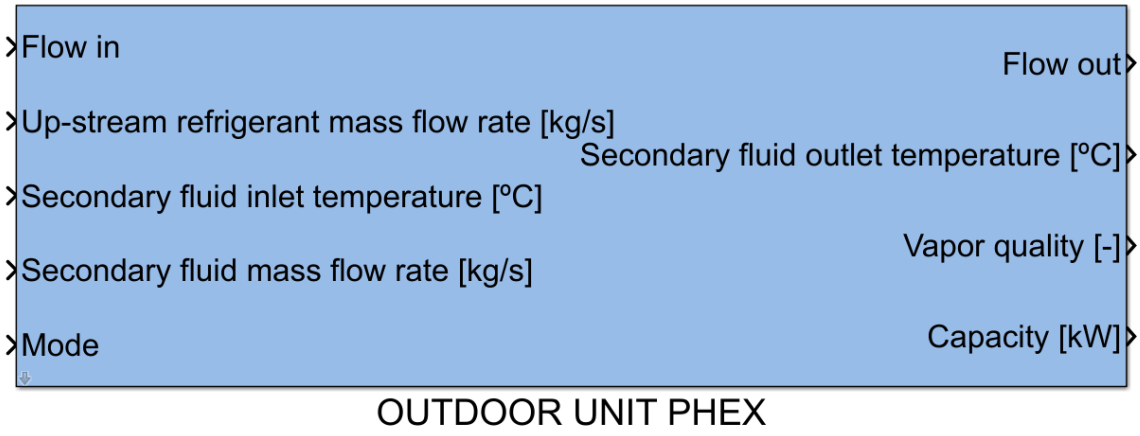

Figure 3.8: Outdoor Unit PHEX model block.

Block inputs

- **Flow in:** This input is a three variables vector with the same variables that the indoor unit. This input port must be connected to 'Flow out' outlet port of the

EEV when working in heating mode and to 'Flow out' of the compressor when working in cooling mode.

- **Up-stream refrigerant mass flow rate:** This input port is a single variable that represents the outlet refrigerant MFR in [kg/s].
- **Secondary fluid inlet temperature:** It is the inlet temperature of the secondary fluid in [°C].
- **Secondary fluid mass flow rate:** It is the MFR of the secondary fluid in [kg/s].
- **Mode:** It is equal to the Mode input explained in the indoor unit PHEX.

Block outputs

- **Flow out:** This output is a vector with the same three variables presented in the indoor unit PHEX.
- **Secondary fluid outlet temperature:** It is the outlet temperature of the secondary fluid in [°C].
- **Vapor quality:** It is a N variables vector that represents the vapor quality of the refrigerant at each FCV of the PHEX.
- **Capacity:** It is the heat transfer given between fluids at each time step expressed in [kW]. As it is a model in which the losses to environment are not taken into account, the sum of the capacity calculated in the evaporator and the compressor work is equal to the capacity calculated in the condenser.

3.4.5 Model inputs

The inputs to the model that are needed to carry out a simulation will be explained. It can be used a constant block for all the simulation or a 'From Workspace' block in order to read a Matlab timeseries. The latter allows to vary input values with the periodicity that the user wants.

– *IU secondary fluid inlet temperature:* Is the inlet temperature of the secondary fluid to indoor unit expressed in [°C].

- *IU secondary fluid mass flow rate:* Is the MFR of the secondary fluid to indoor unit expressed in [kg/s].
- *OU secondary fluid inlet temperature:* Is the inlet temperature of the secondary fluid to outdoor unit expressed in [°C].
- *OU secondary fluid mass flow rate:* Is the MFR of the secondary fluid to outdoor unit expressed in [kg/s].
- *Valve opening:* It represents the current valve opening degree of the EEV.
- *Working mode:* It is the current working mode that wanted to be simulated. It must be manually set before start the simulation.

In the next section they will be seen the inputs located in it correspondent place.

3.4.6 Model interface example

Now, an example of the interface of the whole model will be presented. In Figure 3.9, the model to carry out a heating mode simulation is presented. On the other hand, in Figure 3.10 the interface for cooling mode simulations can be seen.

Dark green boxes are the up-stream MFR or pressure needed for the calculation of the correspondent blocks. Light blue boxes are the secondary fluids inputs to the model presented in the Section 3.4.5 and orange boxes the current working mode of the system.

As can be seen, the only difference between both models is the direction of the refrigerant. While in the heating mode the refrigerant fluid goes from the compressor to the indoor unit, then to the EEV, then to the outdoor unit and finally goes back to the compressor, in the cooling mode it goes from the compressor to the outdoor unit, EEV, indoor unit and back to the compressor.

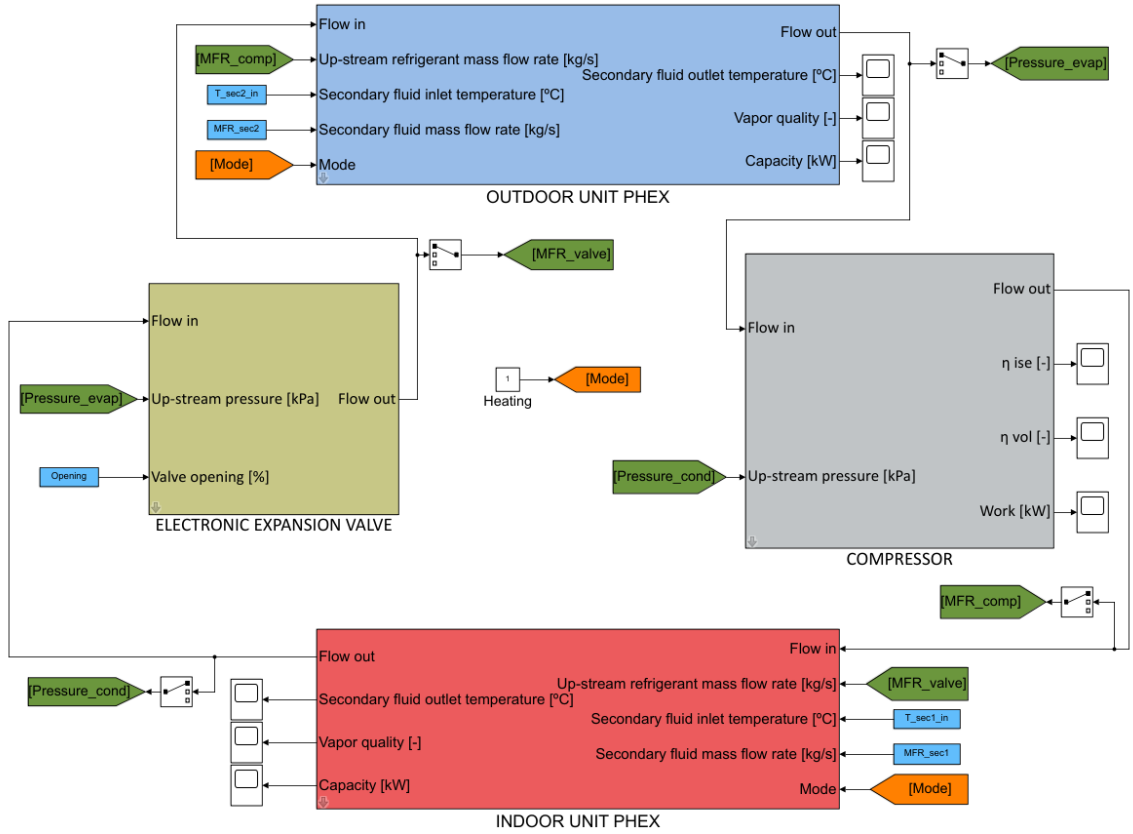

Figure 3.9: Simulation model interface during the heating mode configuration.

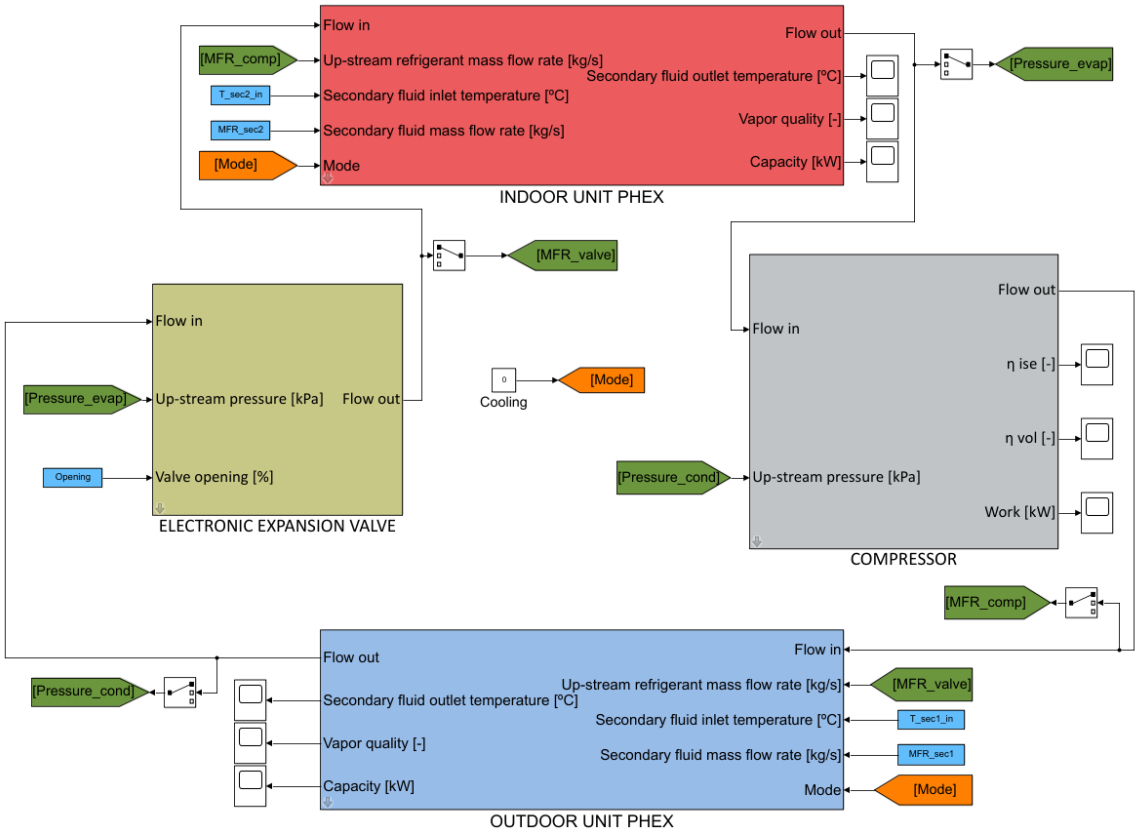

Figure 3.10: Simulation model interface during the cooling mode configuration.

3.5 Model complementary information

The equations presented during the previous sections model the dynamic behavior of the system. They will be the same for any liquid-to-liquid HP that wanted to be simulated. Nevertheless, there is some specific complementary information that must to be added to the model in order to simulate the required specific system.

All this information is added to the model by means of the masks of the correspondent component presented in Section 3.4.

Number of finite control volumes: Inside the mask of the interface of HEXs it must be defined the number of FCV in which the PHEX wanted to be divided. It can be a different number for each PHEX. The accuracy of the model will increase with a higher number of FCV but also the computational time will increase. A study of the appropriate number of FCV is presented in Sections 4.5 and 5.3. In Figure 3.11 can be seen an example of the properties mask of the PHEX model block, where the FCV parameter is highlighted in red.

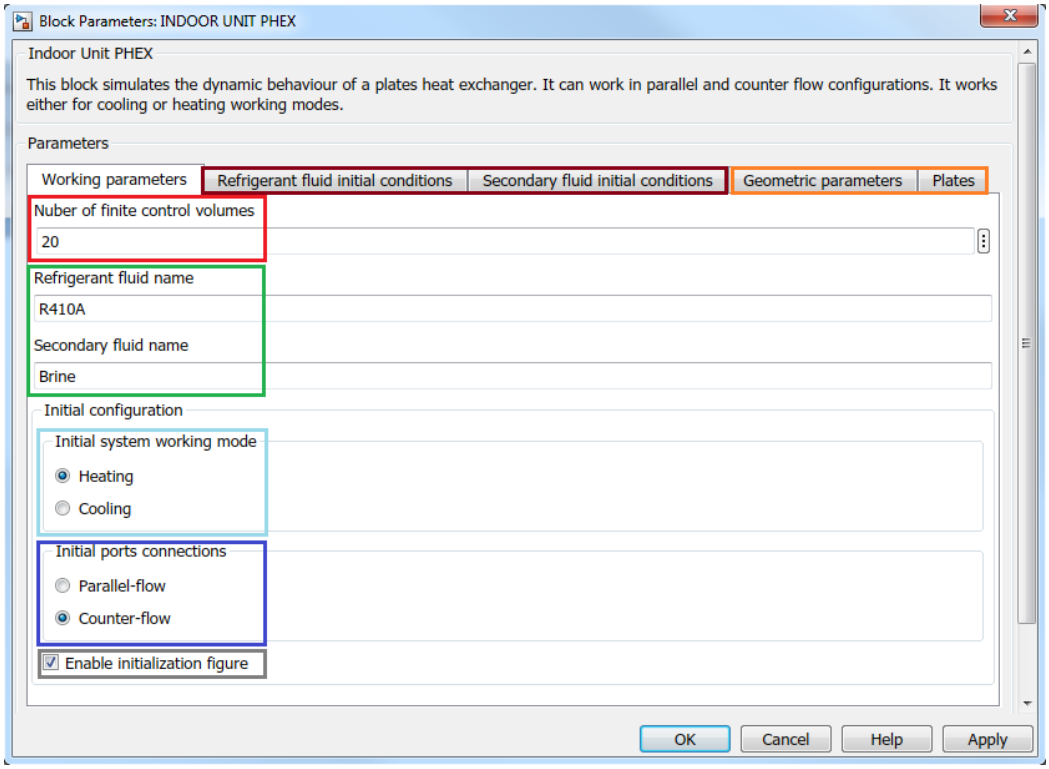

Figure 3.11: Example of a PHEX block mask.

Fluids and fluids properties: The refrigerant fluid that want to be simulated have to be defined in the mask of each component as can be seen highlighted in green in Figure 3.11. Additionally, in the PHEX the secondary fluid must be defined.

Moreover, previously to the simulation, tables of fluids properties must be defined. This tables can be one or two dimensions tables depending on the fluid and properties. The dimension of the table depends on the property that if finding. For instance, the enthalpy of the refrigerant fluid in the superheated area needs a two dimensions table. However, to obtain the specific heat of the water is enough accurate with a one dimension table in function of the temperature.

Fluid tables were obtained by means of the open source software CoolProp [152]. Nevertheless, they can be obtained with other methods such as RefProp [153], EES [154] or the Equations of the State of the fluids [155]. Once the tables are obtained, they must to be saved together in a .mat file. The name of the file is which must be written in the mask of the components. During the initialization of the simulation the tables will be charged.

Initial system working mode: The initial working mode of the system with which the simulation will start must be defined. It can be heating or cooling as can be seen in light blue in Figure 3.11.

Initial PHEX ports connections: The initial ports connections of the PHEX must be defined. During the simulation, if the working mode switches, the connection of the ports will also be switched by reversing the flow of the refrigerant fluid. It can be counter-flow or parallel-flow connections as presented in dark blue in Figure 3.11.

Initial boundary conditions: The boundary conditions for the initialization of the simulation must to be defined in the heat exchanger blocks. In Figure 3.11 is remarked in brown. The initial conditions of the fast-dynamics components such as compressor and EEV are not needed to be defined.

Indistinctly if it is simulating heating or cooling modes, in each PHEX, it must be defined initial conditions for both working modes. Then, during the initialization, depending on the working mode of the system, ones or the others will be taken. Moreover, if user wants, a figure where the temperatures distribution inside PHEXs is seen can be shown

during the initialization. To do it, the box that is highlighted in gray in Figure 3.11 must be checked. An example of the generated figures can be seen in Figure 3.12.

Needed initial boundary conditions for each PHEX are presented in Table 3.2.

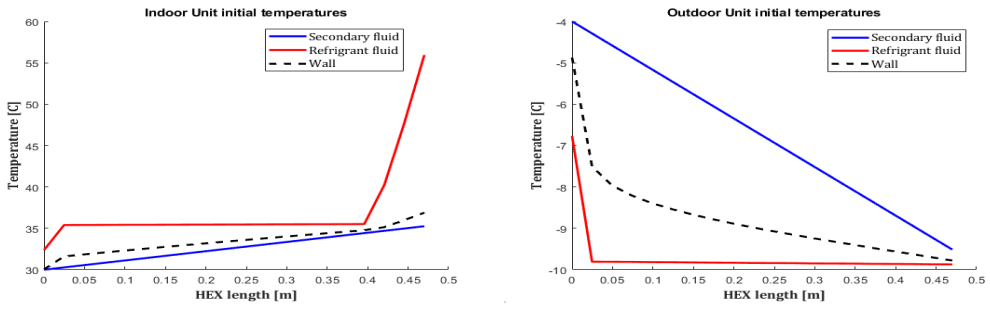

(a) *(b)*

Figure 3.12: Examples of the generated figures during the initialization. Counter-flow condenser (a) and counter-flow evaporator (b).

Table 3.2: Initial boundary conditions for each PHEX.

Refrigerant mass flow rate [kg/s]
Refrigerant condensation pressure [kPa]
Refrigerant evaporation pressure [kPa]
Refrigerant inlet enthalpy (as condenser) [kJ/kg]
Refrigerant inlet enthalpy (as evaporator) [kJ/kg]
Refrigerant subcooling (as condenser) [K]
Refrigerant reheating (as evaporator) [K]
Secondary fluid mass flow rate [kg/s]
Secondary fluid inlet temperature (as condenser) [°C]
Secondary fluid inlet temperature (as evaporator) [°C]

Components dimensions and properties: Utilized components dimensions must be defined. In Table 3.3 the needed dimensions are summarized. Additionally, the specific heat of the heat exchanger plates must be defined. All this can be changed in the mask of the correspondent component. For instance, in the PHEX is changed in the tabs highlighted in orange in Figure 3.11.

Heat transfer coefficients: Inside the PHEX the HTC are calculated for each fluid in each FCV in each time step. This HTC depends between others in the utilized fluids,

Table 3.3: Needed physical dimensions of HP components.

PHEXs	Number of plates
	Plates length [m]
	Distance between plates [m]
	Plates height [m]
	Hydraulic diameter [m]
	Effective surface parameter
	Plates mass [kg]
	Chevron angle [rad]
Compressor	Volumetric displacement [m^3/h]

actual thermal and physical properties of the fluids and geometrical properties of the HEX.

HTC is calculated with Equation 3.42.

$$\alpha = Nu \, \frac{k}{D_h} \tag{3.42}$$

Where Nusselt number (Nu) is obtained by means of empirical correlations that can be found along the literature. There exist some general Nusselt number correlations that can be utilized for different fluids and HEX geometries [156, 157]. Nevertheless, if the accuracy of the simulation wanted to be increased, it is recommended to use more specific correlations in accordance with the used fluid and HEX. For instance, to calculate the HTC of R410A during its evaporation inside brazed plates heat exchangers, it is preferable to use the correlation proposed by Han et al. [158].

Compressor efficiencies: The efficiencies of the compressor must be defined according to the utilized compressor. As briefly explained in Section 3.2.1, both isentropic efficiency and volumetric efficiency are utilized. The irreversibilities inside the compressor are measured with the isentropic efficiency and the frictional and mechanical losses with the volumetric efficiency.

For the simulation, this efficiencies can be defined in different ways depending on the information the user has. It can be defined as a correlation in function of the pressures ratio (or other parameter), a n-dimensional table or even a constant. It will directly affect results accuracy when calculating compressor consumption or refrigerant outlet

properties.

Valve coefficient: In order to define the valve coefficient it can be utilized a correlation, a constant or a table. It depends on the information the user has.

Refrigerant mass flow distributor: As described in Section 3.2.4, in the developed model it is assumed that the refrigerant flow is uniformly distributed in the different channels of the PHEX. Nevertheless, it does not happen. When a single-phase fluid goes into a PHEX, it is generally uniformly distributed along PHEX channels. However, a two-phase fluid is not uniformly distributed and the maldistribution phenomenon is commonly given [159]. This occurs in the inlet of the evaporator since the refrigerant fluid goes out from the EEV as a two-phase fluid.

This phenomenon can be minimized by placing a distributor in the inlet of the evaporator [160, 161]. However, the distributor causes important pressure drops in the refrigerant fluid. This pressure drops are taken into account in the EEV model. The expansion occurred in the distributor is assumed to be isenthalpic.

In the EEV model block mask, a pressure increment can be set, which is added to the low pressure calculated in the evaporator. Therefore, a intermediate pressure level is generated in the model. The EEV model block expands the refrigerant fluid from the high pressure level to the generated intermediate pressure level. A graphic explanation can be seen in Figure 3.13.

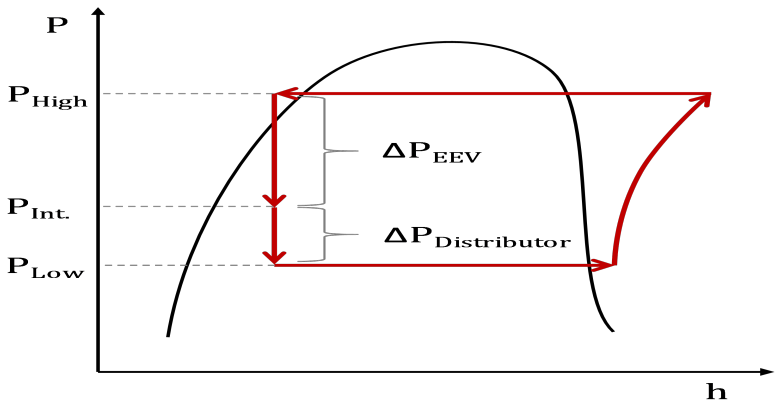

Figure 3.13: Graphic explanation of the intermediate pressure and distributor pressure drop.

Correction factors: As commented before, the calculation of HTC is based on empirical correlations. Some of them are specifics for one fluid and others are more general and can be used with different fluids. However, HTC empirical correlations usually have implied a high degree of uncertainty.

Therefore, correction factors have been implemented in the model. They are applied directly to the HTCs increasing or decreasing the value calculated with the correlations. It affects to the heat transfer between fluids, causing the modification of the operation conditions of the system.

There have been implemented four correction factors. One for each calculated HTC: refrigerant fluid in the indoor unit, secondary fluid in the indoor unit, refrigerant fluid in the outdoor unit and secondary fluid in the outdoor unit. For instance, in Figure 3.14 can be seen the mask of the indoor unit PHEX, where the correction factors can be modified.

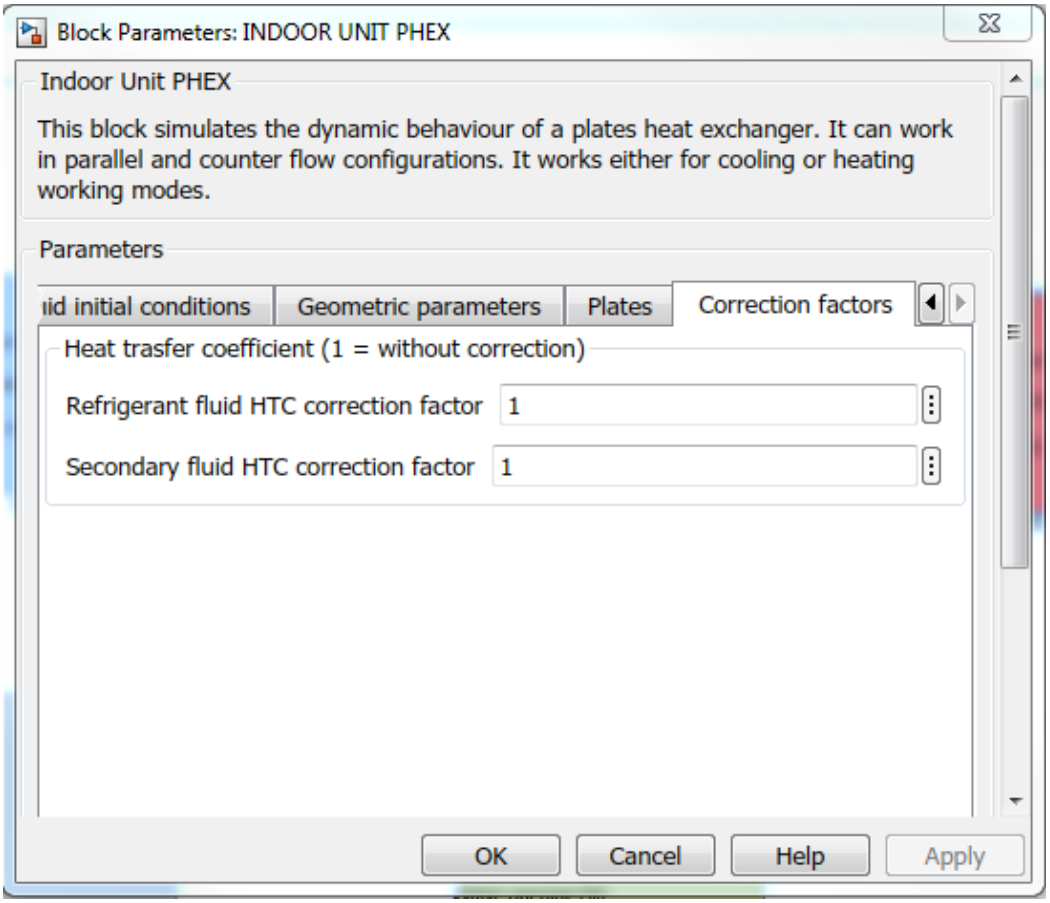

Figure 3.14: Example of a PHEX block mask with the correction factors.

The use of these correction factors is optional and depends on the user. It is important

to remark that in the results presented in all this document there have not been used any correction factor.

Chapter 4

MICRO-SCALE SIMULATIONS

During this chapter, the model developed in the Chapter 3 will be used to simulate fast transient-states. Firstly, the experimental tests will be described, focusing in the used heat pump system, the developed methodology to force the required transient-states and the taken measurements. Then, the model will be validated under three different situations: heating working mode, cooling working mode and an start-up of the system. Finally, the usefulness of the model to simulate working mode switches from the cooling to the heating working mode and vice-versa will be proved.

4.1 Introduction

Once the dynamic model to simulate the behavior of liquid-to-liquid HP systems have been developed, implemented and presented, it must be validated comparing the simulation results with experimental data. In this chapter, it will be validated in micro-scale, focusing in fast transient-states such as changes in the operation conditions and start-ups situations.

Laboratory experimental tests were carried out using a liquid-to-liquid HP system connected to a climatic chamber, which emulates both the heat sources and sinks. The used system is a commercial reversible HP of 5kW of nominal heating capacity. It is compound of two PHEX, one scroll compressor, one EEV and one 4WV. During this chapter, the system, its components and made measurements will be described in detail.

It also will be presented the procedure to carry out the experimental tests, describing the different working conditions of the system, how it have been forced the transient situations and the steps followed to develop each test.

Regarding the comparison of the model with the experimental data, firstly it will be specified the additional information that must be added to the model in relation with the actual HP system, such as used HTC correlations, valve coefficient or compressor efficiencies. Then, it will be compared test data with model simulation results under the heating and the cooling working modes separately. Additionally, a system start-up situation will be validated. The heating and cooling validations will be given against transient situations that have been forced manually in the test bench. On the contrary, the start-up situation has been tested using the control loop of the system.

Finally, a switching mode simulation will be presented in order to prove the validity of the model to simulate the behavior of the system when switching the working mode from the heating to the cooling or vice-versa. It will be explained which have been the changes that had to be made in the model to simulate working mode switches and which are the imposed simulation conditions. Results and a discussion about them will be presented.

To conclude, some comments and conclusions will be drawn.

4.2 Test facility

The test bed is compound by a reversible liquid-to-liquid HP coupled with a climatic chamber. The whole system emulates the behavior of a ground or water source HP facility. The climatic chamber simulates the returning temperatures of secondary fluids to the condenser and evaporator. Photography of the used HP system can be seen in Figure 4.1.

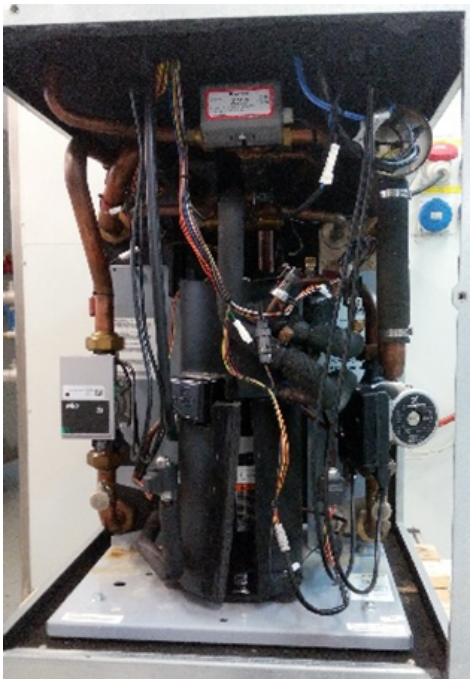

Figure 4.1: Photography of the heat pump system.

The HP is a 5 kW commercial liquid-to-liquid reversible HP. It is compound of one fixed speed and displacement scroll compressor, one EEV, one 4WV and two refrigerant-to-liquid PHEX. In Figure 4.2 a 3D image of the HP and the used mentioned components can be seen.

There are three independent fluids loops. One primary loop and two secondary loops. The working fluid of the primary loop is the R410A commercial refrigerant fluid. It circulates through all the components of the HP. The secondary loops are connected to the PHEXs of the system. The fluids that circulate through secondary loops are Water in one of them and a mixture of 44% Ethylene-Glycol and 56% Water (brine) in the other. Brine is a commonly used fluid in underground boreholes due to the very low freezing temperature. Heat transfer is given between primary and secondary loops inside the PHEX.

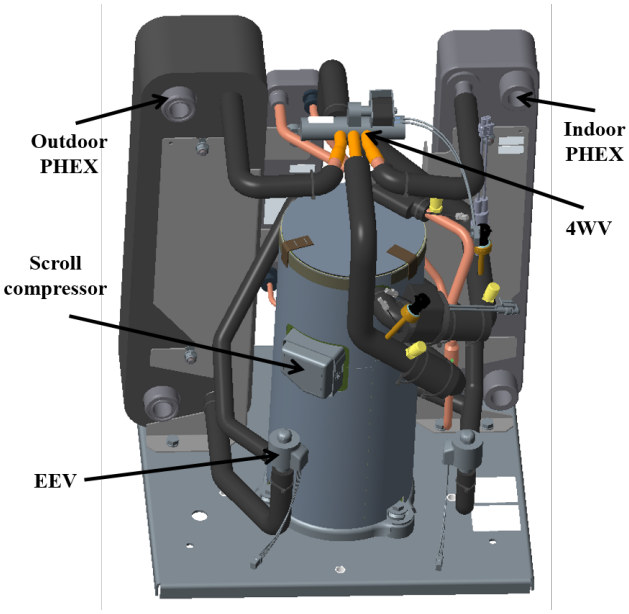

Figure 4.2: 3D image of the heat pump system.

Presented system has two working modes. One is the heating mode where the water is heated and the other one is the cooling mode, where the water is cooled down. During winter seasons, HP works in heating mode, heating the water to be used in space heating. Differently, during summer seasons, HP operates in cooling mode to produce cold water that is used mainly for space cooling.

The different components, fluids loops, measurements points and direction of the refrigerant fluid during both working modes of the system are depicted in Figure 4.3

The used compressor is a commercial fixed speed and displacement scroll compressor that receives the refrigerant fluid in the gas-phase at low pressure and temperature and compresses it increasing the pressure and, therefore, the temperature. Some technical specifications of the scroll compressor can be seen in Table 4.1.

The EEV receives the refrigerant either in liquid-phase or in two-phase at high pressure and expands it decreasing the pressure and temperature. Technical specifications of used EEV can be seen in Table 4.2.

Regarding plates heat exchangers, since the HP is reversible, both PHEX work indistinctly as a condenser and as an evaporator depending on the working mode of the system. PHEXs work always with the same secondary fluid regardless of the working mode. For differentiate them, the PHEX that is connected to the brine loop is the outdoor unit and the PHEX connected to the water loop is the indoor unit. Physical

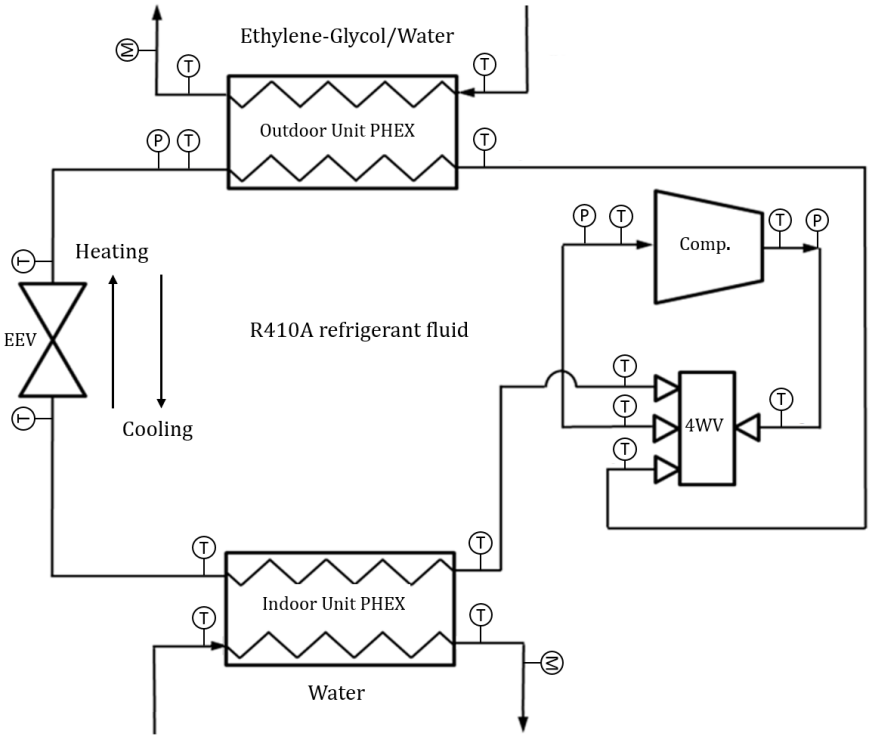

Figure 4.3: Scheme of the heat pump system.

Table 4.1: Specifications of the used scroll compressor.

Electric connection	220/240V 1 50Hz
Nominal heating capacity (kW)	5.0
Displacement (cm^3/rev)	19.34
$T_{evap} = -1°C$, $SH = 4°C$, $T_{cond} = 55°C$, $SC = 3°C$,	
Heating power (kW)	6.2
Absorbed power (kW)	2.03
COP	3.06
Refrigerant mass flow rate (g/s)	23.6

specifications of both PHEX are presented in Table 4.3.

The four ways valve is the component that allows the reversibility of the system. Depending on the working mode of the system, the inlets and outlets ports are internally connected in different ways. In Figure 4.4 the connections of the ports and the refrigerant fluid direction in the 4WV for both the heating and the cooling working modes are presented.

During the heating mode, the refrigerant that leaves the compressor goes into the

Table 4.2: Specifications of the used electronic expansion valve.

Maximum working pressure (kPa)	4700
Maximum working temperature (C)	70
Minimum working temperature (C)	-30
Operation range (pulses)	0 - 480
$T_{evap} = 5°C$, $SH = 0°C$, $T_{cond} = 38°C$, $SC = 0°C$,	
Nominal capacity (kW)	6.8

Table 4.3: Specifications of the used plate heat exchangers.

	Indoor Unit	**Outdoor Unit**
Plates number	26	30
Dimensions (cm)	50 x 10 x 6.2	50 x 10 x 7.1
Chevron angle (rad)	$\pi/4$	$\pi/4$
Primary fluid	R410A	R410A
Secondary fluid	Water	Brine
Total mass (kg)	6.35	7.01
Plates material	Stainless steel	Stainless steel

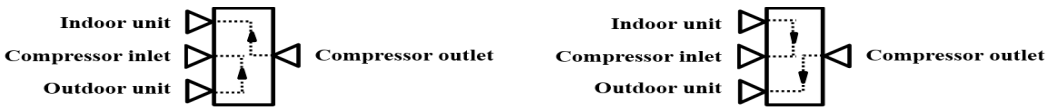

(a) *(b)*

Figure 4.4: Ports connections and refrigerant fluid direction in the 4WV during the heating (a) and the cooling (b) modes.

indoor unit through the 4WV. The indoor unit works as a condenser, so the water increases its temperature while the refrigerant is condensing. Once the refrigerant leaves the indoor unit, it is directed to the EEV and then to the outdoor unit, which works as an evaporator. The brine of the outdoor unit heats the refrigerant and evaporates it, and therefore, the brine temperature decreases. Finally, the refrigerant goes back to the compressor through the 4WV.

When 4WV switches, the system starts working in the cooling mode. The refrigerant reverses its direction, going from the compressor to the outdoor unit through the 4WV. Now, the outdoor unit works as a condenser, so the refrigerant is condensed while the brine is heated. Then it goes to the EEV and the indoor unit, which works as an evaporator, cooling down the temperature of the water. The cycle is closed when the

refrigerant reaches the compressor through the 4WV.

When the working mode changes, the direction of the refrigerant also changes, while the direction of the secondary fluids does not change. Because of this, the interaction between the refrigerant and the secondary fluid changes from counter-flow to parallel-flow or vice versa. It is widely known that a counter-flow connection has a better heat transfer performance than a parallel-flow connection [162, 163]. In the actual system, as the HP was optimized to work in the heating mode, both indoor and outdoor units are connected as counter-flow heat exchangers when the working mode is heating. In cooling mode, both of them are connected in parallel-flow.

In order to understand better the direction of the fluids inside the PHEX, Figure 4.5 shows the indoor PHEX connected in counter-flow (a) and parallel-flow (b). Similarly, the outdoor PHEX in counter-flow (a) and parallel-flow (b) is presented in Figure 4.6. In both PHEX, ports F1 and F2 are the inlet/outlet ports that corresponds to refrigerant fluid. Ports F3 and F4 correspond to the inlet and outlet ports of secondary fluid, respectively. The connections of the PHEX ports with the rest of the components of the system can be seen in Table 4.4.

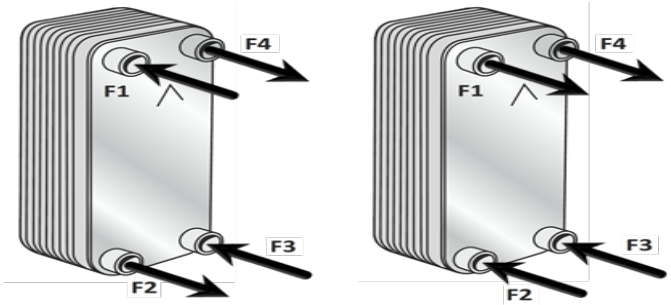

(a) *(b)*

Figure 4.5: Counter-flow (a) and parallel-flow (b) connection ports of the indoor PHEX.

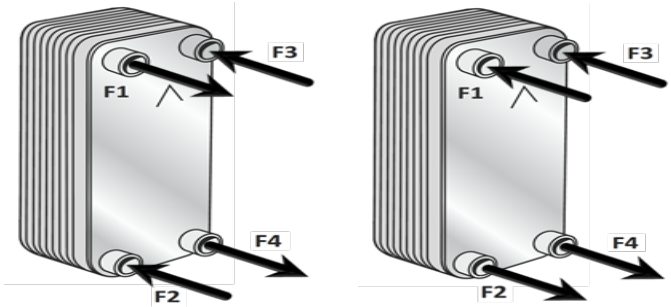

(a) *(b)*

Figure 4.6: Counter-flow (a) and parallel-flow (b) connection ports of the outdoor PHEX.

Table 4.4: Connections of PHEX ports.

		Refrigerant fluid		Secondary fluid	
		Port F1	**Port F2**	**Port F3**	**Port F4**
Cooling mode *(parallel-flow)*	**Indoor Unit**	Outlet to compressor	Inlet from EEV	Water inlet	Water outlet
	Outdoor Unit	Inlet from compressor	Outlet to EEV	Brine inlet	Brine outlet
Heating mode *(counter-flow)*	**Indoor Unit**	Inlet from compressor	Outlet to EEV	Water inlet	Water outlet
	Outdoor Unit	Outlet to compressor	Inlet from EEV	Brine inlet	Brine outlet

On the other hand, in order to decrease the refrigerant fluid mass flow maldistribution phenomenon described in the Section 3.5, a mass flow distributor is used. As the system was optimized for working in the heating mode, the distributor is located in the port F2 of the outdoor unit, which works as an evaporator during the heating mode. A second distributor could be placed in the port F2 of the indoor unit for the cooling mode. However, it is not recommendable to use two distributors because it would generate important pressure drops in the working mode that wanted to be optimized.

The climatic chamber closes the secondary fluid loops cooling down or heating secondary fluids. Regarding water loop, climatic chamber emulates the radiators or cooling systems. During the heating mode, when the water goes out from the indoor unit PHEX, it is cooled down before going back to the indoor unit. On the contrary, during the cooling working mode, the water is heated before going back to the indoor unit.

Regarding the brine loop, the climatic chamber also emulates subsoil boreholes or outdoor water reservoirs. During the heating working mode, brine needs to be heated before returning to the outdoor unit. Instead, in the cooling mode brine is cooled down.

Table 4.5 presents the specifications of the devices used to measure the fluids temperatures, refrigerant pressures and secondary fluids MFRs. Figure 4.3 shows their locations. Each measurement has a different purpose.

Table 4.5: Specifications of the utilized sensors.

Measurement	**Type**	**Uncertainity**
Refrigerant temperature	NTC Thermistor Sensor	$\pm 3\%$
Refrigerant pressure	Pressure sensor 0 – 4600 bar	$\pm 0.8\%$
Secondary fluids temperature	Pt 100 resistance measurers	± 0.1K
Secondary fluids mass flow rate	Flow meter 9 – 150 l/min	$\pm 1 - 2\%$

Secondary fluid sensors, both temperatures and MFR ones, were not located specific-

ally for this tests, they are fixed sensors incorporated in the climatic chamber. Therefore, the accuracy of the obtained data is high. Because of that, inlet temperatures and MFR will be used as inputs to the model and outlet temperatures will be used to validate the model.

Pressure sensors were located at the inlet and outlet pipes of the compressor, pricking the pipe. This data will also be used for the model validations.

On the other hand, the temperature sensors used to measure the refrigerant fluid temperatures were located in the external part of the refrigerant pipes, between the pipe and the insulation. Since the refrigerant fluid is a two-phase fluid and the temperature of the pipe is not the same in the part of the pipe where is the liquid part or the gas part of the fluid, this measurements were only used to figure out the conditions of the refrigerant cycle.

Finally, it also were measured the opening degree of the EEV and the power consumption of the system. The opening degree is taken directly from the control system of the HP and the power consumption is measured with a power meter.

Since the goal of this tests is to validate the model under transient situations and not to analyze the performance of the system, the power consumption of the system will not be used. The opening degree of the EEV will be used as an input to the model.

In table 4.6 is summarized the purpose of each measurement.

Table 4.6: Purposes of the taken measurements.

Measurement	**Purpose**
Refrigerant temperature	Figure out thermodynamic cycle
Refrigerant pressure	Model validation
Inlet secondary fluids temperature	Input to the model
Outlet secondary fluids temperature	Model validation
Secondary fluids mass flow rate	Input to the model
Opening degree of the EEV	Input to the model
Power consumption	-

The tests facility is regulated by a main control loop conditioned by two subordinated control loops. On the one hand, since it is using a fixed speed and displacement compressor, the refrigerant MFR is regulated by the EEV opening degree, which is controlled as a function of the refrigerant reheating at the compressor inlet port.

On the other hand, the climatic chamber regulates the secondary fluids inlet temperatures and MFR. When the set-point of one secondary fluid changes, firstly secondary fluid MFR is modified due to, unlike with the inlet temperature, it can be modified almost instantly. Therefore, since the MFR changes, the outlet temperature also changes. Then, as the inlet temperature goes changing, the mass flow rate recovers its initial value.

Later in this chapter it will be seen how the control systems affect differently to the system working conditions.

4.3 Tests procedure

In order to gather all possible operation conditions, different tests have been carried out. The aim of these tests is to force the system into sudden changes of the operation conditions.

Taking into account that the compressor is a fixed speed compressor, the different operation conditions of the system are limited to the operation conditions of the PHEX. Depending on the outlet fluid-phase of the refrigerant fluid, two working conditions have been differentiated in the condenser and another two in the evaporator. Additionally, it has been varied the set-point temperature of the secondary fluids.

In the aggregated, it has been carried out 14 tests under different working conditions. The methodology to develop each test has been the same and it will be described later in this section. Firstly, the operation conditions of each test will be presented.

4.3.1 Tests operation conditions

Tests conditions have been differentiated into two blocks. The first one regarding to the refrigerant conditions taking into account the refrigerant fluid outlet phases. The second one affects secondary fluids temperature conditions.

Refrigerant working conditions

Concerning refrigerant fluid working conditions, four situations have been taken into account. For a better understanding, regardless of the working mode of the system is heating or cooling, it will be differentiated between condenser and evaporator, not between indoor and outdoor PHEX. Additionally, it does not matter if the PHEX are in parallel- or counter-flow connections.

Regarding the condenser, two different working conditions can be given depending on the outlet refrigerant fluid conditions. In both of them, it is assumed that the fluid goes into the condenser from the compressor as superheated gas. The first working condition that can be found is when the condensing process is completely fulfilled and the refrigerant fluid goes out the condenser as a subcooled liquid with a certain degree of subcooling. This is the most common working condition during the normal operation of the system. Nevertheless, during starts-up or under uncommon external conditions, it can be given that the refrigerant fluid does not completely condensate and goes out from the compressor as a two-phase fluid. Both condenser situations can be seen in Figure 4.7.

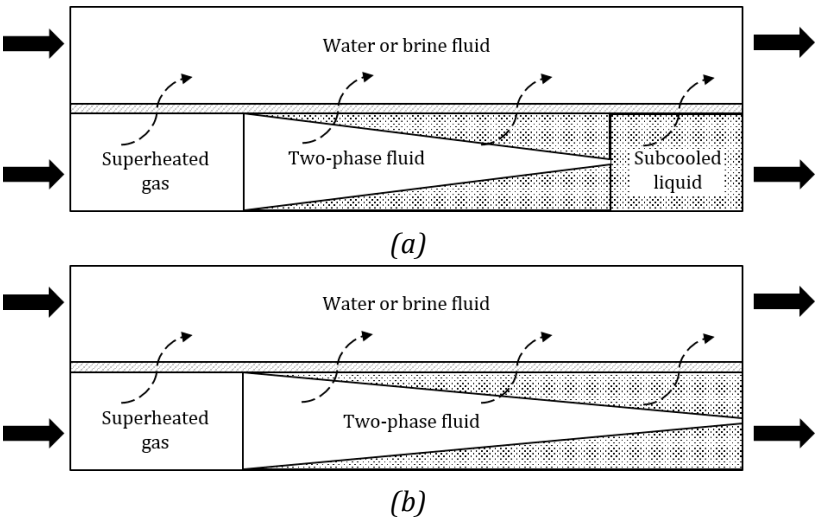

Figure 4.7: Refrigerant working conditions in the condenser. Three zones (a) and two zones (b) condenser.

Concerning the evaporator, another two different operation conditions can be differentiated. Although the most given situation is when refrigerant fluid goes out from evaporator as superheated gas, it also can be found situations in which it goes out as a two-phase fluid. In Figure 4.8, both operation conditions schematically are presented. In both cases, it is assumed that after the expansion of the refrigerant fluid in the EEV, the refrigerant is a two-phase fluid.

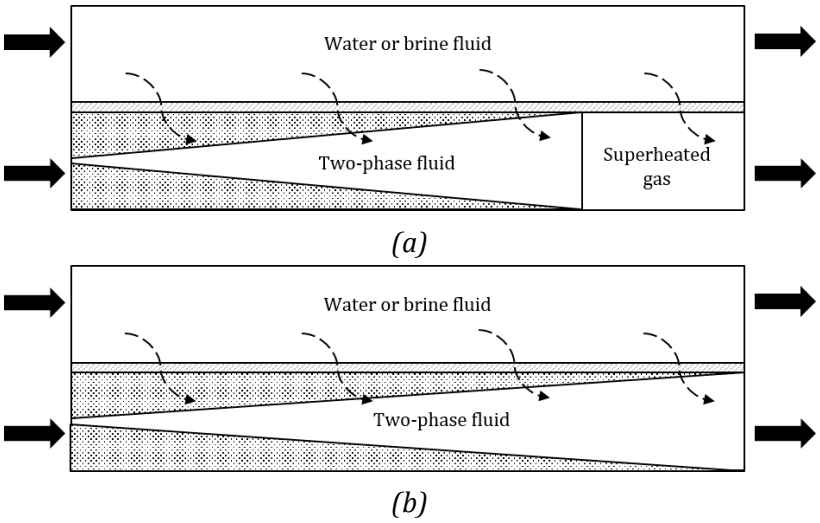

Figure 4.8: Refrigerant working conditions in the evaporator. Two zones (a) and one zone (b) evaporator.

A summary of the refrigerant tests conditions with the chosen nomenclature for this operation conditions can be seen in Table 4.7.

Table 4.7: Tests conditions and nomenclature regarding refrigerant conditions inside the PHEX.

Test condition	Nomenclature
Three zones condenser	C1
Two zones condenser	C2
Two zones evaporator	E1
One zone evaporator	E2

Secondary fluids working conditions

Now, the difference between each test is the set-point temperature of one of the secondary fluids. It is differentiated between the heating and the cooling working modes and between water and brine fluids.

In each test, a previously decided step is given in the outlet of one of the secondary fluids temperatures. That step is given by changing the set-point temperature of the corresponding secondary fluid. The water set-point temperature is referred to the temperature at the outlet of the PHEX. However, the brine set-point temperature is the inlet temperature.

All the initial and final set-point temperatures for each test are collected in Table 4.8. The highlighted cells indicate the secondary fluid in which the temperature change is

applied. The nomenclature for this conditions block is also presented. As can be seen, five types of tests are carried out in the heating mode and two types of tests in the cooling mode.

Table 4.8: Tests conditions and nomenclature regarding secondary fluids conditions.

Working mode	Nomenclature	Affected secondary fluid	Set-point temperature		
			Brine inlet (1)	Water conditions (1)	Conditions (2)
Heating	A	Water	0 °C	40 °C	35 °C
	B	Water	7 °C	50 °C	40 °C
	C	Water	-5 °C	35 °C	30 °C
	D	Brine	0 °C	35 °C	5 °C
	E	Brine	5 °C	45 °C	15 °C
Cooling	G	Brine	35 °C	8 °C	30 °C
	H	Water	30 °C	12 °C	8 °C

Tests summary

To sum up, in the heating mode, ten tests have been carried out. Six of them with a operation conditions step-change in the condenser (indoor unit) and four of them with the step-change in the evaporator (outdoor unit). On the other hand, in the cooling mode, two tests have been developed with a step-change in the condenser (outdoor unit) and another two with a step-change in the evaporator (indoor unit). The summary of developed tests can be seen tabulated in Table 4.9

4.3.2 Test methodology

Each presented test is compound of eight dynamic situations in which different dynamic situations are recorded. The recorded data for each situations is saved in a different file for its later data treatment and use. In Table 4.10 the dynamic situations that compound each test are presented. As can be seen, firstly the control of the system regulates the EEV position. Once the EEV position for each operation condition is known, the rests of the test are carried out with the control of the EEV switched off and regulating the EEV manually. In Figure 4.9 is presented the flowchart of the steps that were followed to carry out each test.

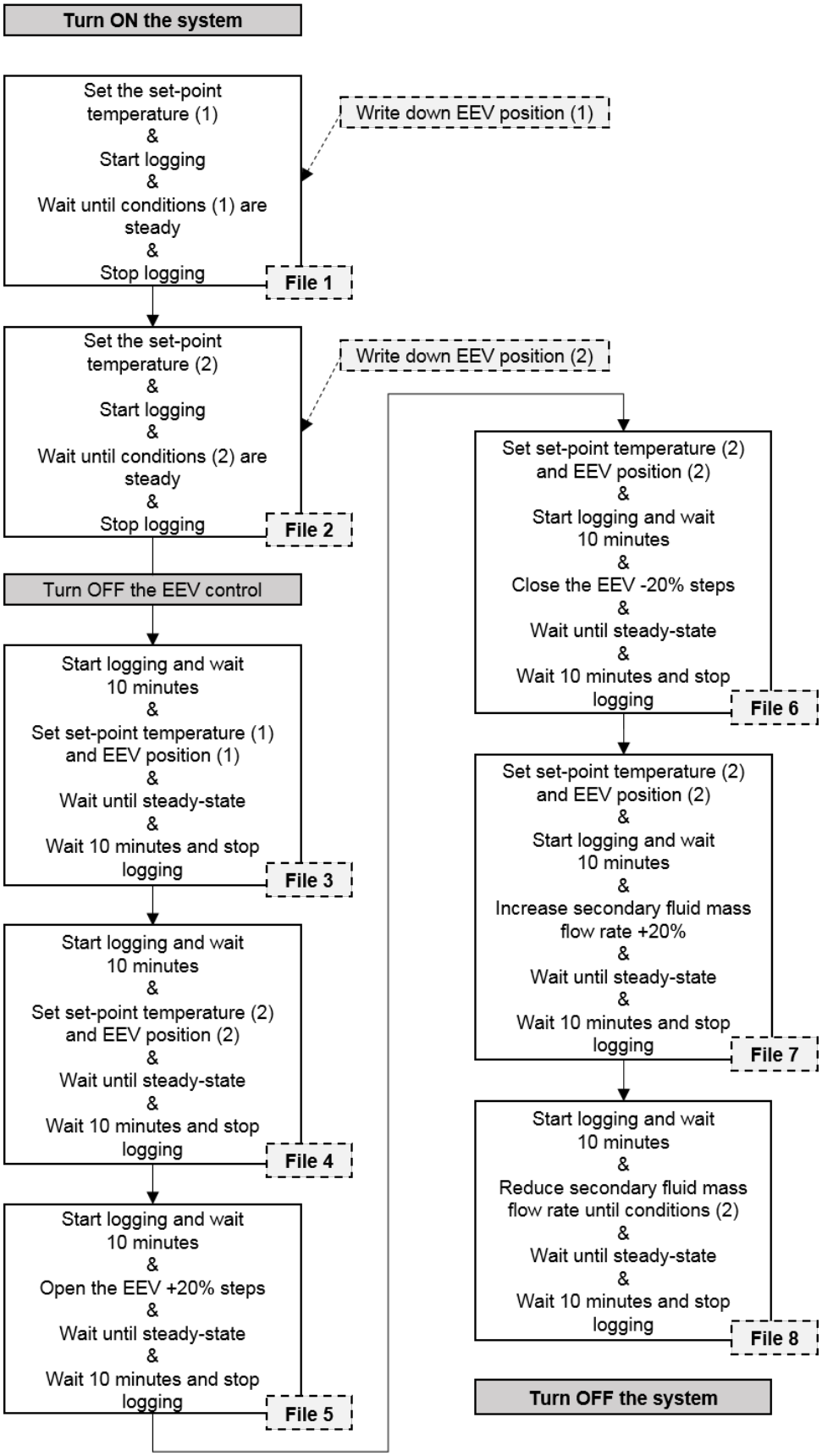

Figure 4.9: Flowchart of the steps followed to carry out each test.

Table 4.9: Summary of developed tests.

Working mode	Affected PHEX	Affected fluid	Refrigerant conditions	Nomenclature
Heating	Condenser (Indoor Unit)	Water	Three zones	A-C1
			Two zones	A-C2
			Three zones	B-C1
			Two zones	B-C2
			Three zones	C-C1
			Two zones	C-C2
	Evaporator (Outdoor Unit)	Brine	Two zones	D-E1
			One zone	D-E2
			Two zones	E-E1
			One zone	E-E2
Cooling	Condenser (Outdoor Unit)	Brine	Three zones	G-C1
			Two zones	G-C2
	Evaporator (Indoor Unit)	Water	Two zones	H-E1
			One zone	H-E2

Table 4.10: Data files for each dynamic situation.

Situations	Dynamic simulation
Situation 1	Start from equilibrium condition until reach set-point temperature (1) with the control of the system.
Situation 2	From set-point temperature (1) to set-point temperature (2) with the control of the system.
Situation 3	From set-point temperature (2) to set-point temperature (1) changing manually the EEV position.
Situation 4	From set-point temperature (1) to set-point temperature (2) changing manually the EEV position.
Situation 5	In operation conditions (2), increase manually the opening degree of the EEV in +20% to augment the refrigerant MFR.
Situation 6	In operation conditions (2), decrease manually the opening degree of the EEV position in -20% to reduce the refrigerant MFR.
Situation 7	In operation conditions (2), increase the secondary fluid MFR in +20%.
Situation 8	In operation conditions (2), reduce the secondary fluid MFR in -20%.

Each test starts switching on the HP and fixing the secondary fluids set-point temperature (1). The control loop of the system regulates the opening degree of the EEV until

reaching the steady-state for the operation conditions (1). The first data file is generated and the current positions of the EEV (1) is written down.

From the steady-state of conditions (1), the set-point temperature of the correspondent secondary fluid for that test is changed to the set-point temperature (2). When the steady-state of the operation conditions (2) is reached, the second data file is saved and the current position of the EEV (2) is written down.

Now, the EEV positions for both operation conditions are known so the EEV control system is switched off in order to move the EEV positions manually during the rest of the test.

The third file is generated starting in the operation conditions (2) and finishing in operation conditions (1) moving manually the EEV position. Equally, the fourth file saves the transient from conditions (1) to conditions (2) moving manually the EEV position.

Starting in the operation conditions (2), fifth and sixth data files are gotten by increasing or decreasing 20% the opening degree of the EEV. It produces an augmentation or reduction of the refrigerant MFR producing a transient-state.

Finally, the last two transients are reached by maintaining the set-point temperature (2) and EEV position (2) fixed and increasing or decreasing 20% the MFR of the corresponding secondary fluid. After that, the HP is turned off and the test is finished.

4.4 Test results

During this section, taking as reference the test B-C1, test results will be presented.

As explained previously, different transient-states were forced, dividing each test in eight transient situations.

On the other hand, it has been presented the measurement equipment and told that the pressures and secondary fluids temperatures will be the data that will be used to validate the model. Refrigerant temperatures at different points of the circuit will only be used to get an idea of the refrigerant fluid working conditions.

The duration of the different situations are not equal since it depends on the time requested by the system to reach the stationary state after the transient forced state. For instance, situations 7 is shorter than situation 3 since the forced transient state is less

aggressive. In the following figures, each dynamic situation is separated by dashed lines and enumerated in correspondence with Table 4.10.

In Figure 4.10 the EEV opening degree during B-C1 test is presented. In situations 1 and 2 it can be appreciated that the system regulates gradually the valve opening by means of the control of the system. In the situations 3-6 the control is switched off and the EEV is regulated manually to the required opening degree for each operation condition. In the situations 7 and 8, the opening degree of the EEV does not change.

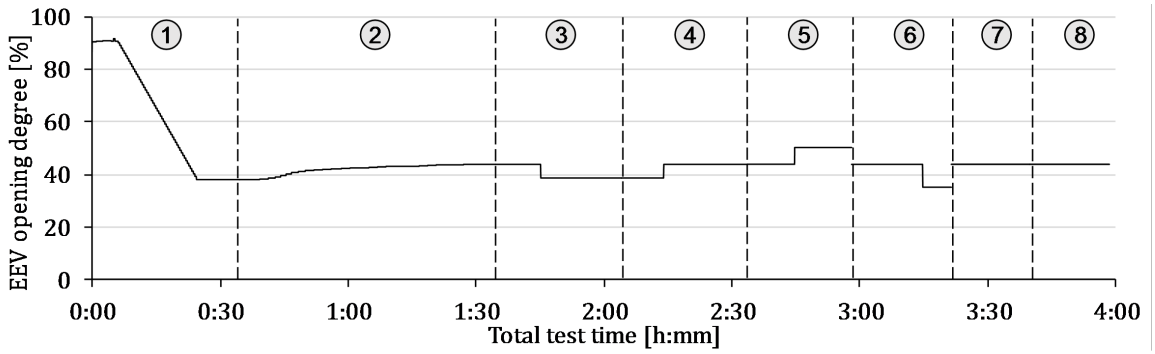

Figure 4.10: Opening degree of the EEV during the different situations of the test B-C1.

In Figure 4.11 the condensation and evaporation pressures are presented.

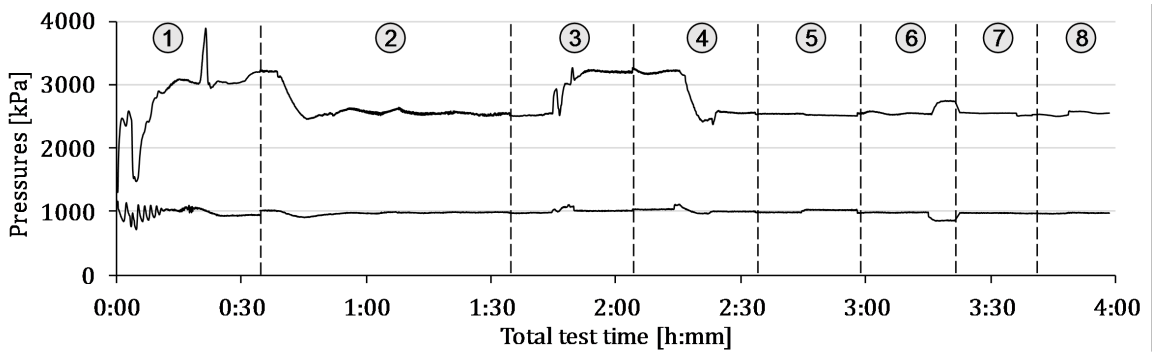

Figure 4.11: Condensation and evaporation pressures during the different situations of the test B-C1.

In Figure 4.12 the inlet and outlet temperatures of the water are presented. During this test the system is working in the heating working mode, so the indoor PHEX works as a condenser. Similarly, In Figure 4.13 the inlet and outlet temperatures of the brine are presented. The outdoor PHEX works as an evaporator.

From Figures 4.11, 4.12 and 4.13 can also appreciate how the temperatures of the system are initially in thermal equilibrium with the ambient and how the pressures of the refrigerant in the condenser and evaporator are equalized.

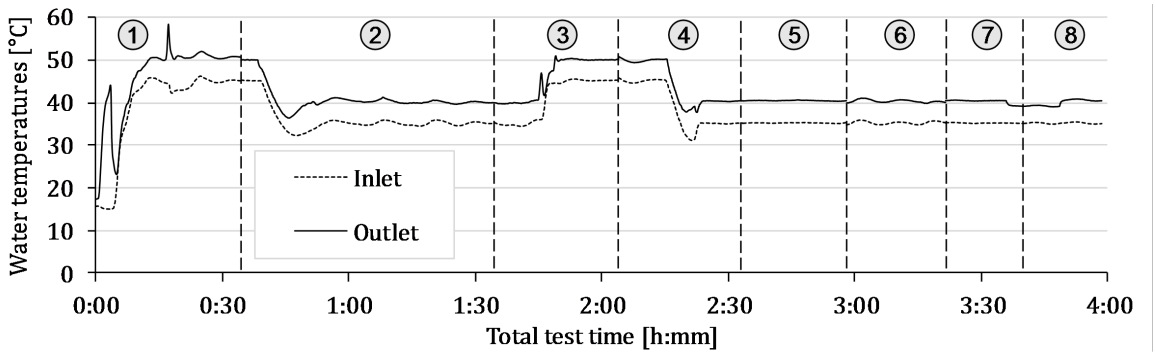

Figure 4.12: Water temperatures in the inlet and outlet ports of the indoor PHEX (condenser) during the different situations of the test B-C1.

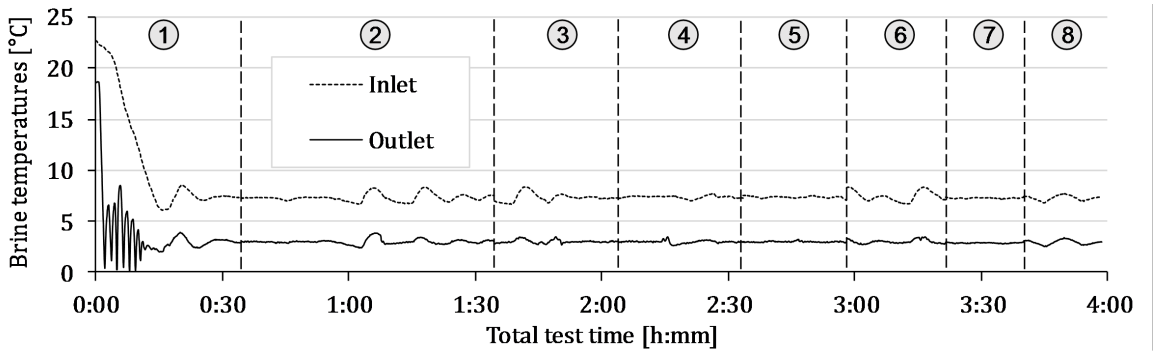

Figure 4.13: Water temperatures in the inlet and outlet ports of the outlet PHEX (evaporator) during the different situations of the test B-C1.

As advanced in the final part of Section 4.2, the effect in the operation conditions of the system is differently affected by the two control loops. For instance, lets take situations 3, 5 and 7 of Figures 4.10 - 4.13. In situation 3, where both EEV opening degree and secondary fluids conditions change, the working conditions change. However, in situation 5, the opening degree changes but the secondary fluid conditions remain constant. It results in almost null variation in the system working conditions. In situation 7, the opposite happens, opening degree remains constant and the MFRs of one secondary fluid changes. In this case, the system working conditions are slightly modified.

Therefore, if the opening degree of the EEV is modified within a moderate percentage from its corresponding degree but the rest of the regulation conditions remain constant, the system working conditions are hardly affected. However, it must be said that the control loop that regulated the opening degree of the EEV is essential for an optimized system, affecting mainly the refrigerant subcooling, reheating and system performance [164–166].

Now, some results regarding the refrigerant temperatures will be presented. It has been chosen the situation 4 of the test B-C1. Nevertheless, before showing measure-

ment results, some comments must be given.

As explained before, this HP was initially optimized to work in heating mode. Therefore, when the system is working on heating mode, both the indoor and outdoor PHEX are connected in counter-flow. During the test B-C1 the system works in heating mode.

On the other hand, the temperatures correct distribution inside a counter-flow condenser and evaporator are shown schematically in Figure 4.14. As can be seen, regarding the evaporator, at any moment, the brine outlet temperature must be higher than refrigerant inlet temperature and brine inlet temperature must be higher than refrigerant outlet temperature. Similarly, during the condensation, water outlet temperature must be lower than refrigerant inlet temperature and water inlet temperature must be lower than refrigerant outlet temperature.

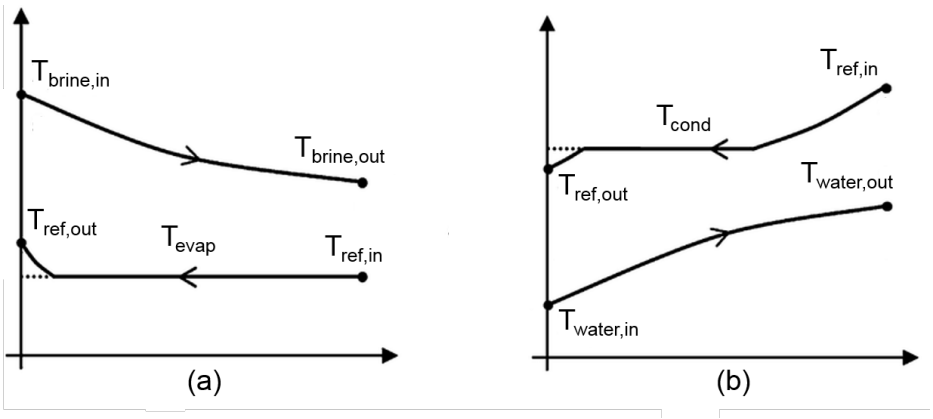

Figure 4.14: Correct temperatures distribution inside a counter-flow evaporator (a) and condenser (b).

Going back to measurements results, Figure 4.15 shows the inlet and outlet temperatures of both water and refrigerant fluids in the indoor unit (condenser) along the situation 4 of the test B-C1. Equally, Figure 4.16 shows the temperatures in the outdoor unit (evaporator).

As can be seen, in both PHEX there is an incorrect distribution of the temperatures. In the indoor unit, which works as a condenser, the inlet water temperature should be lower than outlet refrigerant temperature, but it does not happen. Similarly, in the evaporator, during much of the time, the outlet refrigerant temperature is higher than the inlet brine temperature. It is not possible if the heat flux is supposed to go from the brine to the refrigerant.This kind of situations are repeated many times during the different tests and situations.

Moreover, as explained in the previous section, the sensors utilized to measure the

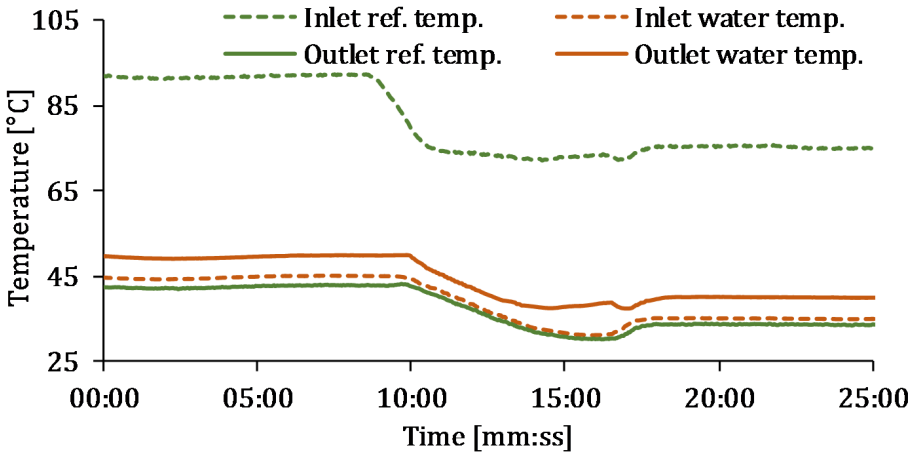

Figure 4.15: Indoor unit (condenser) inlet and outlet temperatures of both water and refrigerant fluids in situation 4 of the test B-C1.

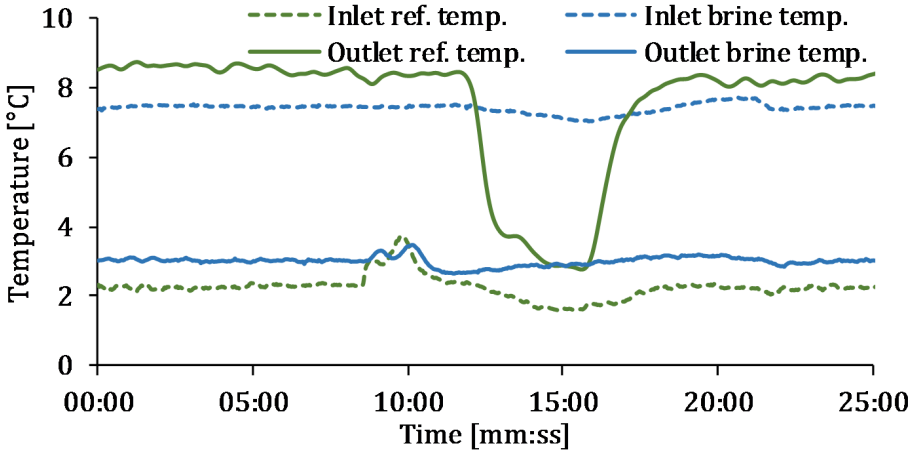

Figure 4.16: Outdoor unit (evaporator) inlet and outlet temperatures of both brine and refrigerant fluids in situation 4 of the test B-C1.

water and brine temperatures are much accurate that the ones utilized to measure the refrigerant temperatures. Consequently, and as it was asserted previously, the refrigerant temperatures measurements will only be used to figure out the thermodynamic cycles but not for the model validation.

4.5 Model specific considerations

In the Chapter 3 it has been presented the physics-based model developed to simulate a liquid-to-liquid HP. However, additionally to the equations, some complementary information must be added to the model depending on the HP that wanted to be simulated, as explained in 3.5.

Now, the specific information that was taken into account to simulate the actual HP will be given.

PHEXs discretization: The PHEX discretization was studied in order to find which is the number of FCV that should be used to reach a good agreement between computational time and results accuracy. Here, it is presented the study carried out with the situation 6 of test C-C2 by increasing the number of FCVs in the PHEXs from 5 to 100. These results were similar for other studied tests and situations.

Figure 4.17 shows the differences in the condensing pressure calculation using a different number of finite volumes. Although the simulation time was 1200 seconds, in the image only is shown the period where the transient occurs in order to perceive better the differences. Figure 4.18 shows the Real Time Factor (RTF) for different number of FCVs.

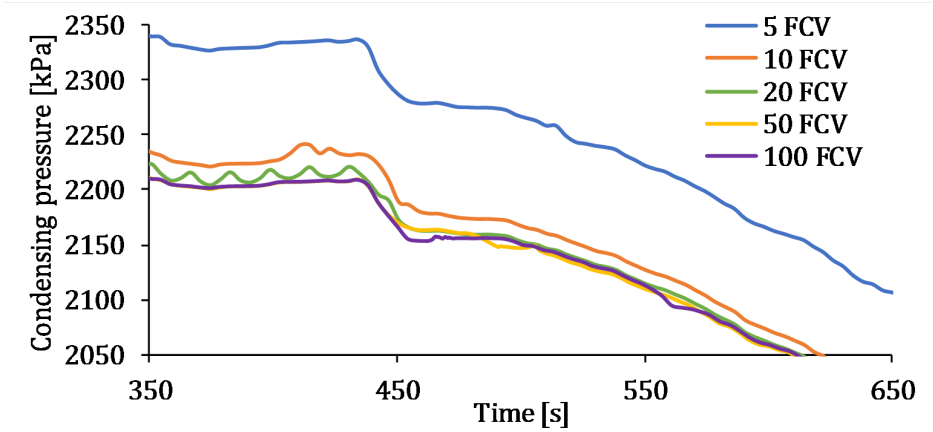

Figure 4.17: Condensing pressure with different numbers of finite control volumes.

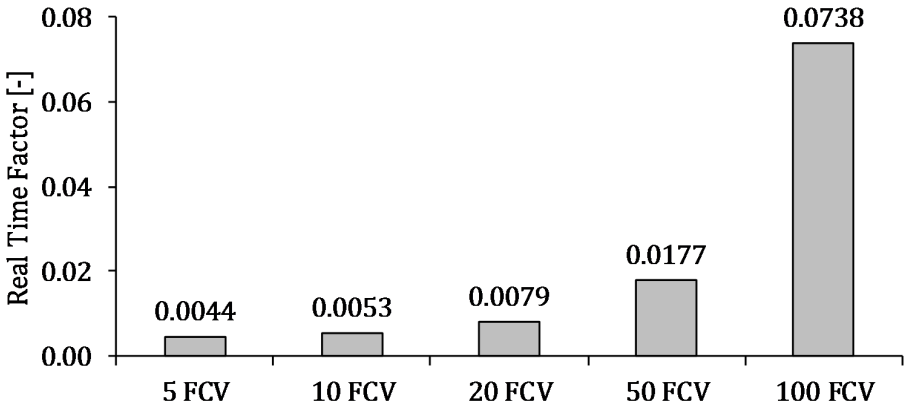

Figure 4.18: Real Time Factor for different numbers of finite control volumes.

As can be appreciated in Figure 4.17, the shape of the system dynamic is well followed, even with a low number of FCVs. Nevertheless, the numerical results do not accurately fit with a low number of FCVs. With ten FCVs, the results can be improved. The numerical results are accurate enough once the number of FCVs are equal or higher than twenty. Regarding the computational time, the RTFs remains low up to 20 FCVs and increases greatly with 100 FCVs.

Therefore, the micro-scale simulations will be carried out discretizing each PHEX into 20 FCVs.

Fluid tables: As explained in Section 4.2, the refrigerant fluid is R410A while the secondary fluids are water in the indoor PHEX and brine in the outdoor PHEX. The needed fluid tables were taken using CoolProp [152].

Nusselt number correlations: For both brine and water, Dittus-Boelter correlations [167] are used to calculate the Nusselt number. Regarding refrigerant fluid, for one-phase HTC, Dittus-Boelter correlation is used. Besides, the correlations presented in Han et al. [158, 168] are used for the two-phase HTC calculation. Evaporation and condensation Nusselt number presented correlations are specific empirical correlations for R410A refrigerant fluid.

In Equations 4.1, 4.2 and 4.3 are presented the one-phase, condensation and evaporation used correlations, respectively. Equation 4.1 is also used for brine and water calculations.

$$Nu = 0.0023\, Re^{0.8}\, Pr^{m} \tag{4.1}$$

Where the exponent of Prandtl number is $m = 0.3$ when the fluid is cooled down and $m = 0.4$ when the fluid is heated.

$$Nu = C_1\, {Re_{Eq}}^{C_2}\, Pr^{0.3} \tag{4.2}$$

$$Nu = C_3\, {Re_{Eq}}^{C_4}\, Pr^{0.4}\, {Bo_{Eq}}^{0.3} \tag{4.3}$$

Where $Re_{Eq} = \dfrac{G_{Eq}\, D_h}{\mu_f}$, $Bo_{Eq} = \dfrac{q}{G_{Eq}\, h_{fg}}$ and C coefficients are non-dimensional geometric parameters presented in Table 4.11.

Table 4.11: C coefficients correlations.

$C_1 = 11.22 \left(\frac{p_{co}}{D_h}\right)^{-2.83} \left(\frac{\pi}{2} - \beta\right)^{-4.5}$
$C_2 = 0.35 \left(\frac{p_{co}}{D_h}\right)^{0.23} \left(\frac{\pi}{2} - \beta\right)^{1.48}$
$C_3 = 2.81 \left(\frac{p_{co}}{D_h}\right)^{-0.041} \left(\frac{\pi}{2} - \beta\right)^{-2.83}$
$C_4 = 0.746 \left(\frac{p_{co}}{D_h}\right)^{-0.082} \left(\frac{\pi}{2} - \beta\right)^{0.61}$

Compressor efficiencies: The volumetric efficiency and the isentropic efficiency of the compressor are calculated as a function of the pressure ratio ($r = P_{comp,out}/P_{comp,in}$).

The curves of both efficiencies are fitted using the information provided by the manufacturer. While the irreversibilities inside the compressor are measured with the isentropic efficiency, which is directly provided by the manufacturer, the friction and mechanical losses are given by the volumetric efficiency. The curve of the volumetric efficiency was fitted using Equation 4.4, which relates the MFR provided by the manufacturer and the MFR calculated analytically with Equation 4.5 for different operation conditions. Table 4.12 presents the equations and R^2 value of both efficiencies correlations.

$$\eta_{vol} = \frac{\dot{m}_{manufacturer}}{\dot{m}_{analitic}} \tag{4.4}$$

$$\dot{m}_{analitic} = \rho_{in} \cdot V_{comp} \tag{4.5}$$

Table 4.12: Equation and R^2 value of volumetric and isentropic efficiencies correlations.

	Volumetric efficiency	**Isentropic efficiency**
Eq.	$\eta_{vol} = 0.005r^2 - 0.099r + 1.176$	$\eta_{ise} = 0.006r^2 - 0.085r + 0.794$
$\boldsymbol{R^2}$	0.926	0.883

EEV coefficient: The valve coefficient depends on the EEV that it is using. For this case, Figure 4.19 shows the C_v used in the presented system, whose data have been provided by the manufacturer.

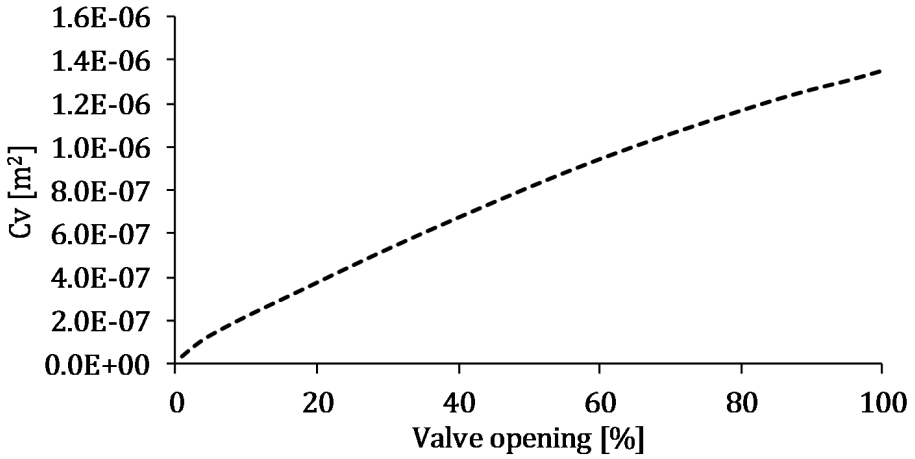

Figure 4.19: Valve coefficient in function of the valve opening.

Components dimensions: The physical specifications of the used PHEXs and compressor are described in Tables 4.3 and 4.1, respectively.

Refrigerant mass flow rate distributor: As described in the Section 4.2, a mass flow distributor was located in the inlet port of the evaporator during the heating mode, to reduce the maldistribution phenomenon. This distributor causes a pressure drop in the refrigerant fluid that must be taken into account during the simulations.

As shown in Figure 4.3, the refrigerant pressure has been measured in three locations: inlet of the compressor, outlet of the compressor and in the pipe that connects the EEV and the outdoor unit PHEX. During the heating mode, assuming that the pressure drops inside PHEXs are negligible, the pressure difference between the inlet of the compressor and the EEV-PHEX connection is the pressure drop generated by the mass flow distributor. That pressure drop has been calculated and taken into account in the EEV calculations. During the cooling mode, there is not a mass flow distributor in the inlet port of the evaporator so only the compressor outlet and inlet pressures are taken into account for the calculations.

Heating and cooling separated interfaces: As seen in Section 3.4, the developed model is able to simulate both the heating and the cooling modes without changing the components. Nevertheless, as explained in Section 3.4.6 it must be manually changed the connections between components to simulate one working mode or the other.

4.6 Validation of the model in micro-scale

Now, the validation of the model under micro-scale transient situations will be presented. It is presented for the heating mode, the cooling mode and during a heating start-up with the situation 4 of C-C2, 3 of G-C1 and 1 of C-C2, respectively. Although these situations were chosen as the representative ones, other comparisons between test data and simulation results are presented in Annex III.

For the validation of the model, it will be taken into account the similarity of the graphics, that indicates if the model follows the dynamics of the system, and the Normalized Error (NE), which shows the numerical divergence between test data and simulation results. NE will be calculated with Equation 4.6.

$$NE = \frac{\sum_{k=1}^{end}(simulation(k) - experimental(k))^2}{\sum_{k=1}^{end}(experimental(k))^2} \tag{4.6}$$

4.6.1 Heating mode validation

Heating mode validation will be given with the situation 4 of test C-C2. During the heating mode, the indoor unit works as a condenser and the outdoor unit as an evaporator. Both are connected in counter-flow.

Water set-point temperature is initially placed at 35°C and is changed to 30°C. The brine set-point temperature remains constant throughout the entire test at -5°C.

Figure 4.20 shows the simulated high and low working pressures compared with test data. As can be seen, the simulation results accurately fit the experimental data. NEs between simulation results and experimental data for the pressure in the outdoor and indoor units are 1.16e-04 and 1.09e-03, respectively.

The comparison for both secondary fluid temperatures is presented in Figure 4.21. The inlet temperature of both secondary fluids has also been drawn. As it has been used as an input in the simulation software, both experimental and simulation inlet temperatures of secondary fluids are the same. The NE of the simulation results with respect to experimental data for the water outlet temperature is 1.83e-04 and for the brine outlet temperatures is 2.72e-03.

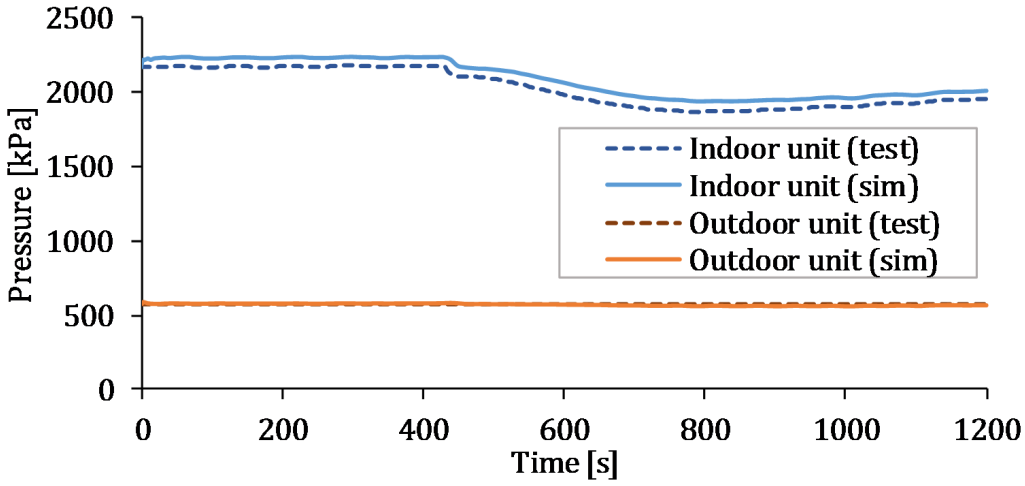

Figure 4.20: Test data and simulation results of the refrigerant pressures during heating mode.

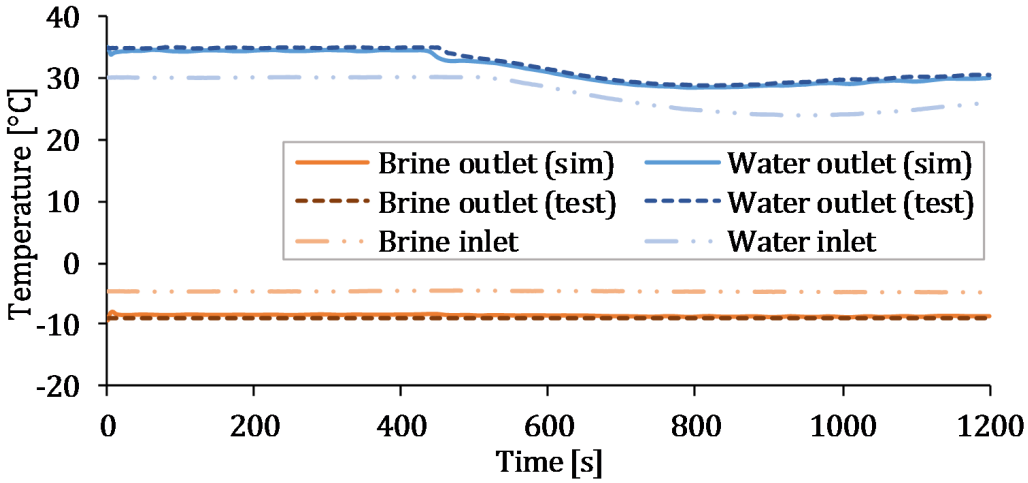

Figure 4.21: Test data and simulation results of water and brine temperatures during heating mode.

4.6.2 Cooling mode validation

Cooling mode validation will carried out with the situation 3 of the tests G-C1. The indoor unit works as an evaporator and the outdoor unit as a condenser. In addition, their connections are in parallel-flow.

In this case, the step in the set-point temperature is in the outdoor unit. Brine set-point temperature starts at 30°C and finishes at 35°C. The water set-point temperature remains constant at 7°C.

The comparison between test data and simulations for refrigerant working pressures and secondary fluid temperatures are presented in Figure 4.22 and Figure 4.23, respectively.

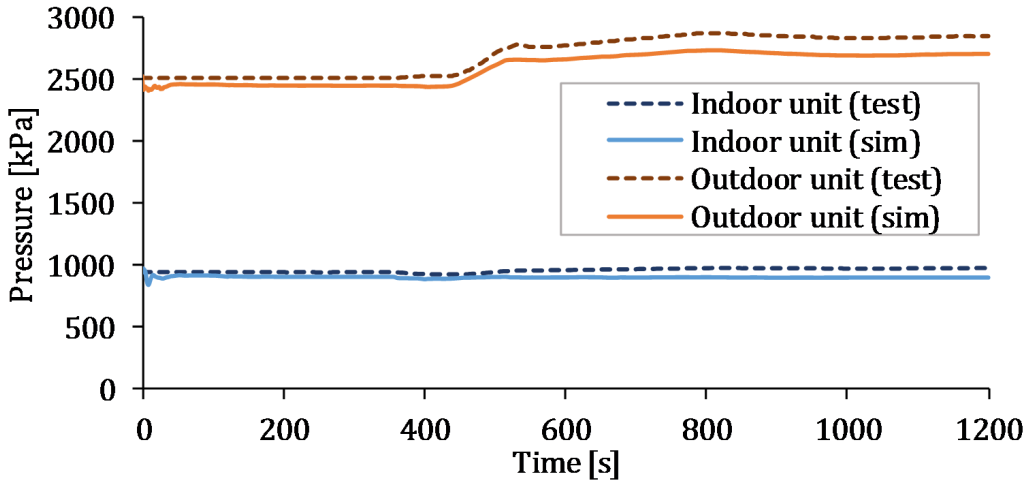

Figure 4.22: Test data and simulation results of the refrigerant pressures during cooling mode.

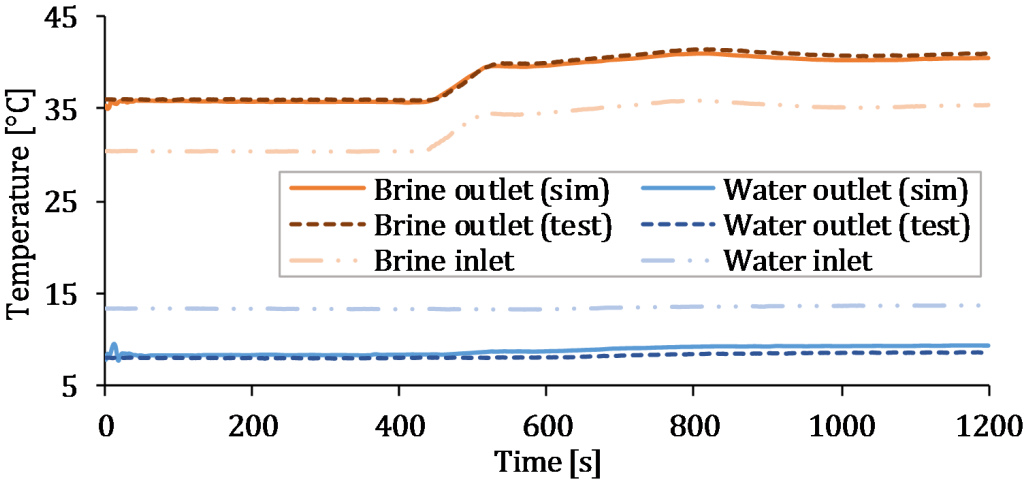

Figure 4.23: Test data and simulation results of water and brine temperatures during cooling mode.

The NE between simulation results and experimental data for the pressure in the outdoor and indoor units are 1.97e-03 and 3.26e-03, respectively. Regarding secondary fluid outlet temperatures, the normalized error is 8.60e-05 for the water and 5.69e-03 for the brine.

4.6.3 System start-up validation

The start-up of the system has also been validated. Here, it will be taken as example the situation 1 of the test C-C2. The start-up is during the heating mode.

Starting from an almost equilibrium conditions, the set-point temperatures are fixed in 35°C for water and -5°C for brine. As explained during the Section 4.3.2, situation

1 is carried out with the control of the HP switched on. Test and measurements go on until the steady state is reached.

Figure 4.24 shows the simulated high and low working pressures compared with test data. Figure 4.25 compares the secondary fluids temperatures.

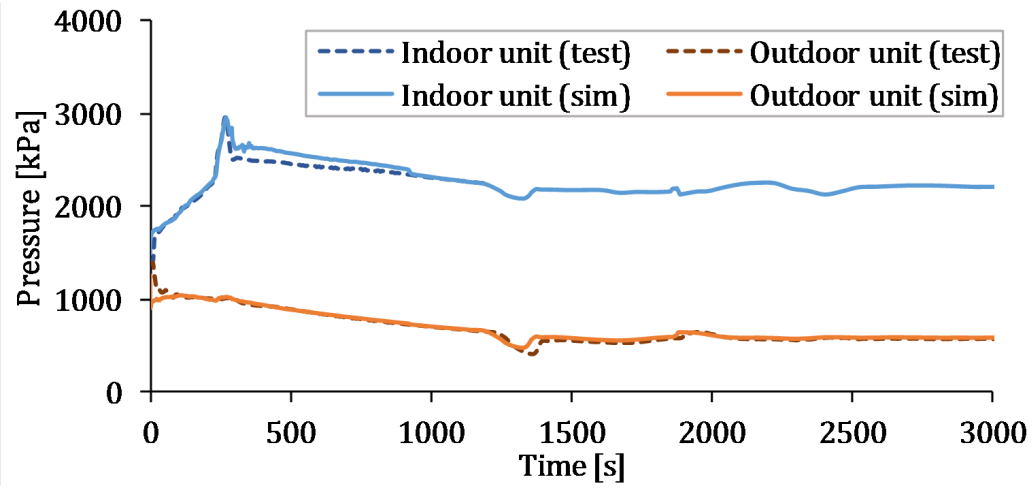

Figure 4.24: Test data and simulation results of the refrigerant pressures during an start-up situation in heating mode.

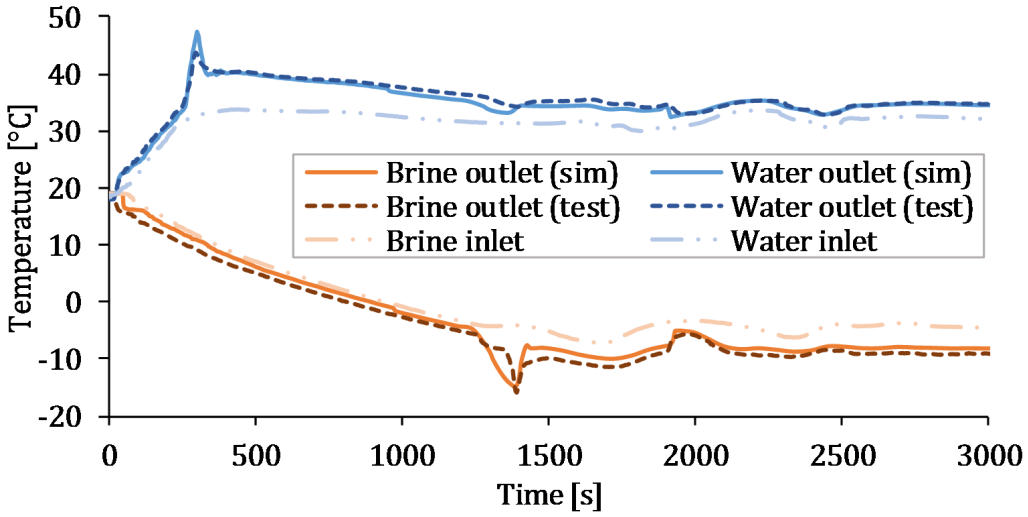

Figure 4.25: Test data and simulation results of water and brine temperatures during an start-up situation in heating mode.

The NE of refrigerant pressures in the outdoor and indoor units are 4.33e-03 and 2.02e-03, respectively. Regarding secondary fluid outlet temperatures, the normalized error is 2.56e-03 for the water and 3.18e-03 for the brine.

As can be seen, although there are some differences between test measurements and

simulation results, the model simulates fairly accurately the transient-states during the system start-up.

4.7 Switching mode simulation

Once the model has been validated in cooling and heating modes separately and also during the start-up of the system, now it will be presented the capability of the model to simulate the switching mode operation.

In a switching mode operation, the system change the working mode from cooling to heating or vice-versa. As explained during the Section 1.2.1, in a liquid-to-liquid HP the switching mode is given, for instance, when the system is working in the cooling mode and, in a given time, it changes to work in the heating mode. In fact, the aim is to simulate a summer period in which, during cooling supply for it use in a refrigeration systems, a demand for DHW is given. After the demand has been covered, the system returns to the cooling mode.

In the actual system, when a switching order is given, firstly the compressor stops working. Then, both indoor and outdoor PHEX pressures are equalized through the EEV. The EEV, which is initially in a given degree of opening, is then opened completely in order to ease the pressure equalization. When the pressures are equalized, the control of the system switches the internal connections of the 4WV and the refrigerant cycle is inverted. At that moment, the compressor is switched on again and the EEV returns to the opening degree commanded by the system control loop. In this case, as in the model the 4WV is expendable, the switches in the connections are given internally in the component blocks.

Input conditions to the system will remain constant throughout the simulation. Being the inlet water temperature 20°C, inlet brine temperature 12°C and the MFR of both water and brine 0.25 kg/s. They have been chosen arbitrary. Nevertheless, 20°C is an acceptable tap water temperature during the summer in a mild weather location and 12°C for the subsoil temperature supposing a vertical ground heat exchanger. Regarding the EEV, it starts working at 45% of the opening grade. When the compressor is switched off, the EEV is fully opened in order to ease the equalization of the pressures. Once the system starts working again, it returns to the previous 45% of the opening grade.

For the simulation, the steady state reached during the cooling mode for given inputs is firstly simulated. After some time, the order to change to the heating mode is given. This order is transmitted to the compressor, which stops working, and to the EEV, which is completely opened to ease the pressures equalization. Once the pressures are equalized, the working mode is switched, the EEV returns to is correspondent opening degree and the compressor starts working again. After some time in the heating mode, the order switching is again given and the system returns to the cooling mode following the same steps before described.

It must take into account that reproducing this switching conditions in a laboratory might not be possible. In fact, in the presented facilities it was not possible.

4.7.1 Reversible model consideration

In Simulink, the connections between blocks are unidirectional. One signal (or signal bus) from an outlet port of one component is sent to one inlet port of the next block and can not be inverted during a simulation. Because of that, as seen in Section 3.4, the difference between the cooling and the heating mode models is the connection between blocks.

Nevertheless, for a reversible simulation in which both working modes wanted to be simulated, the interface and block connections before presented are not valid. Because of that, it is developed a reversible model in which the heating and cooling modes can be simulated in the same simulation.

This model can also be used for single working mode simulations. Moreover, since the model presented in the Chapter 3 and the specific considerations for the actual HP systems presented in 4.5 are the same, the results using one model or the other are equals.

The additional needs of the reversible mode and the differences between reversible and non-reversible models will be now presented.

Components connections: In the non-reversible model presented in Section 3.4, the inlet refrigerant properties port is connected directly with its corresponding anterior block. Nevertheless, in the reversible model, the inlet refrigerant properties port of

each component is duplicated and connected with both anterior and posterior components. Then the correct signal is chosen in function of the working mode of the system.

This must be done because as explained at the beginning of Section 3.4, each component needs to known the pressure or MFR of the anterior and posterior block to solve its respective equations. Moreover, as the model will simulate both working modes at the same simulation, each block need to be fed with both possible refrigerant inlet properties and then, depending on the working mode, use the correct ones.

In Figure 4.26 can be seen the blocks used for the reversible model. There are two differences with the non-reversible model. The first one is that the Mode input port has been added to the compressor and EEV blocks. Secondly, the ”Flow in” and ”Up-stream refrigerant mass flow rate” or ”Up-stream pressure” input ports are substituted by ”Flow in from compressor” and ”Flow in from EEV” or ”Flow in from indoor unit” and ”Flow in from outdoor unit”. During the simulation, the correct signal will be chosen depending on the current working mode.

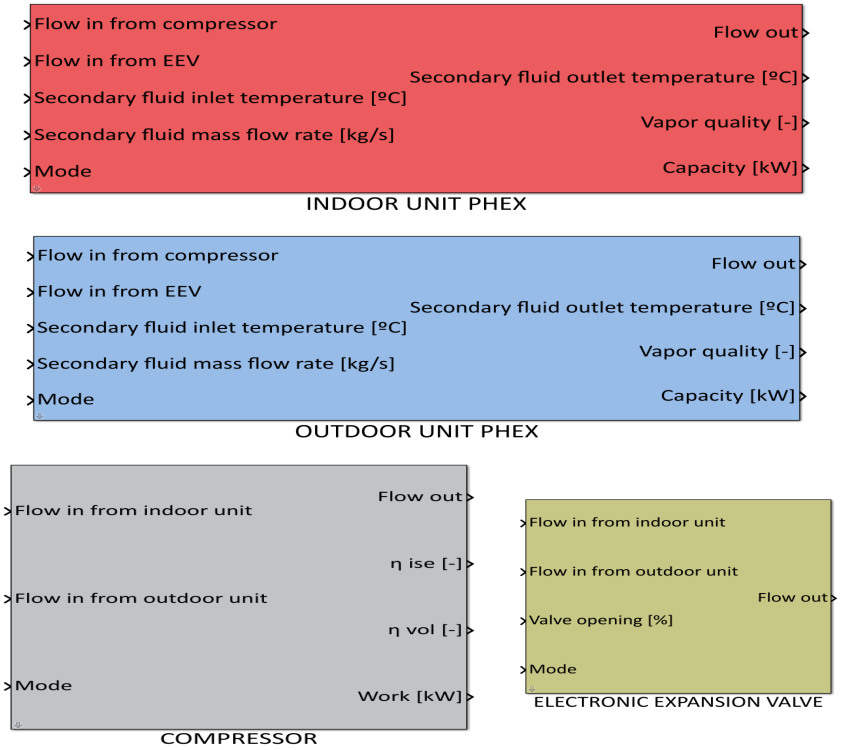

Figure 4.26: Reversible model blocks interface.

Compressor stop and start-up: In the actual system, to carry out a working mode switch, the compressor must be firstly stopped. Nevertheless, there is not information available about the time that is needed from the stop command is given until the compressor completely stops. Moreover, in the simulations, if the compressor is tried to be completely stopped instantaneously in a given time, a discontinuity is given and the simulation stalls. Because of that, according to size of the compressor, it has been assumed that the compressor takes three seconds to completely stop working and another three seconds to completely re-start it.

Working mode switching: Reversible model must be capable to switch between the heating and the cooling modes when is required. After the switching signal or command is given, firstly the compressor stops working, then the pressures are equalized and finally the working mode switch is given. After that, the system re-start working.

In the simulation, indoor and outdoor unit pressures are compared. If the indoor unit pressure is higher than the outdoor unit one, the system is currently working in the heating mode and vice versa. During the equalization of the pressures, when the difference between them is less than 5 kPa, the working mode is inverted. Then, the compressor starts working again.

Refrigerant mass flow rate distributor: As said in Section 4.5, in the current system, the mass flow distributor is only used during the heating mode. In the model, a fixed pressure drops due to the distributor are taken into account in the EEV block calculations during the heating mode. In the cooling mode they are avoided.

Computational height: Although the reversible model can carry out single working mode simulations and the obtained results are equal, the computational height of the reversible model is higher than the non-reversible one. It is due to at each step time, in each component, which is the correct signal depending on the working mode must be chosen. Therefore, the required time to carry out the same simulation is approximately three times higher.

Thus, the reversible model is recommendable only to simulate switching working modes. Otherwise, it is better to use non-reversible mode to simulate single working mode simulations.

4.7.2 Results:

It has been simulated the switching mode operation from the cooling mode to the heating and back to the cooling mode following the conditions described in Section 4.7. In Figure 4.27 is presented the time in which the system is working in heating and cooling modes. It also is marked the moments in which the compressor is stopped and re-started.

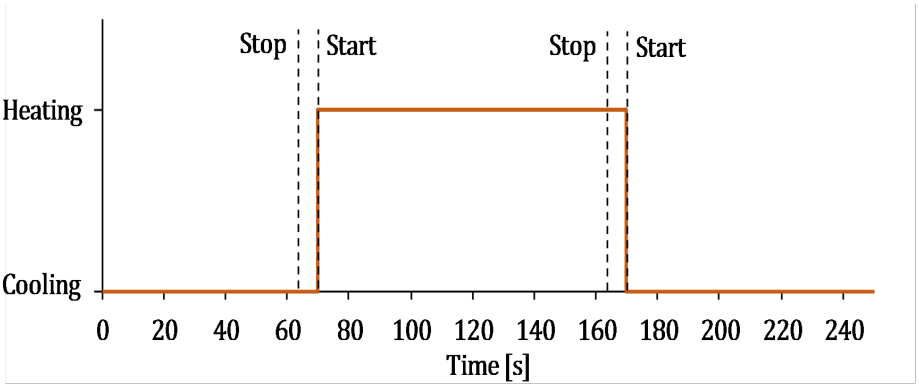

Figure 4.27: Working modes during the reversible simulation.

The simulated MFR of refrigerant is presented in Figure 4.28a. Calculated MFRs in the compressor and EEV are differentiated. In Figures 4.28b and 4.28c are given the zoom in cooling to heating switch and heating to cooling switch respectively. The moments in which the compressor is stopped and re-started are marked. As can be seen, the compressor MFR goes to zero in three seconds, faster than the EEV ones, which depend on the dynamics of the system.

After the mode is switched, the compressors start working again. The MFR in the compressor reaches a high value in a few seconds and oscillates until achieve the equilibrium with the MFR calculated in the EEV. The MFR in the EEV continue decreasing after the switch is given, because of the dynamics of the system, and then increases to reach the equilibrium.

Refrigerant fluid pressures can be seen in Figure 4.29. Initially, in the cooling mode, the outdoor unit PHEX works as a condenser (high pressure), while the indoor unit works as an evaporator (low pressure). During the heating mode, the opposite is true. It is clearly seen both the change in the working mode of the PHEX and the time at which pressures are equalized.

Figure 4.30 shows the refrigerant and brine temperatures in the outdoor PHEX inlet

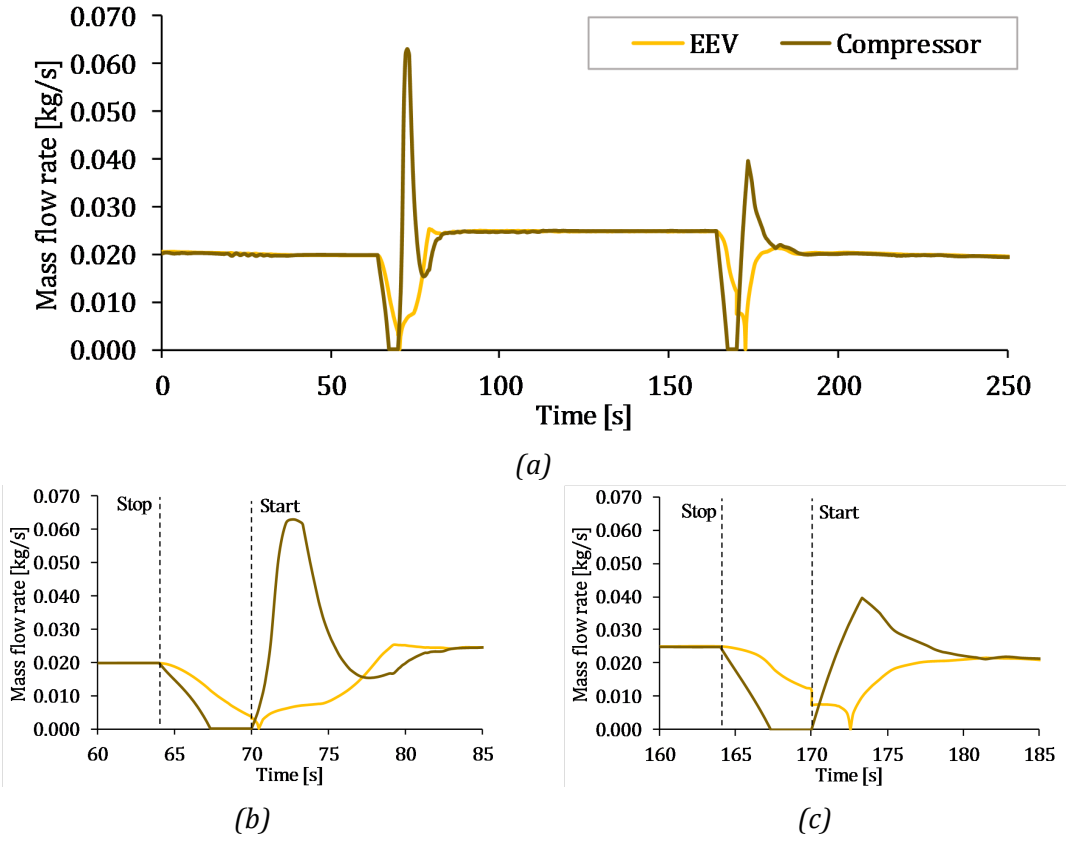

Figure 4.28: Refrigerant MFR during reversible simulation. Entire simulation (a), zoom in cooling to heating (b) and zoom in heating to cooling (c)

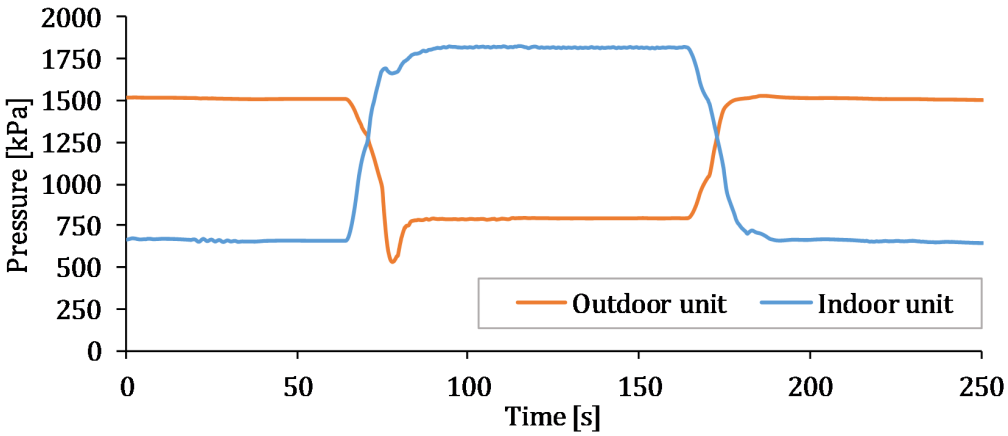

Figure 4.29: Refrigerant pressures during reversible simulation.

and outlet ports. During the cooling mode, port 1 and port 2 are the inlet and the outlet of the refrigerant sides respectively. During the heating mode, the port 2 is the inlet and the port 1 is the outlet. Brine is heated during the cooling mode and cooled down during the heating mode.

During the cooling mode, the temperature of the refrigerant at the port 1 is high be-

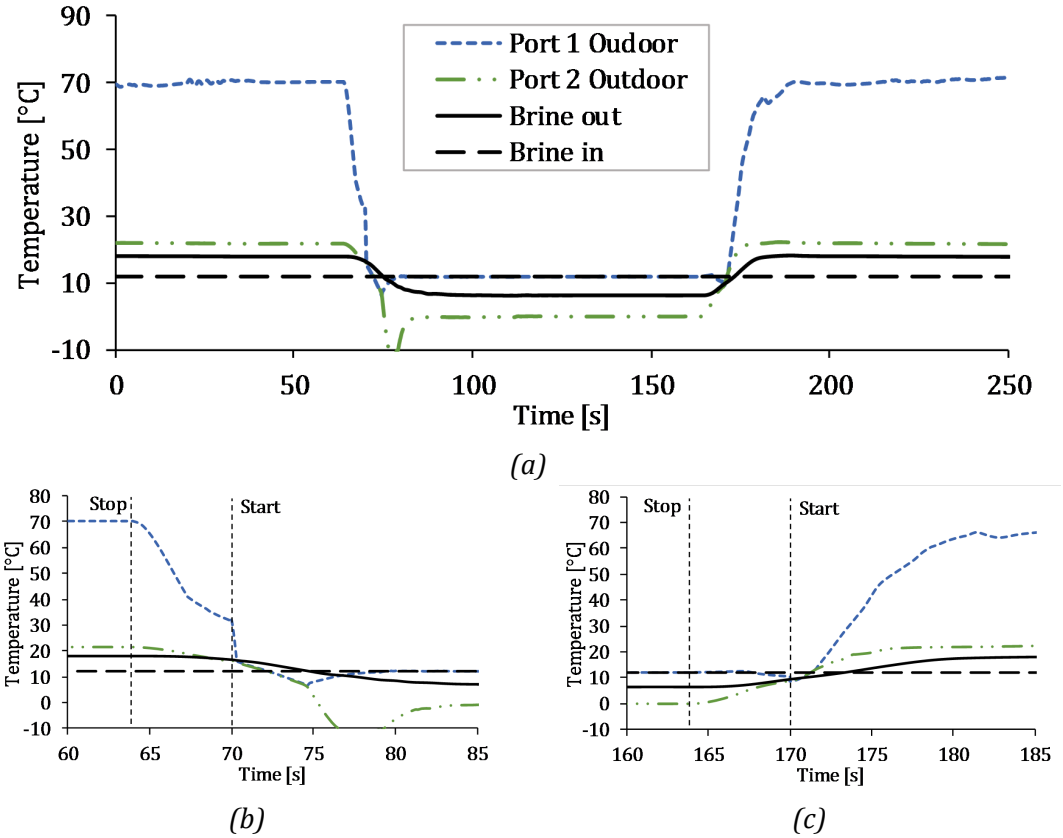

Figure 4.30: Outdoor PHEX inlet and outlet temperatures. Entire simulation (a), zoom in cooling to heating (b) and zoom in heating to cooling (c)

cause it comes as superheated vapor from the compressor. At the port 2, it is near to the brine outlet temperature, which indicate that the PHEX is working in parallel-flow configuration, as described in 4.2. When the compressor stops working, the temperatures of both ports decrease. In the outlet port because although the refrigerant MFR is almost null, the brine keeps flowing and cooling the refrigerant. In port 1, the temperature decreases because the compressor stops compressing the refrigerant. In fact, during the time in which the compressor is switched off, the refrigerant MFR that goes through PHEXs is almost null.

After the switch to the heating mode, the port 1, which now is the outlet port, reach a similar temperature than the inlet of the brine due to the configuration of the PHEX has changed to counter-flow. The refrigerant goes into the PHEX through the port 1 and comes from the EEV at a low pressure and temperature. Then, the steady state in the heating mode is reached.

When the switching order is given again to return to the heating mode, both fluids temperatures are balanced before reach the initial values.

Figure 4.31 shows the refrigerant zones lengths inside the outdoor PHEX along the simulation. During cooling mode, in which the outdoor unit works as a condenser, it can be seen that the refrigerant is divided into three zones: superheated vapor, two-phase fluid and sub-cooled liquid. After the compressor shut-down, the sub-cooled zone disappears and the superheated zone continues decreasing until it disappears. As seen in Figure 4.30, for some time during the compressors shut-down, both refrigerant temperatures are equal. This is because all the fluid inside the PHEX is two-phase fluid, as can be seen in Figure 4.31. After the start-up, as the refrigerant MFR flows constantly again, the temperatures of the refrigerant starts separating one from the other and the superheated zone increases. The outdoor unit is now working as a two-zone evaporator.

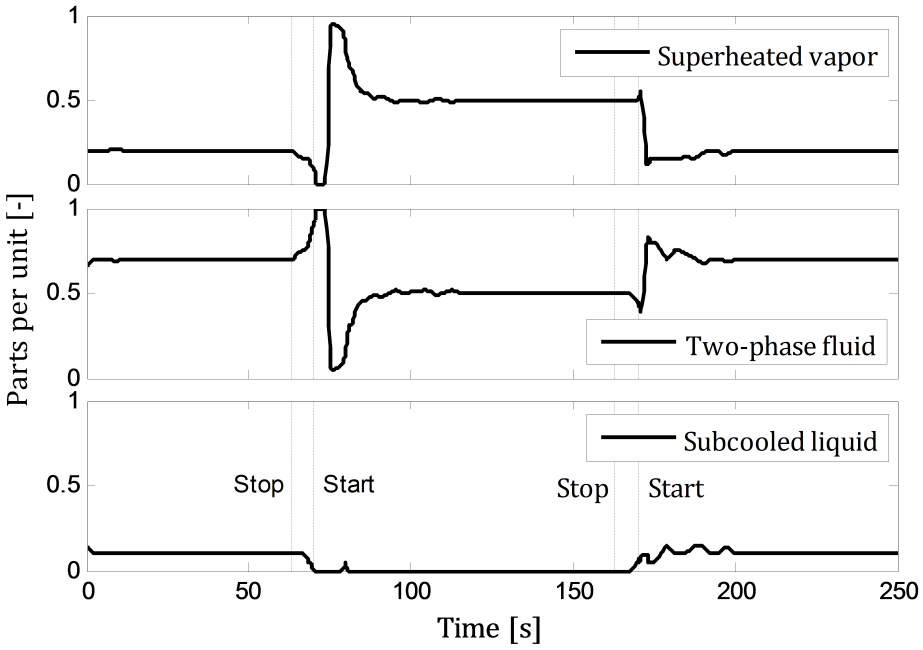

Figure 4.31: Outdoor PHEX vapor-liquid zones length per unit during reversible simulation.

Figure 4.32 shows the refrigerant and water temperatures in the indoor PHEX inlet and outlet ports. The port 2 is the inlet during the cooling mode and the outlet during the heating mode. Water is initially cooled down because the PHEX is working as an evaporator and, after the switch, it is heated due to the PHEX works as a condenser.

As the PHEX is initially working in parallel-flow, the refrigerant outlet temperature is similar to the water outlet temperature. During the heating mode, as the configuration is in counter-flow, the refrigerant outlet temperature defines the maximum temperature at which water can be heated.

Refrigerant temperature in the outlet port increases when the compressor is stopped because the water, which has a higher temperature than the refrigerant, continues circulating and heating the refrigerant. Temperature at the inlet also increases because the refrigerant comes at a higher pressure from the EEV during the equalization of the pressures.

After the switch, inlet port temperature increases considerably because it is superheated vapor that come from the compressor.

When the system switches back to the cooling mode, the transient behavior that occurs is similar to the one described in the first switch of the outdoor unit PHEX.

In Figure 4.33 can be seen the quality of the refrigerant fluid during the switching simulation. During the cooling mode, the PHEX works as a two-zone evaporator. During the heating mode, as a three-zone condenser.

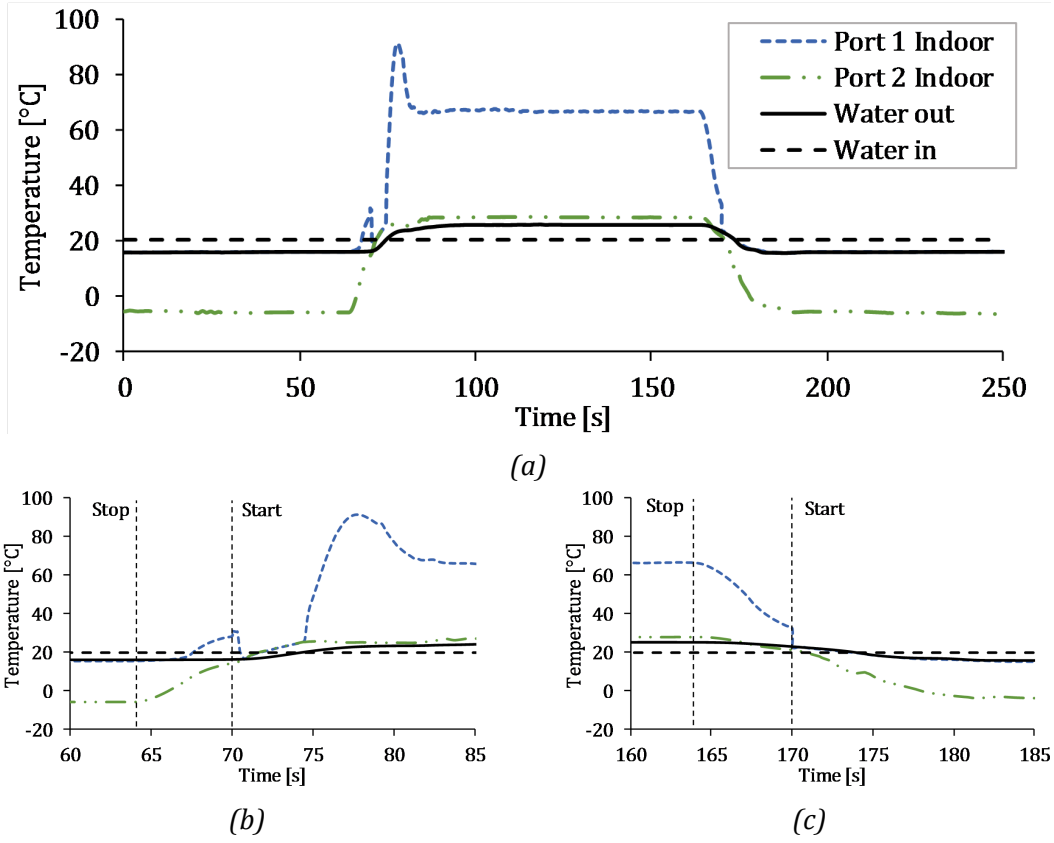

Figure 4.32: Indoor PHEX inlet and outlet temperatures. Entire simulation (a), zoom in cooling to heating (b) and zoom in heating to cooling (c)

The brine is heated 6°C during the cooling mode and is cooled down 5.8°C during the heating mode. The water is cooled down 4.5°C during the cooling mode and heated

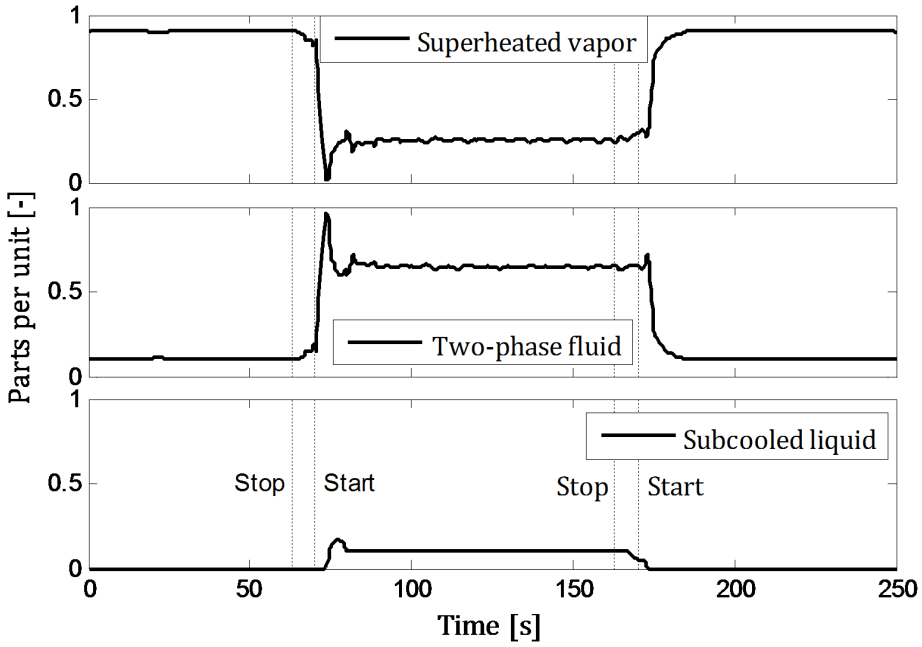

Figure 4.33: Indoor PHEX vapor-liquid zones length per unit during reversible simulation.

5.4°C during the heating mode. The obtained results are similar to the ones obtained in the laboratory tests for the heating and cooling modes separately.

As said before, there is not available experimental test data to compare the simulation results. However, it is important to highlight that the objective is to demonstrate that the developed model is capable to carry out simulations under switching working mode, without focusing in the numerical results. In fact, taken inputs to the model, apart from being arbitrary, are taken as constant and invariant during all the simulation, which is far from the behavior of a real HP.

Moreover, as can be appreciate from Figures 4.31 and 4.33, when the PHEX are working as evaporators, the superheated zones are much longer than they should be, specially the indoor unit during the cooling mode. This denotes that operation conditions have not been studied and much less optimized.

4.8 Conclusions

During this chapter, the model presented in the Chapter 3 has been validated in micro-scale for transient simulations.

The different tests developed to validate the model have been explained. Tests were

carried out with a liquid-to-liquid HP of 5kW of nominal heating capacity connected to a climatic chamber that emulates the heat source and sink. In total, 14 different tests were carried out. Both the heating and the cooling modes were tested. During each test, 8 different situations were given, in which changes in the operation conditions were forced to get transient-states. The tests facility and procedures have been described in detail.

The validation of the model has been presented. It has been validated under the cooling and the heating situations separately and also under a heating start-up situation. In the results can be seen how the model is capable to simulate different transient situations accurately.

Finally, a switching mode was simulated and the results were discussed. The capability of the model to simulate switching modes has been proved. Moreover, although there are not laboratory tests with which compare the simulation results, it can be asserted that they can be a good approach to the real behavior of the system under switching mode operation.

Chapter 5

MACRO-SCALE SIMULATIONS

During this chapter, the model will be validated in macro-scale, which will allow to predict the energy performance of HP systems. The used HP, test methodology and test results will be presented. Then, the model validation will be shown. Finally, an study about the system performance prediction will be presented and some conclusions will be drawn.

5.1 Introduction

The use of dynamic models to simulate the behavior of a thermal facility in macro-scale allows the user to predict the performance of the system under long time operation. For instance, it can be predicted the electricity consumption during the cold season, the COP of the system for space heating or the SPF of the facility. Because of that, it is important that the dynamic model presented in Chapter 3 to be able to simulate HPs in macro-scale.

The model will be validated against macro-scale laboratory experimental tests. They were carried out with a reversible liquid-to-liquid HP of 16 kW of nominal heating capacity working in cooling mode. The system works with Propane (R290) as refrigerant fluid and water as secondary fluids.

Different tests were carried out by varying the cooling loads in the HEX that simulates the building cooling demand. Therefore, seven tests were developed with different ON/OFF time ratios. The duration of tests vary between approximately 40 minutes and 4 hours depending on the test.

Once the model is validated in macro-scale against one of those tests, there will be simulated the rest of them. System performance calculated from simulation results and tests data will be compared and discussed.

5.2 Tests description

5.2.1 Tests facility

Tests have been carried out with a reversible liquid-to-liquid HP joined to two hydraulic groups that simulate the indoor (building) and outdoor (ground/water) secondary loops. In each of these loops, it can be imposed the secondary fluid MFR and set-point temperature or the wanted thermal load. Both secondary loops work with water as secondary fluid. The HP uses Propane (R290) as refrigerant fluid.

A scheme of the used test rig is shown in Figure 5.1. The HP, of 16 kW of nominal heating capacity, is compound by a reciprocating compressor, an EEV, a 4WV and two refrigerant-to-liquid PHEX. Secondary loops are compound by a water pump, a PID

controller to fix set-point temperatures or thermal loads and a HEX to simulate heat sink and source.

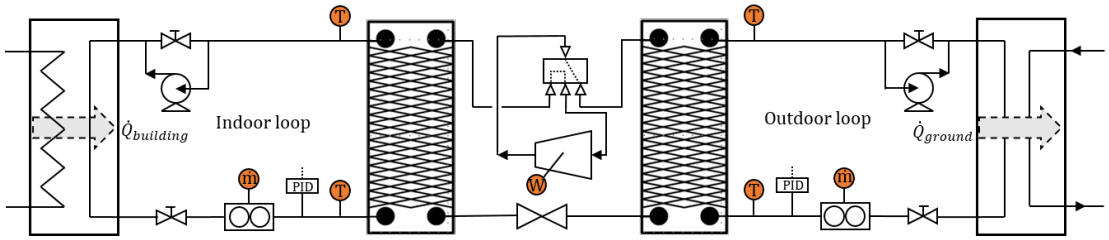

Figure 5.1: Scheme of the used test ring in cooling mode with the measurement points.

Specifications of used PHEXs and compressor are presented in Tables 5.1 and 5.2 respectively.

Table 5.1: Specifications of the used plate heat exchangers.

	Indoor Unit	**Outdoor Unit**
Plates number	26	26
Dimensions (cm)	50 x 10 x 6.2	50 x 10 x 6.2
Primary fluid	R290	R290
Secondary fluid	Water	Water
Heating connections	Parallel-flow (Condenser)	Parallel-flow (Evaporator)
Cooling connections	Counter-flow (Evaporator)	Counter-flow (Condenser)

Table 5.2: Specifications of the used reciprocating compressor.

Electric connection	220/240V 1 50Hz
Maximum power input (kW)	7.9
Displacement (m^3/h)	22.72
$T_{evap} = -1°C$, $SH = 20°C$, $T_{cond} = 55°C$, $SC = 3°C$,	
Heating power (kW)	17.4
Absorbed power (kW)	5.09
COP	2.42
Refrigerant mass flow rate (g/s)	46.25

The operation of the HP is very similar to the one described in Section 4.2. However, in stead of using a climatic chamber to simulate heat source and sink, it is used secondary water loops with HEXs.

During tests, the system is working on cooling mode. Thus, the outdoor unit will work as the condenser and the indoor unit as the evaporator.

Used measurement devices are presented in Table 5.3 and their location is shown in Figure 5.1. When an actual thermal facility of a building wanted to be monitored in order to characterize the performance of the system, the measurements that are accessible are the temperatures and MFR of secondary fluids and the system power consumption. Therefore, as the goal of this tests is to obtain the performance of the system, it has not been measured the refrigerant fluid conditions.

Table 5.3: Specifications of the utilized sensors.

Measurement	Type
Water temperature	Pt 100 resistance measurer
Water mass flow rate	Coriolis effect sensor
Compressor electrical input	Power meter

5.2.2 Tests procedure

The objective is to simulate the performance of a liquid-to-liquid HP during the cooling working mode. Outdoor unit loop is adjusted to simulate the ground or water heat sink and indoor unit loop to simulate the refrigeration facility of the building during warm seasons.

The thermal load of a hypothetical building is varied in order to carry out different tests. Water MFR of both secondary loops remain constant during all tests, being approximately 1 kg/s. The outdoor loop inlet temperature is fixed in 25°C for all tests and it remains constant during all the test. Instead, in the outdoor loop, a specific base ΔT is imposed by the control of the system between the inlet and outlet temperatures of the HEX that simulates the building cooling thermal load. During the operation of the system, a percentage of that base ΔT is fixed. That percentage is varied in each test. Thus, the ON/OFF time ratio of the system is varied. The higher the percentage is, the lower is the ON/OFF ratio and therefore, the lower is the emulated cooling load of the building. There were developed tests with 10, 15, 30, 40, 50, 70 and 90% of cooling load. The based ΔT was fixed in 5K approximately.

Additionally, not all tests have the same cycle time. Understanding as a cycle the sum

of one ON cycle and one OFF cycle. In Table 5.4 are presented the ON time, cycle time and real working percentage for each test.

Table 5.4: Cycles times and real ON/OFF ratios for each test.

Test	ON time [s]	Cycle time [s]	Real ON/OFF ratio
T10	335	2325	14.4%
T15	340	2020	16.8%
T30	405	1430	28.3%
T40	555	1180	47.0%
T50	640	1175	54.5%
T70	925	1360	68.0%
T90	3530	3865	91.3%

As an example, in Figure 5.2 are presented the water temperatures of both secondary loops and the electrical power input for the test T40. As can be seen, approximately the 40% of the time, the system is working and approximately the 60% is switched off.

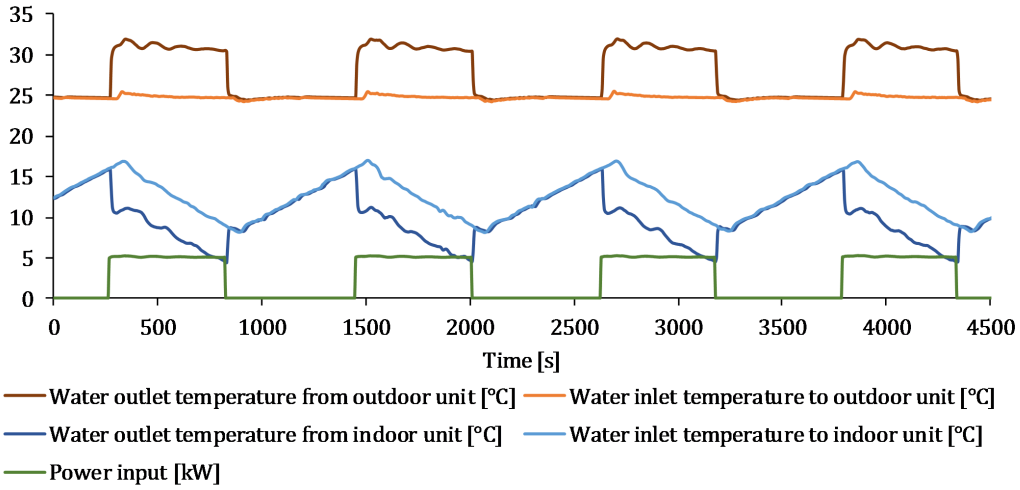

Figure 5.2: Water temperatures and power input T40 test.

5.3 Model specific considerations

Some specific considerations must be taken into account to simulate the system presented in Section 5.2.

PHEXs discretization: The realized study for micro-scale validations regarding the needed number of FCV is repeated with macro-scale tests. T40 test was used and the results are collected in Figure 5.3. As can be seen, in this case, discretizing each PHEX into 5 or more FCVs, accurate results are obtained. However, in order to reach an agreement between computational time and results accuracy, 5 or 10 FCVs are enough. For the following simulations, 10 FCV have been utilized.

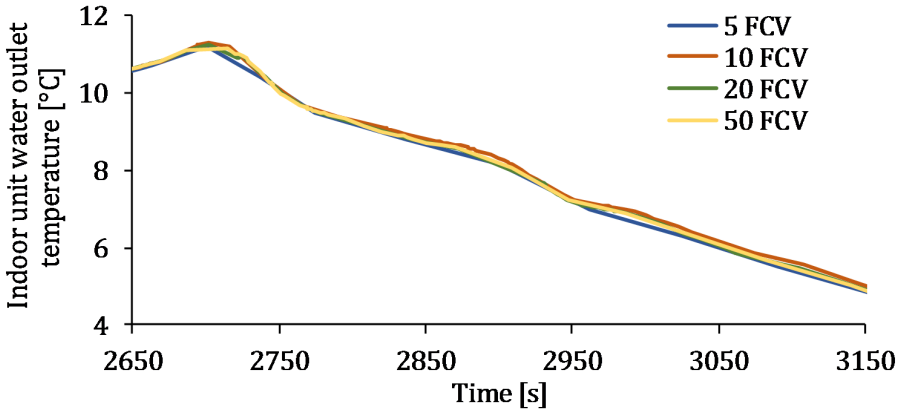

Figure 5.3: Indoor unit water outlet temperature with different numbers of finite control volumes.

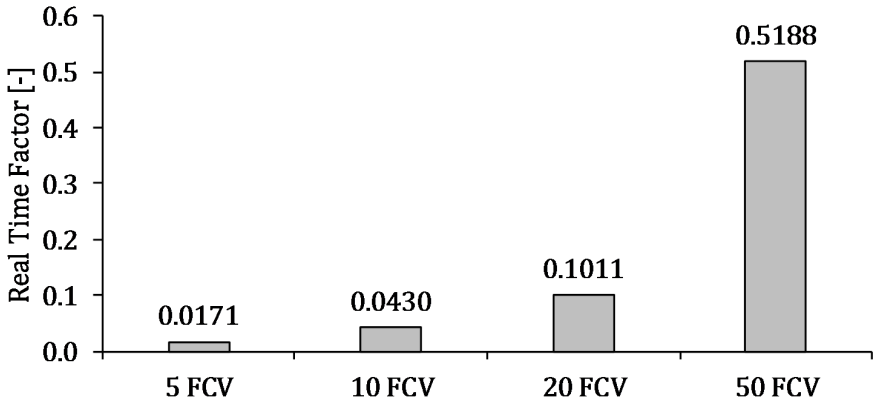

Figure 5.4: Real Time Factor for different numbers of finite control volumes.

Fluid tables: The utilized refrigerant fluid is Propane (R290). The secondary fluid in both PHEXs is water. Again, the needed fluid tables were taken using CoolProp [152].

Nusselt number correlations: Differently from micro-scale validation, instead of using specific Nusselt number correlations for the used refrigerant, it was used more general correlations. Dittus-Boelter correlation [167] is used to calculate the HTCs of

water and single-phase refrigerant and Chisholm correlation [169] to calculate two-phase refrigerant HTCs.

Dittus-Boelter correlation is presented in Equation 4.1 and the Chisholm correlation in Equation 5.1.

$$Nu = 0.724 \left(\frac{6\beta}{pi}\right)^{0.646} Re^{0.583}\, Pr^{m} \tag{5.1}$$

Where the exponent of Prandtl number is $m = 0.3$ when the refrigerant is condensing and $m = 0.4$ when it is evaporating.

Since this correlations are not specific for one refrigerant fluid, it makes the model more suitable to simulate different systems. Moreover, although during the simulations presented in this thesis there have not been used HTC correction factors, it must be take into account that can be utilized to adjust the calculated HTC of each fluid.

Compressor efficiencies: Compressor volumetric and isentropic efficiencies are calculated as a function of the pressure ratio. Used correlations are presented in Table 5.5. This correlations were obtained from a set of tests carried out with the same system under different steady operation conditions.

Table 5.5: Equation and R^2 value of volumetric and isentropic efficiencies correlations.

	Volumetric efficiency	**Isentropic efficiency**
Eq.	$\eta_{vol} = -0.0248r + 1.0231$	$\eta_{ise} = -0.0521r + 0.8749$
$\boldsymbol{R^2}$	0.995	0.998

EEV coefficient: Figure 5.5 shows the C_v of the used EEV in the presented system, whose data was provided by the manufacturer.

Components dimensions: The physical specifications of the used PHEXs and compressor are described in Tables 5.1 and 5.2, respectively. They are both taken from open technical data sheets provided by the manufacturers.

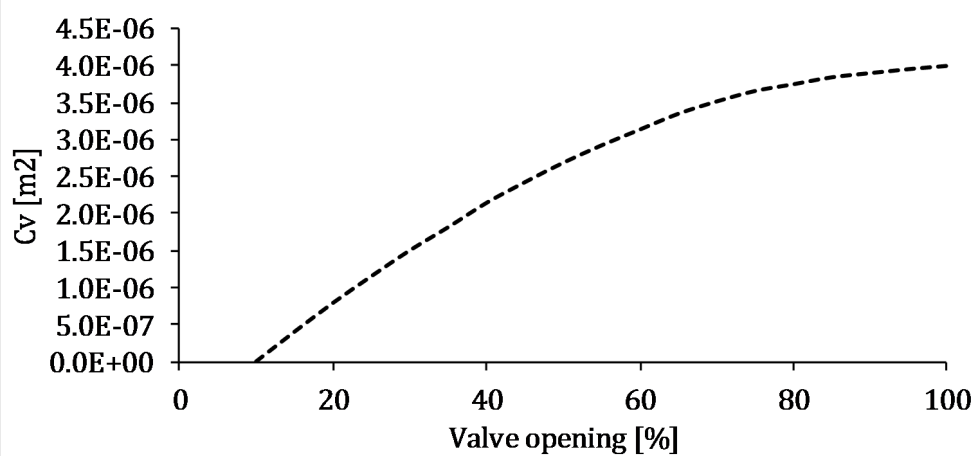

Figure 5.5: Valve coefficient in function of the valve opening.

Refrigerant mass flow rate distributor: Since there is not information about the refrigerant loop, there was not taken into account any pressure drops in the refrigerant distributor.

EEV opening degree Differently from micro-scale tests, in this case it has not been monitored the opening degree of the EEV. However, as seen in Section 4.4, it is not the parameter that most affects the working conditions of the system.

In this case, since there is not implemented a control loop in the model, the opening degree remains constant during all the simulations. Nevertheless, at the time of selecting the opening degree, it was taken into account that for the tests operation conditions, the refrigerant MFR calculated during the simulation was similar to the one given by the compressor manufacturer software for those conditions.

System downtime: In reversible simulation cases, it is interesting to know the behavior of the fluids during the time in which the system is switched off to enable the working mode switch.

On the contrary, at this macro-scale simulations, it is not important the behavior of the system during the off time. It is known that there will be transient-states where the pressures will be equalized, the refrigerant MFR will decrease and the temperatures in HEX will reach an equilibrium. However, that transient-state time is much smaller than the total time where the system will be switched off. Therefore, those transient-states are neglected.

Moreover, in order to accelerate the simulations, the time in which the system is stopped has not been simulated. In the instant in which the system is stopped, the simulation jumps until the time in which the system is restarted. The simulation restarts taking the initially fixed initial conditions.

After the simulation, the results are filtered. During the no simulated stop times, the compressor power input has been set to 0 and the outlet water temperatures have been equated to the inlet ones.

5.4 Validation of the model in macro-scale

Now, simulation results will be compared with experimental data. Here it will shown T70 test. In Annex IV are presented the comparison between test data and simulation results of the rest tests.

In Figure 5.6 and 5.7 are shown the temperatures of the outdoor and indoor PHEXs respectively. As seen, heat transfer between fluids is correctly simulated and therefore, simulation water outlet temperatures are similar to the one from tests.

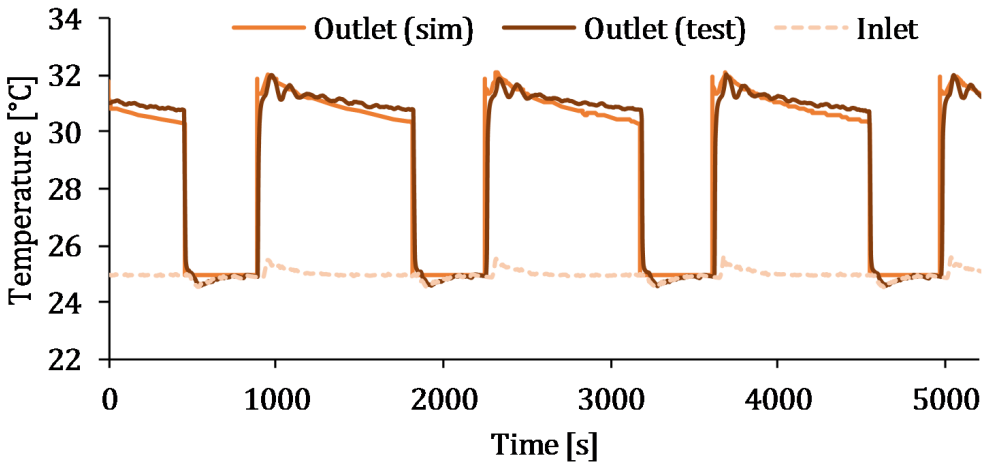

Figure 5.6: Test data and simulation results of water temperatures in the outdoor unit (condenser).

In Figure 5.8 is presented the comparison between the compressor power consumption during the test and the simulation. As can be seen, the model under-calculates the power input to the system.

Finally, the calculated EER is compared. EER is the parameter commonly used to measure the cooling efficiency of an air conditioning system or a reversible HP working in

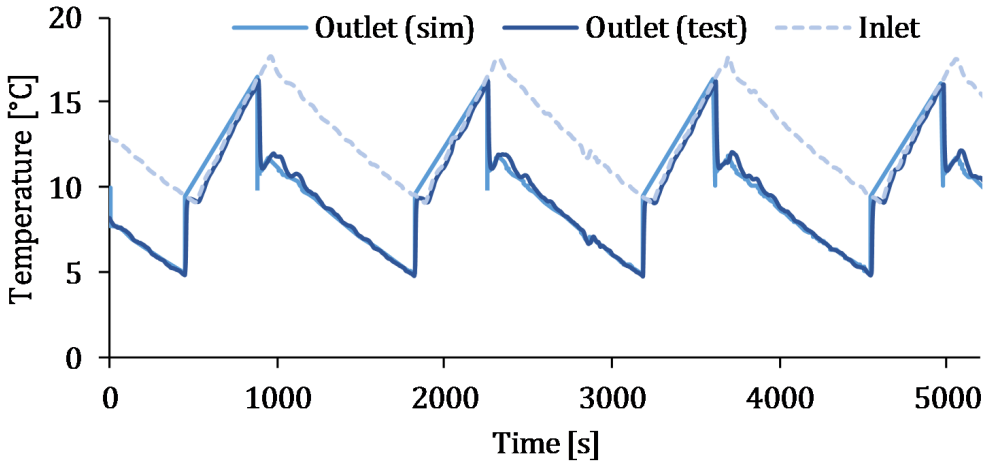

Figure 5.7: Test data and simulation results of water temperatures in the indoor unit (evaporator).

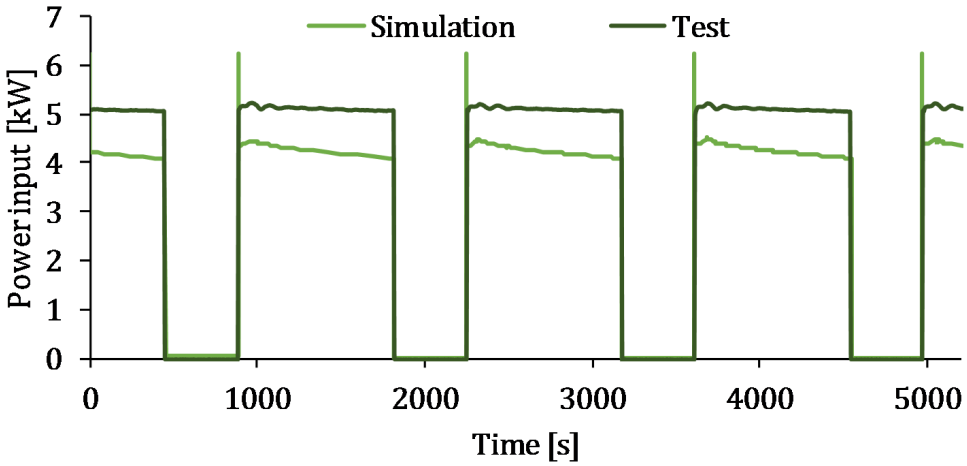

Figure 5.8: Test data and simulation results of compressor power consumption.

the cooling mode. It is calculated by means of Equation 5.2.

$$EER = \frac{\dot{Q}_{cooling}}{\dot{W}_{compressor}} = \frac{\dot{m}_{water\ indoor}(\Delta T_{water\ indoor})}{\dot{W}_{compressor}} \tag{5.2}$$

Calculated EER from simulation results is overestimated in comparison with test data. It is mainly because while the water ΔT is similar in simulation results and test data, the compressor work is under-calculated during the simulations. In next section, where the system performance at different loads is studied, it will be discussed the reasons of the divergences between test data and simulation results.

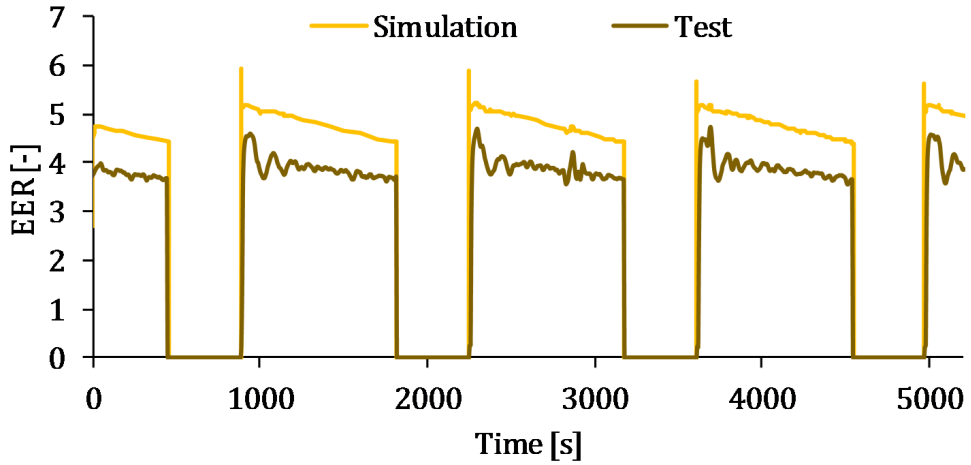

Figure 5.9: Test data and simulation results of calculated EER.

5.5 Model performance study at different cooling loads

The system efficiency at different cooling loads will be studied. Firstly, all test were simulated and the obtained results were treated in order to obtain the EER. Obtained results are presented in Figure 5.10 in comparison with the EER from test data.

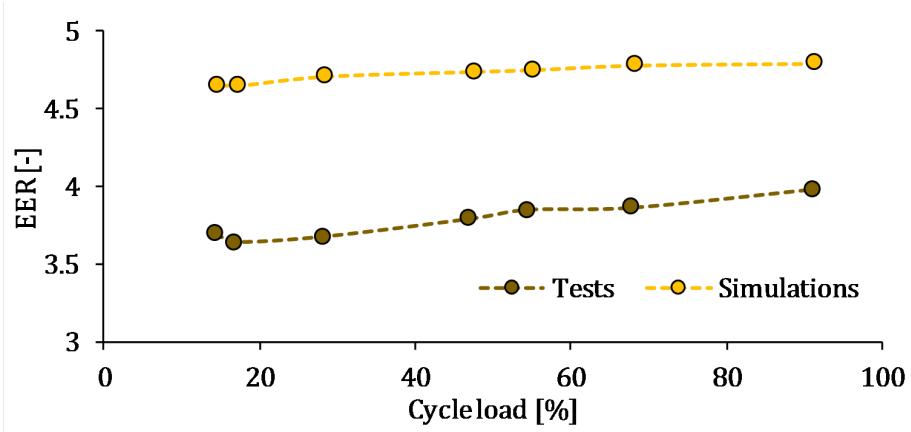

Figure 5.10: Test data and simulation results of calculated EER for different cycle loads.

As can be seen, the model tends to overestimate the system performance. Now, it will be tried to obtain where the observed overestimation comes.

First af all, as seen in Section 5.4, the model simulates accurately the outlet water temperatures in PHEXs but under-predicts the compressor absorbed power. Integrated energy along one cycle in indoor unit, outdoor unit and compressor were calculated for each test and are presented in Figure 5.11. Some differences between simulation

and test data can be appreciate. However, since each test have a different cycle time (Table 5.4), the differences between tests cannot clearly seen.

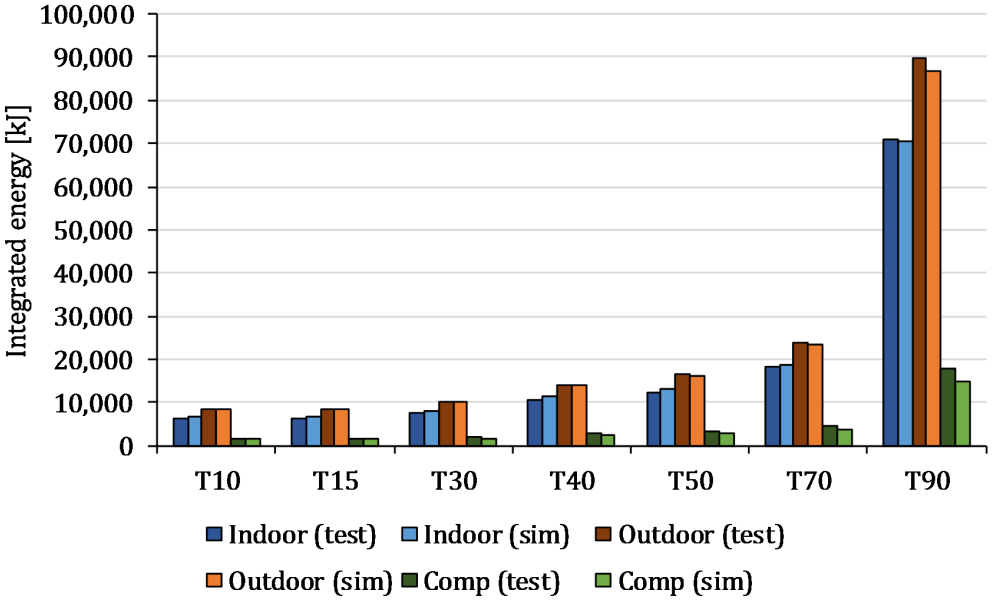

Figure 5.11: Integrated energy along one tested cycle in indoor unit, outdoor unit and compressor.

Because of that, it has been assumed a cycle time of one hour for each test maintaining the real ON/OFF time ratios presented in Table 5.4. Integrated energy in the indoor unit, outdoor unit and compressor were again calculated and are shown in Figure 5.12.

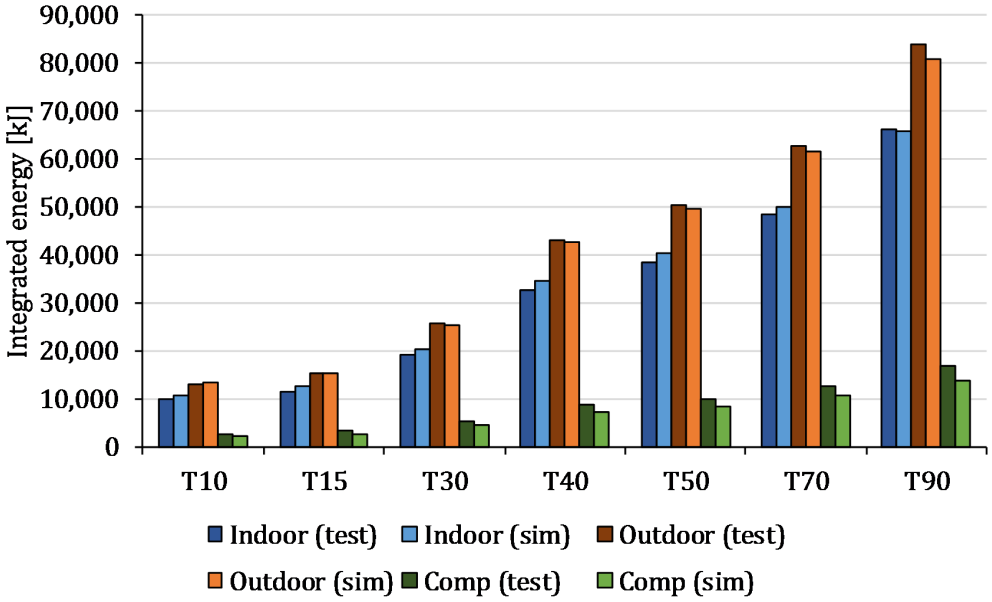

Figure 5.12: Integrated energy along one hour cycle in indoor unit, outdoor unit and compressor.

Now, it can be better seen how the compressor absorbed work is underestimated in all tests. However, integrated energy in the indoor unit, which represents the cooling energy of the system, is generally overestimated.

In order to see it in more detail, In Figure 5.13 it is depicted the relative difference between simulation results and test data in the integrated energy of the indoor unit and compressor.

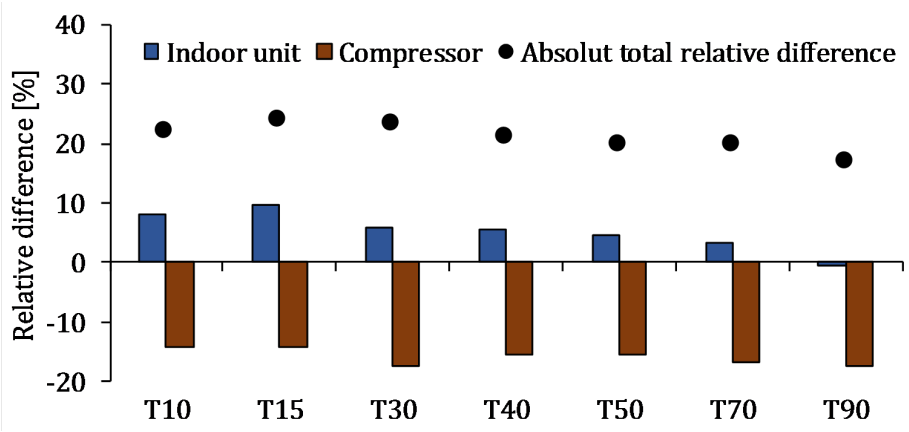

Figure 5.13: Relative difference between simulation results and test data in indoor unit and compressor.

It is observed the overestimation of the cooling capacity against the underestimation of the compressor work. Both of them collaborate in the overestimation of the EER. Additionally, it can be seen that the longer is the ON-cycle time, the smaller the difference is.

Finally, in Figure 5.14 are presented the comparison between simulation results and test data of heating capacity, cooling capacity and compressor power input. It can be asserted that the model simulates fairly accurately the behavior of the systems in macro-scales.

On the other hand, it can be said that the main differences are given in the compressor power input calculation. In fact, compressor model is a basic model which does not simulates the dynamics implicit in its operation and in which only basic thermodynamic laws have been applied. In case the compressor model was improved, the results could be more accurate [137].

Additionally, it must take into account that different assumptions were taken into account in order to simplify the modeling of the system. This directly affects the accuracy of the results.

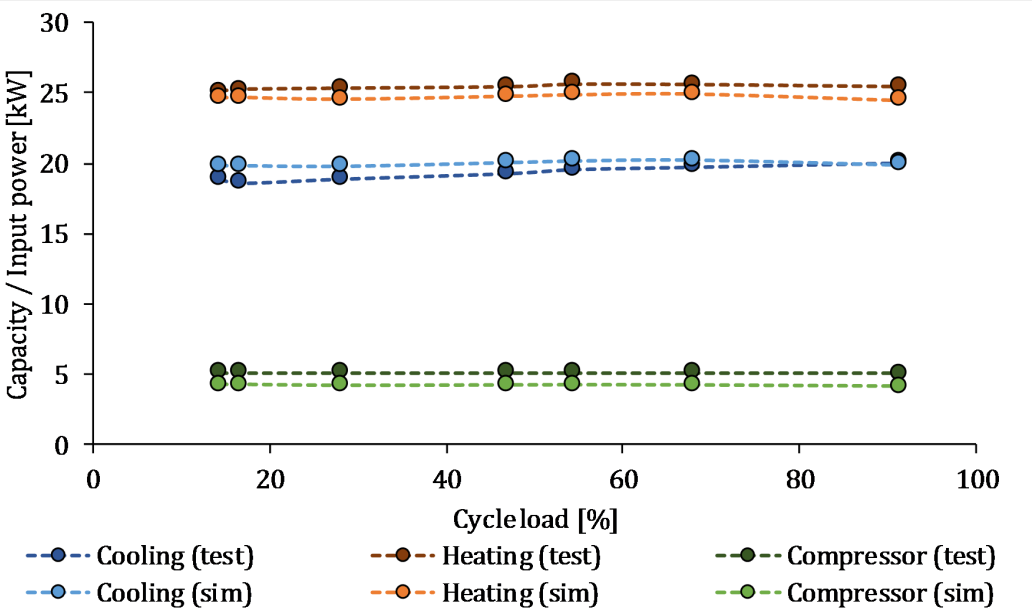

Figure 5.14: Comparison between simulation results and test data of heating capacity, cooling capacity and compressor power input.

5.6 Conclusions

During this chapter, the model presented in the Chapter 3 has been validated in macro-scale obtaining the performance of the system.

Medium-long time scale tests were developed using a reversible liquid-to-liquid HP working in cooling mode. In secondary fluid loops, water was heated or cooled down using secondary HEXs which simulate the demand of the building and the ground/water reservoirs, respectively. Different cooling loads were fixed in order to vary the ON/OFF time ratio of the system. In the aggregate 7 tests were developed.

Using one of those tests, the model was validated. The model predicts accurately the water outlet temperature from both indoor and outdoor PHEX. However, it tends to underestimate the compressor power consumption. It leads to an overestimation of the system performance.

Then, the rest of tests were simulated in order to analyze the system performance. It was seen that the performance overestimation is maintained at different cooling loads. Additionally, it was observed studying the integrated energy in the indoor unit and the compressor that while water outlet temperature is overestimated, power input is underestimated, collaborating both of them in the overestimation of the system perform-

ance.

On the other hand, it was observed that the overestimation of the water outlet temperature decreases with high ON/OFF time ratio. Thus, the differences in the system performance calculation mainly reside in the compressor power input calculation.

Finally, taking into account firstly, that the water temperatures are fairly well simulated but the power consumption is mainly overestimated and, secondly, that the compressor model is a static and basic model, it can be concluded that focusing on the improvement of the compressor model, better results could be obtained.

Chapter 6

ENDING

During this chapter, a summary of the described work along the thesis is presented, remarking the main conclusions. Additionally, the scientific production carried out from the presented work and the future research lines that can be afforded from this work are enumerated.

6.1 Conclusions

HPs are one of the most promising technologies to reduce the use of fossil fuels for heating and DHW production in buildings. Moreover, the capability of reverse the working mode allows them to cover also the refrigeration demand.

In this thesis it was developed a physics-based dynamic model to simulate the behavior of reversible liquid-to-liquid HPs. The model of each component of the HP was separately developed and then they were joined together. The model was implemented in Matlab/Simulink environment.

Since the dynamics of the HEXs are much more slower than the dynamics of components that regulates the refrigerant MFR, such as compressor and valves, these were statically modeled. It simplify the model and decrease considerably the computational time of the model.

HEXs model was developed using the FCV method. With the developed model of refrigerant-to-liquid PHEX, the behavior of PHEXs either if they are working as condensers or as evaporators can be simulated. Moreover, it allows the user to choose the configuration of the PHEX between parallel-flow and counter-flow. The used equations and their implementations were presented.

Then, it was validated the model in micro-scale situations. Different tests under different transient situations were developed. Obtained measurements were used to validate the model under heating, cooling and start-up situations. Simulation results presented good agreement with test data.

After validating the model under different micro-scale transient situations, it was simulated a working mode switch. It was simulated the behavior of the system starting in cooling mode, switching to heating mode and going back to cooling mode. Since there were not available experimental data of working mode switches, it was not possible to compare the simulation results with tests data. However, the obtained results could be a good approach to the actual behavior of the system during a working mode switch.

Finally, the model was used to simulate the behavior of a different HP under macro-scale situations. It was firstly validated under cooling working mode and then a system energy performance study was conducted in order to clarify the divergences between test data and simulation results. It was concluded that, although the results were good,

improving the compressor model more accurate results could be obtained.

To sum up, it can be asserted the validity of the model to simulate reversible liquid-to-liquid HPs obtaining accurate results. It can be used either to simulate micro- and macro-scales simulations under different working modes and configurations of PHEXs. Additionally, working mode switch simulations can be carried out.

6.2 Scientific production

Based on the developed work and the obtained results, it was possible to carry out quality and original scientific contributions during the development of this thesis.

International journals publications

- 'Flexible dynamic model of PHEX for transient simulations in Matlab/Simulink using finite control volume method' Erik Salazar Herrán, Koldobika Martin Escudero, Luis Alfonso del Portillo Valdes, Iván Flores Abascal and Naiara Romero Anton. *International Journal of Refrigeration* [Under 2nd review]
- 'Numerical model for liquid-to-liquid HPs implementing switching mode' Erik Salazar Herrán, Koldobika Martin Escudero, Andrew G. Alleyne, Luis Alfonso del Portillo Valdes and Naiara Romero Anton. *Applied Thermal Engineering*, vol. 160, ar. 114054, 2019.
- 'Solar energy system for heating and domestic hot water supply by means of a heat pump coupled to a photovoltaic ventilated façade' Koldobika Martin Escudero, Erik Salazar Herrán, Álvaro Campos Celador, Gonzalo Diarce Belloso and Iñaki Gómez Arriaran. *Solar Energy*, vol. 183 p. 453-462, 2019.

International conferences publications

- ''Liquid to Liquid Plates Heat Exchanger physics-based dynamic model' Erik Salazar Herrán, Koldobika Martin Escudero, Luis Alfonso del Portillo Valdes, Iván Flores Abascal adn Naiara Romero Anton. *XI National y II International Engineering Thermodynamics Conference*, p. 839-851, 2019.

- 'Analysis of an Air Source Heat Pump Water Heater with Photovoltaic Ventilated Façade for different climatic zones' Erik Salazar Herrán, Koldobika Martin Escudero, Luis Alfonso del Portillo Valdes, Álvaro Campos Celador and Pello Larrinaga Alonso. *9th European Conference on Energy Efficiency and Sustainability in Architecture and Planning*, p. 161–169, 2018.
- 'Experimental study of thermal perofmance of a water-to-water heat pump system' Erik Salazar Herrán, Koldobika Martin Escudero, Iván Flores Abascal and Luis Alfonso del Portillo Valdes. *X National y I International Engineering Thermodynamics Conference*, p. 370-371, 2017.
- 'Residential Heat Pumps as Renewable Energy' Erik Salazar Herrán, Koldobika Martin Escudero, Luis Alfonso del Portillo Valdes, Iván Flores Abascal and Ana Picallo Pérez. *8th European Conference on Energy Efficiency and Sustainability in Architecture and Planning*, p. 163–170, 2017.

National conferences publications

- 'Caracterización experimental de una bomba de calor acoplada a una fachada ventilada para producción de agua caliente' Erik Salazar Herrán, Koldobika Martin Escudero, Ignacio López Paniagua, Álvaro Jiménez Álvaro and Naiara Romero Anton. *I Congreso Ingeniería Energética*, p. 362-374, 2018.

6.3 Future research lines

The present work offers the possibility of deepening in the research lines followed in this thesis as well as using the presented material in other research lines.

Reversible HPs: The use of reversible HPs is spreading. However, the behavior of the system during working mode switches is something that must still be studied in more depth. This model allows simulating the behavior of the system during a working mode switches. Therefore, it can be used in the improvement and development of new reversible systems.

More components models: In this thesis, refrigerant-to-liquid PHEX, EEV and compressor models have been developed. Residing the main contribution in the PHEX model. However, in HP facilities there are used many other components such as refrigerant-to-air HEX, thermal tanks, accumulators, thermostatic valves, long path pipes or internal HEX. The development of those models would allow the user to simulate more complex and actual HP facilities. Moreover, nowadays is growing the relevance of phase change materials, which could be modeled to include them in the simulated facilities.

Model optimization: It would be positive to optimize the model in order to decrease the computational time and enhance it's versatility. "S-functions" block is a useful tool but increase considerably the computational weight of the model. Therefore, remove 'S-function' or at least reduce the calculations made inside them would decrease the weight of the model.

Control system: Control loops is one of the most important things in the actual HPs. Integrating control loops in the model would allow the user to improve existing control strategies or to design new ones.

New refrigerant fluids: Refrigerant policies are increasingly stringent with the use of refrigerants with low levels of greenhouse and ozone layer deployment emissions. Therefore, researches are being conducted on the development of new refrigerants or the use of natural ones. This research line can be assisted with simulation models such as the one presented in this thesis.

Hybrid systems facilities: Hybrid electro-thermal residential facilities are increasingly popular worldwide. The research on the performance and coupling of those systems could be benefited from this kind of simulation models.

Buildings thermal demand supply: The model could be transformed in order to switch on/off depending on the thermal demand of a building. There exist different software that calculate the thermal demand of buildings. Thus, using the calculated thermal demand as an input to the model, it would be capable to switch on/off the system and obtain daily, monthly or yearly performance parameters for a studied building.

Bibliography

[1] R. G. Newell, D. Raimi and G. Aldana, 'Global Energy Outlook 2019: The Next Generation of Energy', Tech. Rep., 2019.

[2] Enerdata, 'Global Energy Statistical Yearbook 2019', Tech. Rep., 2019.

[3] International Energy Agency, 'Energy Statistics', *IEA Publications*, p. 81, 2019.

[4] K. Guo, 'Current issues of fossil fuels and their future prospects', in *Fossil Fuels: Sources, Environmental Concerns and Waste Management Practices*, 2013, pp. 85–99.

[5] International Energy Agency, 'Global Energy & CO2 Status Report', Tech. Rep., 2018.

[6] S. Shafiee and E. Topal, 'When will fossil fuel reserves be diminished?', *Energy Policy*, vol. 37, no. 1, pp. 181–189, 2009.

[7] *International Energy Agency*.

[8] C. Pirlogea and C. Cicea, 'Econometric perspective of the energy consumption and economic growth relation in European Union', *Renewable and Sustainable Energy Reviews*, vol. 16, no. 8, pp. 5718–5726, 2012.

[9] M. Azam, A. Q. Khan, B. Bakhtyar and C. Emirullah, 'The causal relationship between energy consumption and economic growth in the ASEAN-5 countries', *Renewable and Sustainable Energy Reviews*, vol. 47, pp. 732–745, 2015.

[10] A. Carfora, R. V. Pansini and G. Scandurra, 'The causal relationship between energy consumption, energy prices and economic growth in Asian developing countries: A replication', *Energy Strategy Reviews*, vol. 23, pp. 81–85, 2019.

[11] *European Environmental Agency*.

[12] Eurostat, 'Energy consumption in households', Tech. Rep., 2019.

[13] U.S. Energy Information Administration, 'Monthly Energy Review', Tech. Rep., 2019.

[14] International Energy Agency, 'The Future of Cooling', Tech. Rep., 2018, p. 92.

[15] ——, 'Energy Efficiency 2018', Tech. Rep., 2018, p. 172.

[16] ——, *Market Report Series: Renewables 2018*. 2018, p. 211.

[17] A. M. Omer, 'Direct expansion ground source heat pumps for heating and cooling', *International Research Journal on Engineering*, vol. 1, no. 2, pp. 27–48, 2013.

[18] European Commission, 'An EU Strategy on Heating and Cooling', pp. 1–13, 2016.

[19] D. Keating, 'Decarbonising Heat', *EURACTIV*, no. September, 2012.

[20] Institute for Energy Diversification and Saving - IDAE, 'Analysis of the Energetic Consumption of the Residential Sector in Spain', Tech. Rep., 2016, p. 76.

[21] UN Environment, 'UN Environment fights to cut cooling and heating emissions', Tech. Rep., 2018.

[22] United Nations and European Union, *Montreal Protocol on Substances that Deplete the Ozone Layer*, 1987.

[23] United Nations, 'United Nations Framework Convention', vol. 62220, 1992.

[24] European Council, 'Council Directive 93/76/EEC to limit carbon dioxide emissions by improving energy efficiency (SAVE)', *Official Journal of the European Communities*, vol. 237, pp. 28–30, 1993.

[25] United Nations, 'Kyoto Protocol Reference Manual', *United Nations Framework Convention on Climate Change*, pp. 1–130, 2008. eprint: 92-9219-055-5.

[26] European Parliament; European Council, 'Directive 2002/91/EC on the energy performance of buildings', *Official Journal Of The European Union*, vol. 1, pp. 65–71, 2002.

[27] ——, 'Directive 2006/32/EC on energy end-use efficiency and energy services', *Official Journal Of The European Union*, vol. 114, pp. 64–85, 2006.

[28] ——, 'Directive 2009/28/EC on the promotion of the use of energy from renewable sources', *Official Journal of the European Union*, vol. 140, pp. 16–62, 2009.

[29] R. Nordman, K. Andersson, M. Axell and M. Lindahl, *Calculation methods for SPF for heat pump systems for comparison, system choice and dimensioning*. 2010, p. 82.

[30] European Comission, 'Action Plan for Energy Efficiency: Realising the Potential', *Official Journal of the European Union*, pp. 1–25, 2006.

[31] European Parliament; European Council, 'Directive 2010/31/EU on the nergy performance of buildings', *Oficial Journal of the European Union*, vol. 153, pp. 13–35, 2010.

[32] ——, 'Directive 2012/27/EU on energy efficiency', vol. 315, pp. 1–56, 2012.

[33] United Nations, 'Paris Agreement', vol. 21, no. December 2015, pp. 1–7, 2017.

[34] K. Heinloth, *Energy Technologies. Renewable Energy*. 2006.

[35] Y. Zhang, G. Zhang, A. Zhang, Y. Jin, R. Ru and M. Tian, 'Frosting Phenomenon and Frost-Free Technology of Outdoor Air Heat Exchanger for an Air-Source Heat Pump System in China: An Analysis and Review', *Energies*, vol. 11, no. 10, 2018.

[36] S. N. Kondepudi and D. L. O'Neal, 'Frosting performance of tube fin heat exchangers with wavy and corrugated fins', *Experimental Thermal and Fluid Science*, vol. 4, no. 5, pp. 613–618, 1991.

[37] A. Amirirad, R. Kumar, A. S. Fung and W. H. Leong, 'Experimental and simulation studies on air source heat pump water heater for year-round applications in Canada', *Energy and Buildings*, vol. 165, pp. 141–149, 2018.

[38] Y. Wang, S. You, Y. Sun and Z. Li, 'Experimental investigations and operational performance analysis on an air source heat pump unit for domestic hot water supply in South China', *Procedia Engineering*, vol. 205, pp. 2407–2414, 2017.

[39] G.-H. Shi, L. Aye, D. Li and X.-J. Du, 'Recent advances in direct expansion solar assisted heat pump systems: A review', *Renewable and Sustainable Energy Reviews*, vol. 109, pp. 349–366, 2019.

[40] J. Cai, Z. Li, J. Ji and F. Zhou, 'Performance analysis of a novel air source hybrid solar assisted heat pump', *Renewable Energy*, vol. 139, pp. 1133–1145, 2019.

[41] S. Vaishak and P. V. Bhale, 'Photovoltaic/thermal-solar assisted heat pump system: Current status and future prospects', *Solar Energy*, vol. 189, pp. 268–284, 2019.

[42] M. Wang and C. A. Infante Ferreira, 'Absorption heat pump cycles with NH3 – ionic liquid working pairs', *Applied Energy*, vol. 204, pp. 819–830, 2017.

[43] A. Goyal, M. A. Staedter and S. Garimella, 'A review of control methodologies for vapor compression and absorption heat pumps', *International Journal of Refrigeration*, vol. 97, pp. 1–20, 2019.

[44] C. M. Keinath, S. Garimella and M. A. Garrabrant, 'Modeling of an ammonia–water absorption heat pump water heater for residential applications', *International Journal of Refrigeration*, vol. 83, pp. 39–50, 2017.

[45] J. M. Corberán, A. Cazorla-Marín, J. Marchante-Avellaneda and C. Montagud, 'Dual source heat pump, a high efficiency and cost-effective alternative for heating, cooling and DHW production', *International Journal of Low-Carbon Technologies*, vol. 13, no. 2, pp. 161–176, 2018.

[46] H. Wang, X. Liu, G. Feng, Z. Kang, Y. Luo, B. Bai and L. Chi, 'Simulation and Analysis of Air-Ground Dual source Heat Pump Operating Efficiency', *Procedia Engineering*, vol. 121, pp. 1413–1419, 2015.

[47] P. Byrne, R. Ghoubali and J. Miriel, 'Scroll compressor modelling for heat pumps using hydrocarbons as refrigerants', *International Journal of Refrigeration*, vol. 41, pp. 1–13, 2014.

[48] International Renewable Energy Agency, *Energy Transition*.

[49] International Energy Agency, '2018 Global Status Report', *IEA Publications*, 2018.

[50] P. Poredoš, T. Čož, A. Kitanovski and A. Poredoš, 'Thermo-economic and primary-energy-factor assessment based on the field test of an air-to-water heat pump', *International Journal of Refrigeration*, 2017.

[51] O. Ibrahim, F. Fardoun and H. Louahlia-gualous, 'Air source heat pump water heater : Dynamic modeling , optimal energy management and mini-tubes condensers', vol. 64, pp. 1102–1116, 2014.

[52] L. Schibuola and M. Scarpa, 'Experimental analysis of the performances of a surface water source heat pump', *Energy and Buildings*, vol. 113, pp. 182–188, 2016.

[53] W. Zheng, T. Ye, S. You and H. Zhang, 'The thermal performance of seawater-source heat pump systems in areas of severe cold during winter', *Energy Conversion and Management*, vol. 90, pp. 166–174, 2015.

[54] D. Klip, 'The transition of the residential heating system', Clingendael International Energy Programme, Tech. Rep., 2017.

[55] S. R. Asaee, V. I. Ugursal and I. Beausoleil-Morrison, 'Techno-economic feasibility evaluation of air to water heat pump retrofit in the Canadian housing stock', *Applied Thermal Engineering*, vol. 111, pp. 936–949, 2017.

[56] 'Heat pump sales 2018 in Finland shot up by 22% – investments exceed half a billion', *Eusopean HEat Pump Association*, 2019.

[57] 'Heat pumps & mechanical ventilation start to dominate new homes market', *PASSIVE HOUSE +*, 2019.

[58] 'BWP Marktzahlen 2018: Nachhaltiges Wachstum mit Luft nach Oben, Deutliches Signal für die Politik', *Bundesverband Wärmepumpe e.V.*, 2019.

[59] P. Byrne, J. Miriel and Y. Lenat, *Experimental study of an air-source heat pump for simultaneous heating and cooling - Part 1: Basic concepts and performance verification*, 2011.

[60] ——, 'Experimental study of an air-source heat pump for simultaneous heating and cooling - Part 2: Dynamic behaviour and two-phase thermosiphon defrosting technique', *Applied Energy*, vol. 88, no. 9, pp. 3072–3078, 2011.

[61] X. Sun, J. Wu and R. Wang, 'Exergy analysis and comparison of multi-functional heat pump and conventional heat pump systems', *Energy Conversion and Management*, vol. 73, pp. 51–56, 2013.

[62] J. Dong, S. Deng, Y. Jiang, L. Xia and Y. Yao, 'An experimental study on defrosting heat supplies and energy consumptions during a reverse cycle defrost operation for an air source heat pump', *Applied Thermal Engineering*, vol. 37, pp. 380–387, 2012.

[63] Y. Ding, G. Ma, Q. Chai and Y. Jiang, 'Experiment investigation of reverse cycle defrosting methods on air source heat pump with TXV as the throttle regulator', *International Journal of Refrigeration*, vol. 27, no. 6, pp. 671–678, 2004.

[64] U. Çakır, K. Çomaklı, Ö. Çomaklı and S. Karslı, 'An experimental exergetic comparison of four different heat pump systems working at same conditions: As air to air, air to water, water to water and water to air', *Energy*, vol. 58, pp. 210–219, 2013.

[65] C. Sebarchievici and I. Sarbu, 'Performance of an experimental ground-coupled heat pump system for heating, cooling and domestic hot-water operation', *Renewable Energy*, vol. 76, pp. 148–159, 2015.

[66] M. Pitarch, E. Navarro-Peris, J. Gonzálvez-Maciá and J. M. Corberán, 'Experimental study of a subcritical heat pump booster for sanitary hot water production using a subcooler in order to enhance the efficiency of the system with a natural refrigerant (R290)', *International Journal of Refrigeration*, vol. 73, pp. 226–234, 2017.

[67] J. Luo, J. Rohn, M. Bayer, A. Priess, L. Wilkmann and W. Xiang, 'Heating and cooling performance analysis of a ground source heat pump system in Southern Germany', *Geothermics*, vol. 53, pp. 57–66, 2015.

[68] H. Wang, Y. Luo, G. Feng, G. Li, X. Liu, B. Bai and L. Chi, 'Measurement and Analysis of the Groundwater Source Heat Pump System in Shenyang', *Procedia Engineering*, vol. 121, pp. 1389–1396, 2015.

[69] S. Lu and J. Wu, 'Optimal selection among different domestic energy consumption patterns based on energy and exergy analysis', *Energy Conversion and Management*, vol. 51, no. 7, pp. 1398–1406, 2010.

[70] T. Sivasakthivel, K. Murugesan, S. Kumar, P. Hu and P. Kobiga, 'Experimental study of thermal performance of a ground source heat pump system installed in a Himalayan city of India for composite climatic conditions', *Energy and Buildings*, vol. 131, pp. 193–206, 2016.

[71] L. Yan, P. Hu, C. Li, Y. Yao, L. Xing, F. Lei and N. Zhu, 'The performance prediction of ground source heat pump system based on monitoring data and data mining technology', *Energy and Buildings*, vol. 127, pp. 1085–1095, 2016.

[72] J. F. Urchueguía, M. Zacarés, J. M. Corberán, Á. Montero, J. Martos and H. Witte, 'Comparison between the energy performance of a ground coupled water to water heat pump system and an air to water heat pump system for heating and cooling in typical conditions of the European Mediterranean coast', *Energy Conversion and Management*, vol. 49, no. 10, pp. 2917–2923, 2008.

[73] J. Romaní, G. Pérez and A. de Gracia, 'Experimental evaluation of a cooling radiant wall coupled to a ground heat exchanger', *Energy and Buildings*, vol. 129, pp. 484–490, 2016.

[74] ——, 'Experimental evaluation of a heating radiant wall coupled to a ground source heat pump', *Renewable Energy*, vol. 105, pp. 520–529, 2017.

[75] A. Dikici and A. Akbulut, 'Exergetic performance evaluation of heat pump systems having various heat sources', *International journal of Energy Research*, vol. 32, pp. 1279–1296, 2008. eprint: arXiv:1011.1669v3.

[76] L. Dai, S. Li, L. DuanMu, X. Li, Y. Shang and M. Dong, 'Experimental performance analysis of a solar assisted ground source heat pump system under different heating operation modes', *Applied Thermal Engineering*, vol. 75, pp. 325–333, 2015.

[77] V. Verma and K. Murugesan, 'Experimental study of solar energy storage and space heating using solar assisted ground source heat pump system for Indian climatic conditions', *Energy and Buildings*, vol. 139, pp. 569–577, 2017.

[78] F. J. da Silva, 'Dynamic Process Simulation: When do we really need it?', *Process Ecology*, pp. 1–4,

[79] J. Hensen, 'Application of modelling and simulation to HVAC systems', *30th International Conference MOSIS*, no. January 1999, pp. 1–6, 1996.

[80] C. P. Underwood, M. Royapoor and B. Sturm, 'Parametric modelling of domestic air-source heat pumps', *Energy and Buildings*, vol. 139, pp. 578–589, 2017.

[81] C.-t. Tran, P. Riviere and P. Waide, 'Energy efficiency modelling of residential heat pump water heater', *9th Conference on Sustainable Development of Energy, Water and Environment Systems*, vol. 4, no. 1, pp. 69–88, 2016.

[82] E. Kinab, D. Marchio, P. Rivière and A. Zoughaib, 'Reversible heat pump model for seasonal performance optimization', *Energy and Buildings*, vol. 42, no. 12, pp. 2269–2280, 2010.

[83] Oak Ridge National Laboratory (ORNL), *DOE/ORNL Heat Pump Design Model*, 1998.

[84] National Institute of Standards and Technology (NIST), *CYCLE_D-HX*.

[85] I. d.I. E. Thermal Area, *IMST-ART*.

[86] Center of Environmental Energy Engineering, *VapCyc*.

[87] R. Gupta and R. Irving, 'Development and application of a domestic heat pump model for estimating CO2 emissions reductions from domestic space heating, hot water and potential cooling demand in the future', *Energy and Buildings*, vol. 60, pp. 60–74, 2013.

[88] Y. Wang, W. Li, Z. Zhang, J. Shi and J. Chen, 'Performance evaluation and prediction for electric vehicle heat pump using machine learning method', *Applied Thermal Engineering*, vol. 159, p. 113 901, 2019.

[89] S. Tangwe, M. Simon and E. Meyer, 'Mathematical modeling and simulation application to visualize the performance of retrofit heat pump water heater under first hour heating rating', *Renewable Energy*, vol. 72, pp. 203–211, 2014.

[90] C. Underwood, *Heat pump modelling*. Elsevier Ltd, 2016, pp. 387–421.

[91] B. P. Rasmussen, 'Dynamic modeling for vapor compression systems — Part I : Literature review Review Article Dynamic modeling for vapor compression systems — Part I : Literature review', vol. 9669, 2012.

[92] A. Alleyne, B. Rasmussen and J. Jeddeloh, *Thermosys Toolbox*.

[93] A. Alleyne, B. Rasmussen, M. Keir and B. Eldredge, 'Advances in Energy Systems Modeling and Control', in *2007 American Control Conference*, IEEE, 2007, pp. 4363–4373.

[94] MathWorks and C. Moler, *Matlab/Simulink*, 1984.

[95] J. M. Fasl, 'Modeling and Control of Hybrid Vapor Compression Cycles', 2013.

[96] B. Li and A. G. Alleyne, 'A dynamic model of a vapor compression cycle with shut-down and start-up operations', *International Journal of Refrigeration*, vol. 33, no. 3, pp. 538–552, 2010.

[97] Modelica Association, *Modelica*.

[98] TLK-Thermo GmbH, *TIL Suite Library*.

[99] S. Quoilin, A. Desideri, J. Wronski and I. H. Bell, *ThermoCycle Library*.

[100] H. Qiao, V. Aute and R. Radermacher, 'Transient modeling of a flash tank vapor injection heat pump system – Part I: Model development', *International Journal of Refrigeration*, vol. 49, pp. 169–182, 2015.

[101] H. Qiao, X. Xu, V. Aute and R. Radermacher, 'Transient modeling of a flash tank vapor injection heat pump system – Part II: Simulation results and experimental validation', *International Journal of Refrigeration*, vol. 49, pp. 183–194, 2015.

[102] H. Qiao, V. Aute and R. Radermacher, 'Dynamic modeling and characteristic analysis of a two-stage vapor injection heat pump system under frosting conditions', *International Journal of Refrigeration*, vol. 84, pp. 181–197, 2017.

[103] R. Koury, R. Faria, R. Nunes, K. Ismail and L. Machado, 'Dynamic model and experimental study of an air–water heat pump for residential use', *International Journal of Refrigeration*, vol. 36, no. 3, pp. 674–688, 2013.

[104] H.-S. Lee and M.-Y. Lee, 'Steady state and start-up performance characteristics of air source heat pump for cabin heating in an electric passenger vehicle', *International Journal of Refrigeration*, vol. 69, pp. 232–242, 2016.

[105] C. J. Hermes and C. Melo, 'A first-principles simulation model for the start-up and cycling transients of household refrigerators', *International Journal of Refrigeration*, vol. 31, no. 8, pp. 1341–1357, 2008.

[106] D. E. Andrade and C. O. Negrão, 'Analysis of start-up tests of household refrigeration systems. A potential for on-line predictions of test results', *Applied Thermal Engineering*, vol. 54, no. 1, pp. 255–263, 2013.

[107] J. Jeong, A. Lubis, K. Saito, S. Karng, S. Kim and K. Kim, 'Start-up behaviour of a combined air-conditioning system in cooling and heating operating modes', *Energy and Buildings*, vol. 158, pp. 1346–1357, 2018.

[108] H. Qiao, V. Aute and R. Radermacher, 'Modeling of transient characteristics of an air source heat pump with vapor injection during reverse-cycle defrosting', *International Journal of Refrigeration*, vol. 88, pp. 24–34, 2018.

[109] F. Calise, M. Dentice d'Accadia and A. Palombo, 'Transient analysis and energy optimization of solar heating and cooling systems in various configurations', *Solar Energy*, vol. 84, no. 3, pp. 432–449, 2010.

[110] A. Buonomano, F. Calise and A. Palombo, 'Buildings dynamic simulation: Water loop heat pump systems analysis for European climates', *Applied Energy*, vol. 91, no. 1, pp. 222–234, 2012.

[111] I. Grossi, M. Dongellini, A. Piazzi and G. L. Morini, 'Dynamic modelling and energy performance analysis of an innovative dual-source heat pump system', *Applied Thermal Engineering*, vol. 142, pp. 745–759, 2018.

[112] F. Calise, R. D. Figaj and L. Vanoli, 'A novel polygeneration system integrating photovoltaic/thermal collectors, solar assisted heat pump, adsorption chiller

and electrical energy storage: Dynamic and energy-economic analysis', *Energy Conversion and Management*, vol. 149, pp. 798–814, 2017.

[113] R Shah, A. G. Alleyne, C. W. Bullard, B. P. Rasmussen and P. S. P. Hrnjak, 'Dynamic modeling and control of single and multi-evaporator subcritical vapor compression systems', *Industrial Engineering*, vol. 61801, no. 217, p. 207, 2003.

[114] A. Rasmussen, Bryan P; Alleyne, 'Dynamic modeling and advanced control of air conditioning and refrigeration systems', PhD thesis, University of Illinois at Urbana-Champaign, 2005.

[115] E. W. Grald and J. MacArthur, 'A moving-boundary formulation for modeling time-dependent two-phase flows', *International Journal of Heat and Fluid Flow*, vol. 13, no. 3, pp. 266–272, 1992.

[116] J. MacArthur, 'Transient heat pump behaviour: a theoretical investigation', *International Journal of Refrigeration*, vol. 7, no. 2, pp. 123–132, 1984.

[117] G. Wedekind, B. Bhatt and B. Beck, 'A system mean void fraction model for predicting various transient phenomena associated with two-phase evaporating and condensing flows', *International Journal of Multiphase Flow*, vol. 4, no. 1, pp. 97–114, 1978.

[118] J. Garcia, T. Ali, W. M. Duarte, A. Khosravi and L. Machado, 'Comparison of transient response of an evaporator model for water refrigeration system working with R1234yf as a drop-in replacement for R134a', *International Journal of Refrigeration*, vol. 91, pp. 211–222, 2018.

[119] S. Bendapudi, J. E. Braun and E. A. Groll, 'A comparison of moving-boundary and finite-volume formulations for transients in centrifugal chillers', *International Journal of Refrigeration*, vol. 31, no. 8, pp. 1437–1452, 2008.

[120] H. Pangborn, A. G. Alleyne and N. Wu, 'A comparison between finite volume and switched moving boundary approaches for dynamic vapor compression system modeling', *International Journal of Refrigeration*, vol. 53, pp. 101–114, 2015.

[121] A. Desideri, B. Dechesne, J. Wronski, M. van den Broek, S. Gusev, V. Lemort and S. Quoilin, 'Comparison of Moving Boundary and Finite-Volume Heat Exchanger Models in the Modelica Language', *Energies*, vol. 9, no. 5, p. 339, 2016.

[122] J. Bonilla, S. Dormido and F. E. Cellier, 'Switching moving boundary models for two-phase flow evaporators and condensers', *Communications in Nonlinear Science and Numerical Simulation*, vol. 20, no. 3, pp. 743–768, 2015.

[123] E. Rodriguez and B. Rasmussen, 'A comparison of modeling paradigms for dynamic evaporator simulations with variable fluid phases', *Applied Thermal Engineering*, vol. 112, pp. 1326–1342, 2017.

[124] B. P. Rasmussen, B. Shenoy, B. P. Rasmussen and B. Shenoy, 'Dynamic modeling for vapor compression systems — Part II : Simulation tutorial Review Article Dynamic modeling for vapor compression systems — Part II : Simulation tutorial', vol. 9669, 2012.

[125] H. Qiao, C. R. Laughman, V. Aute and R. Radermacher, 'An advanced switching moving boundary heat exchanger model with pressure drop', *International Journal of Refrigeration*, vol. 65, pp. 154–171, 2016.

[126] T. L. McKinley and A. G. Alleyne, 'An advanced nonlinear switched heat exchanger model for vapor compression cycles using the moving boundary method', *International Journal of Refrigeration*, vol. 31, no. 7, pp. 1253–1264, 2008.

[127] R. Sangi, P. Jahangiri and D. Müller, 'A combined moving boundary and discretized approach for dynamic modeling and simulation of geothermal heat pump systems', *Thermal Science and Engineering Progress*, 2019.

[128] D. Li, K. Luo and J. Dang, 'A moving boundary model for two-phase flow heat exchanger incorporated with relative velocities between boundaries and fluid', *International Journal of Heat and Mass Transfer*, 2016.

[129] I. H. Bell, S. Quoilin, E. Georges, J. E. Braun, E. A. Groll, W. T. Horton and V. Lemort, 'A generalized moving-boundary algorithm to predict the heat transfer rate of counter fl ow heat exchangers for any phase con fi guration', *Applied Thermal Engineering*, vol. 79, pp. 192–201, 2015.

[130] Z. Chu and W. Zhang, 'Moving-boundary and finite volume coupling algorithm for heat exchanger with fluid phase change', *International Journal of Heat and Mass Transfer*, vol. 131, pp. 313–328, 2019.

[131] S. Ozana and M. Pies, 'Using Simulink S-Functions with Finite Difference Method Applied for Heat Exchangers', pp. 210–215,

[132] S Bendapudi, J. E. Braun and E. A. Groll, 'Dynamic model of a centrifugal chiller system - Model development, numerical study, and validation', in *ASHRAE Transactions*, vol. 111 PART 1, 2005, pp. 132–148.

[133] N. Srihari, B. Prabhakara Rao, B. Sunden and S. K. Das, 'Transient response of plate heat exchangers considering effect of flow maldistribution', *International Journal of Heat and Mass Transfer*, vol. 48, no. 15, pp. 3231–3243, 2005.

[134] T. Gao and J. Gong, 'Modeling the airside dynamic behavior of a heat exchanger under frosting conditions', *Journal of Mechanical Science and Technology*, vol. 25, no. 10, pp. 2719–2728, 2011.

[135] R. Link and C. J. Deschamps, 'Numerical modeling of startup and shutdown transients in reciprocating compressors', *International Journal of Refrigeration*, vol. 34, no. 6, pp. 1398–1414, 2011.

[136] B. Li and A. G. Alleyne, 'Dynamic modeling, simulation, and control of transportation HVAC systems', PhD thesis, University of Illinois at Urbana-Champaign, 2013.

[137] C. T. Aksland, J. P. Koeln and A. G. Alleyne, 'A graph-based approach for dynamic compressor modeling in vapor compression systems', *ASME 2017 Dynamic Systems and Control Conference, DSCC 2017*, vol. 3, pp. 1–8, 2017.

[138] G. Hundy, A. Trott and T. Welch, 'Expansion Valves', *Refrigeration, Air Conditioning and Heat Pumps*, pp. 135–146, 2016.

[139] R. Lazzarin and M. Noro, 'Experimental comparison of electronic and thermostatic expansion valves performances in an air conditioning plant', *International Journal of Refrigeration*, vol. 31, no. 1, pp. 113–118, 2008.

[140] C. Chinnaraj, P. Govindarajan and R. Vijayan, 'Influence of electronic expansion valve on the performance of small window air conditioner retrofitted with R407C and R290', *Thermal Science*, vol. 15, no. SUPPL.2, pp. 327–339, 2011.

[141] X. Cao, Z.-Y. Li, L.-L. Shao and C.-L. Zhang, 'Refrigerant flow through electronic expansion valve: Experiment and neural network modeling', *Applied Thermal Engineering*, vol. 92, pp. 210–218, 2016.

[142] D. Ndiaye and M. Bernier, 'Modelling the bleed port of a thermostatic expansion valve', *International Journal of Refrigeration*, vol. 32, no. 5, pp. 826–836, 2009.

[143] T. Abergel and J. Dulac, 'Heat Pumps - Tracking Clean Energy Progress', Tech. Rep., 2019.

[144] Siemens, *AMESim*.

[145] P. Li, Y. Li and J. E. Seem, 'Modelica Based Dynamic Modeling of Water- Cooled Centrifugal Chillers', *International Refrigeration and Air Conditioning Conference at Purdue*, 2010.

[146] P. Nevriva, S. Ozana and L. Vilimec, 'Simulation of the heat exchangers dynamics in Matlab&Simulink', *WSEAS Transactions on Systems and Control*, vol. 4, no. 10, pp. 519–530, 2009.

[147] G Damasceno, S Rooke and V. Goldschmidt, 'Effects of reversing valves on heat pump performance', *International Journal of Refrigeration*, vol. 14, no. 2, pp. 93 –97, 1991.

[148] M. Amala Justus Selvam, P. Senthil Kumar and S. Muthuraman, 'The characteristics of brazed plate heat exchangers with different chevron angles', *Journal of Engineering and Applied Sciences*, vol. 4, no. 10, pp. 19–26, 2009.

[149] D. Lee, D. Kim, S. Park, J. Lim and Y. Kim, 'Evaporation heat transfer coefficient and pressure drop of r-1233zd(e) in a brazed plate heat exchanger', *Applied Thermal Engineering*, vol. 130, pp. 1147 –1155, 2018.

[150] M. H. Protter and C. B. Morrey, 'Differentiation under the Integral Sign. Improper Integrals. The Gamma Function', in *Intermediate Calculus*. New York, NY: Springer New York, 1985, pp. 421–453.

[151] M. Thorade and A. Saadat, 'Partial derivatives of thermodynamic state properties for dynamic simulation', *Environmental Earth Sciences*, vol. 70, no. 8, pp. 3497–3503, 2013.

[152] I. H. Bell, J. Wronski, S. Quoilin and V. Lemort, 'Pure and pseudo-pure fluid thermophysical property evaluation and the open-source thermophysical property library coolprop', *Industrial & Engineering Chemistry Research*, vol. 53, no. 6, pp. 2498–2508, 2014.

[153] Applied Chemicals and Materials Division, *RefProp*.

[154] F-Chart Software, *Engineering Equation Solver*.

[155] 'Equations of State and Formulations for Mixtures', *Supercritical Fluid Science and Technology*, vol. 4, pp. 333–480, 2013.

[156] D. Chisholm, 'A theoretical basis for the Lockhart-Martinelli correlation for two-phase flow', *International Journal of Heat and Mass Transfer*, vol. 10, no. 12, pp. 1767–1778, 1967.

[157] M. Cooper, 'SATURATION NUCLEATE POOL BOILING - a SIMPLE CORRELATION', pp. 785–793, 1984.

[158] D. Han, K. Lee and Y. Kim, 'Experiments on the characteristics of evaporation of R410A in brazed plate heat exchangers with different geometric configuration', *Applied Thermal Engineering*, vol. 23, pp. 1209–1225, 2003.

[159] B. Prabhakara Rao, P. Krishna Kumar and S. K. Das, 'Effect of flow distribution to the channels on the thermal performance of a plate heat exchanger', *Chemical Engineering and Processing: Process Intensification*, vol. 41, no. 1, pp. 49–58, 2002.

[160] Z. Zhang, S. Mehendale, J. Tian and Y. Li, 'Experimental investigation of distributor configuration on flow maldistribution in plate-fin heat exchangers', *Applied Thermal Engineering*, vol. 85, pp. 111–123, 2015.

[161] P. Yuan, G. Jiang, Y. He and W. Tao, 'Performance simulation of a two-phase flow distributor for plate-fin heat exchanger', *Applied Thermal Engineering*, vol. 99, pp. 1236–1245, 2016.

[162] Y. A. Çengel and A. J. Ghajar, *Heat and mass transfer*. McGraw Hill, 2004, p. 570.

[163] T.-L. Liu, B.-R. Fu and C. Pan, 'Boiling two-phase flow and efficiency of co- and counter-current microchannel heat exchangers with gas heating', *International Journal of Heat and Mass Transfer*, vol. 55, no. 21-22, pp. 6130–6141, 2012.

[164] W. Kim, J. Choi and H. Cho, 'Performance analysis of hybrid solar-geothermal CO 2 heat pump system for residential heating', *Renewable Energy*, vol. 50, pp. 596–604, 2013.

[165] Y. Zhao, Q. Liu and J. Gao, 'Experimental study on influence of electronic expansion valve opening on performance of water source heat pump unit', *IOP Conference Series: Earth and Environmental Science*, vol. 186, p. 012 039, 2018.

[166] J. Chen and J. Yu, 'Dynamic simulation of an air-source heat pump water heater using novel modified evaporator model', *Applied Thermal Engineering*, vol. 144, pp. 469 –478, 2018.

[167] F. W. Dittus and L. M. Boelter, 'Heat transfer in automobile radiators of the tubular type', *International Communications in Heat and Mass Transfer*, vol. 12, no. 1, pp. 3–22, 1985.

[168] D. Han, K. Lee and Y. Kim, 'The characteristics of brazed plate heat exchangers with different chevron angles', *Journal of the Korean Physical Society*, vol. 43, pp. 66–73, 2003.

[169] D. Chisholm and A. Wanniarachchi, 'Layout of plate heat exchangers', in *ASME/JSME Thermal Engineering Proceedings*, ASME, Ed., New York, NY, 1991, pp. 433–438.

List of Figures

List of Tables

ANNEX I

Model interface and subsystems

In this annex, the subsystems of the blocks presented in Section 3.4 are shown. Both indoor and outdoor units use the same subsystem changing only the "S-function".

Compressor block

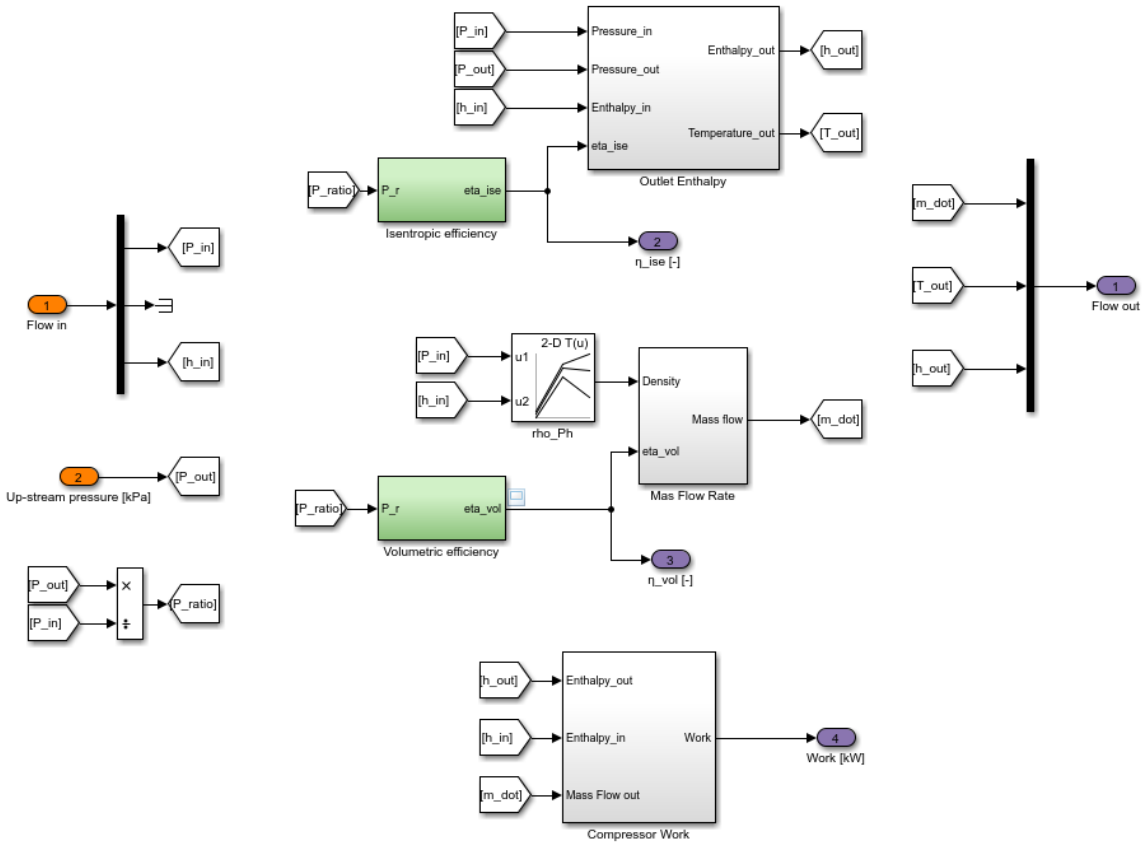

Compressor subsystem.

EEV block

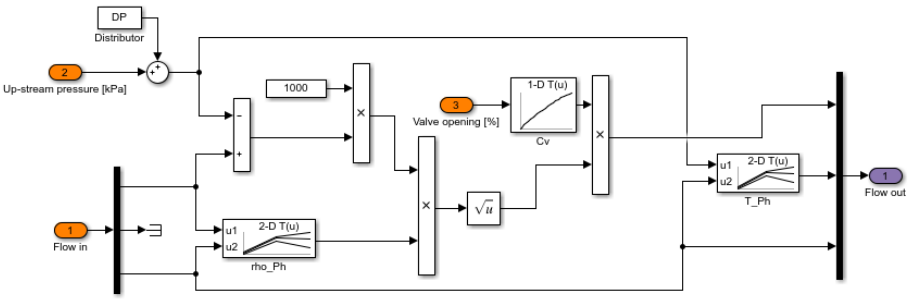

EEV subsystem.

PHEX block

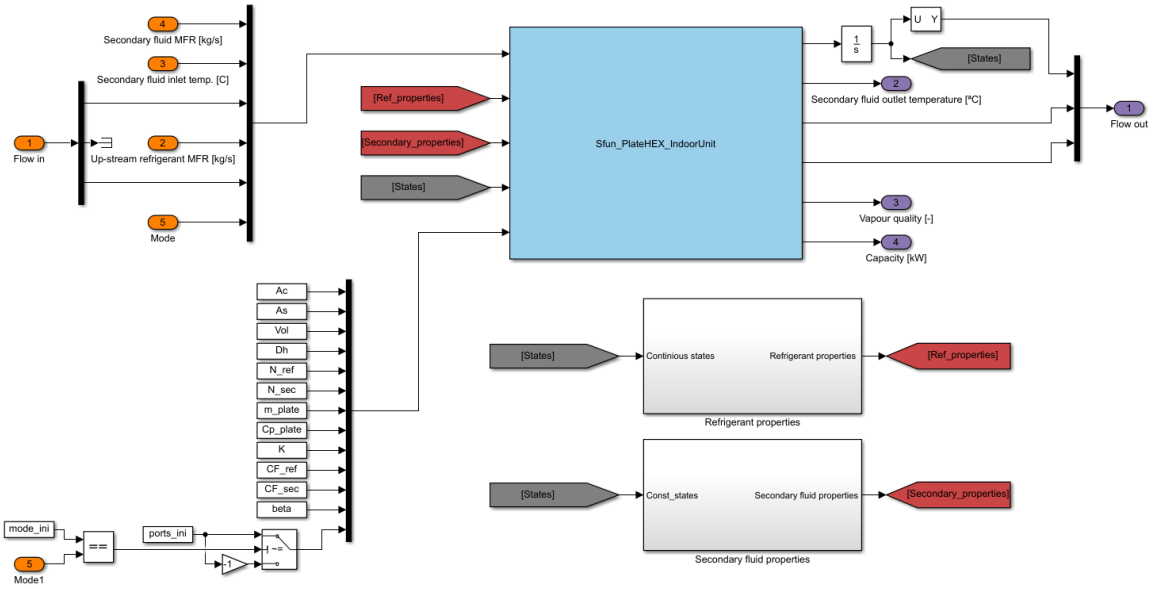

PHEX subsystem.

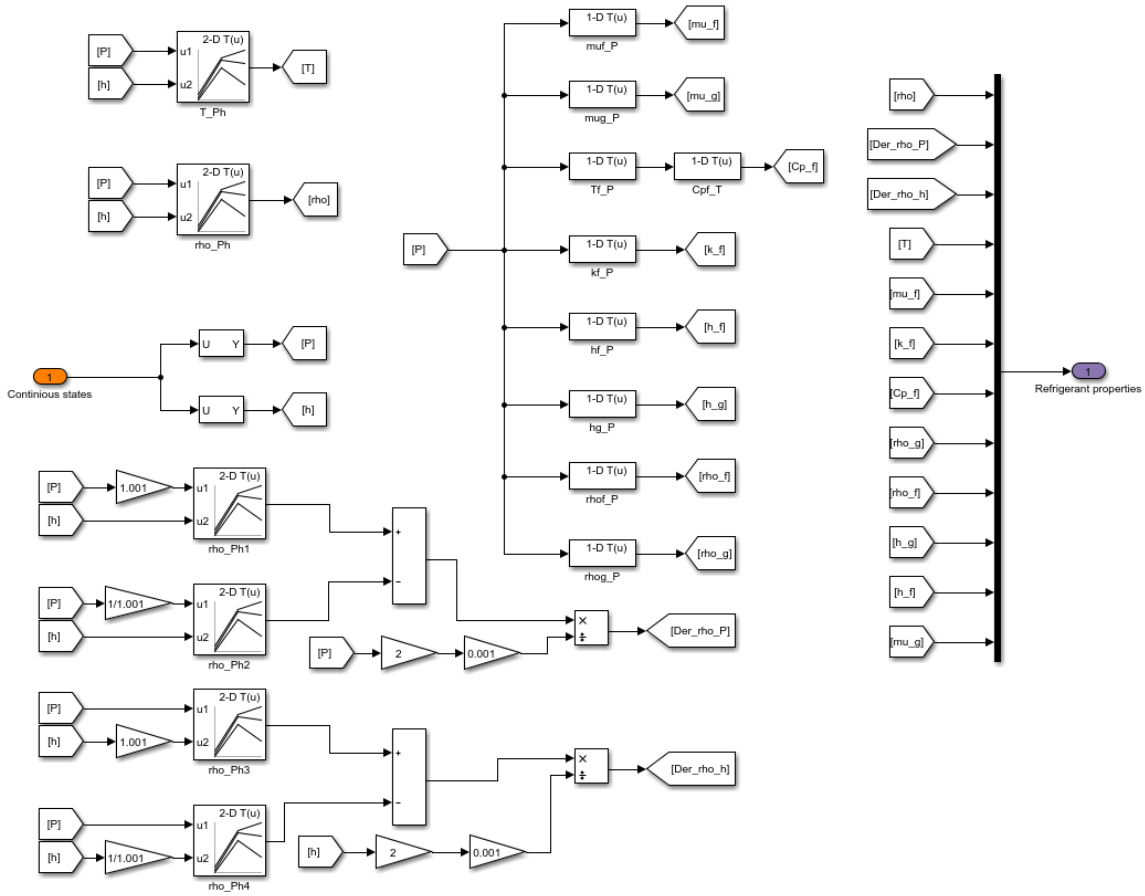

Refrigerant properties subsystem.

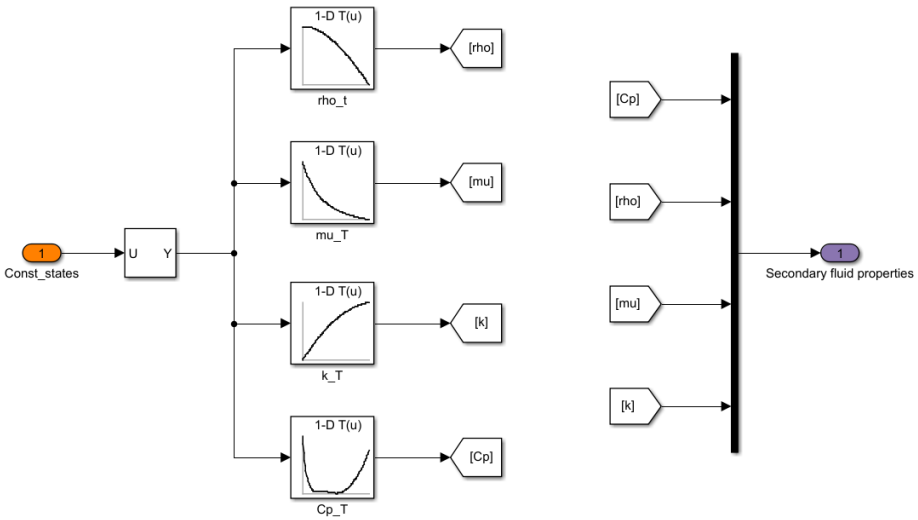

Secondary fluid properties subsystem.

ANNEX II

PHEX ”S-function” code

In this annex, the S-funtion used to simulate the heat transfer and the properties variation inside a PHEX is presented. Equations presented in the Chapter 3 are implemented.

Indoor unit PHEX ”S-funtion”

The ”S-function” used to simulate the indoor unit PHEX is presented. The only difference between the indoor unit and outdoor unit ”S-funtion”-s is that the behavior of the PHEX is inverted in the system working modes.

Therefore, during the heating mode, the indoor unit works as a condenser and the outdoor unit as an evaporator. In the cooling mode, the indoor unit works as an evaporator and the outdoor unit as a condenser.

The only change that must to be made to use this function in the outdoor unit is to replace ”mode == 1” with ”mode == 0” in line 160 of the code.

```
1  function Sfun_PlateHEX_IndoorUnit(block)
2
3  setup(block);
4  end
5
6  %%%%%%%%%% DESCRIPTION %%%%%%%%%%%%%%%%%%%%%%%%%%%%
7  % This S-funtion implements the matrix equation that calculates the ...
       time
8  % derivatives of the refrigerant pressure, temperature and
9  % enthalpy; secondary fluid temperature; and plate temperature in ...
       an indoor
10 % unit PHEX by applying the FCV method.
11 %%%%%%%%%%%%%%%%%%%%%%%%%%%%%%%%%%%%%%%%%%%%%%%%%%%%
12
13 function setup(block)
14
15 % Register parameters
16 block.NumDialogPrms  = 1;
17
18 % Register number of ports
19 block.NumInputPorts  = 5;
20 block.NumOutputPorts = 6;
21 block.NumContStates  = 0;
22
23 % Setup port properties
24 block.SetPreCompInpPortInfoToDynamic;
25 block.SetPreCompOutPortInfoToDynamic;
```

```
26
27 N  = block.DialogPrm(1).Data; % number of volumes
28
29 block.InputPort(1).Dimensions          = 6;
30 block.InputPort(2).Dimensions          = 4*N+8;
31 block.InputPort(3).Dimensions          = 4*N;
32 block.InputPort(4).Dimensions          = 4*N+1;
33 block.InputPort(5).Dimensions          = 13;
34
35 block.InputPort(1).SamplingMode        = 'Sample';
36 block.InputPort(2).SamplingMode        = 'Sample';
37 block.InputPort(3).SamplingMode        = 'Sample';
38 block.InputPort(4).SamplingMode        = 'Sample';
39 block.InputPort(5).SamplingMode        = 'Sample';
40
41 block.OutputPort(1).Dimensions         = 4*N+1;
42 block.OutputPort(2).Dimensions         = 1;
43 block.OutputPort(3).Dimensions         = 1;
44 block.OutputPort(4).Dimensions         = 1;
45 block.OutputPort(5).Dimensions         = 2*N;
46 block.OutputPort(6).Dimensions         = N;
47
48 block.OutputPort(1).SamplingMode       = 'Sample';
49 block.OutputPort(2).SamplingMode       = 'Sample';
50 block.OutputPort(3).SamplingMode       = 'Sample';
51 block.OutputPort(4).SamplingMode       = 'Sample';
52 block.OutputPort(5).SamplingMode       = 'Sample';
53 block.OutputPort(6).SamplingMode       = 'Sample';
54
55 block.SampleTimes = [0  0];
56 block.SimStateCompliance = 'DefaultSimState';
57
58 block.RegBlockMethod('Outputs', @Outputs);
59
60 end
61
62 function Outputs(block)
63
64 %% PARAMETERS
65 Ac          = block.InputPort(5).Data(1);  % Cross-sectional area
66 As          = block.InputPort(5).Data(2);  % Contact area
67 Vol         = block.InputPort(5).Data(3);  % Total volume
68 Dh          = block.InputPort(5).Data(4);  % Hydraulic diameter
```

```
69  N_ref        = block.InputPort(5).Data(5);  % Number of refrigerant ...
        channels
70  N_sec        = block.InputPort(5).Data(6);  % Numer of secondary ...
        channels
71  mass_wall    = block.InputPort(5).Data(7);  % Plates mass
72  cp_wall      = block.InputPort(5).Data(8);  % Plates specific heat
73  K            = block.InputPort(5).Data(9);  % Number of FCV
74  CF_ref       = block.InputPort(5).Data(10); % Ref. correcrion factor
75  CF_sec       = block.InputPort(5).Data(11); % Sec. correction factor
76  beta         = block.InputPort(5).Data(12); % Chevron angle
77  ports        = block.InputPort(5).Data(13); % 1 = counter-flow // -1 ...
        = parallel-flow
78
79  %% INPUTS
80  mdot_sec         = block.InputPort(1).Data(1)/N_sec;
81  T_sec_in         = block.InputPort(1).Data(2);
82  mdot_ref_in      = block.InputPort(1).Data(3)/N_ref;
83  mdot_ref_out     = block.InputPort(1).Data(4)/N_ref;
84  h_in             = block.InputPort(1).Data(5);
85  mode             = block.InputPort(1).Data(6); % 1 = ...
        heating(condenser) // 0 = cooling(evaporator)
86
87  %% CONTINUOUS STATE CALLBACKS
88  P_ref        = block.InputPort(4).Data(1);
89  h_ref        = block.InputPort(4).Data(2:K+1);
90  Tw           = block.InputPort(4).Data(K+2:2*K+1);
91  mdot_ref     = block.InputPort(4).Data(2*K+2:3*K+1);
92  T_sec        = block.InputPort(4).Data(3*K+2:4*K+1);
93
94  %% REFRIGERANT PROPERTIES
95  rho_ref      = block.InputPort(2).Data(1:K);
96  d_rho_P      = block.InputPort(2).Data(1*K+1:2*K);
97  d_rho_h      = block.InputPort(2).Data(2*K+1:3*K);
98  T_ref        = block.InputPort(2).Data(3*K+1:4*K);
99  mu_liq       = block.InputPort(2).Data(4*K+1);
100 k_liq        = block.InputPort(2).Data(4*K+2);
101 Cp_liq       = block.InputPort(2).Data(4*K+3);
102 rho_gas      = block.InputPort(2).Data(4*K+4);
103 rho_liq      = block.InputPort(2).Data(4*K+5);
104 h_gas        = block.InputPort(2).Data(4*K+6);
105 h_liq        = block.InputPort(2).Data(4*K+7);
106 mu_gas       = block.InputPort(2).Data(4*K+8);
107
```

```
%% SECONDARY FLUID PROPERTIES
cp_sec        = block.InputPort(3).Data(1:K);
rho_sec       = block.InputPort(3).Data(1*K+1:2*K);
mu_sec        = block.InputPort(3).Data(2*K+1:3*K);
k_sec         = block.InputPort(3).Data(3*K+1:4*K);

%%%%%%%%%%%%%%%%%%%%%%%%%%%%%%%%%%%%%%%%%%%%%
%% CALCULATES FLUIDS CURRENT PROPERTIES %%
%%%%%%%%%%%%%%%%%%%%%%%%%%%%%%%%%%%%%%%%%%%%%

% Calculate refrigerant enthalpies at volume bounds
if ports == -1 % Parallel-flow
    h_bound =  [h_in;(h_ref(1:K-1)+h_ref(2:K))/2;...
                    (h_ref(K)+(h_ref(K)-h_ref(K-1))/2)];
else
     h_bound = [(h_ref(1)+(h_ref(1)-h_ref(2))/2);...
                    (h_ref(1:K-1)+h_ref(2:K))/2; h_in];
end

% Calculate refrigerant outlet temperatures
if ports == -1 % Parallel-flow
     T_ref_out = T_ref(K)+(T_ref(K)-T_ref(K-1))/2;
     h_ref_out = h_bound(end);
else
     T_ref_out = T_ref(1)+(T_ref(1)-T_ref(2))/2;
     h_ref_out = h_bound(1);
end

% Calculate refrigerant quality
h_fg = (h_gas - h_liq);
quality = (h_ref-h_liq)/h_fg;
quality(quality<0) = 0;
quality(quality>1) = 1;

% Calculate secondary temperatures at volume bounds
T_sec_bound = [T_sec_in;(T_sec(1:K-1)+T_sec(2:K))/2;...
                    (T_sec(K)+((T_sec(K)-T_sec(K-1))/2))];

%%%%%%%%%%%%%%%%%%%%%%%%%%%%%%%%%%
%% CALCULATE REFRIGERANT HTC %%
%%%%%%%%%%%%%%%%%%%%%%%%%%%%%%%%%%

p_co = (21.01*beta^2 - 19.022*beta + 8.98)/1000;
```

```
151
152 G_ref    = abs(mdot_ref)/Ac;
153 G_Eq     = G_ref .* ((1-quality) + quality *((rho_liq/rho_gas)^0.5));
154 Re_Eq    = G_Eq * Dh / mu_liq;
155 Re_liq   = G_ref * Dh / mu_liq;
156 Re_gas   = G_ref * Dh / mu_gas;
157 Pr       = Cp_liq * mu_liq /k_liq;
158
159 alpha_ref = zeros(K,1);
160 if mode == 1 % Condenser
161     C_1 = 11.22 * (p_co/Dh)^-2.83 * (pi/2 - beta)^-4.5;
162     C_2 = 0.35 * (p_co/Dh)^0.23 * (pi/2 - beta)^1.48;
163
164     alpha_2p  = (k_liq/Dh) * (C_1 * Re_Eq.^C_2 * Pr^0.3);
165     alpha_gas = 0.023 * (k_liq/Dh) * Re_gas.^0.8 * Pr^0.3;
166     alpha_liq = 0.023 * (k_liq/Dh) * Re_liq.^0.8 * Pr^0.3;
167
168     for n = 1:K
169         if quality(n) == 1
170             alpha_ref(n) = CF_ref * alpha_gas(n);
171             else if quality(n) == 0
172                 alpha_ref(n) = CF_ref * alpha_liq(n);
173                 else
174                 alpha_ref(n) = CF_ref * alpha_2p(n);
175                 end
176         end
177     end
178 else        % Evaporator
179     q = abs(mdot_ref) .* (h_gas-h_ref) ./ (As/K);
180     Bo_Eq = abs(q) ./ G_Eq ./ h_fg;
181
182     C_1 = 2.81 * (p_co/Dh)^-0.041 * (pi/2 - beta)^-2.83;
183     C_2 = 0.746 * (p_co/Dh)^-0.082 * (pi/2 - beta)^0.61;
184
185     alpha_2p = (k_liq/Dh) * (C_1 * Re_Eq.^C_2 .* Pr^0.4 .* ...
        Bo_Eq.^0.3);
186     alpha_1p = 0.023 * (k_liq/Dh) * Re_gas.^0.8 * Pr^0.4;
187
188     alpha_ref = zeros(K,1);
189     for n = 1:K
190         if quality(n) == 1
191             alpha_ref(n) = CF_ref * alpha_1p(n);
192         else
```

```
                alpha_ref(n) = CF_ref * alpha_2p(n);
            end
        end
    end

    %%%%%%%%%%%%%%%%%%%%%%%%%%%%%%%%%%%%%%%%
    %%  CALCULATE SECONDARY FLUID HTC %%
    %%%%%%%%%%%%%%%%%%%%%%%%%%%%%%%%%%%%%%%%

    mass_sec = mean(rho_sec)*(Vol/K);

    G_sec = mdot_sec / Ac;
    Re_sec = G_sec * Dh ./ mu_sec;
    Pr_sec = mu_sec .* cp_sec ./ k_sec;

    alpha_ref = zeros(K,1);
    if mode == 1 % Condenser
        alpha_sec = CF_sec * (k_sec/Dh) * 0.023 .* Re_sec.^0.8 .* ...
            Pr_sec.^0.4;
    else
        alpha_sec = CF_sec * (k_sec/Dh) * 0.023 .* Re_sec.^0.8 .* ...
            Pr_sec.^0.3;
    end

    %%%%%%%%%%%%%%%%%%%%%%%%%%%%%%%%%%%%%%%%%%%%%%%%%
    %%  CALCULATE SECONDARY FLUID DERIVATIVES %%
    %%%%%%%%%%%%%%%%%%%%%%%%%%%%%%%%%%%%%%%%%%%%%%%%%

    Q_sec =  alpha_sec * (As/K) .* (Tw - T_sec);

    T_sec_dot = (mdot_sec*cp_sec.*(T_sec_bound(1:end-1)-...
                    T_sec_bound(2:end)) + (2*Q_sec))/...
                    (mean(cp_sec)*mass_sec);

    %%%%%%%%%%%%%%%%%%%%%%%%%%%%%%%%%%%%%%%%%%%%
    %%  CALCULATE REFRIGERANT DERIVATIVES %%
    %%%%%%%%%%%%%%%%%%%%%%%%%%%%%%%%%%%%%%%%%%%%

    Q_ref =  alpha_ref.*(As/K).*(T_ref-Tw);

    % Matrixes
    Z = zeros(2*K,2*K);
    s = zeros(2*K,1);
```

```
234
235 % P_dot
236 Z(1:K,1)       = ((d_rho_P.*h_ref)-1)*Vol/K;
237 Z(K+1:K*2,1) = d_rho_P.*Vol/K;
238
239 % h_dot
240 Z(1:K,2:K+1)       = diag(((d_rho_h.*h_ref)+rho_ref)*Vol/K);
241 Z(K+1:K*2,2:K+1) = diag(d_rho_h.*Vol/K);
242
243 % m_dot
244 h_diag = diag(h_bound(2:end))+diag(-h_bound(2:end-1),-1);
245 m_diag = diag(ones(K,1))+diag(-ones(K-1,1),-1);
246
247 if ports == -1 % Parallel-flow
248     Z(1:K,K+2:end)       = h_diag(:,1:end-1);
249     Z(K+1:end,K+2:end) = m_diag(:,1:end-1);
250 else
251     Z(1:K,K+2:end)       = -h_diag(:,1:end-1);
252     Z(K+1:end,K+2:end) = -m_diag(:,1:end-1);
253 end
254
255 % Solution
256 if ports == -1 % Parallel-flow
257     s(1)     = (mdot_ref_in*h_in)-(Q_ref(1)*2);
258     s(K)     = -(mdot_ref_out*h_bound(end))-(Q_ref(K)*2);
259     s(K+1)   = mdot_ref_in;
260     s(2*K)   = -mdot_ref_out;
261 else
262     s(1)     = -(mdot_ref_out*h_bound(1))-(Q_ref(1)*2);
263     s(K)     = (mdot_ref_in*h_in)-(Q_ref(K)*2);
264     s(K+1)   = -mdot_ref_out;
265     s(2*K)   = mdot_ref_in;
266 end
267
268 s(2:K-1) = -(Q_ref(2:K-1)*2);
269
270
271 % Solve
272 x_dot = Z\s;
273 P_dot = x_dot(1);
274 h_dot = x_dot(2:K+1);
275 mdot  = ([mdot_ref_in;x_dot(K+2:2*K)]+...
276             [x_dot(K+2:2*K);mdot_ref_out])/2;
```

```
277 mdot_new = (mdot-mdot_ref);
278
279 %%%%%%%%%%%%%%%%%%%%%%%%%%%%%%%%%%%%
280 %%  CALCULATE PLATE DERIVATIVES %%
281 %%%%%%%%%%%%%%%%%%%%%%%%%%%%%%%%%%%%
282
283 Tw_dot = ((Q_ref)-(Q_sec))/(cp_wall*mass_wall/K);
284
285 %%%%%%%%%%%%%
286 %%  OUTPUT %%
287 %%%%%%%%%%%%%
288
289 % Derivatives vector
290 block.OutputPort(1).Data(1:4*K+1) = [P_dot; h_dot; Tw_dot; ...
        mdot_new; T_sec_dot];
291
292 % Secondary fluid outlet temperature
293 block.OutputPort(2).Data = T_sec_bound(K);
294
295 % Refrigerant outlet temperature
296 block.OutputPort(3).Data = T_ref_out;
297
298 % Refrigerant outlet enthalpy
299 block.OutputPort(4).Data = h_ref_out;
300
301 % Refrigerant HTC
302 block.OutputPort(5).Data = [alpha_ref; alpha_sec];
303
304 % Refrigerant quality
305 block.OutputPort(6).Data = quality;
306
307 end
```

ANNEX III

Micro-scale validations

In this annex, the remaining comparisons between experimental data and simulation results in micro-scale that have not been presented in Chapter 4 are presented. It is included the comparison of high and low working pressures and the water outlet temperature of both indoor and outdoor PHEXs.

All tests that were carried out and their conditions are summarized in Table 4.9. Similarly, different transient-states forced in each test situation are described in 4.10.

Initially, it was thought that the model could need some different corrections for different operation conditions. Thus, in total, 14 test with 8 situations each are carried out. However, after start comparing test data with simulation results it was observed that, having enough information from the manufacturers, the model was able to simulate the behavior of the system under different working conditions without the need of any kind of corrections. Therefore, not all the tests where finally used.

Representative results were presented in Section 4.6. Here, the rest of the simulated test results are presented.

On the other hand, there are situations in which the forced change in the operation conditions affects the refrigerant fluid circuit but that barely has influence in secondary fluids (i.e. situations 5 and 6). Therefore, could be that in the presented figures it seems as an stationary situations.

For anyone interested in seeing more test or simulation results, contact the thesis author.

Test A-C1

Situation 1

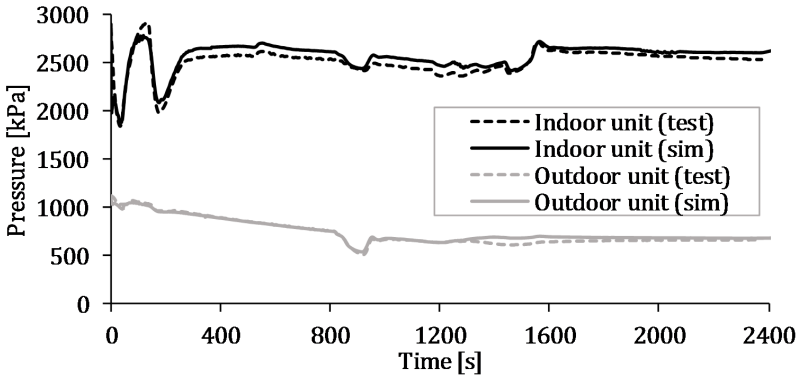

Refrigerant pressures.

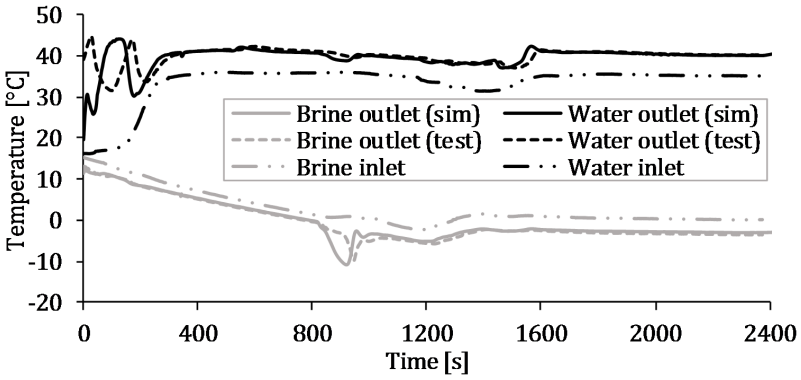

Water and brine temperatures.

Situation 2

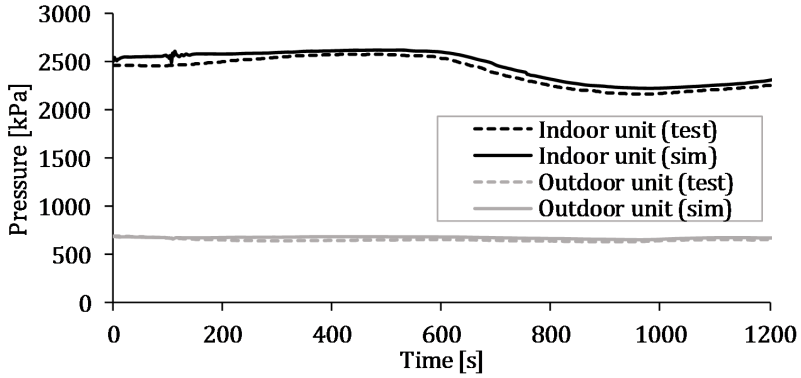

Refrigerant pressures.

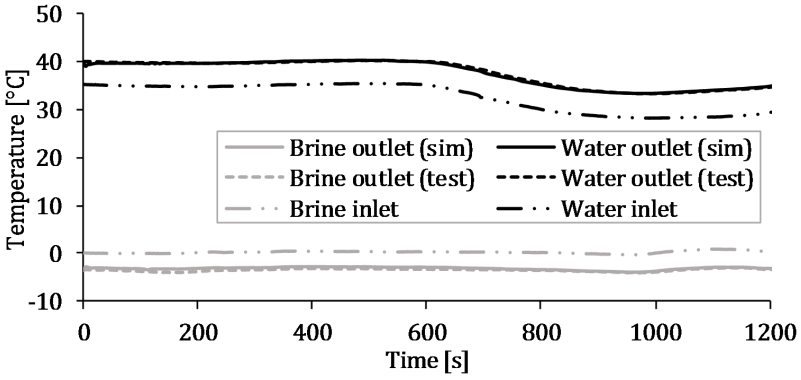

Water and brine temperatures.

Situation 3

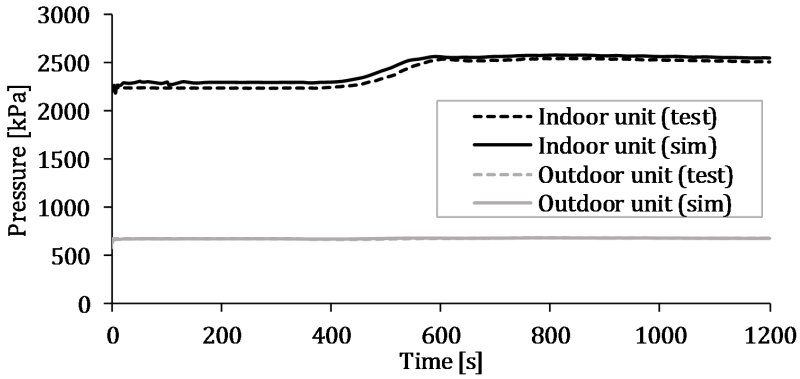

Refrigerant pressures.

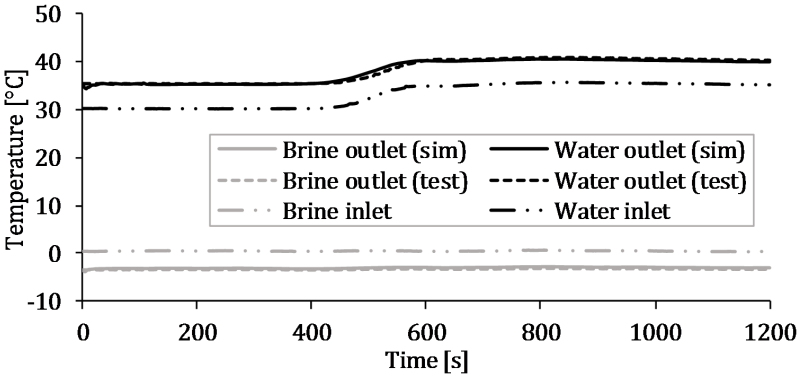

Water and brine temperatures.

Situation 4

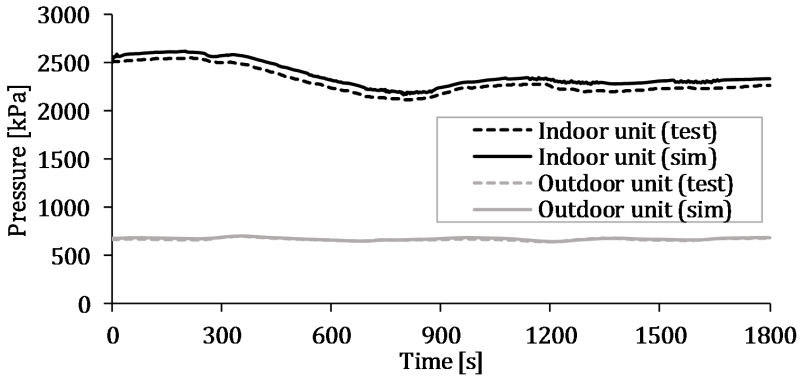

Refrigerant pressures.

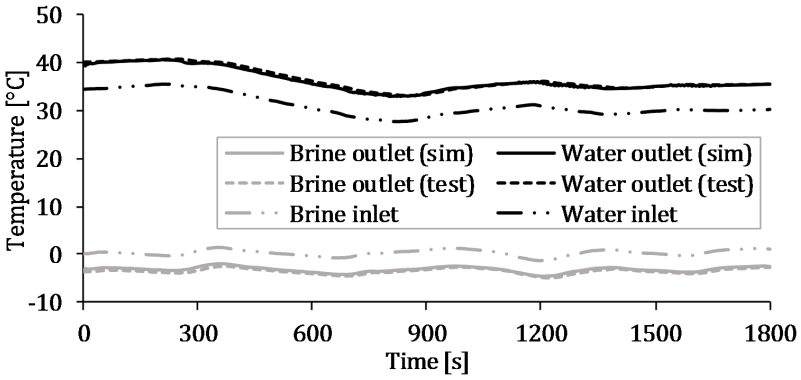

Water and brine temperatures.

Situation 5

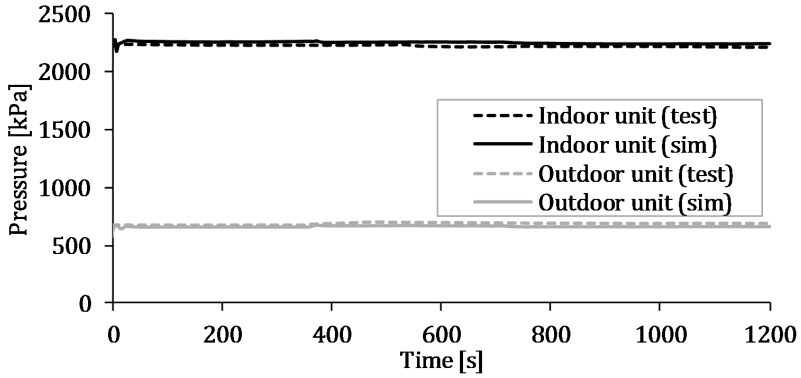

Refrigerant pressures.

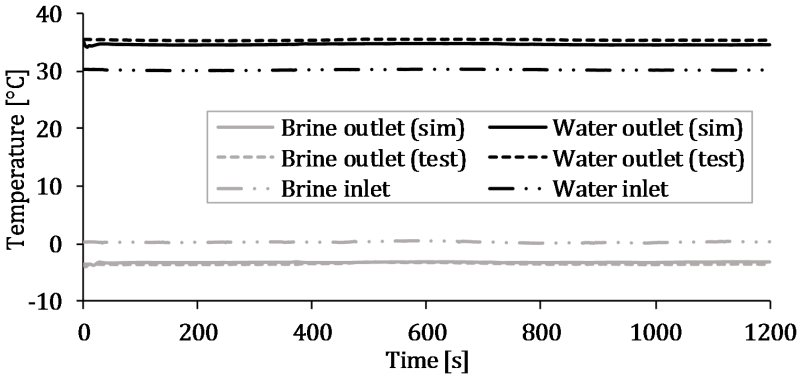

Water and brine temperatures.

Situation 6

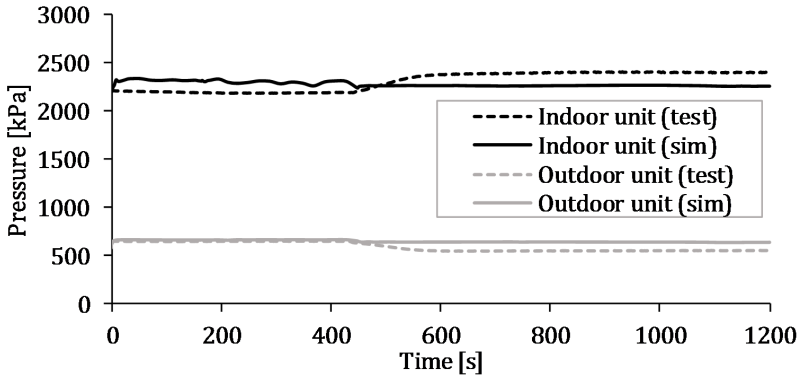

Refrigerant pressures.

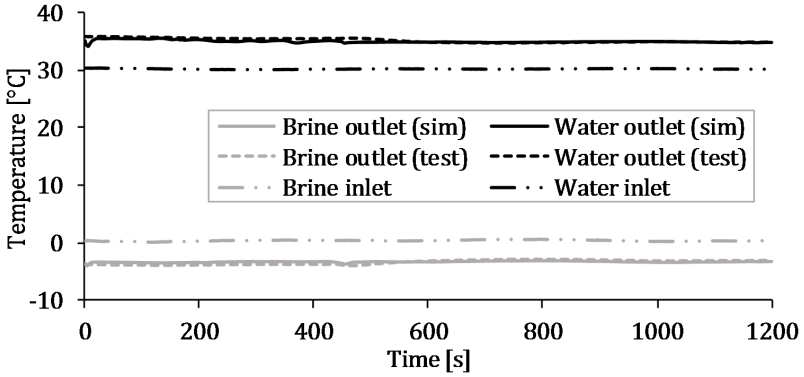

Water and brine temperatures.

Situation 7

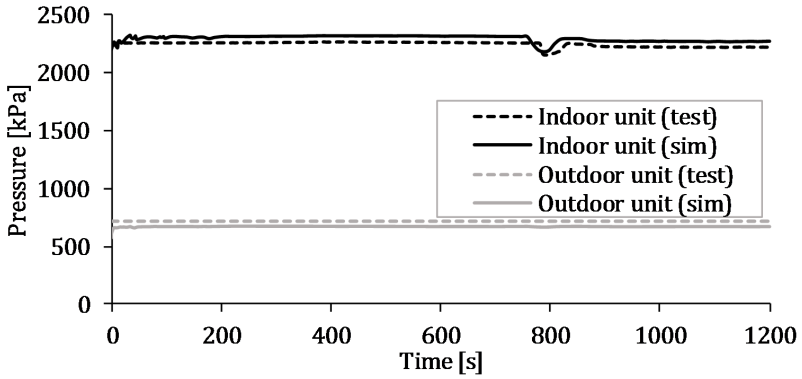

Refrigerant pressures.

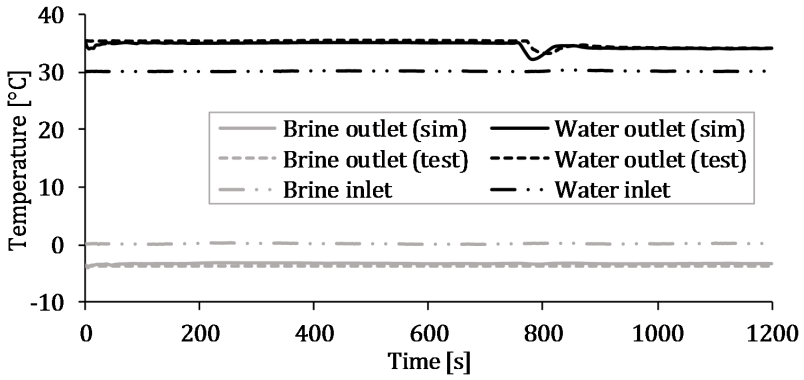

Water and brine temperatures.

Situation 8

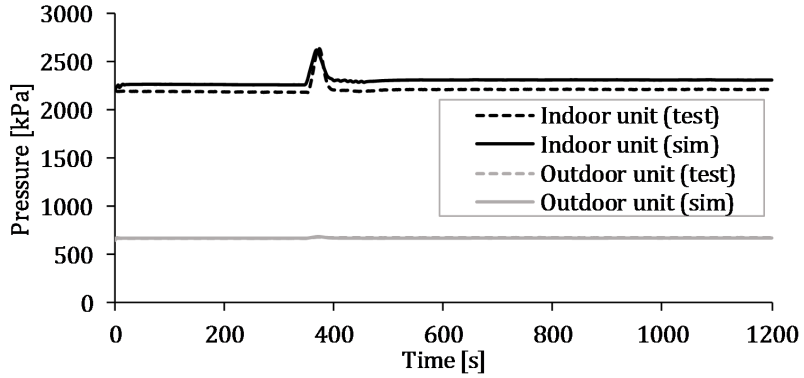

Refrigerant pressures.

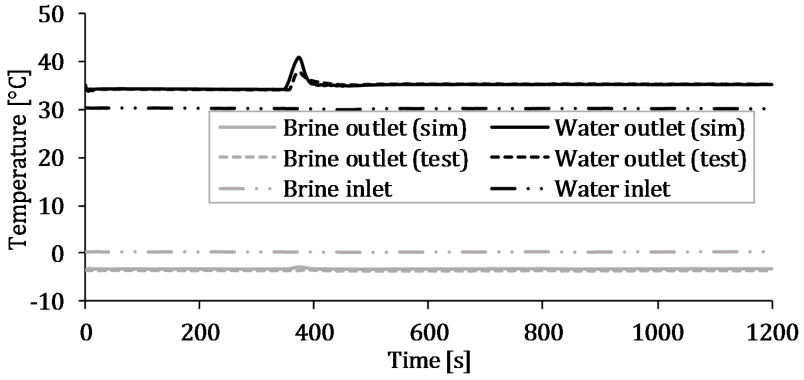

Water and brine temperatures.

Test A-C2

Situation 3

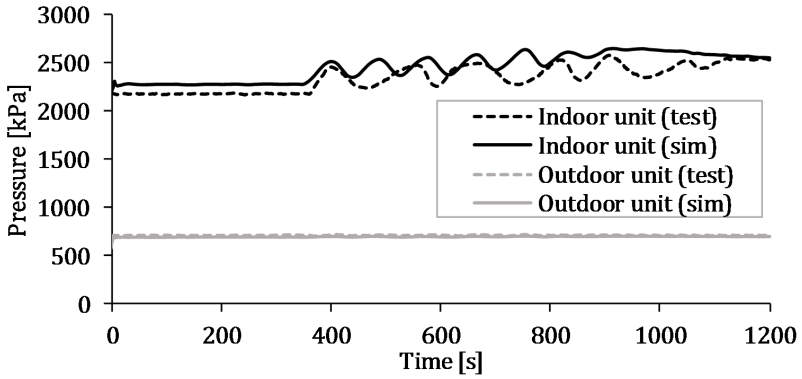

Refrigerant pressures.

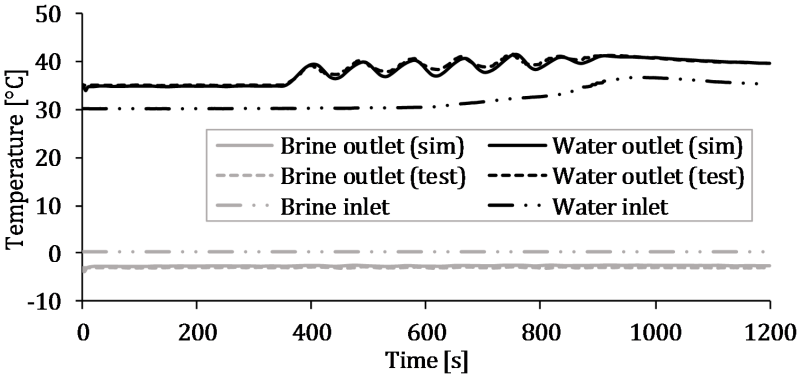

Water and brine temperatures.

Situation 4

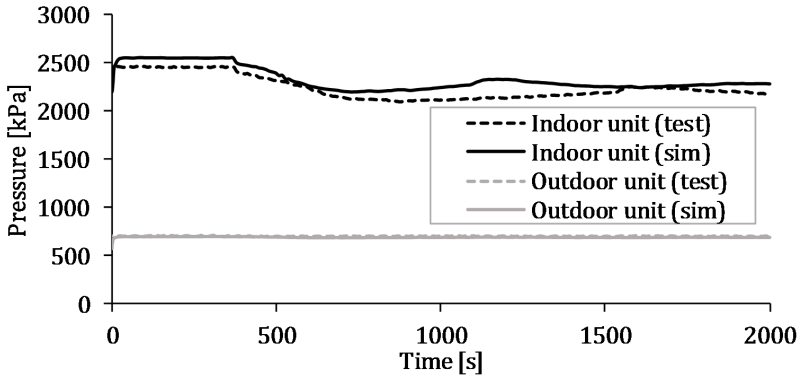

Refrigerant pressures.

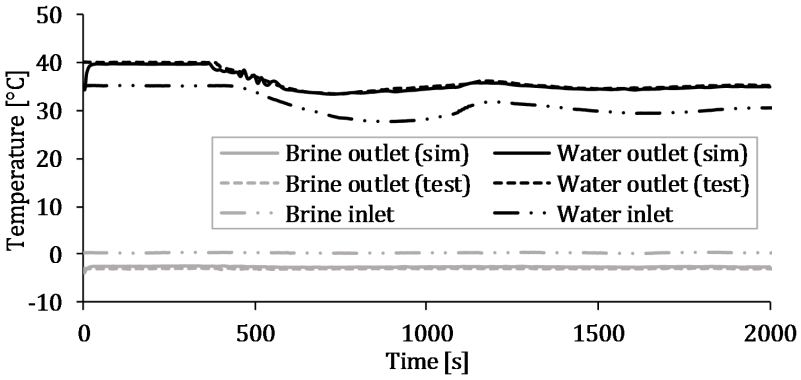

Water and brine temperatures.

Situation 5

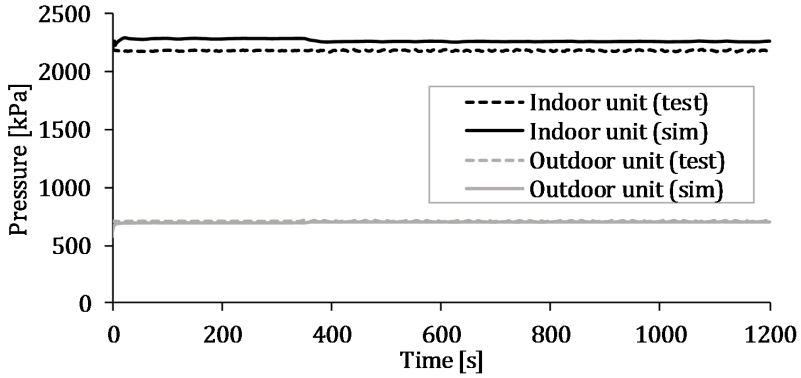

Refrigerant pressures.

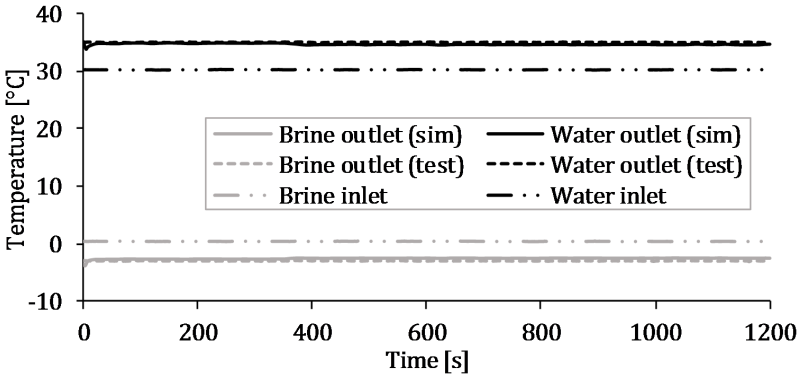

Water and brine temperatures.

Situation 6

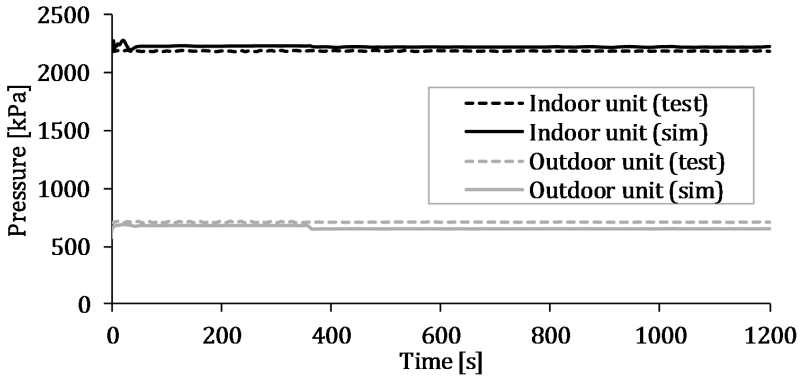

Refrigerant pressures.

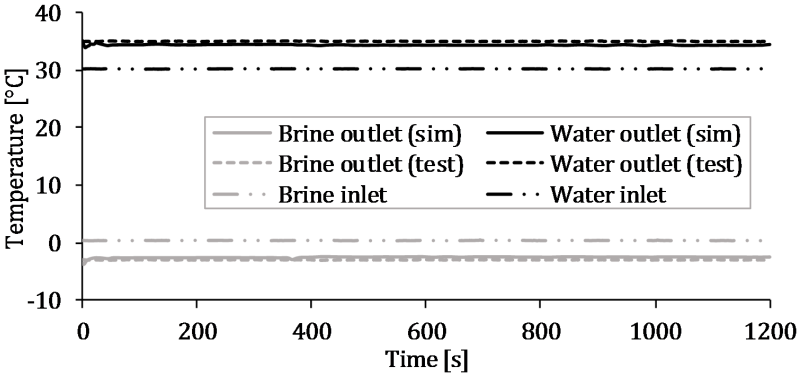

Water and brine temperatures.

Situation 7

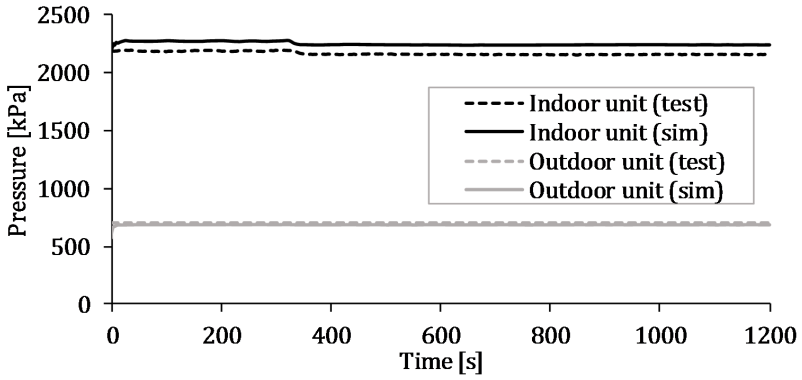

Refrigerant pressures.

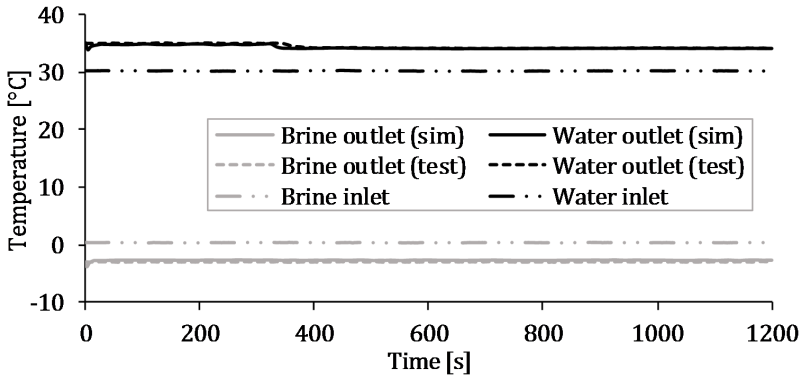

Water and brine temperatures.

Situation 8

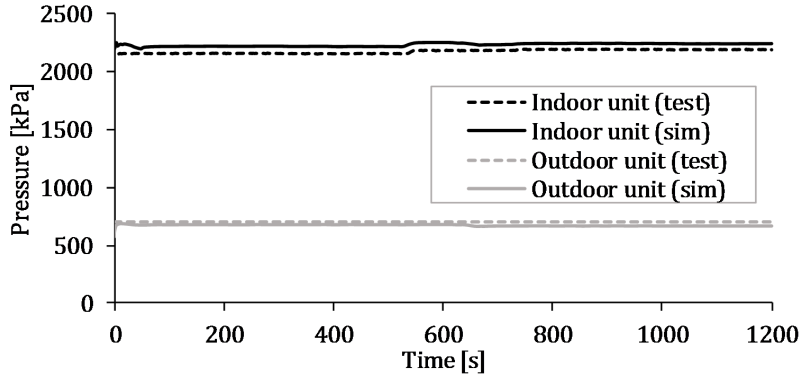

Refrigerant pressures.

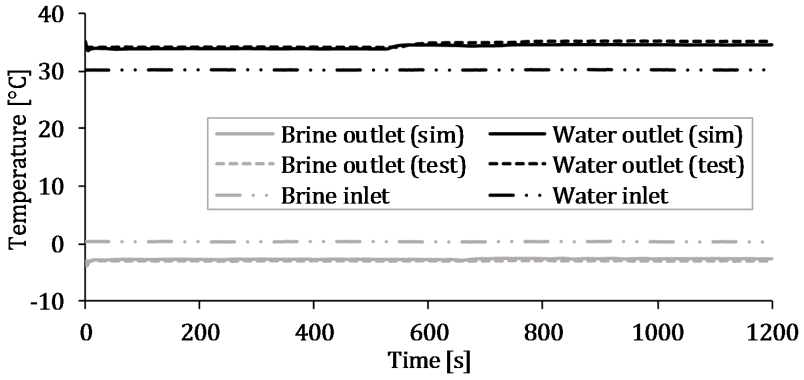

Water and brine temperatures.

Test C-C1

Situation 2

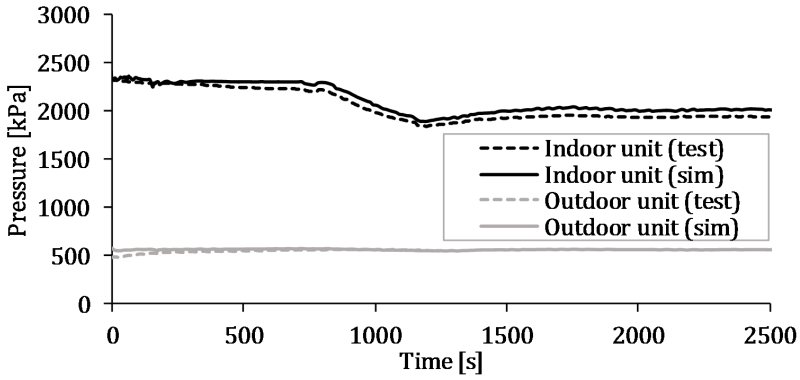

Refrigerant pressures.

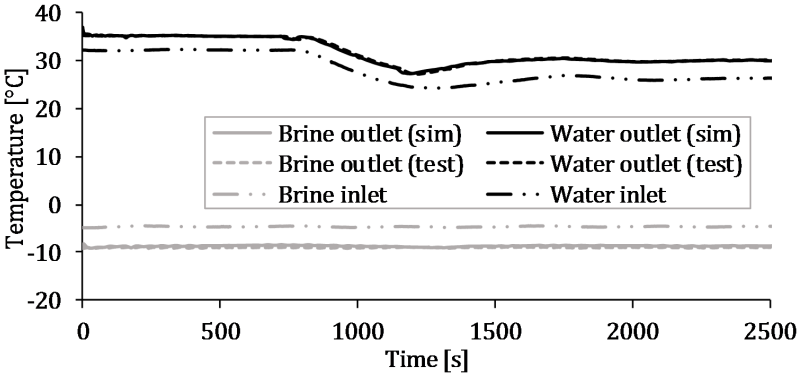

Water and brine temperatures.

Situation 3

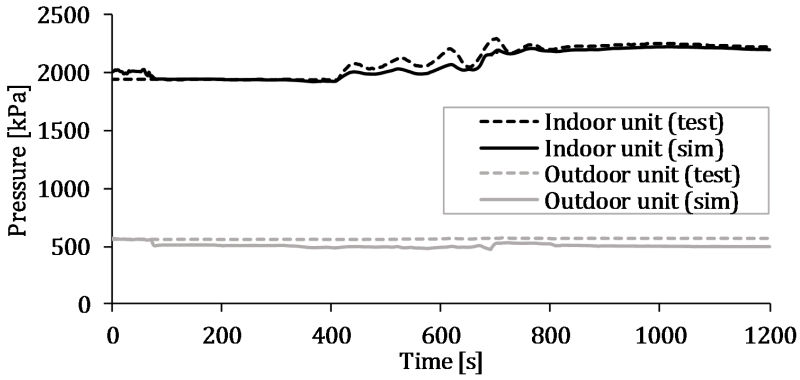

Refrigerant pressures.

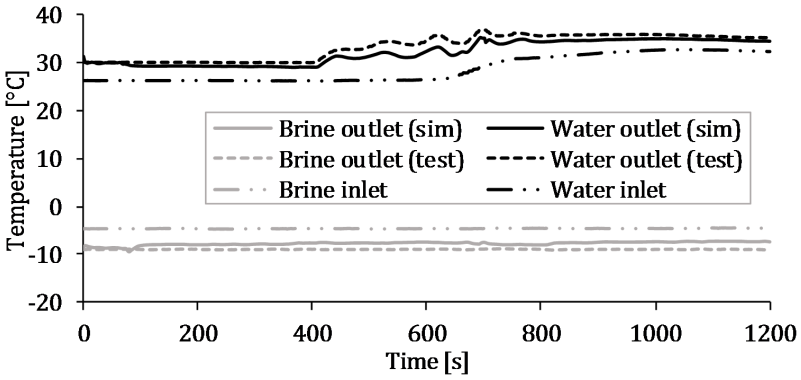

Water and brine temperatures.

Situation 4

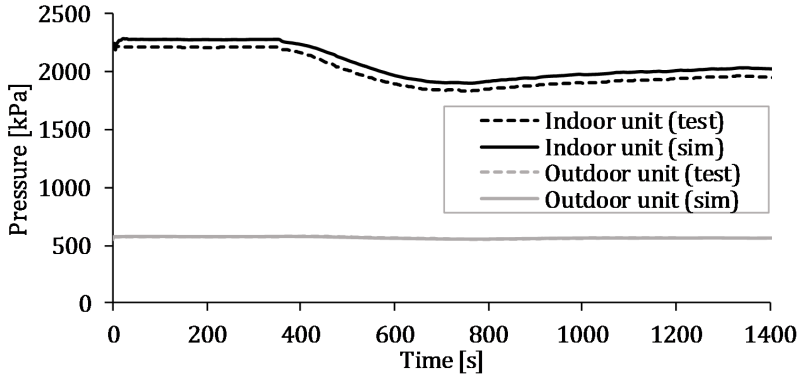

Refrigerant pressures.

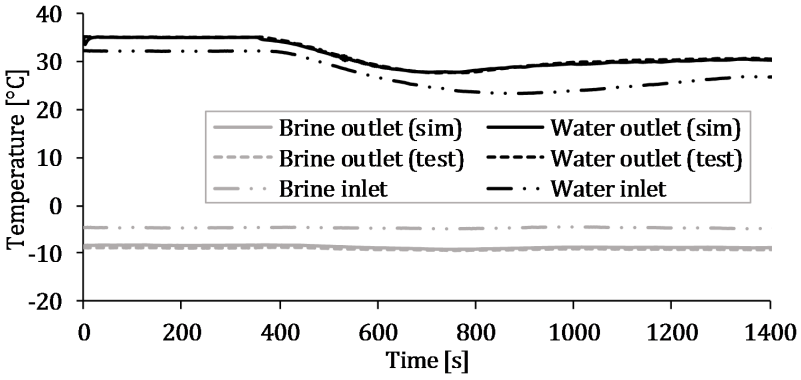

Water and brine temperatures.

Test E-E1

Situation 4

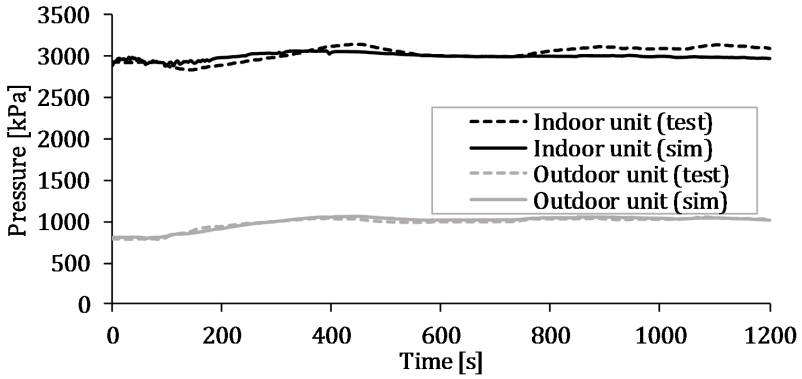

Refrigerant pressures.

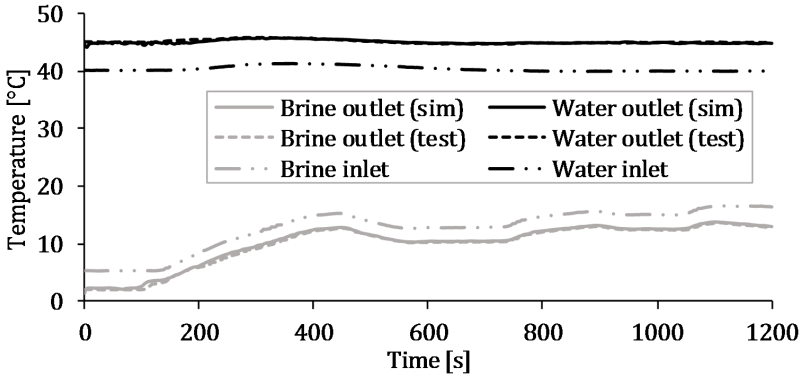

Water and brine temperatures.

Test E-E2

Situation 3

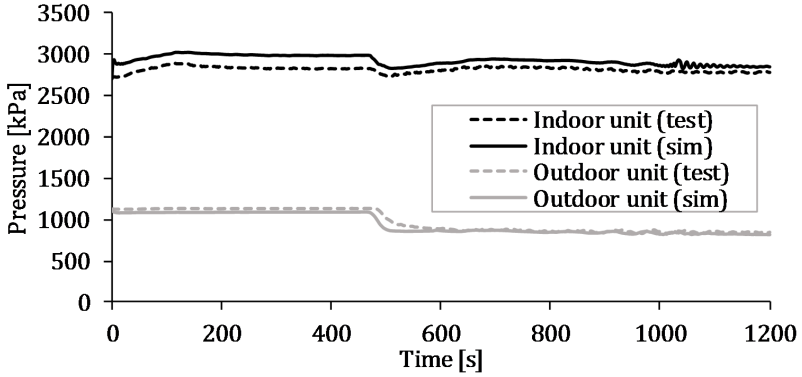

Refrigerant pressures.

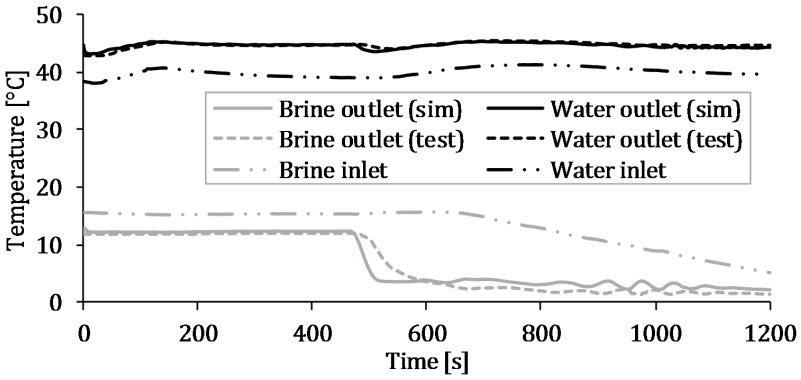

Water and brine temperatures.

Test G-C1

Situation 1

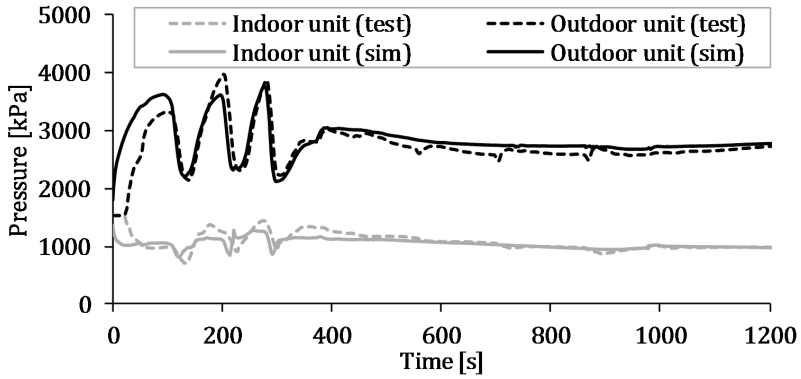

Refrigerant pressures.

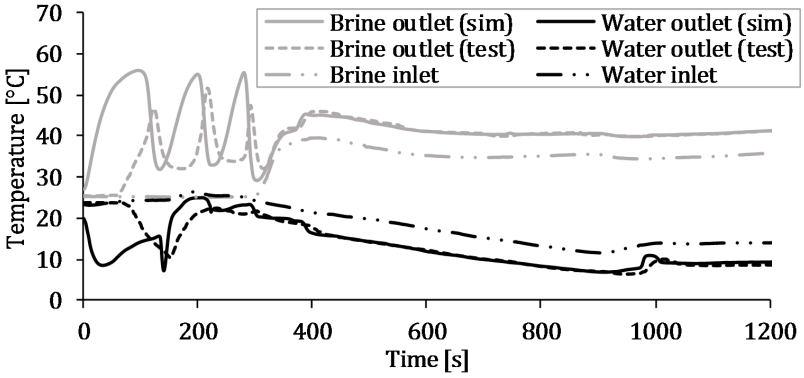

Water and brine temperatures.

Test G-C2

Situation 4

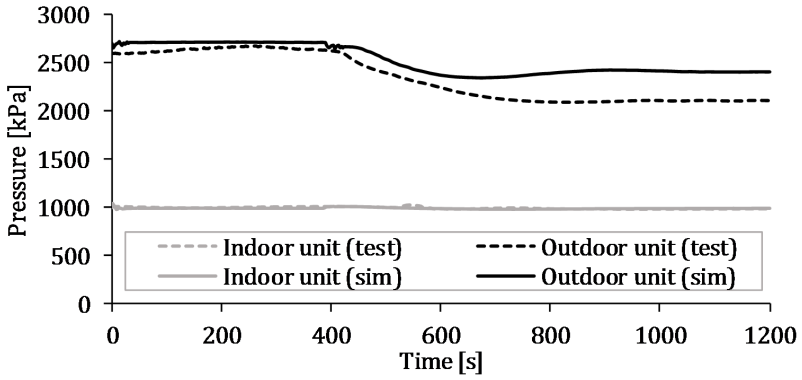

Refrigerant pressures.

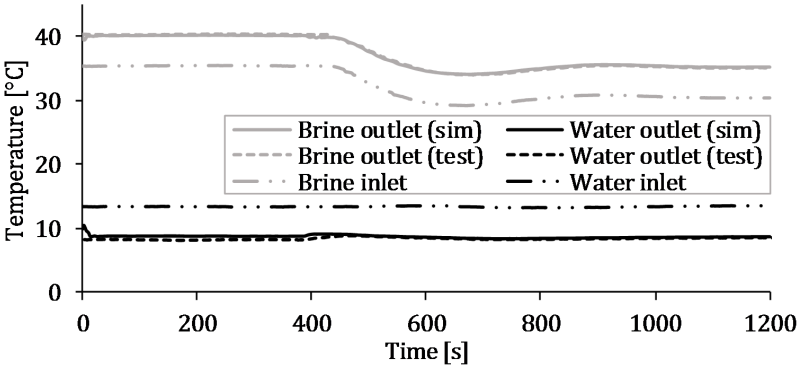

Water and brine temperatures.

Test H-E1

Situation 4

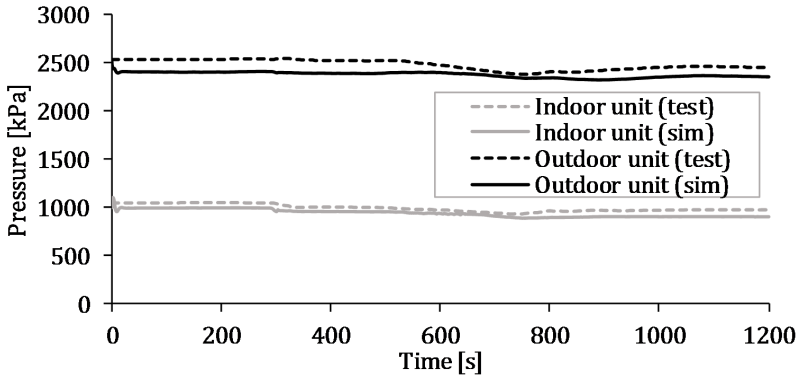

Refrigerant pressures.

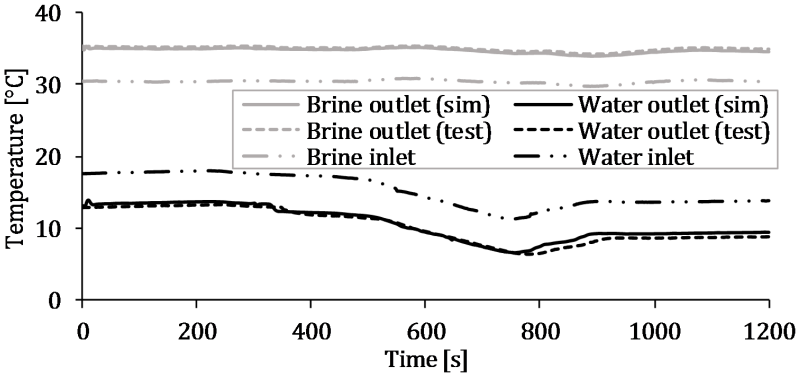

Water and brine temperatures.

ANNEX IV

Macro-scale validations

In this annex, the remaining comparisons between experimental data and simulation results in macro-scale that have not been presented in Chapter 5 are presented. It is included the comparison of the water outlet temperature of both indoor and outdoor PHEXs and the compressor power consumption.

Test T10

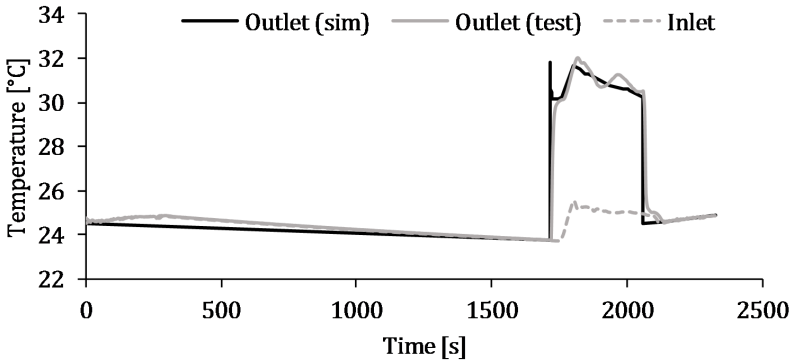

T10 test data and simulation results of water temperatures in the outdoor unit (condenser).

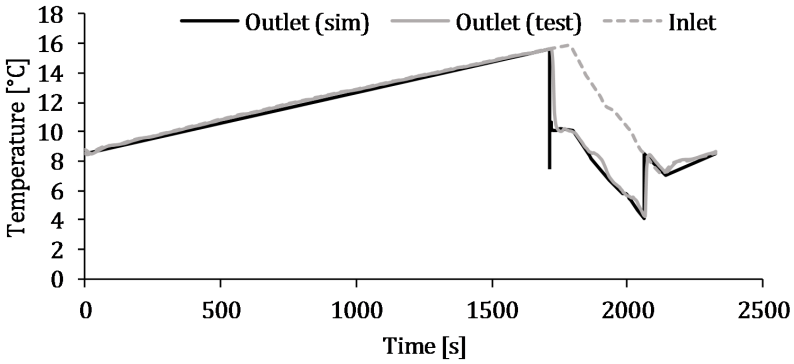

T10 test data and simulation results of water temperatures in the indoor unit (evaporator).

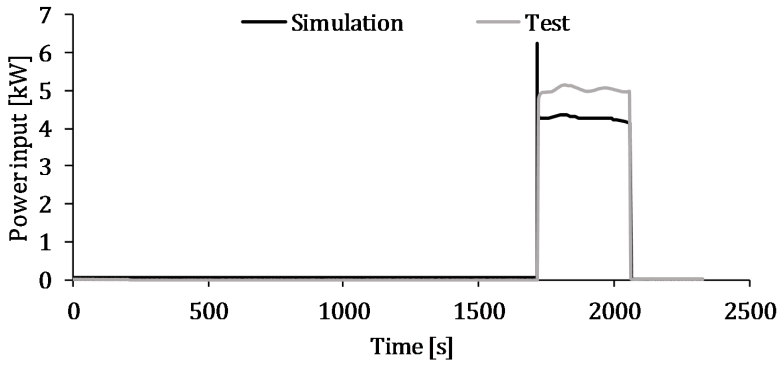

T10 test data and simulation results of compressor power consumption.

Test T15

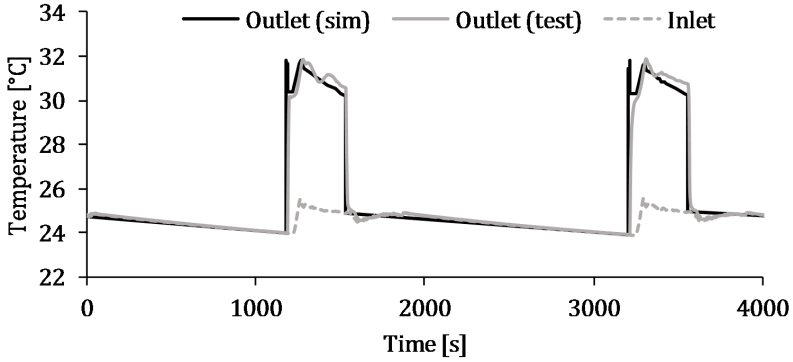

T15 test data and simulation results of water temperatures in the outdoor unit (condenser).

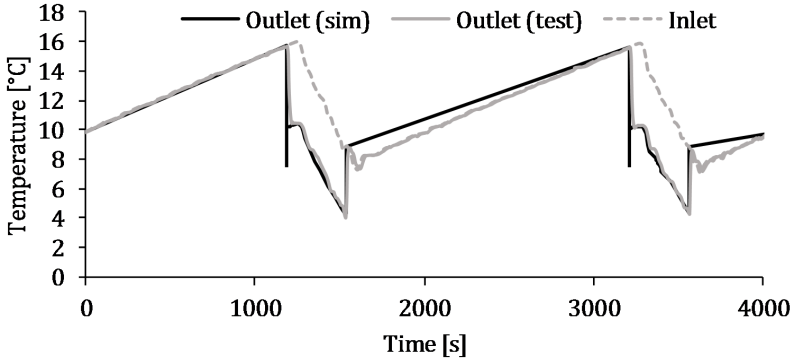

T15 test data and simulation results of water temperatures in the indoor unit (evaporator).

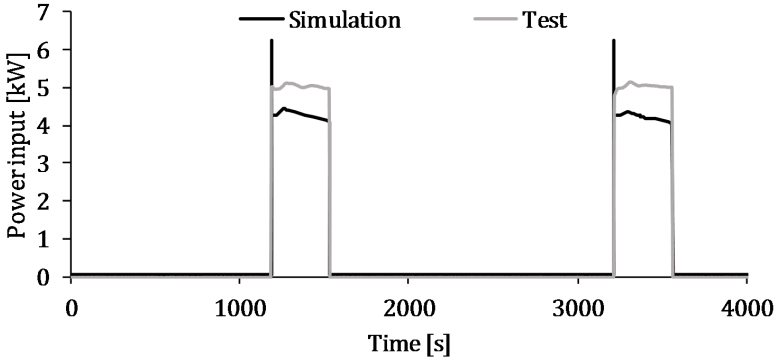

T15 test data and simulation results of compressor power consumption.

Test T30

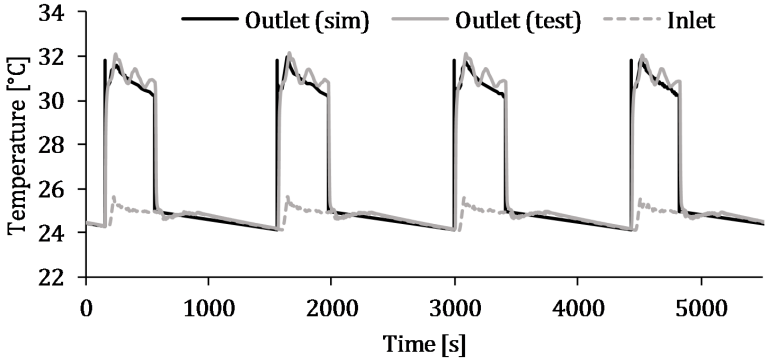

T30 test data and simulation results of water temperatures in the outdoor unit (condenser).

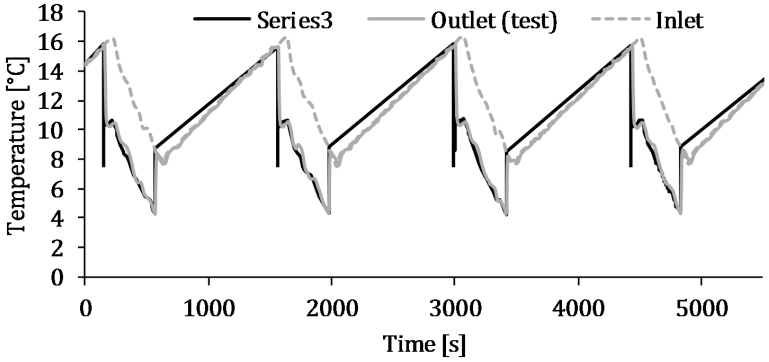

T30 test data and simulation results of water temperatures in the indoor unit (evaporator).

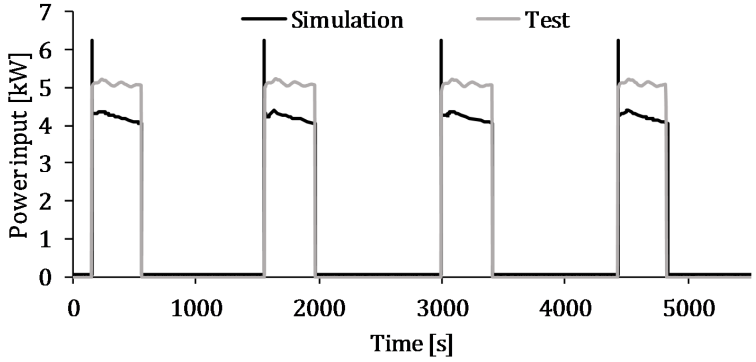

T30 test data and simulation results of compressor power consumption.

Test T40

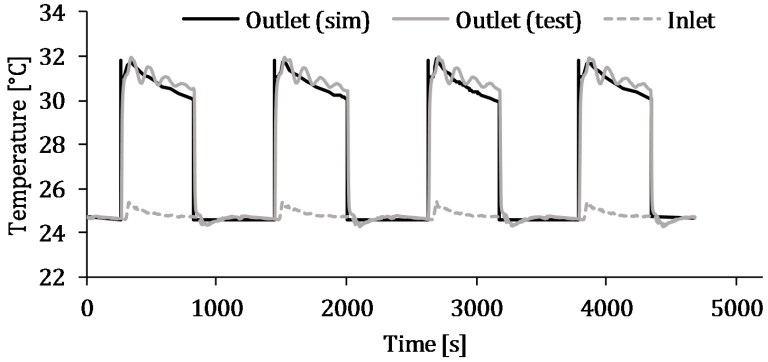

T40 test data and simulation results of water temperatures in the outdoor unit (condenser).

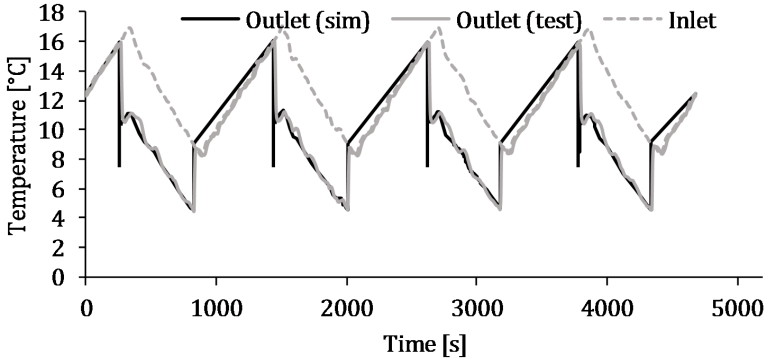

T40 test data and simulation results of water temperatures in the indoor unit (evaporator).

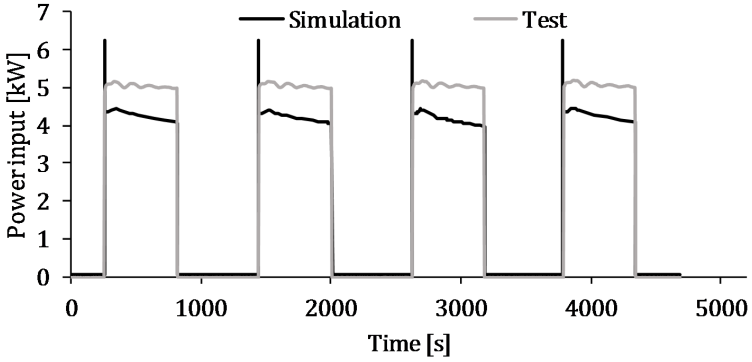

T40 test data and simulation results of compressor power consumption.

Test T50

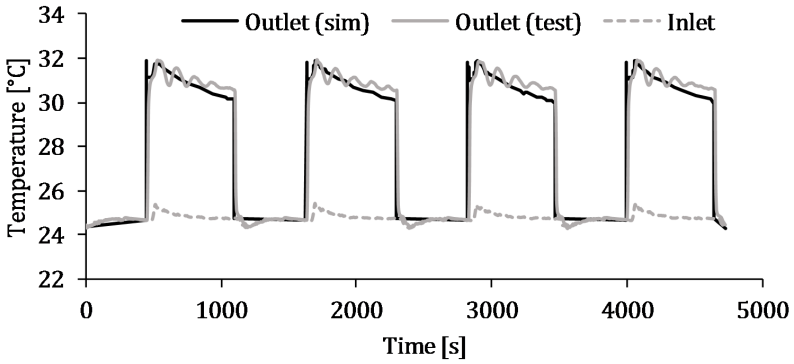

T50 test data and simulation results of water temperatures in the outdoor unit (condenser).

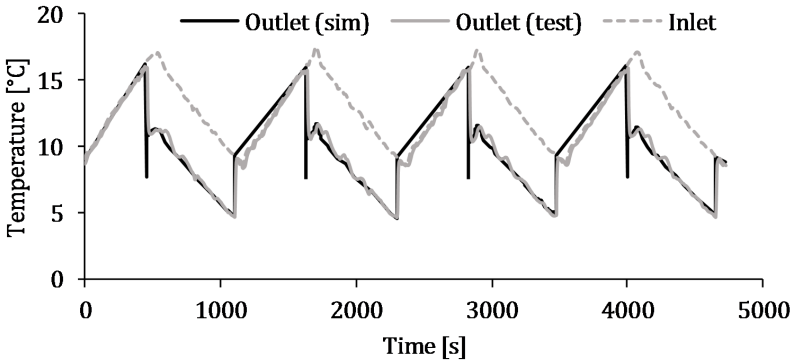

T50 test data and simulation results of water temperatures in the indoor unit (evaporator).

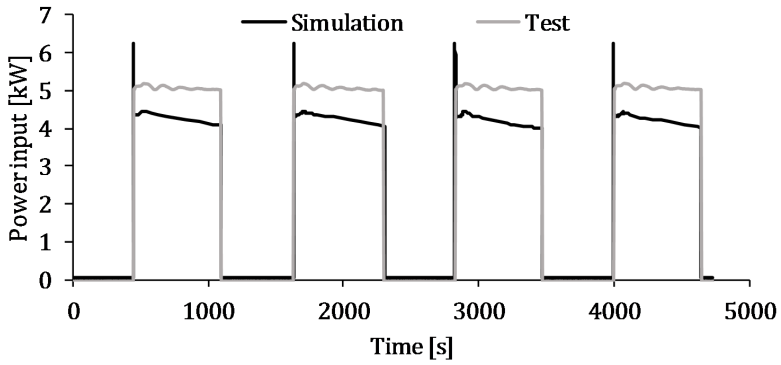

T50 test data and simulation results of compressor power consumption.

Test T70

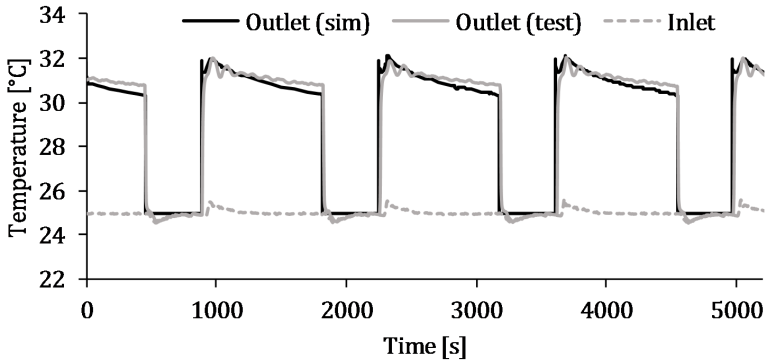

T70 test data and simulation results of water temperatures in the outdoor unit (condenser).

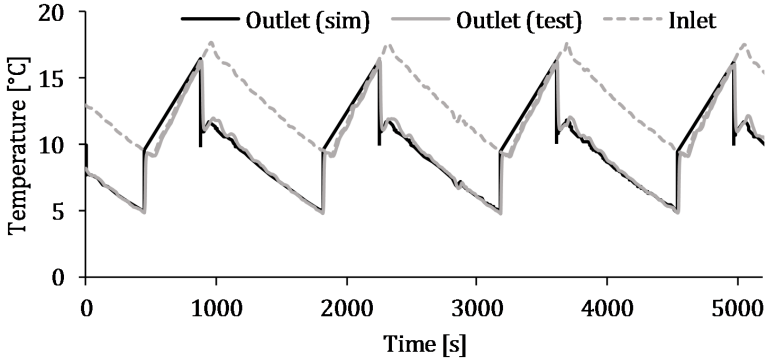

T70 test data and simulation results of water temperatures in the indoor unit (evaporator).

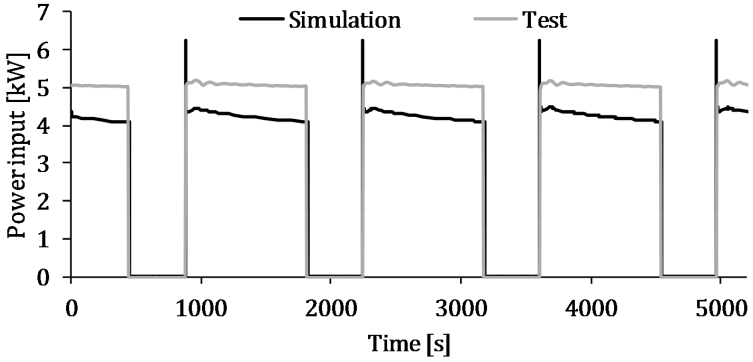

T70 test data and simulation results of compressor power consumption.

Test T90

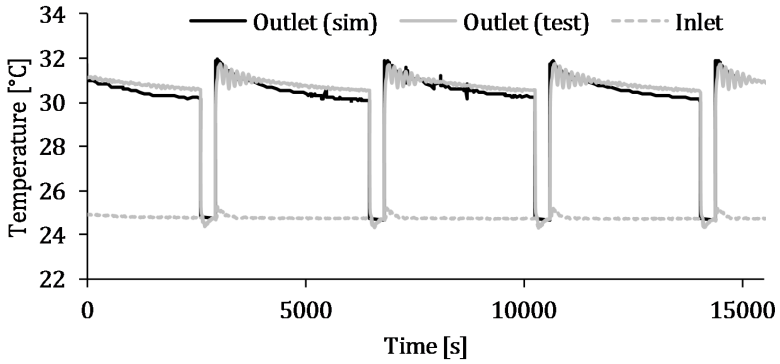

T90 test data and simulation results of water temperatures in the outdoor unit (condenser).

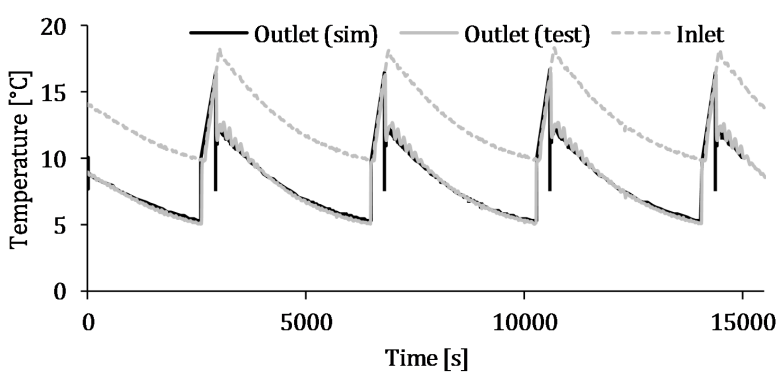

T90 test data and simulation results of water temperatures in the indoor unit (evaporator).

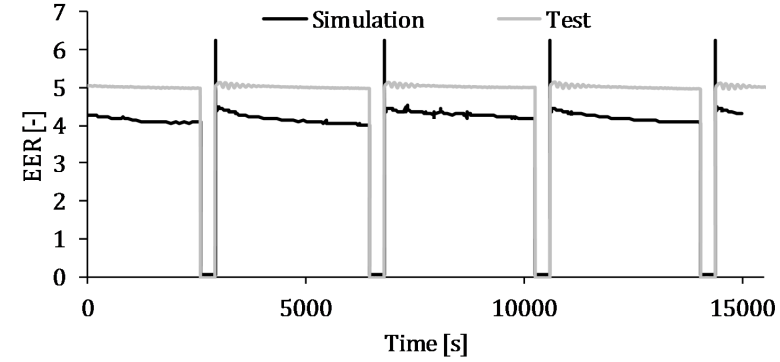

T90 test data and simulation results of compressor power consumption.